# Rhenium(I)/Manganese(I)-based Supramolecular Cages, Tubes and Acyclic Complexes

### A Thesis Submitted for the Degree of DOCTOR OF PHILOSOPHY

By Isha Mishra



School of Chemistry
University of Hyderabad
Hyderabad 500046
INDIA

**JUNE 2023** 

# Dedicated to My FAMILY

#### **CONTENTS**

STATEMENT DECLARATION CERTIFICATE ACKNOWLEDGEMENT List of Abbreviations and Symbols SYNOPSIS		
Chapter 1	Introduction	
1.1.	Overview	1
1.2.	Tetranuclear SCCs from neutral benzimidazolyl/imidazolyl based ligands	6
1.3.	Tetranuclear SCCs from benzimidazolate/imidazolate-based ligands	10
1.4.	Trinuclear SCCs from rigid bidentate ligands	12
1.5.	Re(I)-based SCCs from phenoxybenzimidazolyl ligands	19
1.6.	Re(I)-based acyclic complexes from phenoxybenzimidazole ligand	22
1.7.	Manganese tricarbonyl core containing SCCs and acyclic complexes	24
1.8.	Scope of the present work	27
1.9.	References	29
Chapter 2	Flexible Coordination Cages with Polarized C-H donors for the Recog	gnition of
	Spherical and Linear Anions	
	Abstract	35
2.1.	Introduction	36
2.2.	Results and Discussion	38
2.3.	Experimental Section	67
2.4.	Conclusions	70
2.5.	References	71

Chapter 3	Fluorine	assisted	self-assembly	approach	for	tubular	architecture	of	cyclic
	trinuclear rhenium(I)-fluorothiabendazolate complex								

	Abstract	74
3.1.	Introduction	76
3.2.	Results and Discussion	78
3.3.	Experimental Section	117
3.4.	Conclusions	121
3.5.	References	122
Chapter 4	Luminescent [fac-Re(CO) <sub>3</sub> -N $\cap$ O-phenylimidazole] complexes with arrangement of twisted ligand motifs	h parallel
	Abstract	126
4.1.	Introduction	127
4.2.	Results and Discussion	128
4.3.	Experimental Section	150
4.4.	Conclusions	153
4.5.	References	154
Chapter 5a	Rhenium(I) complexes from 2-(2'-hydroxyphenyl)benzimidazolyl	based bis-
	chelating ligand and 4-aminopyridine/4-dimethylaminopyridine	
	Abstract	158
5a.1.	Introduction	159
5a.2.	Results and Discussion	161
5a.3.	Experimental Section	169
5a.4.	Conclusions	172
5a.5.	References	173

### Chapter 5b Synthesis and characterization of binuclear manganese carbonyl complex of 1,4-bis(2-(2'-hydroxyphenyl)benzimidazol-1-yl)benzene and dimethylaminopyridine

	Abstract	175
5b.1.	Introduction	176
5b.2.	Results and Discussion	178
5b.3.	Experimental Section	185
5b.4.	Conclusions	187
5b.5.	References	188

**Publications and Presentations** 

Plagiarism Report



#### **STATEMENT**

I hereby declare that the matter embodied in this thesis is the result of investigations carried out by me in the School of Chemistry, University of Hyderabad, Hyderabad, under the supervision of **Prof. M. Sathiyendiran**.

In keeping with the general practice of reporting scientific observations, due acknowledgements have been made wherever the work described is based on the findings of other investigators.

Hyderabad JUNE 2023

> Isha Mishra (17CHPH03)

#### **DECLARATION**

I, Isha Mishra, hereby declare that this thesis entitled "Rhenium(I)/Manganese(I)-based Supramolecular Cages, Tubes and Acyclic Complexes" submitted by me under the guidance and supervision of Prof. M. Sathiyendiran, is a bonafide research work which is also free from plagiarism. I also declare that it has not been submitted previously in part or in full to this university or any other university or institution for the award of any degree or diploma. I hereby agree that my thesis can be deposited in Shodhganga/INFLIBNET.

A report on plagiarism statistics from the University Librarian is enclosed.

Date: June 19, 2023

Isha Mishra (17CHPH03)

Signature of the student

M. Satly Liva.
Signature of the Supervisor

Dr. M.Sathiyendiran
Professor
School of Chemistry
University of Hyderabad
Hyderabad - 500 046, India.



#### UNIVERSITY OF HYDERABAD

Prof. M. Sathiyendiran

#### SCHOOL OF CHEMISTRY

HYDERABAD-500046, INDIA

Phone: +91-40-2313-4811 (Office), 2313-4911 (Lab) E-mail: msathi@uohyd.ac.in

#### CERTIFICATE

This is to certify that the thesis entitled "Rhenium(I)/Manganese(I)-based Supramolecular Cages, Tubes and Acyclic Complexes" submitted by Isha Mishra bearing registration number 17CHPH03 in partial fulfillment of the requirements for the award of Doctor of Philosophy (Ph. D.) is a bonafide work carried out by her under my supervision and guidance in School of Chemistry, University of Hyderabad. This thesis is free from plagiarism and has not been submitted previously in part or in full to this or any other University or Institution for the award of any degree or diploma. Further, the student has seven publications before submission of the thesis for adjudication and has produced shreds of evidence for the same in the form of reprints.

#### Parts of this thesis have been published as the following articles:

- 1. I. Mishra, M. Sathiyendiran, J. Organomet. Chem. 2019, 895, 1–6 (Chapter 4).
- 2. I. Mishra, M. Priyatharsini, M. Sathiyendiran, J. Organomet. Chem. 2020, 927, 121521 (Chapter 5a).
- 3. I. Mishra, M. Priyatharsini, M. Sathiyendiran, J. Organomet. Chem. 2021, 949, 121934 (Chapter 5b).

#### She has also made presentations in the following conferences:

- Poster: "Light emitting heteroleptic rhenium complexes" in Chemfest 2018 (In-house symposium) at University of Hyderabad.
- Poster: "fac-Mn(CO)<sub>3</sub> core based neutral dinuclear complexes" in Chemfest 2019 at (Inhouse symposium) University of Hyderabad.
- 3. Poster: "Dinuclear Rhenium (I) Acyclic complexes: Photophysical and Electrochemical studies" in Chemfest 2020 (In-house symposium) at University of Hyderabad.
- 4. Oral and Poster: "Rhenium(I) based Metallocage and Tubes" in Chemfest 2023 at University of Hyderabad. (Best oral presentation)

Further the student has passed the following courses towards the fulfilment of coursework requirement for Ph. D.

Sl. No.	Course No.	Title of the Course	No. of Credits	Result Pass Pass	
1.	CY801	Research Proposal	4		
2.	CY805	Instrumental Methods-A	4		
3. CY806		Instrumental Methods-B	4	Pass	

Hyderabad

M. Satlylra.
Prof. M. Sathiyendiran

(Thesis Supervisor)

Dr. M.Sathiyendiran
Professor
School of Chemistry
University of Hyderabad
Hyderabad - 500 046, India.

Dean

School of Chemistry

University of Hyderabad

Hyderabad- 500046, INDIA Dean

SCHOOL OF CHEMISTRY

University of Hyderabad Hyderabad-500 046.

#### **ACKNOWLEDGEMENTS**

I would like to express my sincere gratitude and heartfelt appreciation to the following individuals and groups, without whom the completion of this thesis would not have been possible:

I extend my deepest gratitude to my supervisor Prof. M. Sathiyendiran for his support, guidance, and invaluable expertise that have been instrumental in shaping this research endeavour.

I am equally indebted to the members of my doctoral committee, Prof. V. Baskar and Prof. K. Muralidharan for their insightful suggestions. I am grateful for their time, dedication, and willingness to share their knowledge.

I want to thank present and former deans, School of Chemistry, University of Hyderabad, and all the faculty members of the School of chemistry for their help and support on various occasions.

I am highly grateful to Prof. Ulrich Abram (Institute for Chemistry and Biochemistry, Freie Universität Berlin) for providing me an excellent opportunity to explore a new field, <sup>99</sup>Tc-chemistry. I am highly grateful for his valuable guidance, great care and immense support during my stay in Germany.

I want to acknowledge DST-INSPIRE, and Erasmus+ Exchange Program, Berlin (Erasmus+ Grant) for financial support during my Ph.D. research tenure.

My heartfelt appreciation extends to Mr. Durgesh and Mr. Mahender (NMR, School of Chemistry), Mr. Mahesh (SC–XRD, School of Chemistry), Mrs. Asia Parwez and Dr. Manasi Dalai (HRMS, School of Chemistry), Mr. Anand (IR, School of Chemistry) and Mr. Abraham for his help in official work (School Office). Their constant support, from administrative assistance to technical expertise, has been crucial throughout my academic journey. I am grateful for their tireless efforts behind the scenes, which have made the pursuit of knowledge a seamless and enriching experience.

I am highly indebted to Dr. Chandrakanta Dash (School of chemical sciences, Central University of Rajasthan) who has sown the seeds of research in my mind. I will always be thankful for his constant guidance, support and motivation.

I am thankful to Dr. P. Kalimuthu (Gandhigram rural institute, Tamil Nadu) for his time, willingness to share his knowledge, constant support and help for my research problems.

I would also like to thank all my lab seniors, Dr. B. Shankar, Dr. P. Rajakannu, Dr. R. Arumugam, Dr. Soumya K. R. and Dr. Mamina bhol for their constructive comments and helpful discussions. I am very grateful to all my colleagues, Moon, Upasana, Reema, Vengadesh and Sujeet for their help and creating a pleasant research environment, making it a memorable and enjoyable journey. I would specially like to thank Dr. Soumya for always being there in my highs and lows, motivating me to pursue the research and always having open ears for my personal and professional problems. I extend my gratitude to all the project students who have worked with me, Priya, Soumik and Sanjit.

I am thankful to my dear friends, Noorul, Ishfaq, Mujahid, Asif, Navneetha, Daradi and Dr. Bilal Ahmed for their unwavering support, understanding, and encouragement that have been a constant source of motivation. My special thanks to Noorul for believing in my abilities, shared laughter, and moments of respite from academic rigors that have played a pivotal role in keeping me inspired and focused. Your presence has made this journey all the more meaningful, and I am grateful for the enduring bond we share. Especially, I would like to thank Dr. Ankit K. Srivastav who always had an open ear for my worries and guided me through my Ph.D. studies. I thank Dr. Jagjeet gujral, Intezar, Vamshi, Tousif, Irfan, Vinay and Shruti, for their help and support on several occasions.

I would like to express my heartfelt gratitude to my best friend, Monica for her support and encouragement throughout my journey. Your presence has provided me strength, motivation, and moments of laughter when I needed it the most. Your willingness to lend an ear, offer insightful perspectives, and engage in meaningful discussions has greatly enriched my research experience. I am truly fortunate to have you in my life and forever grateful for this friendship.

Last but certainly not least, I would like to express my deepest gratitude to my family. To my parents, Mr. Anil Mishra and Mrs. Sarita Mishra for their unwavering love, support, and sacrifices that have been the foundation upon which my achievements rest. Your beliefs in my abilities, constant encouragement, and sacrifices have fuelled my determination to succeed. I am forever grateful for your unyielding faith in me.

To my siblings, Ishank and Aditi, my extended family, and loved ones, your unwavering support and words of encouragement have provided me with the strength to overcome challenges along the way. Your understanding, love, and encouragement have been a constant source of inspiration. I am grateful for the countless ways you have uplifted me throughout this journey.

This thesis stands as a testament to the collaborative efforts and support of the aforementioned individuals and groups. Their contributions have left an indelible mark on this research, and I am humbled by their generosity and belief in my abilities. It is with heartfelt gratitude that I acknowledge their immense impact on my academic and personal growth. Finally, I thank almighty for making this happen.

Isha Mishra

#### List of abbreviations and symbols

SCC Supramolecular Coordination Complex

fac facial

SARS-COV Severe Acute Respiratory Syndrome Corona Virus

CORMs CO-Releasing Molecules

H<sub>2</sub>-BBim 2,2'-bisbenzimidazole

2-PyTz 2-pyridyltetrazolate

DMSO Dimethyl Sulfoxide

MLCT Metal-to-Ligand Charge Transfer

MLLCT Metal-to-Ligand-Ligand Charge Transfer

ILCT Intra-Ligand Charge Transfer

N-donor Nitrogen donor

Bpy Bipyridine

OTf Triflate

DMF N,N-Dimethylformamide

DCM Dichloromethane

THF Tetrahydrofuran

CDCl<sub>3</sub> Deuterated Chloroform

DMSO-*d*<sub>6</sub> Deuterated Dimethyl Sulphoxide

UV-Vis Ultraviolet-Visible

ATR-IR Attenuated Total Reflectance Infrared spectroscopy

FT-IR Fourier-transform Infrared Spectroscopy

NMR Nuclear Magnetic Resonance

DOSY Diffusion Ordered Spectroscopy

ESI- HR-MS Electron Spray Ionization High Resolution Mass Spectrometry

SCXRD Single Crystal X-Ray Diffraction

ppm Parts per million

H<sub>2</sub>-CA Chloranilic acid

H<sub>2</sub>-dhbq 2,5-dihydroxy-1,4-benzoquinone

H<sub>2</sub>-dhaq 1,4-dihydroxy-9,10-anthraquinone

H<sub>2</sub>-dhnq 6,11-dihydroxy-5,12-naphthacenedione

H<sub>2</sub>-RBC 2-(2'-hydroxyphenyl)benzimidazole

Å Angstrom

h Hour

m/z Mass to charge ratio

nm Nanometer

δ Chemical shift

 $\lambda_{abs}$  Absorption wavelength

 $\lambda_{max}$  Absorption maxima

 $\lambda_{exc}$  Excitation wavelength

 $\lambda_{em}$  Emission wavelength

J Coupling constant

K Binding constant

#### **SYNOPSIS**

The thesis entitled "Rhenium(I)/Manganese(I)-based Supramolecular Cages, Tubes and Acyclic Complexes" consists of six chapters.

#### **Chapter 1: Introduction**

Chapter 1 contains brief literature overview on rhenium(I)/manganese(I) tricarbonyl-based discrete cyclic supramolecules and acyclic systems. Based on different shapes, sizes and nuclearity, the rhenium(I) complexes are subdivided into four classes i.e., tetranuclear, trinuclear, dinuclear and acyclic complexes. The general overview describes the significance of Re(I) and Mn(I) complexes and their potential utility in material and medicinal sciences. The chapter mainly highlights the imidazole/benzimidazole scaffold containing ligands and their self-assembly with rhenium metal core. Further, the importance of photo-active units is discussed to assemble visible light absorbing and emitting mono- and dinuclear acyclic complexes. The discussions on manganese (I) tricarbonyl complexes describes the synthetic strategy and their use as photocatalyst and photo-CO releasing molecules.

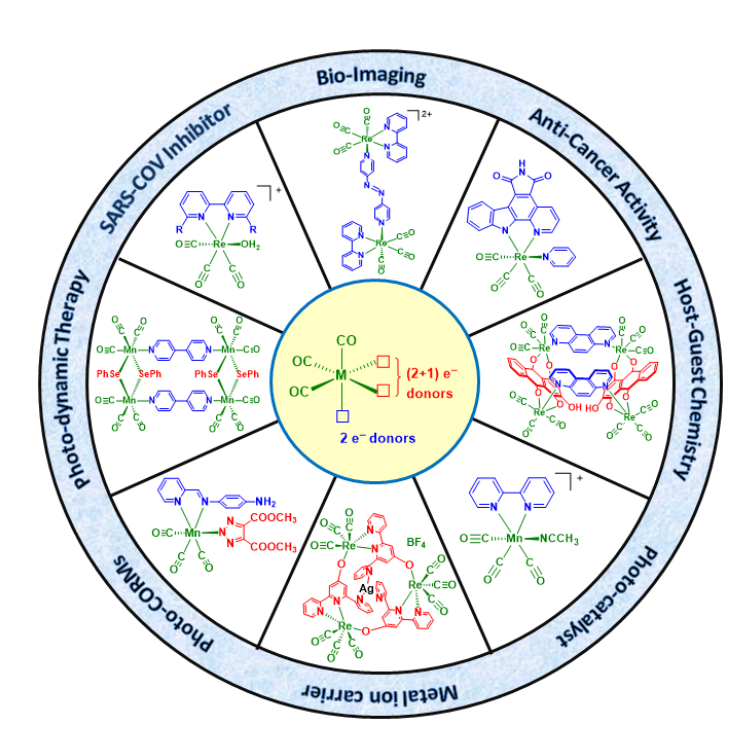
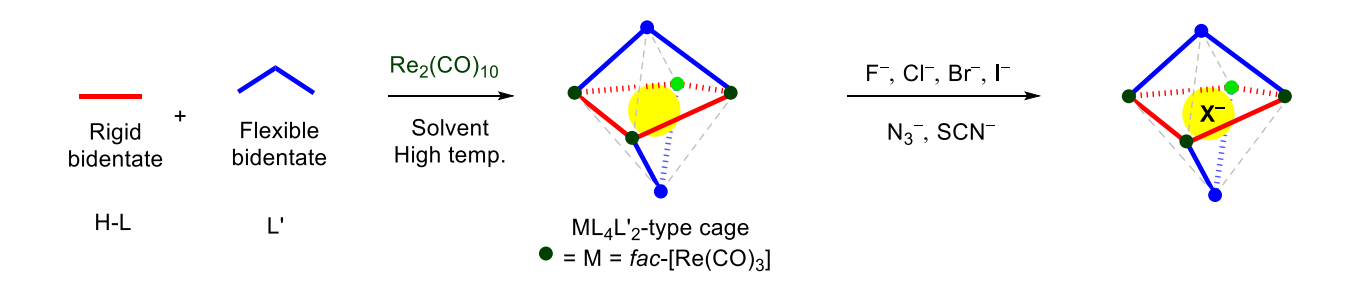


**Figure 1.** Various known examples of M(I) core-based (M = Re/Mn) complexes and applications.

#### Chapter 2: Flexible Coordination Cages with Polarized C-H Donors for the Recognition of Spherical and Linear Anions

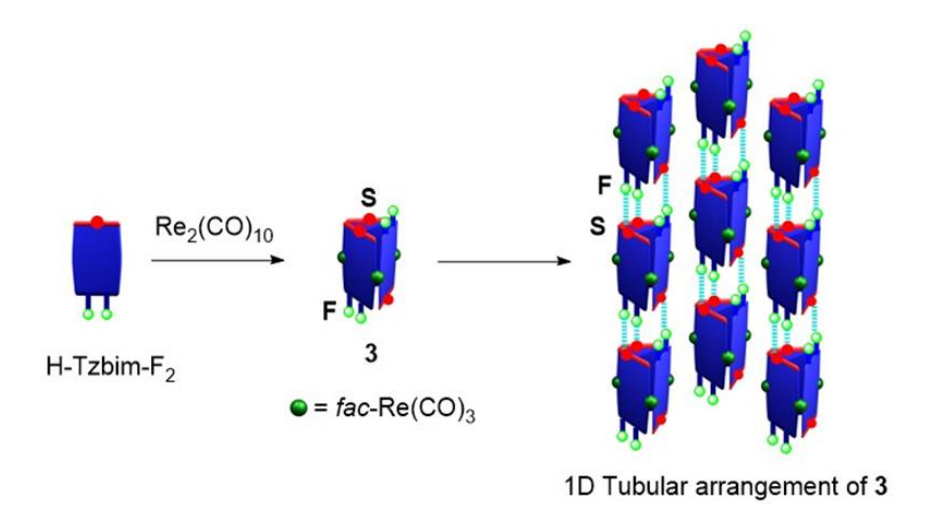
This chapter describes the design and synthesis of neutral heteroleptic flexible tetranuclear coordination cages possessing flexible multiple electron deficient C–H donors self-assembled using Re<sub>2</sub>(CO)<sub>10</sub>, carbonyldiimidazole/1,2,4–triazole and bis(benzimidazol-1-yl)methane via one pot solvothermal approach. The cages were characterized using various analytical and spectroscopic techniques such as ATR–IR, NMR spectroscopy, mass spectrometry, single crystal X–ray diffraction analysis, and fluorescence spectroscopy. The molecular structure of the cages reveals that it consists of a butterfly-like cyclic core capped with two neutral N-donor ligands lying above and below the cycle. The semi-flexible neutral donor and bridged imidazolate/triazolate units imparts flexibility to the cages. The dynamic behavior of the cage 1 was studied using variable temperature <sup>1</sup>H–NMR spectroscopy. The ability of cage 1 to interact with anions of different shapes and sizes was further investigated using <sup>1</sup>H–NMR and fluorescence spectroscopy. The thermally stable, flexible cage 1 transforms into restricted cage in the presence of spherical and linear anions, and has more binding affinity for fluoride. The extent of association of anions with cage 1 was determined using fluorescence spectroscopy. The binding constant values were calculated using Benesi-Hildebrand equation for 1:1 host-guest stoichiometry.



**Scheme 1.** Self–assembly of  $ML_4L'_2$ –type cage and its interaction with various anionic guests.

### Chapter 3: Fluorine Assisted Self-assembly Approach for Tubular Architecture of Cyclic Trinuclear Rhenium(I)-Fluorothiabendazolate Complex

Chapter 3 describes the synthetic strategy, structural aspects and properties of three neutral trinuclear rhenium(I)-organic cyclic complexes, fac-[{Re(CO)<sub>3</sub>(L)}<sub>3</sub>] (1–3), self-assembled from Re<sub>2</sub>(CO)<sub>10</sub> and thiabendazole/thiazolylnaphthanoimidazole/difluorothiabendazole in a one-pot approach. The molecular structures established by X-ray analysis revealed that all three complexes adopt M<sub>3</sub>L<sub>3</sub>-type metal-organic triangular tube structure which consists of alternatively arranged three fac-[Re(CO)<sub>3</sub>] cores and three anionic ligand motifs. All three metal-organic tubes possess uncoordinated sulfur atoms from thiazolyl motif that are directed along the tube axis. Metal-organic tube 3 additionally possesses six C–F bonds, four at one end and two at rear, lateral to the tube axis and further self-organizes into 1D supramolecular tubular architecture via fluorine assisted noncovalent C–F···S contacts. The photophysical properties of 1–3 were studied using UV-Visible and fluorescence spectroscopy and further validated using time-dependent density functional theory (TDDFT) calculations. The electrochemical properties of 1–3 were studied using cyclic voltammetry.



**Scheme 2.** Synthetic approach for discrete tube **3** and its self-organization into 1D-tubular architecture via fluorine assisted C–F···S non-covalent contacts.

### Chapter 4: Luminescent [fac-Re(CO)<sub>3</sub>-N∩O-phenylimidazole] Complexes with Parallel Arrangement of Twisted Ligand Motifs

In chapter 4, Luminescent complexes [fac-Re(CO)<sub>3</sub>(Y $\cap$ X)(ph-imz)] where (Y $\cap$ XH) = H<sub>2</sub>–PBI = 2-(2'-hydroxyphenyl)benzimidazole for **1**, H–PBO = 2-(2'-hydroxyphenyl)benzoxazole for **2**, and H–PBT = 2-(2'-hydroxyphenyl)benzothiazole for **3** and ph-imz = 2-phenylimidazole) were synthesized using Re<sub>2</sub>(CO)<sub>10</sub>, H<sub>2</sub>–PBI/H–PBO/H–PBT and ph-imz via one-pot approach. All three complexes were characterized using FT–IR,  $^1$ H–NMR, and single crystal X–ray diffraction analysis. The two twisted coordinated ligand motifs are arranged closely parallel to each other and interact through  $\pi$ ··· $\pi$  stacking interactions in the solid state. The photophysical properties of the complexes were also studied. All the complexes display emission both in the solution and solid state at room temperature.

Re<sub>2</sub>(CO)<sub>10</sub>

$$Re_{2}(CO)_{10}$$

$$Re_{2}(CO)_{10}$$

$$Re_{2}(CO)_{10}$$

$$Re_{2}(CO)_{10}$$

$$Re_{3}(CO)_{10}$$

$$Re_{4}(CO)_{10}$$

$$Re_{5}(CO)_{10}$$

$$Re_{6}(CO)_{10}$$

$$Re_{7}(CO)_{10}$$

$$Re_{7}(CO)_{10$$

Scheme 3. Synthetic approach for complexes 1–3.

### Chapter 5a: Rhenium(I) Complexes from 2-(2'-hydroxyphenyl) benzimidazolyl Based Bis-chelating Ligand and 4-Aminopyridine/4-Dimethylaminopyridine

In Chapter 5, two fac-Re(CO)<sub>3</sub> core based dinuclear complexes obtained from Re<sub>2</sub>(CO)<sub>10</sub>, 1,4phenylene-bis(2-(2'-hydroxyphenyl)benzimidazole)  $(H_2-L)$ and neutral N-donors (4-(amino)pyridine for 1/4-(dimethylamino)pyridine for 2) are discussed. Both the complexes were characterized using various analytical and spectroscopic techniques. The molecular structure of 2 from single crystal X-ray diffraction analysis shows that two anionic phenoxybenzimidazolyl motifs of L<sup>2-</sup> are twisted, resulting in an acyclic dinuclear helical structure. Both the complexes display strong emission in the solution state at room temperature.

HO H<sub>2</sub>-L 
$$\rightarrow$$
 OC  $\rightarrow$  O

**Scheme 4.** Synthetic approach for dinuclear Re(CO)<sub>3</sub> core-based complexes (1–2).

## Chapter 5b: Synthesis and Characterization of Binuclear Manganese Carbonyl Complex of 1,4-Bis(2-(2'-hydroxyphenyl)benzimidazolyl)benzene and Dimethylaminopyridine

Chapter 5b describes the design and synthetic approach for a neutral heteroleptic binuclear complex fac-[{Mn(CO)<sub>3</sub>(Py')}<sub>2</sub>(L)] synthesized using Mn<sub>2</sub>(CO)<sub>10</sub>, 1,4-bis(2-(2'-hydroxyphenyl)benzimidazolyl)benzene (H<sub>2</sub>-L<sup>1</sup>), 4-dimethylaminopyridine (Py'), and trimethylamine-N-oxide (Me<sub>3</sub>NO) via conventional one-pot approach. The complex was characterized using FT-IR,  $^1$ H-NMR,  $^{13}$ C-NMR, mass spectrometry and single crystal X-ray diffraction analysis. The molecular structure of the complex reveals that it adopts a helical structure in the solid state due to twisted arrangement of ligand framework.

$$\begin{array}{c} CO \\ OC \\ Mn_2(CO)_{10} \end{array}$$

**Scheme 5.** Synthetic approach for binuclear manganese complex.

#### **Chapter 6: Conclusion and Future Prospects**

This chapter provides a brief summary of the thesis along with future prospects of the performed work. The thesis is mainly divided into two parts that discusses about Re(I) based supramolecules and Re(I)/Mn(I) based mono- and dinuclear acyclic complexes. The structural aspects and properties of the complexes are studied using various spectroscopic and analytical techniques. We have developed new synthetic combinations for assembling metal-organic cages with better adaptability using N-donor flexible ligand and anionic counterpart with Re<sub>2</sub>(CO)<sub>10</sub> in a one-pot solvothermal approach. The incorporation of flexible N-donor ligand facilitates the adaptive behavior of the cage. The other part describes Re(I) based metal-organic tubes decorated with chalcogen/halogen donor acceptor atoms that undergo self-organization to form 1D-tubular architectures from discrete small molecular tubes. The study suggested that incorporation of chalcogen/halogen donor acceptor groups in the ligand framework can provide a way to assemble hierarchical superstructures from small SCCs.

The study on synthetic strategy and photophysical properties of mono and dinuclear Re(I)/Mn(I) based acyclic complexes based on photo-active motifs, 2-(2'-hydroxyphenyl)benzimidazole and its analogues have also been discussed. Considering the labile character of *fac*–Mn(CO)<sub>3</sub>–core based complexes upon irradiation of light and good photophysical properties of 2-(2'-hydroxyphenyl)benzimidazole core, the research was directed towards combining these two units to form a potential photo-CO releasing molecule. This is the first report on *fac*-Mn(CO)<sub>3</sub> core containing acyclic dinuclear complexes assembled using rigid bis-chelating ligand. This field is ever growing with new synthetic combinations for assembling *fac*-Re(CO)<sub>3</sub>/Mn(CO)<sub>3</sub> based acyclic and discrete cyclic complexes. The current research is directed towards modulating the building units through functionalization or incorporation of biologically relevant or photo-active groups that can be used to construct SCCs or acyclic complexes for wide range of applications.

#### **Chapter 1**

#### Introduction

#### 1.1. Overview

The self-assembly of supramolecular coordination complexes (SCCs) i.e., discrete metal-organic cyclic complexes assembled using pre-designed metal ion sources and organic donors is among the most explored classes in supramolecular chemistry. 1-7 Various types of two and three dimensional supramolecules have been constructed using this synthetic approach and explored for their potential utility in different fields including material and medicinal sciences. <sup>1-7</sup> The supramolecular metalligand self-assembly can have various non-covalent interactions due to the presence of functionalized ligand cores which can be helpful in biological applications and in building superstructures or macrocycles. Among various types of metal precursors usually employed in the synthesis of these SCCs, rhenium tricarbonyl core is one of the most promising metal cores for constructing small to complex supramolecular architectures (Chart 1-2).<sup>3-7</sup> Multiple types of metal precursors including  $Re_2(CO)_{10}$ ,  $[Re(CO)_3(DMSO)_3](OTf)$ ,  $Re(CO)_5X$  (X = Cl, Br, OTf) are utilized for making these complexes. The rhenium tricarbonyl core offers three orthogonal vacant sites for coordination by accepting [3+2] electrons. This chemistry have been growing since decades and modifications of the coordinating units have provided numerous complexes possessing intriguing properties and wide range of applications in diverse fields.<sup>3-7</sup> Several robust architectures including mononuclear cycles (ML); dinuclear cycles (helicates: double stranded (M<sub>2</sub>L<sub>2</sub> or M<sub>2</sub>LL') and triple stranded (M<sub>2</sub>L<sub>3</sub> or M<sub>2</sub>L<sub>2</sub>L'), mesocates (M<sub>2</sub>L<sub>2</sub> or M<sub>2</sub>LL'); trinuclear (metallacycles  $(M_3L_3L')$ , triangles or metallacalix[3]arenes  $(M_3L_3)$ ; tetranuclear (squares or rhombus  $(M_4L_4)$ , rectangles  $(M_4L_2L_2')$ , tetrahedrons  $(M_4L_2L_2')$ ); hexanuclear (trigonal prisms  $(M_6L_2L_3')$ , spheroids

 $(M_6LL_6')$  and octanuclear prisms  $(M_8L_2L_8')$  (1-14) have been reported (Chart 1–2).<sup>3-7</sup> The basic coordination framework for SCCs consists of neutral rigid or flexible ligands with pyridyl/imidazolyl/benzimidazolyl N-donors and RX<sup>-</sup> (where X<sup>-</sup> = O/S, R = -H, aryl or alkyl) as anionic counterparts.

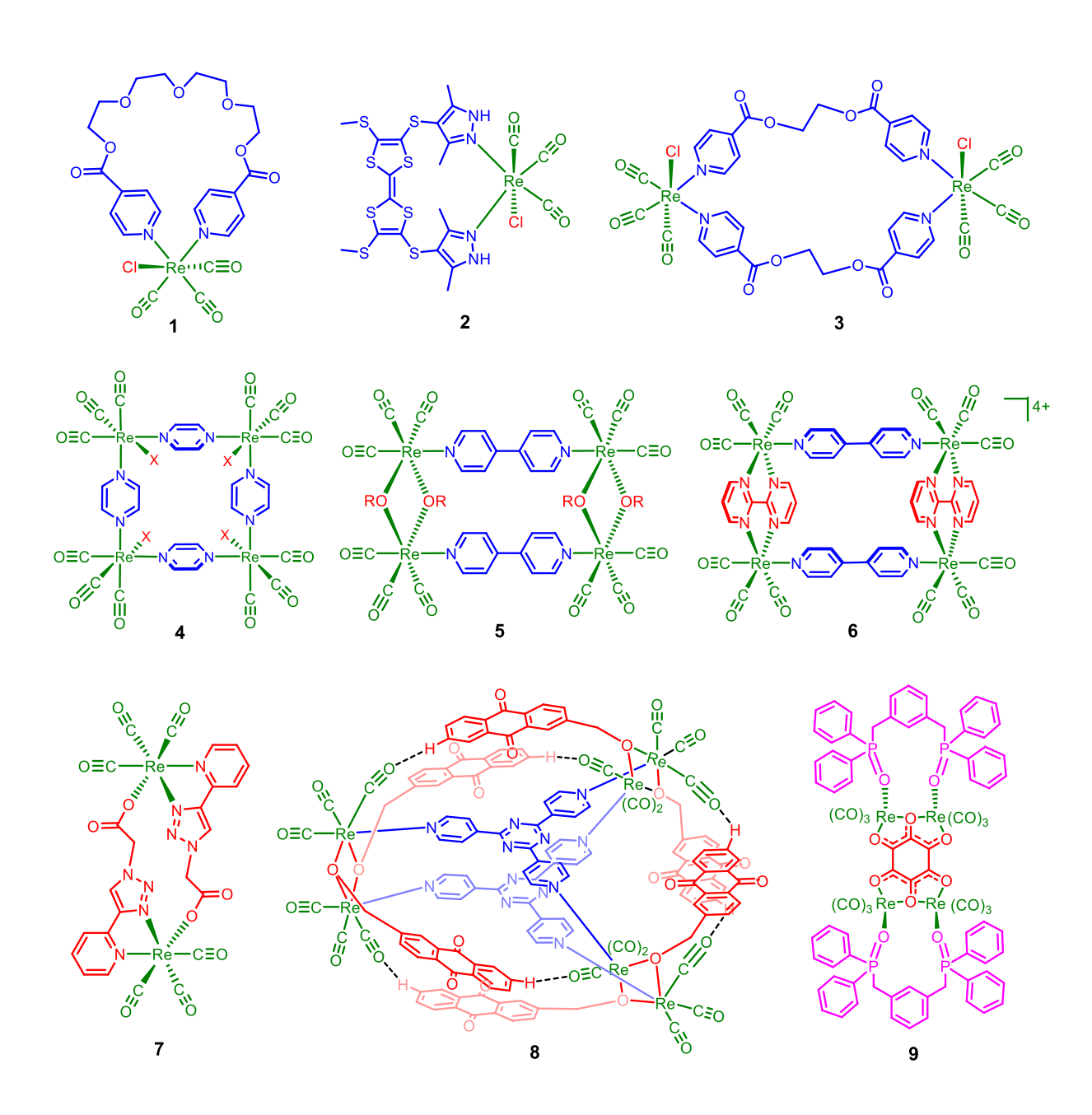
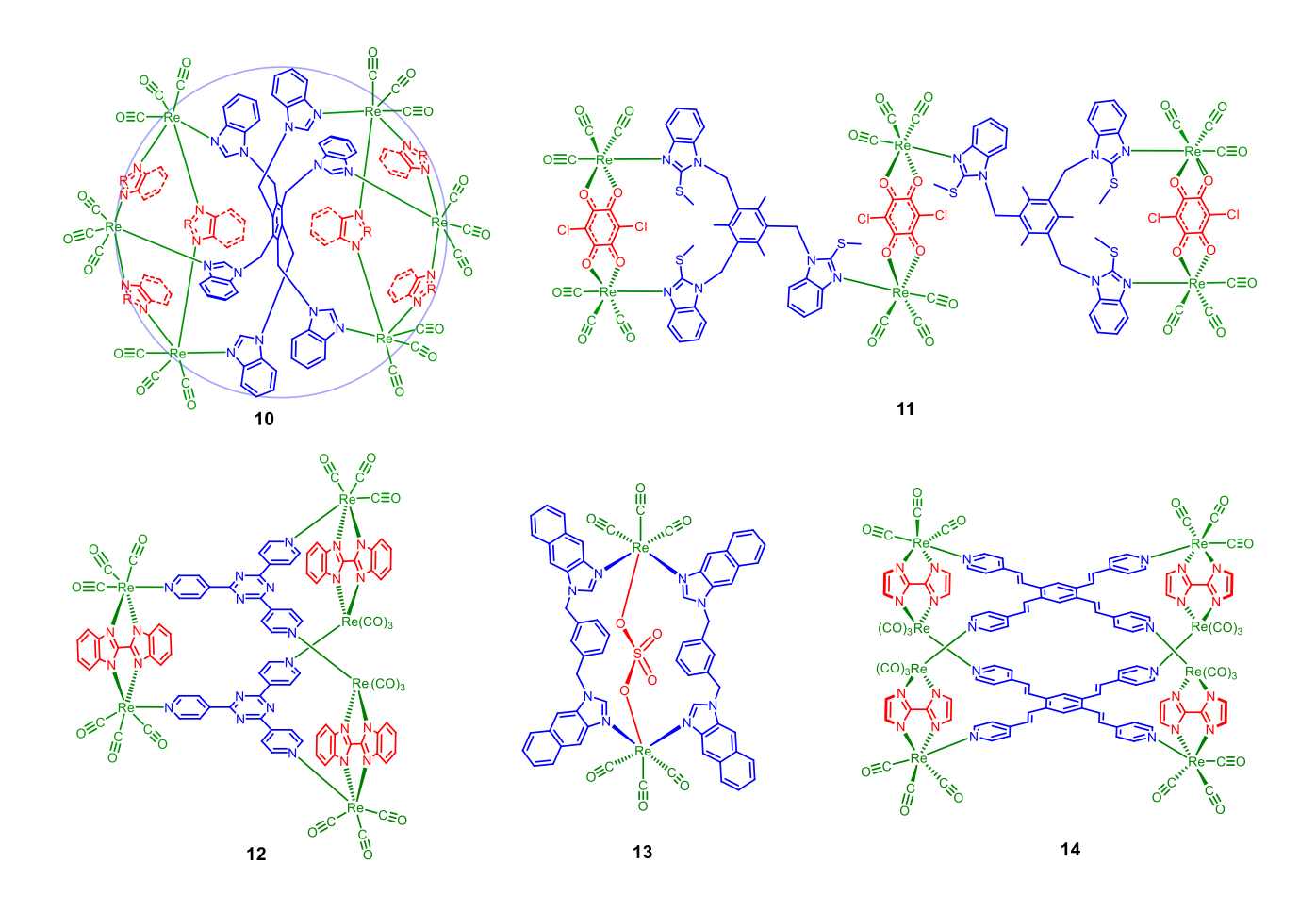


Chart 1. Different types of Re(I) based mono- and multinuclear complexes.<sup>3-7</sup>



**Chart 2.** Chem draw representations of rhenium(I)-based di-, hexa- and octanuclear SCCs.

The interesting properties of Re(I) complexes including kinetic inertness, thermal and photo-stability, long-lived excited states, large Stokes shift, presence of strong field CO ligands have paved way for these complexes to be utilized for molecular recognition, bio-imaging, anti-cancer activity, photosensitizers, photo/electro-catalysts for CO<sub>2</sub> reduction and drug delivery. Both acyclic and cyclic complexes have been explored for such applications and have provided promising results (Chart 3). However, study on cyclic Re(I) complexes is still at a very nascent stage. Recent study by Cohen and co-workers has shown activity of these mononuclear complexes (15) towards SARS-COV virus.

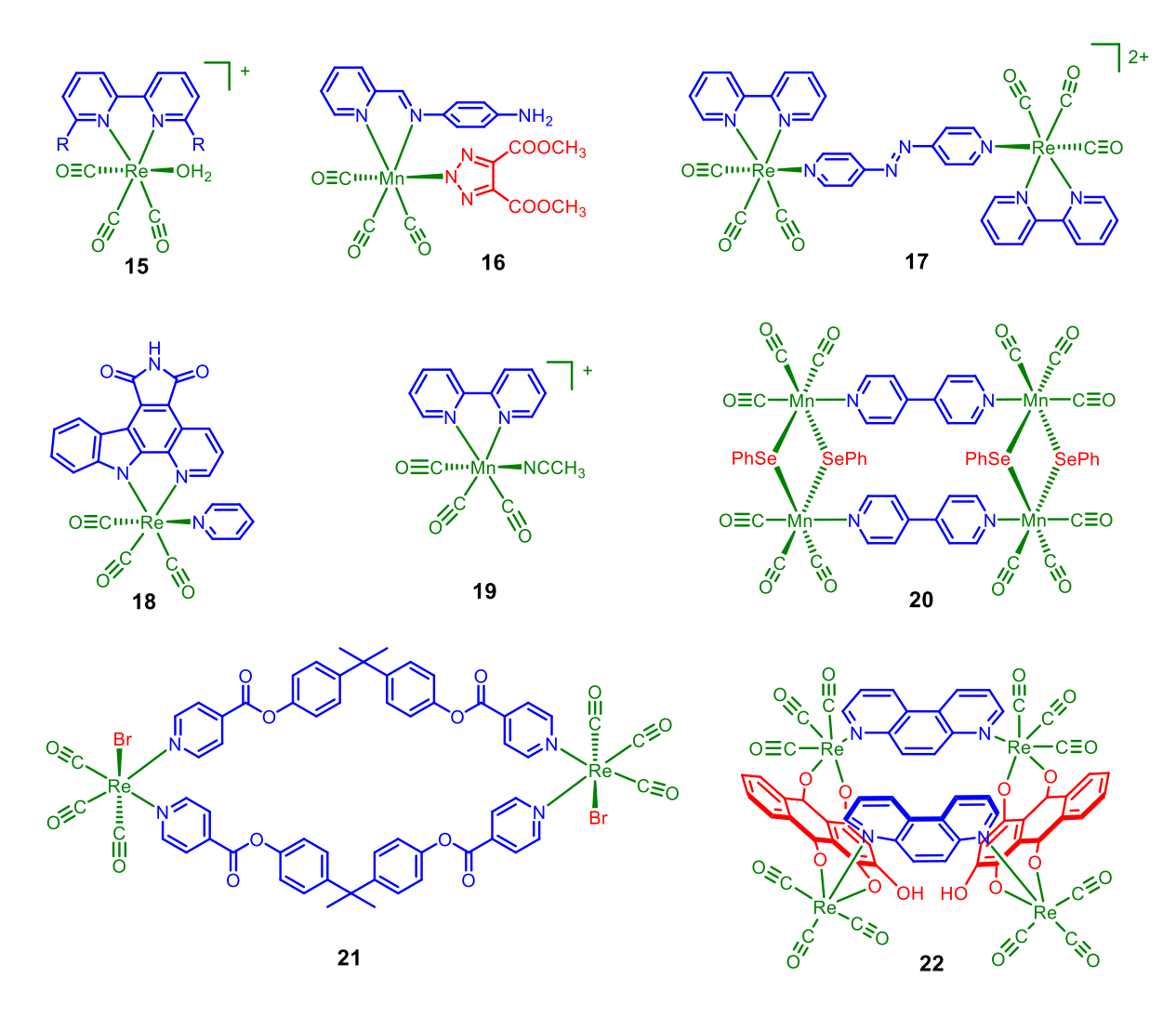


Chart 3. fac-M(CO)<sub>3</sub> (M = Mn, Re) core-based complexes with applications in material science and biology.

The anti-cancer properties of both cyclic and acyclic systems have been explored by several groups providing an insight on Re(I) and Mn(I) complexes as emerging class of bio-active compounds (15-21). The typical arrangement of rigid ligands in Re(I) complex reported by Lu et al., showcases the ability of cavity containing supramolecules to interact with suitable guest molecules through non-covalent interactions (22).<sup>7d</sup>

Along with Re(I), its congener manganese tricarbonyl complexes have also evolved tremendously due to their ability to release CO upon irradiation of light. The highly labile character

of Mn(I) complexes have proved to be advantageous for their use in anti-cancer activity, as photo-CO releasing molecules (photo-CORMs) and photo catalyst (16, 19, 20). One such report by Manimaran et al., demonstrated the anti-cancer activity of tetranuclear Mn(I) complexes (20) and several reports are available on acyclic Mn(I) complexes that have been tested for their ability to act as photo-CORMs (16, 19). Most of the literature reports use pyridine based flexible or rigid ligands as building blocks for SCCs. The literature overview mentioned in this thesis primarily focuses on synthetic combinations utilized for assembling Re(I) complexes using imidazole/benzimidazole units and their functionalized analogues as ligands. Imidazole and benzimidazole scaffolds are advantageous in terms of their biological relevance. Thus, incorporation of these scaffolds on ligand framework and its combination with rhenium tricarbonyl core has yielded numerous 2D and 3D architectures which can have potential use as bio-active molecules. The scale of the property of the scale of the scale

The major portion of rhenium tricarbonyl chemistry consists of mono and dinuclear acyclic complexes and studies on their physico-chemical properties with relevant applications. Most of these complexes contain N^N<sup>-</sup> donor based anionic bis-chelating ligands i.e., bipyridine and/or phenanthroline as the coordinating motifs. Some examples also include O^O<sup>-</sup> and N^O<sup>-</sup> chelating ligands as a part of their coordination framework. 3b,4b,7a-d Now, since these types of complexes displayed good biological activity, the incorporation of biologically relevant scaffolds and/or motifs which can exhibit absorption and emission properties in the visible-region becomes a key factor for assembling such complexes. One such highly relevant motif is 2-(2'-hydroxyphenyl)benzimidazole and its derivatives with rich photophysical and redox properties which can serve as a building unit for making visible-light absorbing and emitting complexes. <sup>11b</sup> Hence, a portion of this thesis also describes the advantages of using such building blocks and their use for constructing acyclic M(I) (M = Re or Mn) complexes using these photo-active units.

#### 1.2. Tetranuclear SCCs from neutral benzimidazolyl/imidazolyl based ligands

Tetranuclear metallacycles having  $[Re(CO)_3]^+$  core and benzimidazolyl-/imidazolyl-based neutral ligands are quite limited. Most of the tetranuclear complexes are either square or rectangle shaped with rigid or flexible pyridine ligand framework. Only a few known examples of rhenium(I)-tetranuclear metallacycles utilizes flexible ditopic ligands as ligand backbone (Scheme 1).

**Scheme 1.** Possible dinuclear and tetranuclear metallacycles from flexible ditopic ligand (blue) and rigid chelating ligand (red).

**Scheme 2.** Self-assembly of tetranuclear metallacycles from flexible ditopic ligand. <sup>17</sup>

The incorporation of methylene groups in ditopic ligand provides flexibility, thereby, resulting in various conformers in the solution. Therefore due to flexible nature, the coordination angles of such ligands are less anticipated in solution state. The flexible ligands in the metallacycles provide several advantages including breathing ability in the solid state and better adaptability towards guest molecules.

Lu et al., reported first synthetic strategy i.e., *rigidity-modulated approach* to incorporate flexible ditopic ligands as one of the structural frameworks in making Re(I) metallacycles (23) (Schemes 1-2).<sup>17</sup> In this approach, rigid bis-chelating ligand fixes the distance of M···M core which indirectly dictates the arrangement of flexible ditopic ligand in the final complex. For example, flexible ligand  $\alpha,\alpha'$ -bis(benzimidazol-1-yl)- $\alpha$ -xylene (L1) containing two methylene spacers and two terminal benzimidazolyl coordinating units can adopt minimum three conformers i.e., *syn*, *anti* and intermediate in solution state. The reaction of L1 with Re<sub>2</sub>(CO)<sub>10</sub> and 6,11-dihydroxy-5,12-naphthacenedione (H<sub>2</sub>-dhnq) yielded tetranuclear metallacycles (23) with *anti*-conformation of L1, whereas treatment of L1 with 2,2'-bis-benzimidazolyl (H<sub>2</sub>-BBim), and Re<sub>2</sub>(CO)<sub>10</sub> resulted in binuclear metallacycles in which L1 adopts *syn*-conformation.

This strategy was also used to control highly flexible tetratopic benzimidazole donor having four methylene units attached to phenyl as spacer. The ligand 1,2,4,5-tetrakis(5,6-dimethylbenzimidazol-1-ylmethyl)benzene (L2) can have various conformations in solution due to the arrangement of four terminal benzimidazolyl motifs. Rigid ancillary bis-chelating ligand H<sub>2</sub>-BBim and chloranilic acid (H<sub>2</sub>-CA) were used for controlling conformational dynamics of flexible ligand during the self-assembly process (Scheme 3).<sup>18</sup>

**Scheme 3.** Synthetic approach for bicyclic metallacycles *via* rigidity modulated approach. <sup>18</sup>

The bridging bis-benzimidazolate ligand resulted in shorter Re···Re distance leading to *syn,anti,syn,anti*-conformation of L2 in the final metallacycle (24), whereas H<sub>2</sub>-CA as bridging ligand provided longer Re···Re distance and directs L2 to adopt a different conformational mode in the metallacyclic structure (25).<sup>18</sup> Similar strategy was employed by incorporating a tetratopic ligand possessing biphenylene spacer (L3) in the design of neutral metallacycles (Scheme 4). The treatment of L3, H<sub>2</sub>-dhnq or H<sub>2</sub>-dhaq with Re<sub>2</sub>(CO)<sub>10</sub> resulted in a bicyclic metallacycle consisting of two dinuclear metallacavitands (26–27) which are similar to calix[4]arene. This study not only provides a way to fix the conformational dynamics of flexible ligand through appropriate anionic counterpart but also to prepare metallacavitands with tunable properties in a simple one-pot approach.<sup>19</sup>

**Scheme 4.** Synthesis of bicyclic metallacavitand from flexible tetradentate ligand. <sup>19</sup>

Another tetranuclear metallacycle was constructed using rigid angular ligand 2-(4-pyridyl)-1-ethyl-benzimidazole (L4) possessing a coordination angle of  $\sim 80^{\circ}$ . The treatment of L4, H<sub>2</sub>-CA and Re<sub>2</sub>(CO)<sub>10</sub> resulted in neutral tetranuclear heteroleptic chair-shaped metallacycle (**28**) (Scheme 5).<sup>20</sup> This study provided a new synthetic strategy for assembling chair-conformation based tetranuclear metallacycles via orthogonal bonding approach.

$$H_2$$
-CA  $L_4$ 
 $Re_2(CO)_{10}$ 
 $Re_2(CO)_{10}$ 
 $Re_2(CO)_{10}$ 
 $Re_2(CO)_{10}$ 
 $Re_2(CO)_{10}$ 
 $Re_2(CO)_{10}$ 
 $Re_2(CO)_{10}$ 
 $Re_2(CO)_{10}$ 
 $Re_2(CO)_{10}$ 

**Scheme 5.** Synthesis of tetranuclear molecular chair. <sup>20</sup>

#### 1.3. Tetranuclear SCCs from benzimidazolate/imidazolate-based ligands

Rhenium(I) tricarbonyl based tetranuclear rectangle shaped metallacycles consisting of ditopic pyridine donor with different types of spacer units and  $RX^-$  (X = O/S) motif are well-known. However, the use of imidazolate/benzimidazolate as anionic ligands for assembling such metallacycles is scarce. One such example is bis-imidazolate bridged molecular rectangles (29–31) self-assembled using bis-imidazole, 1,2-bis(4-pyridyl)ethylene motif and  $Re_2(CO)_{10}$  (Scheme 6).<sup>21</sup>

**Scheme 6.** Self-assembly of molecular rectangles possessing bis-imidazolate ligands.<sup>21</sup>

**Scheme 7.** Photo-responsive molecular rectangles having bis-imidazolate anionic ligand core.

This method provided synthetic approach to assemble two double bonds in close-proximity with each other in a photo-responsive metallacyclic structure. These discrete rhenium(I) based metallacycles undergo [2+2] cycloaddition upon irradiation of light which provided one of the rare example of metallacycles (32–34) undergoing interconversion via photo-cycloaddition (Scheme 7). A series of bis-benzimidazolate based neutral heteroleptic rectangles (35–42) with different types of rigid ditopic donor were reported by Hupp and co-workers (Scheme 8). Functional spacer such as naphthalimide, porphyrins and salen were also incorporated on structural framework of molecular rectangle using similar approach.

**Scheme 8**. Molecular rectangles (35–42) possessing bis-benzimidazolate ligand.<sup>22</sup>

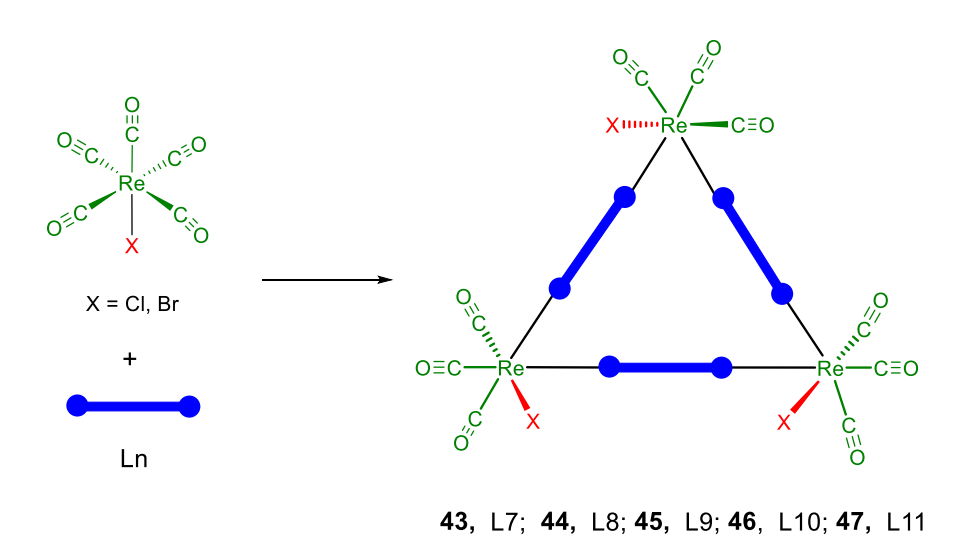
The spectro-electrochemical properties of these rectangles suggested that complexes possess rich redox chemistry and undergo intra-molecular charge transfer via through space mechanism upon reduction. This class of rectangles having bis-benzimidazolate anionic ligand is a rare example of complexes showing ligand-based mixed valence properties and hence, can further exhibit catalytic activity. <sup>22</sup>

#### 1.4. Trinuclear SCCs from rigid bidentate ligands

Rigid bidentate and tridentate pyridine-based bridging ligands are commonly used in the construction of neutral or ionic trinuclear metallacycles (Chart 4).  $^{23-28}$  Generally, upon treatment of Re(CO)<sub>5</sub>X where X = Cl or Br, with rigid bidentate ligands, *fac*-[Re(CO)<sub>3</sub>X]-based molecular squares are formed. On the other hand use of angular spacers indirectly favours the formation of a molecular triangle rather than square.

Chart 4. Rigid bidentate ligands used for the synthesis of trinuclear metallacycles. <sup>23-28</sup>

These molecular triangles (43–47) possess inner cavity suitable for accommodating guests of different sizes and shapes. Rigid bidentate ligands with different types of spacer units were also employed to construct molecular triangles.



**Scheme 9.** Synthetic approach for assembling molecular triangles using pyridine-based bridging ligands.<sup>23</sup>

The rigid ditopic N-donors possessing alkoxy/alkyl chain substituted spacers i.e., 1,4-bis(4'-pyridylethynyl)-2,5-dihexyloxybenzene for **43**, 1,4-bis(4'-pyridylethynyl)-2,5-didodecanoloxybenzene for **44** upon treatment with Re(CO)<sub>5</sub>Br under reflux conditions yielded trinuclear metallacycles (Scheme 9). The long alkyl chains hinders the accessibility of cavity to the small guest molecules. <sup>23</sup> Similar approach was used to assemble trinuclear metallacycles (**46-47**) using alkyl group substituted carbazole spacer based dipyridyl ligand and Re(CO)<sub>5</sub>Cl. Lee and coworkers introduced thiophene-ethyne spacer with pyridine coordinating motifs to build molecular triangle (**45**) along with dinuclear metallacycles as the major product. <sup>23</sup>

Vazquez-Lopez et al., utilized thiosemicarbazone based ligand for assembling Re(I) based trinuclear metallacycles (48). Upon incorporation of rhenium precursor,  $\beta$ -keto ester monothiosemicarbazones undergo chain-ring tautomeric conversion (Scheme 10). This study provides an insight on in-situ conversion of open-form of thiosemicarbazones to cyclic pyrazolane form upon coordination to Re(I) metal centre. <sup>24</sup>

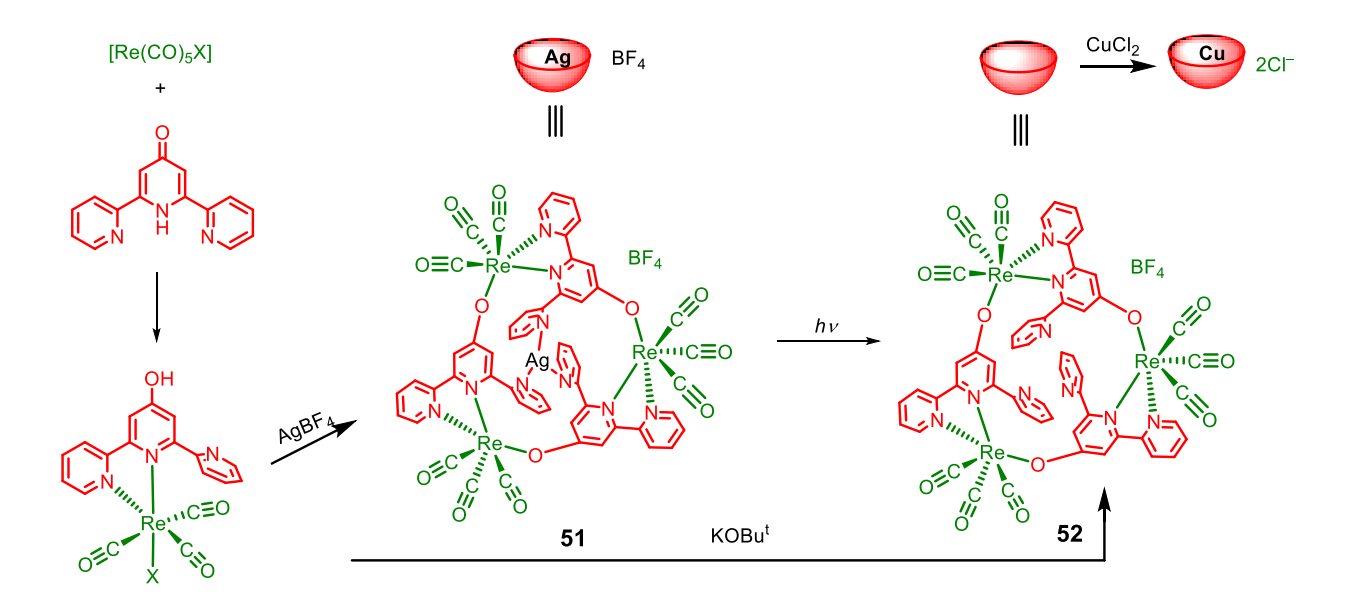
**Scheme 10.** Self-assembly of trinuclear metallacycles.<sup>24</sup>

Another type of molecular triangle was prepared using  $Re(CO)_5X$  where X = Cl, Br and tridentate bridging ligand either *via* two steps or single step approach. Severin and co-workers prepared metallacyclic triangle (**49**) stabilized via  $[Ag(benzene)_3]BF_4$  counter ion. The molecule adopts bowl structure and accommodates  $BF_4^-$  unit in its internal cavity. The initial reaction of  $[Re(CO)_3Br_3](NEt_4)$  and 3-hydroxy-1,2,3-benzotriazine-4(3*H*)-one yielded a mononuclear compound having labile bromide ancillary ligand, the addition of  $AgBF_4$  induces cyclization process to form a trinuclear metallacycle (Scheme 11). <sup>25</sup>

**Scheme 11.** Two step approach for the self-assembly of trinuclear metallacycle. <sup>25</sup>

Massi et al., reported a trinuclear metallacalix[3]arene using 2-pyridyltetrazolate ligand (2-PyTz) serving as both anionic donor and a bis-chelating ligand. Using a conventional one pot reflux approach, 2-PyTz and  $Re(CO)_5X$  (where X = Cl, Br) were reacted in presence of triethylamine as base forming a trinuclear metallacalix[3]arene (50) which adopts partial cone conformation creating a very small cavity (Scheme 12). The reduced conjugation and structural rigidity of 2-PyTz upon coordinating with Re(I) centre provided a trinuclear metallacycle that exhibits good photophysical and redox properties. <sup>26</sup>

**Scheme 12.** Self-assembly of trinuclear metallacalix[3]arene. <sup>26</sup>



**Scheme 13.** Synthetic approach for a trinuclear molecular stopper. <sup>27,28</sup>

Coogan et al., reported a synthetic approach to assemble trinuclear metallacycle (51–52) with rigid tridentate ligands and three *fac*-Re(CO)<sub>3</sub> cores arranged alternatively (Scheme 13). Interestingly, the metallacycles serve as stopper by coordinating to silver ion using free pyridyl units. Upon irradiation of light (405 nm), the silver ion detaches from the complex and provides a neutral system. Hence, such type of systems can be useful in transporting ions like silver.<sup>27,28</sup> Similarly, Thorp-Greenwood and co-workers utilized the same system to trap copper ions (52).

The previous synthetic approaches used to build trinuclear cycles utilized rigid ligand framework due to its fix coordination angle in the final assembly. On contrary, use of flexible ligands provides adaptability to the final architecture (Figure 1).

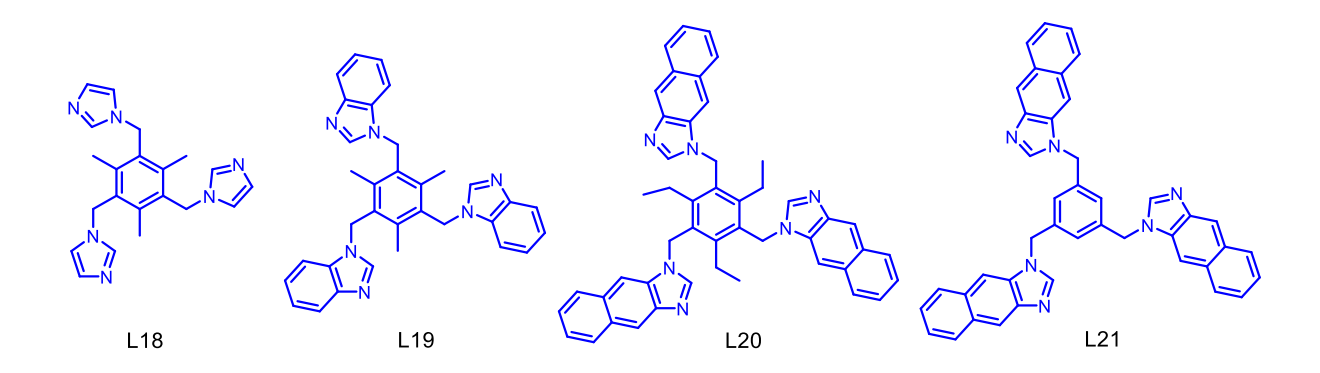
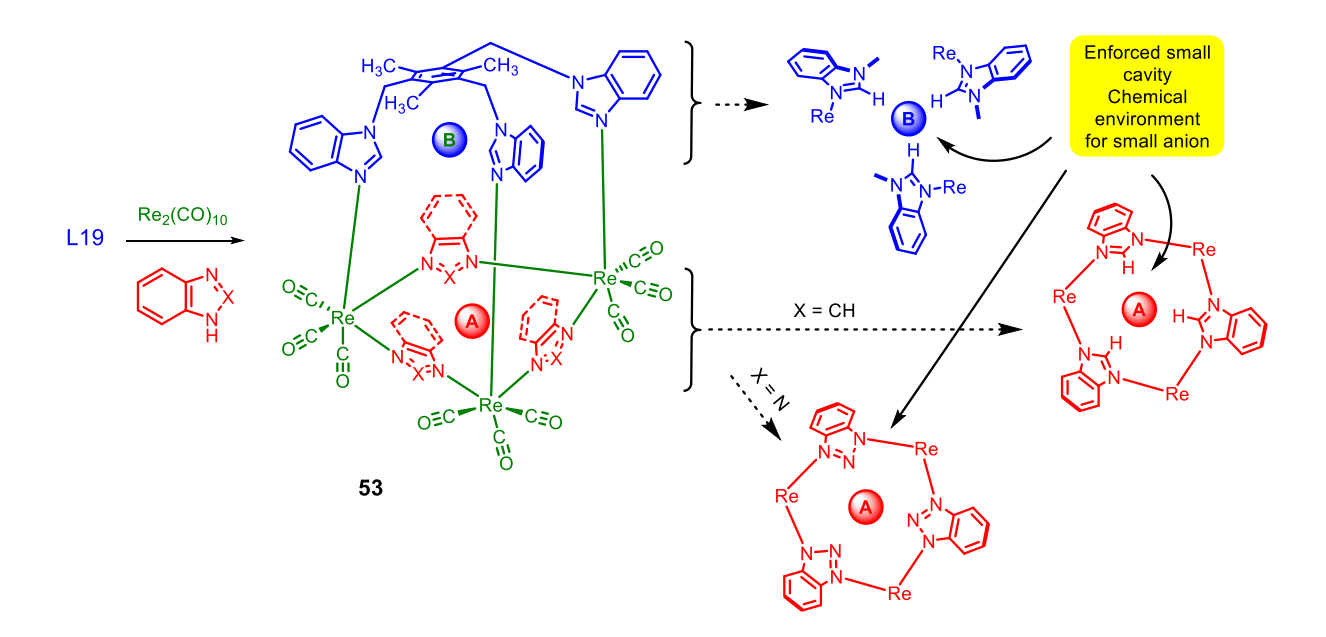


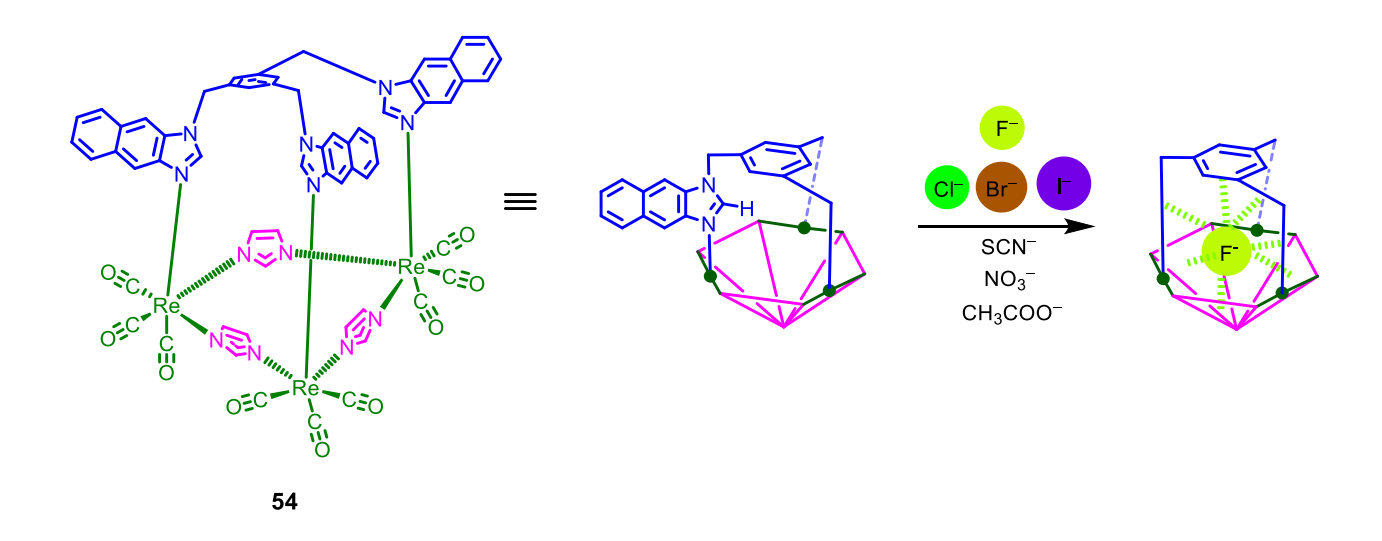
**Figure 1.** Flexible tripodal ligands used for the synthesis of trinuclear metallacycles.<sup>29</sup>

Our group reported a different synthetic approach for assembling trinuclear metallacycles (53) using imidazolyl/benzimidazolyl/napthanoimidazolyl-based flexible tripodal ligands as coordinating units and imidazolate/benzimidazolate/naphthanoimidazolate as anionic counterparts (Scheme 14). The resulting metallacycles contains an exocyclic and an endocyclic cavity useful for accommodating small ions/molecules. <sup>29</sup>



**Scheme 14.** Self–assembly of trinuclear metallacycle (**53**) with two types of cavities.<sup>29</sup>

Recently, ability of these metallacycles to accommodate small ions was explored (Scheme 15). The arrangement of benzimidazolyl/napthanoimidazolyl pendants with electron deficient C–H units pointing towards the cavity helps in stabilizing fluoride ion selectively *via* various non-covalent interactions (54).



**Scheme 15.** Trinuclear metallacycle with selective recognition ability for fluoride.<sup>30</sup>

Also, the anionic counterparts forming the base of metallacycles provide an exocyclic cavity where DMSO solvent molecule was found interacting. The presence of recognition units facilitates the interaction of the metallacycles with guest molecules and stabilizes it *via* multiple non-covalent interactions. The modification of the ligand framework can tune the number of recognition sites that can accommodate neutral or ionic guest molecules. <sup>30</sup>

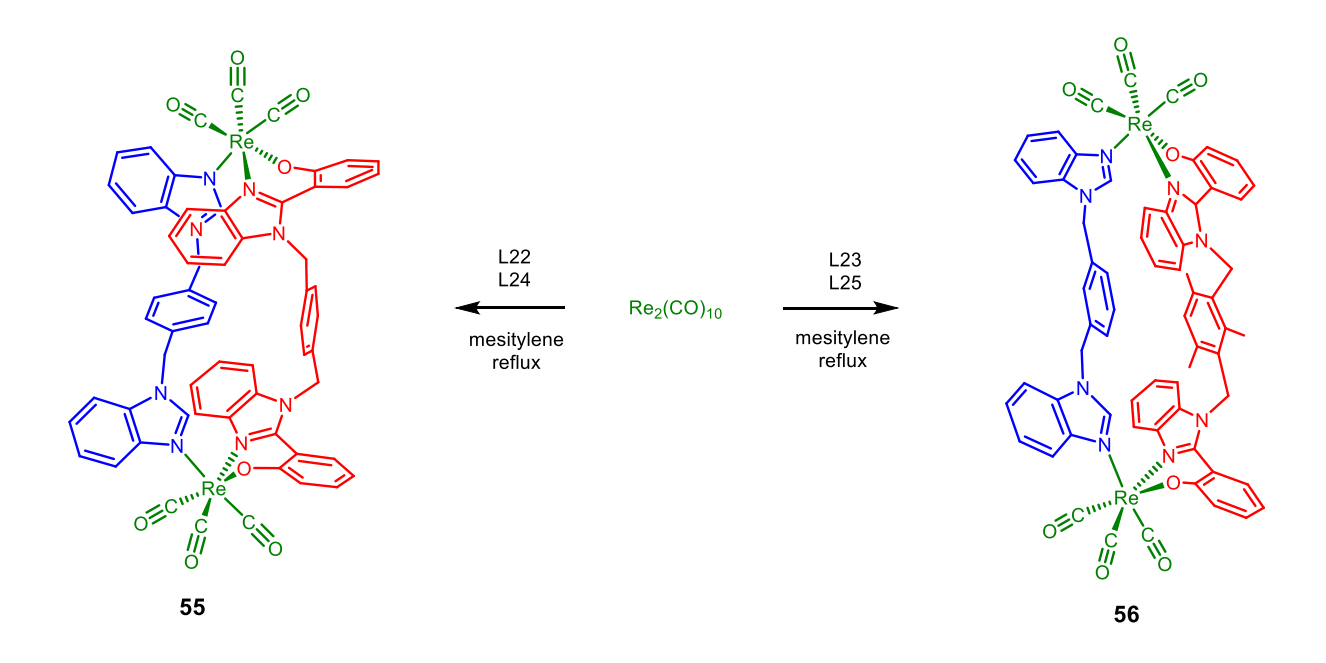
#### 1.5. Re(I)-based SCCs from phenoxybenzimidazolyl ligands

2,2'-bipyridine is one of the well-known chelating ligands widely used for making Re(I)tricarbonyl based complexes. The derivatives of these complexes have found enormous applications in medicinal and material sciences. More often such complexes display weak absorption in UV-Vis region ( $\lambda_{max} = \sim 350$  nm).

**Figure 2.** (A) Stereoelectronic requirement of rhenium(I)tricarbonyl core, (B) flexible neutral bidentate and rigid bis-chelating ligands.

In order to make visible light absorbing and emitting complexes, chelating units can be modified accordingly. One way to achieve this is to opt for the chelating ligand which absorbs and emits in the visible region. Among various types of known chelating ligands, 2-(2'-hydroxyphenyl)benzimidazole (H<sub>2</sub>–L) is an attractive candidate to construct Re(I) complexes due to its interesting photophysical properties in solid and solution state and also potential utility as photo-active unit for making fluorescent sensors, switches and dyes. In an attempt to prepare visible light absorbing and emitting complexes, our group has synthesized a flexible bis-chelating ligand

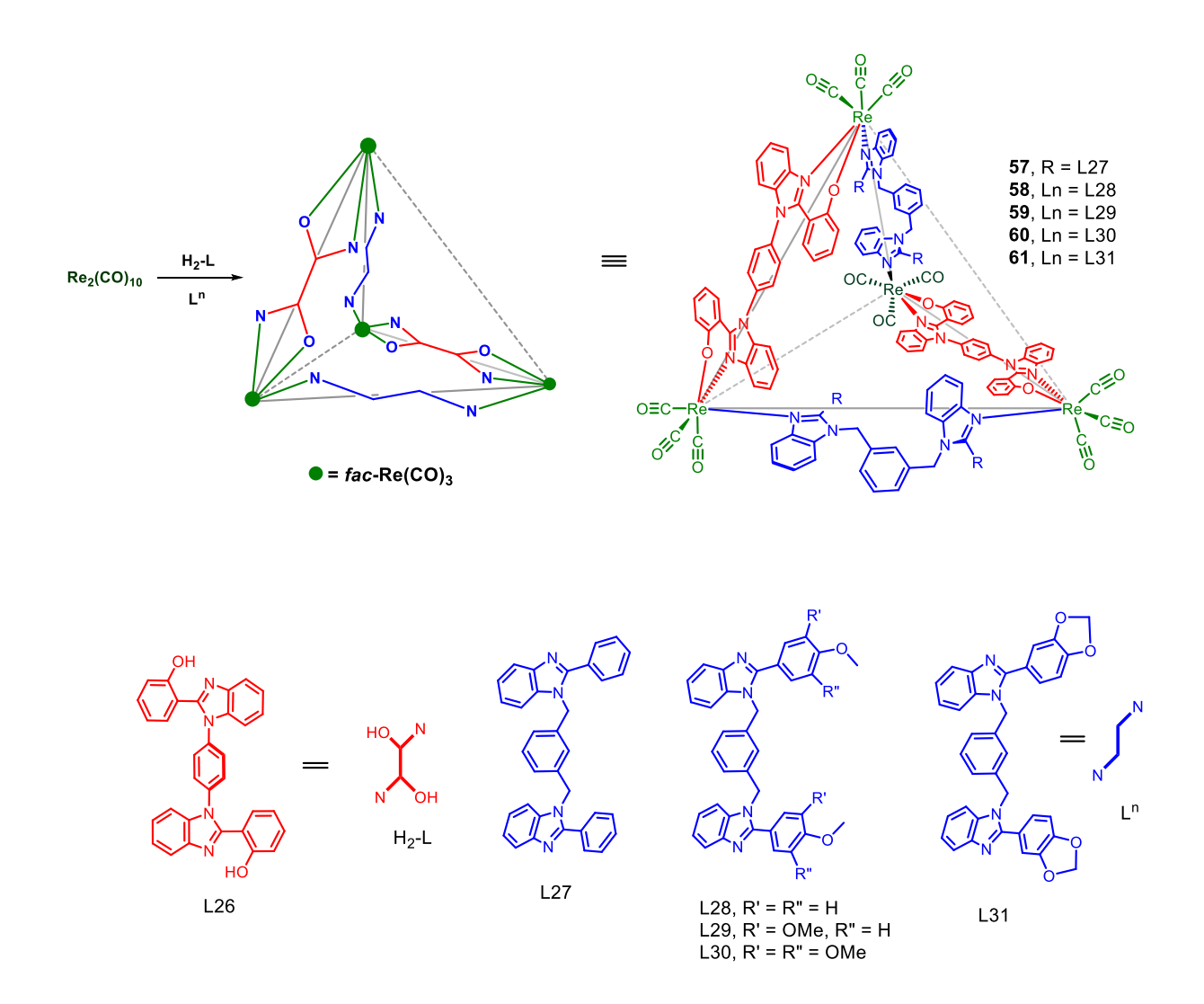
possessing two motifs of  $H_2$ –L connected *via p*-xylene/mesitylene spacer and used it for the construction of double stranded helicates and mesocates (55–56, Figure 2, Scheme 16). The spacer unit and steric factors play an important role in dictating the final supramolecular architecture.<sup>31</sup>



**Scheme 16.** Self-assembly of helicate (**55**) and mesocate (**56**). <sup>31</sup>

The combination of p-phenylene spacer based bis-chelating ligand and neutral benzimidazolyl flexible ligand with Re<sub>2</sub>(CO)<sub>10</sub> resulted in helicate (55) whereas m-phenyl spacer and mesitylene spacer provided mesocate (56) structure (Scheme 16). The complexes exhibit dual emission i.e., both fluorescence and phosphorescence in solution state while in solid state, aggregation induced phosphorescence from two states ( $^3$ MLCT and  $^3$ MLLCT) were observed due to aggregation between two adjacent molecules via  $\pi$ - $\pi$  stacking interactions. This work provides a methodology to assemble unsaturated redox active helicates of varying shapes and sizes. Different types of Re(I) based supramolecules including helicates, mesocates, bowls, square, rectangle,

trigonal and tetragonal prisms, spheroids have been designed and synthesized. However, Re(I) tricarbonyl based SCCs having tetrahedral topology were unknown.



**Scheme 17.** Self-assembly of Re(I) tricarbonyl based tetrahedron.<sup>32</sup>

Our group reported synthetic combination of 2-(2'-hydroxyphenyl)benzimidazole based rigid bis-chelating ligand (H<sub>2</sub>-L), neutral flexible ditopic N-donor ( $L^n$ ) and Re<sub>2</sub>(CO)<sub>10</sub> to yield neutral heteroleptic tetrahedrons with two missing edges (Scheme 17). The arrangement of coordination framework provides a scalene triangular face which can accommodate guest molecules. Until now this is the only report on Re(I) tricarbonyl based tetrahedrons (**57–61**). <sup>32</sup>

### 1.6. Re(I)-based acyclic complexes from phenoxybenzimidazolyl ligand

The acyclic systems with general formula, fac-[Re(CO)<sub>3</sub>(N^N)X] (where X = Cl, Br, O, N) have been explored enormously because of their interesting physico-chemical properties and spectroscopic aspects. Such complexes find applications as sensors, photo-switches, laser dyes, catalysts and therapeutic agents. Though countless examples of such complexes are known, this section specifically highlights mononuclear and dinuclear complexes based on 2-phenoxybenzimidazole (N^O<sup>-</sup>) scaffold (Chart 5). The properties of 2-phenoxybenzimidazole and its structural analogues show their ability to act as photo-active units which upon incorporation in the coordination framework can provide complexes with absorption and emission in the visible region which will be advantageous for biological applications and material sciences. The properties of complexes can be altered by tuning either of the ligand core i.e., bis-chelating unit and/or anionic ancillary ligand. <sup>13b,33</sup>

Chart 5. Acyclic mononuclear complexes with N^O bis-chelating donor motifs. 13b,33

Kapturkiewicz and Sathiyendiran et al., used different types of bis-chelating N^O<sup>-</sup> donors with pyridine as ancillary ligand, studied their structural and photophysical aspects (62–66). The mononuclear complexes reported by Kapturkiewicz and co-workers were synthesized using

substituted 2-(2'-hydroxyphenyl)benzimidazole and its derivatives *via* two-step synthetic strategy. The first step involves formation of a dinuclear complex with the O-atom serving as a bridge between the two Re-centers and further upon addition of pyridine ligand, a mononuclear complex consisting of both the coordinating units was obtained (**62–64** and **67–69**; **Chart 6**).

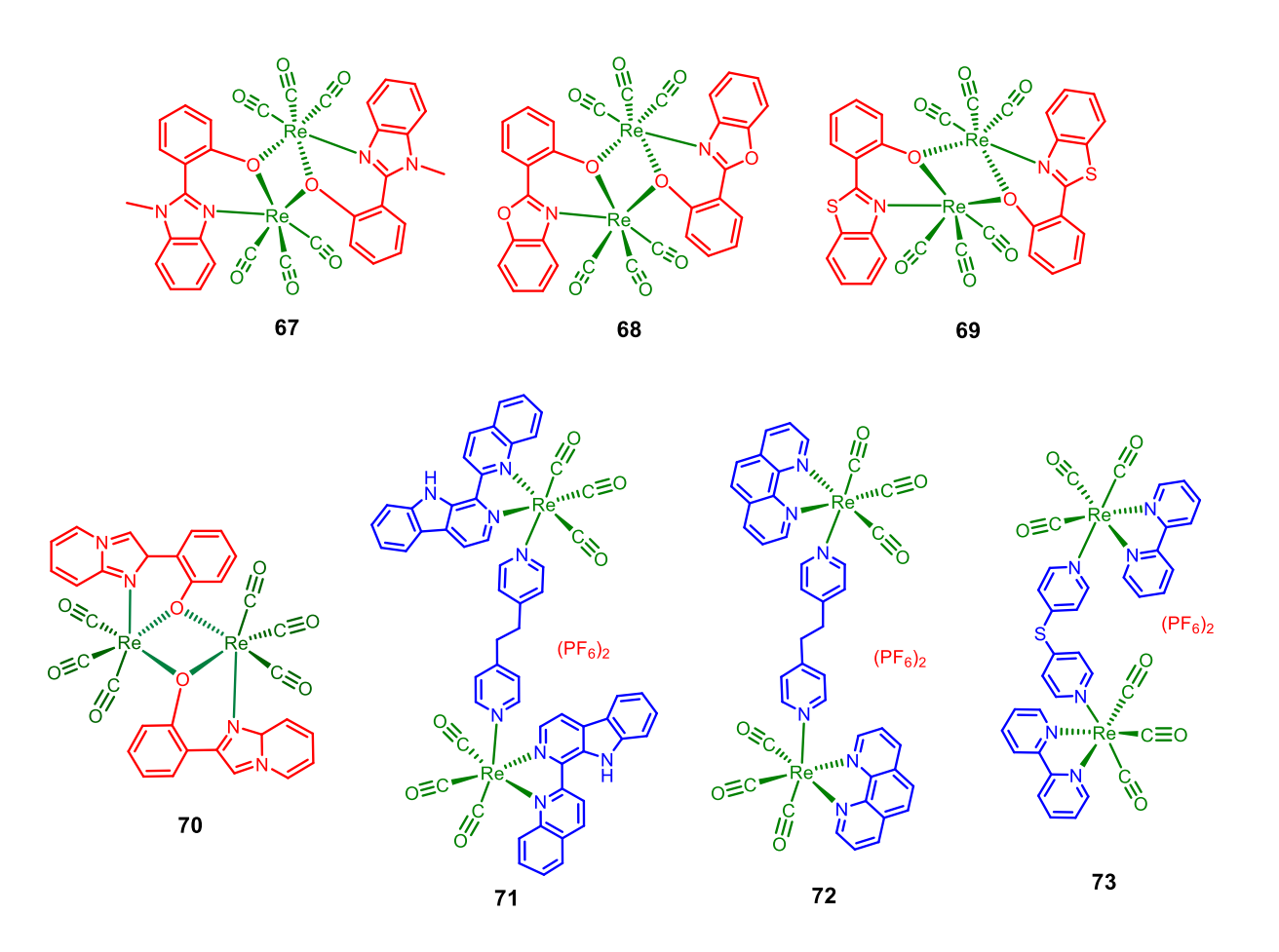


Chart 6. Acyclic dinuclear complexes with N^N and N^O $^-$  donor motifs.  $^{13b,\ 33-35}$ 

Similarly, Sathiyendiran and co-workers utilized N-fused ring-based N^O<sup>-</sup> chelating unit and pyridine derivative for making mononuclear complexes (**70**) and studied them using various analytical and spectroscopic techniques. <sup>13b, 33-35</sup> He and Pan reported two dinuclear phosphorescent

Re(I) complexes using carboline containing ligands (71–72). Both the complexes displayed high anti-cancer activity against various cancer cell lines and were also effective in generating singlet oxygen useful in photo-dynamic therapy. Gomez et al., reported thiopyridine based dinuclear complex (73) using monothiopyridine-based ligands and [Re(bpy)(CO)<sub>3</sub>OTf] precursor. The complex (73) displayed good photophysical properties. Some literature reports have also mentioned about the better efficacy of dinuclear complexes over mononuclear counterparts indicating the synergistic effect between the two metal ions.

#### 1.7. Manganese tricarbonyl core containing SCCs and acyclic complexes

Rhenium is one of the most widely used 7<sup>th</sup> group element for making acyclic as well as discrete cyclic complexes. The efforts are now being directed towards the use of manganese in design and synthesis such complexes (**74–78**) (Chart 7). This congener of rhenium(I) offers high lability of the coordinated ligands when prompted by internal or external trigger such as irradiation of light and hence, can serve as suitable candidate as photo CO-releasing molecule with use in therapeutics.

HOOC

$$CF_3SO_3$$
 $CF_3SO_3$ 
 $CF_3SO_3$ 

Chart 7. Examples of mononuclear manganese tricarbonyl complexes. 36-38

The design of bio-active complexes requires crucial selection of ligand framework which can offer good photophysical properties in the visible region. Some of the complexes reported so far have utilized bipyridine or pyridine substituted ligand systems to serve the purpose. However, use of such chromophoric ligands which have absorption and emission in the visible region is being encouraged for building visible light absorbing complexes. 36-38

Manimaran and co-workers reported a set of dinuclear supramolecules (**79-82**) by treatment of aminoquinonato-bridged flexible pyridine ligands and anionic bis-chelating ligand with  $Mn_2(CO)_{10}$  under dark conditions (Scheme 18). The complexes displayed good anti-cancer activity towards various cancer cell lines. <sup>39</sup> The increasing interest in Mn-based CO releasing molecules in the research community is due to the possibility of controlled and targeted delivery of CO molecules at specific sites of action in the biological targets.

**Scheme 18.** Self-assembly of Mn(I) tricarbonyl based dinuclear complexes.<sup>39</sup>

Mansour and co-workers reported fac-Mn(CO)<sub>3</sub>Br and benzimidazole ligand containing mono- and binuclear complexes bearing sulfonate and phosphonium groups (Scheme 19). Complex with  $N_3^-$  as ancillary ligand (83) undergo in situ transformation into triazole via [3+2] cycloaddition iclick reaction and forms a triazole-based dinuclear complex (84). Further, the CO-releasing ability of this complex was compared with other complexes containing Br<sup>-</sup> and NCS<sup>-</sup> ligands.

**Scheme 19.** Self-assembly of Mn(I) tricarbonyl complex *via* cycloaddition iClick reaction. <sup>40</sup>

## 1.8. Scope of the present work

The chapter provides an insight on rhenium(I) based acyclic and discrete cyclic metal-organic complexes i.e., supramolecular coordination complexes along with brief literature overview on manganese tricarbonyl complexes. The increase in the number of mononuclear/dinuclear acyclic and simple to complex SCCs is due to their wide range of applications in material science and biology. Among different metal ions-based SCCs, Re(I) tricarbonyl core containing complexes is an important class of complexes with potential applications in catalysis, molecular recognition, bioimaging, sensors and as anti-cancer agents. The building units play a significant role in deciding the properties and functions of final architectures.

The first part of the thesis describes the synthetic combinations used for making Re(I) based cyclic complexes followed by study of their structural aspects and properties. The rhenium(I) supramolecules with flexible ligands mostly contains arene spacer motif, herein, alkyl spacer have been utilized in place of aryl spacer to provide breathing ability in solid state and better adaptability in solution. The incorporation of these flexible units is fruitful in making flexible adaptive cages containing multiple C—H polarized sites for molecular recognition of neutral/ionic guests. Although various shapes of Re(I) tricarbonyl based SCCs including mononuclear/dinuclear cycles, squares, rectangles, prisms are known, molecular tubular architectures having properly arranged chalcogen(S)/halogen(F) donor/acceptor and multinuclear cages with multiple electron deficient recognition sites are scarce. The incorporation of chalcogen/halogen donor on the cyclic framework would result in functional metallacycles which can further self-organize into 1D-tubular architecture or hierarchical superstructures via chalcogen···halogen interactions.

The other part of thesis describes design and synthesis of mono- and dinuclear complexes using 2-(2'-hydroxyphenyl)benzimidazole motif and its analogues as chelating unit due to its

remarkable photophysical properties which make them suitable building block for constructing photo-active switches, sensors and dyes. Such units can be used to prepare flexible or rigid bischelating ligands which can further be utilized for making dinuclear Re(I)/Mn(I) complexes. The dinuclear Re(I)/Mn(I) tricarbonyl complexes holds potential utility to serve as photo-CO releasing molecules with ability to release CO upon irradiation of light or other external trigger and also as photocatalysts.

Therefore, the objectives of present work are as follows:

- Design and synthesis of metal—organic cages and study on their molecular recognition properties towards various anions.
- Design and synthesis of metal—organic tubes functionalized with chalcogen and halogen donor/acceptor groups, study of their photophysical and electrochemical properties.
- Design, synthesis, and photophysical studies of neutral acyclic mono- and dinuclear heteroleptic Mn(I)/Re(I) tricarbonyl complexes.

#### 1.9. References

- a) D. Chakraborty, R. Saha, J. K. Clegg, P. S. Mukherjee, *Chem. Sci.*, 2022, 13, 11764–11771;
   b) N. Dey, C. J. Haynes, *ChemPlusChem* 2021, 86, 418-433;
   c) Z. Cui, G. Jin, *Nat. Synth.*, 2022, 1, 635-640;
   d) D. Zhang, T. K. Ronson, Y. Zou, J. R. Nitschke, *Nat Rev Chem.*, 2021, 5, 168–182;
   e) I. Mishra, M. Bhol, P. Kalimuthu, M. Sathiyendiran, *Chem. Rec.*, 2021, 21, 1–22;
   f) A. Kumar, P. S. Mukherjee, *Chem. Eur. J.* 2020, 26, 4842–4849;
   g) G. Moreno-Alcantarand, A. Casini, *FEBS Letters* 2023, 597, 191–202.
- a) H. Sepehrpour, W. Fu, Y. Sun, P. J. Stang, J. Am. Chem. Soc. 2019, 141, 14005–14020; b)
   M. PanKai, W. Zhang, C. Su, Coord. Chem. Rev. 2019, 378, 333–349; c) Y. Sun, C. Chen, J. Liu, P. J. Stang, Chem. Soc. Rev., 2020, 49, 3889–3919; d) S. Samantray, S. Krishnaswamy, D. K. Chand, Nat Commun, 2020, 11, 880; e) J. E. M. Lewis, J. D. Crowley, ChemPlusChem 2020, 85, 815–827; f) T. Tateishi, Y. Yasutake, T. Kojima, S. Takahashi, S. Hiraoka, CommunChem, 2019, 25, 1–9; g) Z. Huang, J. J. Wilson, Eur. J. Inorg. Chem. 2021, 1312–1324; h) W. Gao, H. Zhang, G. Jin, Coord. Chem. Rev., 2019, 386, 69–84.
- 3. a) K. R. Soumya, I. Mishra, M. Kedia, U. Phukon, R. Borkar, M. Sathiyendiran, Rhenium (I)-based supramolecular coordination complexes: Synthesis and functional properties. In Supramolecular Coordination Complexes: Design, Synthesis and Applications, 1st Ed.; Elseiver, 2022, 133-153; b) D. Gupta, M. Sathiyendiran, *ChemistrySelect* 2018, **3**, 7439 7458.
- a) A. A. Haase, E. B. Bauer, F. E. Kühn, D. C. Crans, *Coord. Chem. Rev.*, 2019, 394, 135–161;
   b) R. Govindarajan, R. Nagarajaprakash, V. Veena, N. Sakthivel, B. Manimaran, *Polyhedron* 2018, 139, 229–236;
   c) J. Rohacova, O. Ishitani, *Dalton Trans.*, 2017, 46, 8899–8919.
- a) P. Thanasekaran, C. Lee, K. L. Lu, Acc. Chem. Res. 2012, 45, 1404–1418; b) F. Würthner, C.
   You, C. R. Saha-Möller, Chem. Soc. Rev. 2004, 33, 133–146; c) K. K. Lo, M. Louie, K. Y.

- Zhang, *Coord. Chem. Rev.* 2010, **254**, 2603–2622; d) M. Panigati, M. Mauro, D. Donghi, P. Mercandellic, P. Mussini, L. De Cola, G. D'Alfonso, *Coord. Chem. Rev.* 2012, **256**, 1621–1643; e) W. Gao, H. Zhang, G. Jin, *Coord. Chem. Rev.* 2019, **386**, 69–84; f) V. Sathish, A. Ramdass, M. Velayudham, K. L. Lu, P. Thanasekaran, S. Rajagopal, *Dalton Trans.*, 2017, **46**, 16738–16769.
- a) R. Govindarajan, R. Nagarajaprakash, V. Veena, N. Sakthivel, B. Manimaran, *Polyhedron* 2018, 139, 229–236; b) M. Saldías, J. Manzur, R. E. Palacios, M. L. Gómez, J. De La Fuente, G. Günther, N. Pizarroa, A. Vega, *Dalton Trans.*, 2017, 46, 1567–1576; c) B. Shankar, P. Elumalai, R. Shanmugam, M. Sathiyendiran, *J. Organomet. Chem.* 2014, 749, 224–232; d) K. R. J. Thomas, J. T. Lin, Y. Lin, C. Tsai, S. Sun, *Organometallics* 2001, 20, 2262–2269; e) S. Sun, A. J. Lees, *J. Am. Chem. Soc.* 2000, 122, 8956–8967.
- a) M. L. Merlau, M. P. Mejia, S. T. Nguyen, J. T. Hupp, *Angew. Chem. Int. Ed.* 2001, 40, 4239–4242; b) M. Boccalon, E. Iengo, P. Tecilla, *Org. Biomol. Chem.*, 2013, 11, 4056–4067; c)
   R. Govindarajan, R. Nagarajaprakash, B. Manimaran, *Inorg. Chem.* 2015, 54, 10686–10694; d)
   B. Manimaran, P. Thanasekaran, T. Rajendran, R. Lin, I. Chang, G. Lee, S. Peng, S. Rajagopal, K. L. Lu, *Inorg. Chem.* 2002, 41, 5323–5325; e) M. Sathiyendiran, R. Liao, P. Thanasekaran, T. Luo, N. S. Venkataramanan, G. Lee, S. Peng, K. L. Lu, *Inorg. Chem.* 2006, 45, 10052–10054.
- a) X. Yi, J. Zhao, J. Sun, S. Guo, H. Zhang, *Dalton Trans.*, 2013, 42, 2062–2074; b) R. Fernandez-Teran, L. Severy, *Inorg. Chem.* 2021, 60, 1334–1343; c) K. K. Lo, K. Y. Zhang, S. P. Li, *Eur. J. Inorg. Chem.* 2011, 3551–3568; d) F. Wang, J. Liang, H. Zhang, Z. Wang, Q. Wan, C. Tan, L. Ji, Z. Mao, *ACS Appl. Mater. Interfaces* 2019, 11, 13123–13133; e) A. Kastl, S. Dieckmann, K. Wähler, T. Vçlker, L. Kastl, A. L. Merkel, A. Vultur, B. Shannan, K. Harms, M. Ocker, W. J. Parak, M. Herlyn, E. Meggers, *ChemMedChem* 2013, 8, 924–927; f) B.

- Merillas, E. Cuellar, A. Diez-Varga, T. Torroba, G. García-Herbosa, S. Fernandez, J. Lloret-Fillol, J. M. Martín-Alvarez, D. Miguel, F. Villafañe, *Inorg. Chem.* 2020, **59**, 11152–11165.
- a) J. D. B. Koenig, W. E. Piers, G. C. Welch, *Chem. Sci.*, 2022, 13, 1049–1059; b) T. Klemens,
   A. Switlicka-Olszewska, B. Machura, M. Grucela, E. Schab-Balcerzak, K. Smolarek, S. Mackowski, A. Szlapa, S. Kula, S. Krompiec, P. Lodowski, A. Chrobok, *Dalton Trans.*, 2016,
   45, 1746–1762; c) T. Klemens, A. Switlicka-Olszewska, B. Machura, M. Grucela, H. Janeczek,
   E. Schab-Balcerzak, A. Szlapa, S. Kula, S. Krompiec, K. Smolarek, D. Kowalska, S. Mackowski, K. Erfurtf, P. Lodowsk, *RSC Adv.* 2016, 6, 56335–56352.
- a) A. Sharma, N. Vaibhavi, B. Kar, U. Das, P. Paira, RSC Adv., 2022, 12, 20264–20295; b) Z.
   Pan, D. Cai, L. He, Dalton Trans. 2020, 49, 11583–11590.
- a) J. Karges, M. Kalaj, M. Gembicky, S. M. Cohen, *Angew. Chem. Int. Ed.* 2021, 60, 10716–10723;
   b) R. Czerwieniec, A. Kapturkiewicz, R. Anulewicz-Ostrowska, J. Nowacki, *J. Chem. Soc.*, *Dalton Trans.* 2002, 3434–3441.
- a) H. G. Daniels, O. G. Fast, S. M. Shell, F. A. Beckford, *J. Photochem. & Photobio. A: Chem.* 2019, 374, 84–94; b) U. Kumar, B. Ramakrishna, J. Varghese, P. Vidhyapriya, N. Sakthivel, B. Manimaran, *Inorg. Chem.* 2021, 60, 13284–13298; c) P. Guntzel, C. Nagel, J. Weigelt, J. W. Betts, C. A. Pattrick, H. M. Southam, R. M. La Ragione, R. K. Pool, U. Schatzschneider, *Metallomics* 2019, 11, 2033–2042.
- a) S. Bélanger, M. Gilbertson, D. I. Yoon, C. L. Stern, X. Dang, J. T. Hupp, J. Chem. Soc., Dalton Trans. 1999, 3407–3412; b) S. Y. Chang, H. Y. Jang, K. S. Jeong, Chem. Eur. J. 2003,
   9, 1535–1541; c) A. K. Chowan, S. Karthikeyan, B. Varghese, V. Veena, N. Sakthivel, B. Manimaran, J. Organomet. Chem. 2014, 766, 86–94; d) T. Rajendran, B. Manimaran, F. Y.

- Lee, P. J. Chen, S. C. Lin, G. H. Lee, S. M. Peng, Y. J. Chen, K. L. Lu, *J. Chem. Soc., Dalton Trans.* 2001, 3346–3351; e) P. Singla, V. Luxami, K. Paul, *RSC Adv.* 2014, **4**, 12422–12440.
- 14. a) S. M. Woessner, J. B. Helms, Y. Shen, B. P. Sullivan, *Inorg. Chem.* 1998, 37, 5406–5407; b)
  A. Boulay, A. Seridi, C. Zedde, S. Laderia, C. Picard, L. Maron, E. Benoist, *Eur. J. Inorg. Chem.*, 2010, 5058–5062; c) D. Gupta, P. Rajakannu, B. Shankar, R. Shanmugam, F. Hussain, B. Sarkar, M. Sathiyendiran, *Dalton Trans.* 2011, 40, 5433–5435; d) B. Shankar, P. Elumalai, R. Shanmugam, V. Singh, D. T. Masram, M. Sathiyendiran, *Inorg. Chem.*, 2013, 52, 10217–10219.
- a) P. Rajakannu, P. Elumalai, B. Shankar, F. Hussain, M. Sathiyendiran *Dalton Trans*. 2013, 42, 11359–11362;
   b) P. H. Dinolfo, V. Coropceanu, J. L. Bredas, J. T. Hupp, *J. Am. Chem. Soc.* 2006, 128, 12592–12593;
   c) K. R. Soumya, R. Arumugam, B. Shankar, M. Sathiyendiran, *Inorg. Chem.* 2018, 57, 10718–10725.
- 16. B. Shankar, P. Elumalai, F. Hussain, M. Sathiyendiran, *J. Organomet. Chem.* 2013, **732**, 130–136.
- 17. M. Sathiyendiran, C. Chang, C. Chuang, T. Luo, Y. Wen, K. L. Lu, *Dalton Trans*. 2007, 1872–1874
- 18. C. Chuang, M. Sathiyendiran, Y. Tseng, J. Wu, K. Hsu, C. Hung, Y. Wen, K. L. Lu, Organometallics 2010, 29, 283–285.
- 19. P. Elumalai, R. Kanagaraj, R. Marimuthu, B. Shankar, A. Ch. Kalita, M. Sathiyendiran, *Dalton Trans.*, 2015, **44**, 11274–11277.
- 20. B. Shankar, P. Rajakannu, S. Kumar, D. Gupta, K. Tharanikkarasu, M. Sathiyendiran, *Inorg. Chem. Commun.* 2011, **14**, 374–376.

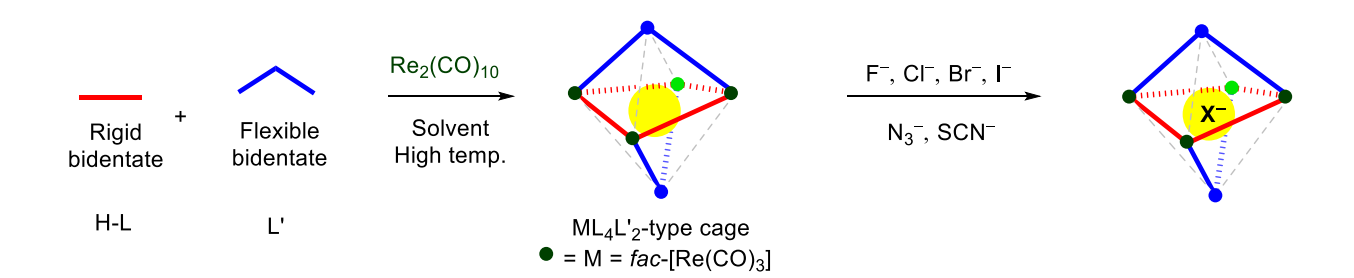
- Z. Z. Lu, C. C. Lee, M. Velayudham, L. W. Lee, J. Y. Wu, T. S. Kuo, K. L. Lu, *Chem. Eur. J.* 2012, 18, 15714–15721.
- a) K. D. Benkstein, J. T. Hupp, C. L. Stern, *Angew. Chem. Int. Ed.* 2000, 39, 2891–2893; b) K.
   E. Splan, A. M. Massari, G. A. Morris, S. S. Sun, E. Reina, S. T. Nguyen, J. T. Hupp, *Eur. J. Inorg. Chem.* 2003, 2348–2351; c) P. H. Dinolfo, M. E. Williams, C. L. Stern, J. T. Hupp, *J. Am. Chem. Soc.* 2004, 126, 12989–13001; d) P. H. Dinolfo, S. J. Lee, V. Coropceanu, J. L. Bredas, J. T. Hupp, *Inorg. Chem.* 2005, 44, 5789–5797; e) K. D. Benkstein, J. T. Hupp, *Mol. Cryst. Liq. Cryst.* 2000, 342, 151–158; f) P. H. Dinolfo, J. T. Hupp, *J. Am. Chem. Soc.* 2004, 126, 16814–16819.
- 23. a) S. S. Sun, A. J. Lees, J. Am. Chem. Soc. 2000, 122, 8956–8967; b) K. R. J. Thomas, J. T. Lin,
  Y. Y. Lin, C. Tsai, S. S. Sun, Organometallics 2001, 20, 2262–2269.
- 24. T. Brasey, A. Buryak, R. Scopelliti, K. Severin, Eur. J. Inorg. Chem. 2004, 964–967.
- 25. P. Barbazán, R. Carballo, J. S. Casas, E. Garcia-Martinez, G. Pereiras-Gabián, A. Sánches, E. M. Vázquez-Lopez, *Inorg. Chem.* 2006, **45**, 7323–7330.
- 26. P. J. Wright, S. Muzzioli, B. W. Skelton, P. Raiteri, J. Lee, G. Koutsantonis, D. S. Silvester, S. Stagni, M. Massi, *Dalton Trans.* 2013, **42**, 8188–8191.
- 27. M. P. Coogan, V. Fernández-Moreira, B. M. Kariuki, S. A. J. Pope, F. L. Thorp-Greenwood, *Angew. Chem. Int. Ed.* 2009, **48**, 4965–4968.
- 28. F. L. Thorp-Greenwood, V. Fernández-Moreira, C. O. Millet, C. F. Williams, J. Cable, J. B. Court, A. J. Hayes, D. Lloyd, M. P. Coogan, *Chem. Commun.* 2011, **47**, 3096–3098.
- 29. B. Shankar, F. Hussain, M. Sathiyendiran, J. Organomet. Chem. 2012, 719, 26–29.
- 30. M. Kedia, B. Shankar, M. Sathiyendiran, *Inorg. Chem.* 2022, **61**, 14506–14510.
- 31. B. Shankar, S. Sahu, N. Deibel, D. Schweinfurth, B. Sarkar, P. Elumalai, D. Gupta, F. Hussain, G. Krishnamoorthy, M. Sathiyendiran, *Inorg. Chem.*, 2014, **53**, 922–930.

- 32. R. Arumugam, B. Shankar, K. R. Soumya, M. Sathiyendiran, *Dalton Trans*. 2019, **48**, 7425–7431.
- 33. P. Saxena, B. Shankar, M. Sathiyendiran, J. Organomet. Chem. 2015, 799-800, 82-89.
- 34. R. Ye, C. Tan, M. Chen, L. Hao, L. Ji, Z. Mao, *Chem. Eur. J.* 2016, **22**, 7800–7809.
- 35. B. S. Murray, P. J. Dyson, Curr. Opin. Chem. Biol. 2020, 56, 28–34.
- 36. J. J. Walsh, C. L. Smith, G. Neri, G. F. S. Whitehead, C. M. Robertson, A. J. Cowan, *Faraday Discuss*. 2015, **183**, 147–160.
- 37. I. Chakraborty, S. J. Carrington, G. Roseman, P. K. Mascharak, *Inorg. Chem.* 2017, **56**, 1534–1545.
- 38. R. M. Khaled, D. A. Habashy, A. Y. Ahmed, O. S. Ismael, S. S. Ibrahim, M. Abdelfatah, K. Radacki, A. M. Mansour, *Polyhedron* 2022, **225**, 116048.
- 39. B. Ramakrishna, D. Divya, P. V. Monisha, B. Manimaran, Eur. J. Inorg. Chem. 2015, 5839–5846.
- 40. A. M. Mansour, A. Friedrich, New J. Chem., 2018, 42, 18418–18425.

# **Chapter-2**

# Flexible Coordination Cages with Polarized C-H donors for the Recognition of Spherical and Linear Anions

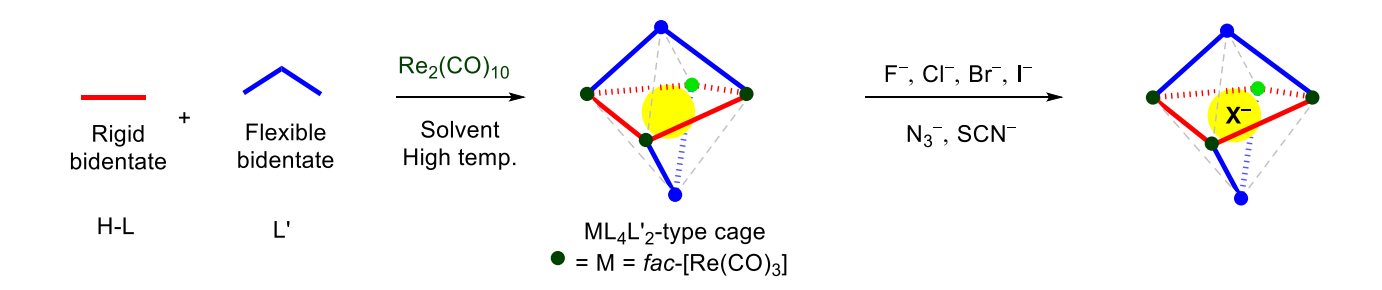
ABSTRACT: Neutral heteroleptic flexible tetranuclear coordination cages possessing flexible multiple electron deficient C-H donors was self-assembled using  $Re_2(CO)_{10}$ , carbonyldiimidazole/1,2,4-triazole, and bis(benzimidazol-1-yl)methane via one pot solvothermal approach. The cages (1-2) were characterized using various analytical and spectroscopic techniques such as ATR-IR, NMR spectroscopy, mass spectrometry, single crystal X-ray diffraction analysis, and fluorescence spectroscopy. The molecular structure of the cages reveals that it consists of a butterfly-like cyclic core capped with two neutral N-donor ligands lying above and below the cycle. The semi-flexible neutral donor and bridged imidazolate/tetrazolate units imparts flexibility to the cage. The dynamic behavior of the cage was studied using variable temperature <sup>1</sup>H-NMR spectroscopy. The ability of cage 1 to interact with anions of different shapes and sizes was further investigated using <sup>1</sup>H-NMR and fluorescence spectroscopy. The thermally stable, flexible cage 1 transforms into restricted cage in the presence of spherical and linear anions, and selectively recognizes fluoride. The extent of association of anions with 1 was determined using fluorescence spectroscopy. The binding constant values were calculated using Benesi-Hildebrand equation for 1:1 host-guest stoichiometry.



#### 2.1. Introduction

The design and synthesis of coordination cages capable of accommodating anionic guests in their inner cavities have been getting immense interest because of their importance in anion sensing, separation, transport, catalysis, and material chemistry. 1-6 The nature of the cage i.e., ionic or neutral; position of the N–H groups; the shape and size of the inner cavity play a vital role in selective anion recognition. The choice of metal precursors and organic ligands play a crucial role in getting the desired cage. Naked metal ions/partially protected metal complexes and organic ligands containing N-H functional groups such as imine, amide, urea, pyrrole are generally used for the self-assembly of ionic/neutral cages for anion sensing. 4,5 Cages possessing properly positioned multiple non-traditional electron deficient C-H groups acting as hydrogen bond donors have been emerging parallelly as potential hosts for anions.<sup>6-8</sup> The C-H group is mostly from heterocyclic ring and acquires electron deficient nature by coordination of its adjacent nitrogen to metal ion. Recently our group reported design strategy for neutral capped electron deficient bowl-shaped trinuclear coordination cages fac-[{Re(CO)<sub>3</sub>(im)}<sub>3</sub>L'] (I) (im = imidazolate; L' = 1,3,5tris(naphthanoimidazol-1-ylmethyl)benzene its derivatives) and containing symmetrically arranged three C-H donors directed towards the centre of small cavity for fluoride recognition. 8a Cage I was obtained by the combination of Re<sub>2</sub>(CO)<sub>10</sub>, carbonyldiimidazole (CO-im<sub>2</sub>), and L'. In order to increase the number of cavities in the cage, flexible ditopic donor bis(benzimidazol-1-yl)methane (L) is chosen instead of L'. In principle, L-type capsule-like cage with two separate electron deficient bowls, [{fac-Re(CO)<sub>3</sub>(im)<sub>3</sub>]<sub>2</sub>, at each end connected by three L motifs was expected. However, the above bonding combinations resulted in tetranuclear cage that possesses a cavity surrounded

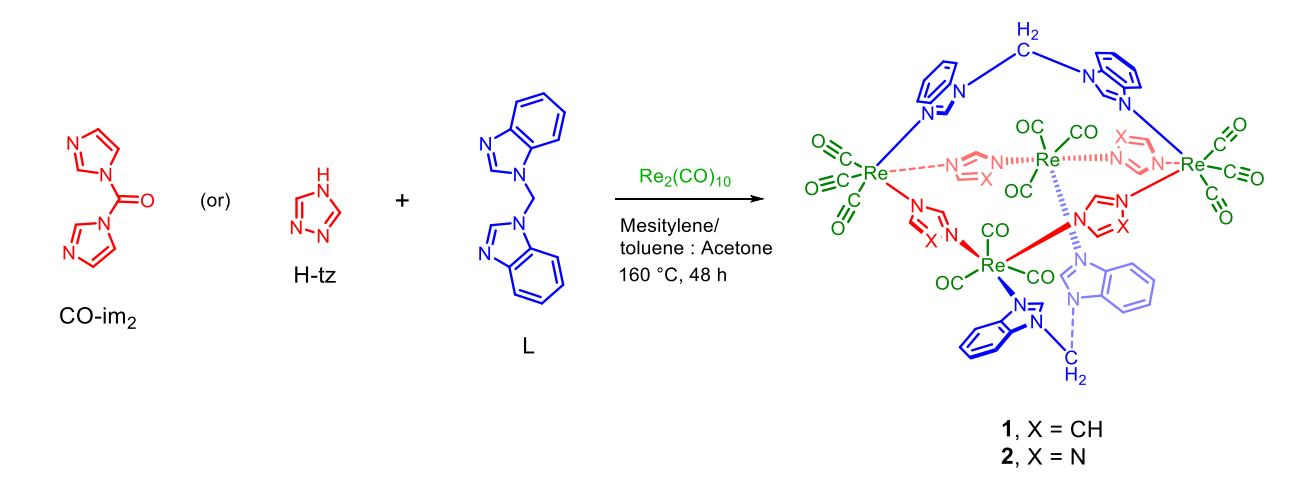
by eight or twelve electron deficient C–H groups as H-bond donor, capable of participating in anion coordination. Herein, we report the self-assembly of flexible neutral heteroleptic tetranuclear fac-Re(CO)<sub>3</sub> core-based cages fac-[{Re(CO)<sub>3</sub>(im)}<sub>3</sub>L] (1) and fac-[{Re(CO)<sub>3</sub>(1,4-tz)}<sub>3</sub>L] (2), where im = imidazolate and 1,4-tz = 1,4-triazolate. Further, the flexible cage 1 was studied for molecular recognition of various anions. The cage 1 recognizes spherical halides and linear anions by transforming flexible structural framework into restricted framework (Scheme 1).



**Scheme 1.** Schematic representation for the self-assembly of ML<sub>4</sub>L'<sub>2</sub>-type cage and its interaction with various anionic guests.

#### 2.2. Results and Discussions

**Synthesis of complexes 1–2.** The cages fac-[{Re(CO)<sub>3</sub>(im)}<sub>3</sub>L] (1) and fac-[{Re(CO)<sub>3</sub>(1,4-tz)}<sub>3</sub>L] (2) were synthesized using Re<sub>2</sub>(CO)<sub>10</sub>, carbonyldiimidazole (CO-im<sub>2</sub>) for 1/1,2,4-triazole (H–tz) for 2 and L in mesitylene/toluene:acetone via one-pot solvothermal approach (Scheme 2). The cages were air and moisture stable and soluble in DMSO and acetone upon slight heating.



Scheme 2. Self-assembly of cages 1–2.

The ATR-IR spectrum of **1–2** shows three distinct bands which confirms the presence of [fac-Re(CO)<sub>3</sub>] motif (Figure 1).<sup>8</sup>

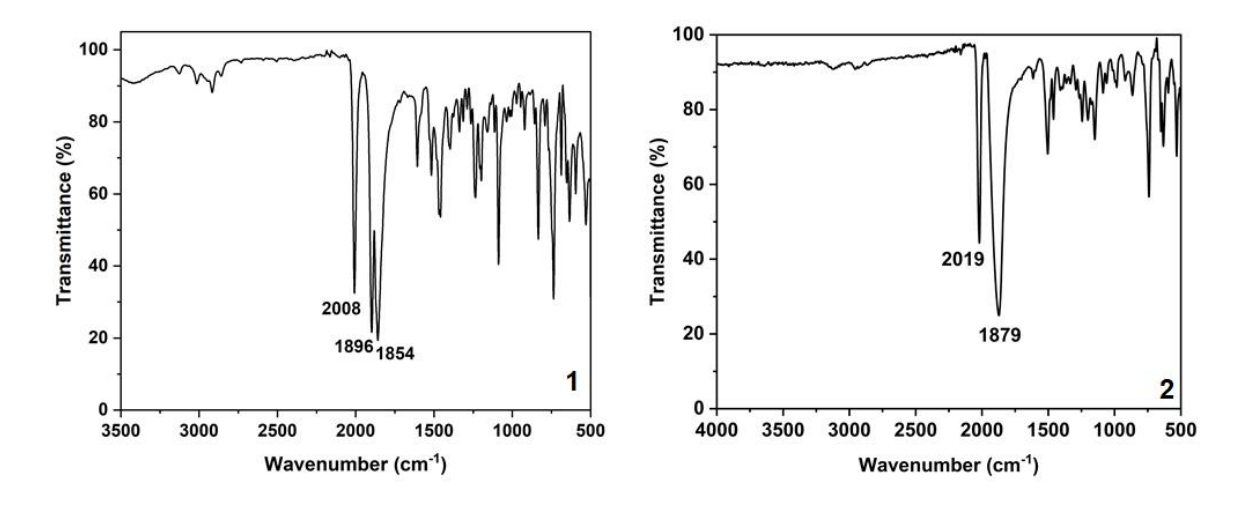
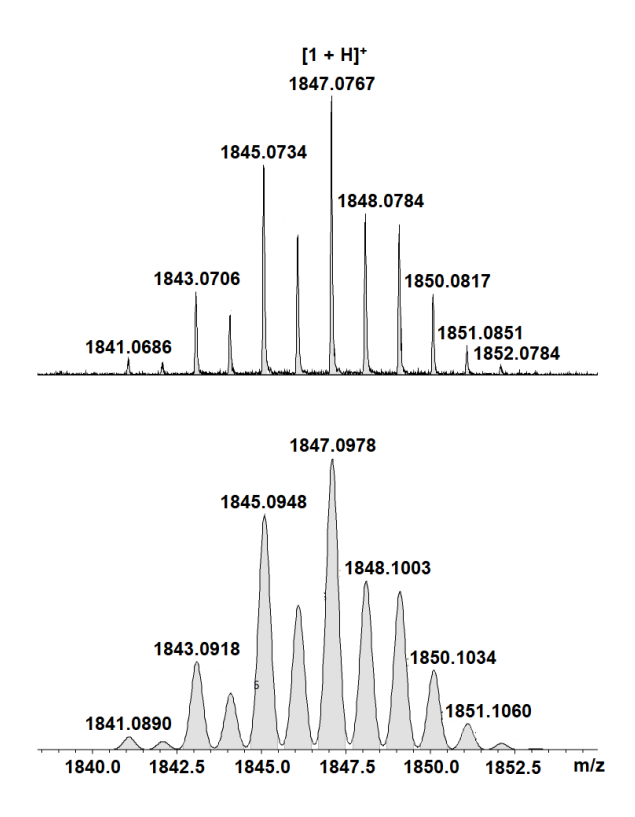


Figure 1. ATR-IR spectrum of cages 1 and 2.

The ESI–MS spectrum of **1-2** displays peak corresponding to molecular ion  $(m/z = 1847.0767 \text{ for } [\mathbf{1} + H]^+)$ , and  $(m/z 1851.0789 \text{ for } [\mathbf{2} + H]^+)$  which matches well with the theoretical value (Figure 2).



**Figure 2.** Experimental (top) and calculated (bottom) ESI mass spectra of  $[1 + H]^+$  in positive ion mode.

**Molecular structure of 1.** The single crystal X-ray analysis of **1-2** reveals that it adopts cage structure (Figure 3). The cages are made up of four *fac*-Re(CO)<sub>3</sub> cores, four imidazolate/tetrazolate motifs, and two neutral L motifs. Four rhenium ions and four imidazolate/tetrazolate motifs acting as bridging units are arranged alternatively, resulting in butterfly like cyclic structure. However, there is no direct bond present between any two rhenium ions in the butterfly cyclic core. Each

rhenium in the cyclic structure is surrounded by three facial carbonyl groups, which are directed outward. The remaining coordination site of rhenium in **1-2** is occupied by neutral nitrogen donor (L). The alternatively arranged two rhenium cores in the butterfly cycle are coordinated by ditopic nitrogen donor L i.e., one L is capped on top of the cycle and another is capped at the bottom of the cycle. This arrangement of the ligand motifs provides the cage structure to **1** and **2**.

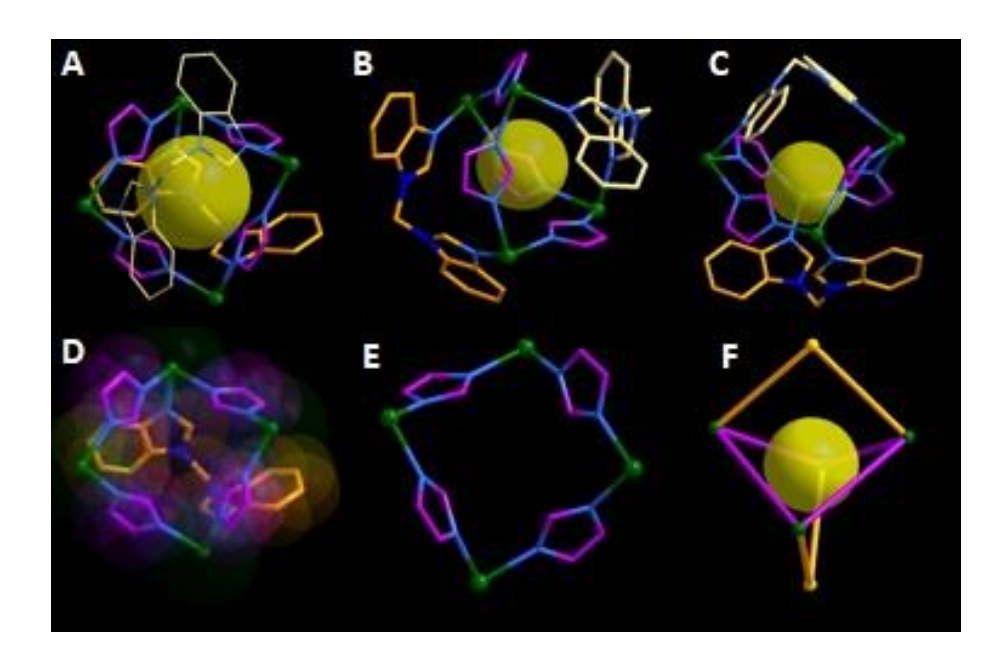


**Figure 3.** (A–C) Various views of molecular structure of **1** (H atoms and CO groups are removed for clarity & yellow sphere indicates empty space in the cage). (D) One of L and all CO groups are removed to show inner space of **1**. (E)  $[Re(im)_4]$  cycle in **1**. (F) Skeleton of **1** (green = fac- $[Re(CO)_3]$ , red line = im and orange V = L).

The four Re<sup>I</sup> ions form a butterfly cyclic core with Re···Re distances of  $\sim$ 6.41 Å. The two N-CH-N units of the two imidazolate/tetrazolate motifs are above the plane and the other two points below the plane. The imidazolate/tetrazolate units acquire alternate syn, anti-arrangement.

The two benzimidazolyl motifs are arranged in a *trans* arrangement w.r.t each other. The overall height of structure of **1-2** from the C-atom of methylene group of L from above to below the cyclic plane of Re(im)<sub>4</sub> is ~10.63 Å. The distances of Re–N (2.196 Å, 2.147 Å), Re–C (1.894–1.905 Å), and C–O (1.136–1.174 Å) are within the expected range found for complexes containing *fac*-Re(CO)<sub>3</sub>, imidazolate and benzimidazolyl cores.<sup>8</sup>

**Molecular structure for 1·(H<sub>2</sub>O)·(DMSO)**. Several attempts to grow crystals of **1** with various anions proved to be fruitless. The single crystals obtained for **1** with TBAClO<sub>4</sub> resulted in  $1 \cdot (H_2O) \cdot (DMSO)$  without TBAClO<sub>4</sub> (Figure 4).

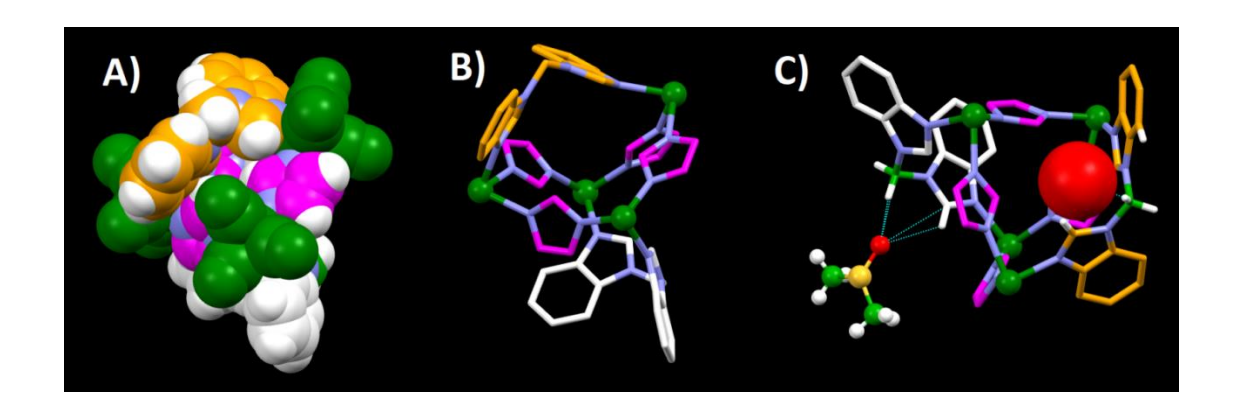


**Figure 4.** Molecular structure of  $1 \cdot (H_2O) \cdot (DMSO)$ . Space filling view (A) and stick view (B) without solvent molecules (hydrogen atoms are omitted in the cage B and C; carbon atoms of two L motifs are shown in orange and white). Color code:  $[Re(CO)_3] = green$  and im = C, pink, N = blue, H = white.

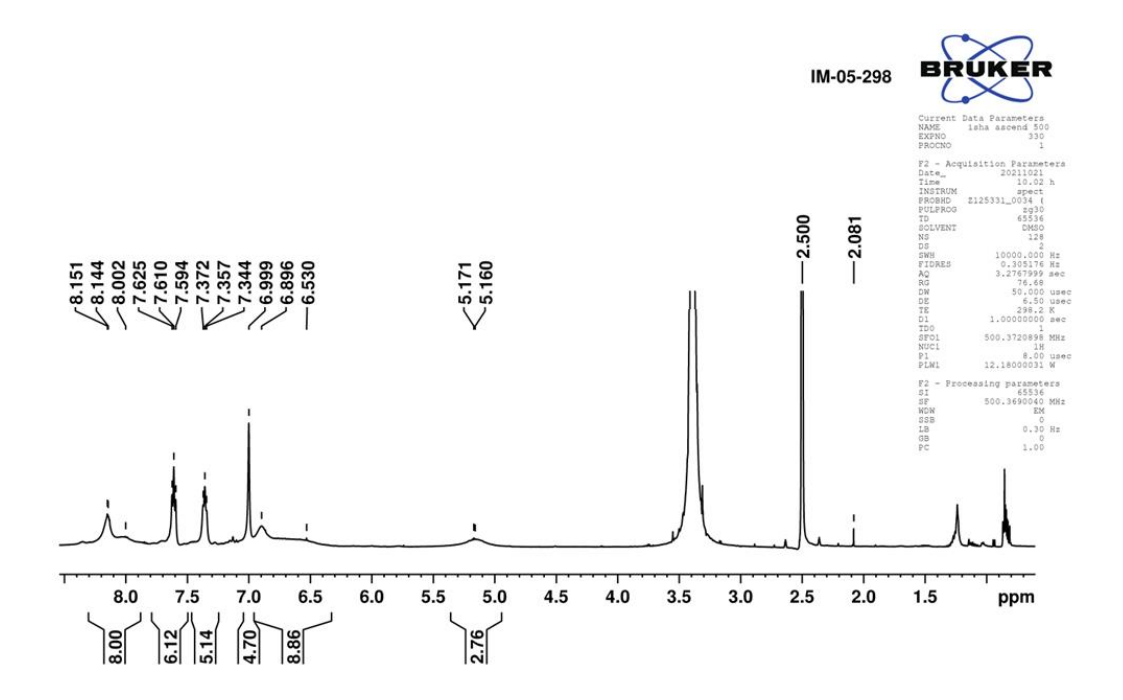
However, the data provides information about the flexibility and stability of the cage in the presence of anion. The main difference between molecular structure of 1 and  $1 \cdot (H_2O) \cdot (DMSO)$  is

the conformation of neutral ligand motifs i.e., *anti*-conformer of L and *intermediate*-conformer of L. The benzimidazolyl motif almost acts as a portal for accessing the inner cavity of 1. The data further supports that the benzimidazolyl hydrogen atoms are capable of acting as H-bond donor to electron rich atoms. Non-covalent contacts were observed between 1 and DMSO solvent molecule, present above the exocavity (shown as blue dotted line, Figure 4). The oxygen atom from  $H_2O$  molecule almost sits in the exocavity/portal, created upon rearrangement of the benzimidazolyl motifs of L, of 1. The crystallographic parameters for 1,  $1 \cdot (H_2O) \cdot (DMSO)$  and 2 are mentioned in Table 1.

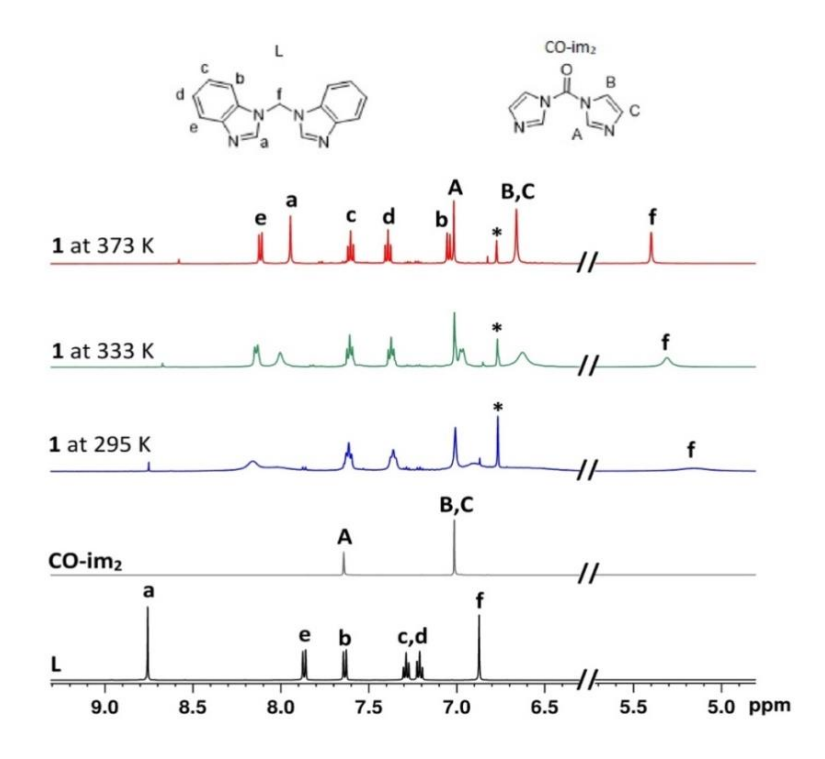
**Table 1.** Crystallographic structural parameters of **1** and  $1 \cdot (H_2O) \cdot (DMSO)$ .

Crystal data	1	$1 \cdot (H_2O) \cdot (DMSO)$
Empirical Formula	$C_{54}H_{36}N_{16}O_{12}Re_4$	C <sub>56</sub> H <sub>36</sub> N <sub>16</sub> O <sub>12</sub> Re <sub>4</sub> S
Formula Mass, $M_r$	1845.79	1939.91
Crystal system	Tetragonal	Triclinic
Space group	I-42d	P-1
a (Å)	14.4758 (7)	11.4283 (2)
b (Å)	14.4758 (7)	13.9624 (4)
c (Å)	39.543 (3)	23.2688 (5)
α(°)	90	105.171
β(°)	90	98.106
γ(°)	90	95.298
$V(\mathring{A}^3)$	8286.1 (10)	3515.12 (15)
$d (g/cm^3)$	1.480	1.833
Z	4	2
T(K)	296	296
R factor $(I > 2\sigma(I))$	0.0305	0.0871
$wR_2 (I > 2\sigma(I))$	0.0723	0.2245
R factor (all data)	0.0373	0.1418
$wR_2$ (all data)	0.0789	0.2978
GooF	1.156	1.074
CCDC	2216292	2216293

**Dynamic behavior of cage 1**. The  ${}^{1}$ H NMR spectrum of **1** in  $d_{6}$ -DMSO at room temperature shows one singlet, two triplets and four broad chemical resonances. The broad resonances are almost merged with the baseline (Figure 5). The protons of the free ligands are well-separated. Comparison of the  ${}^{1}$ H-NMR spectra of the free ligands with **1** clearly indicates that no impurity is present in **1** (Figure 6).

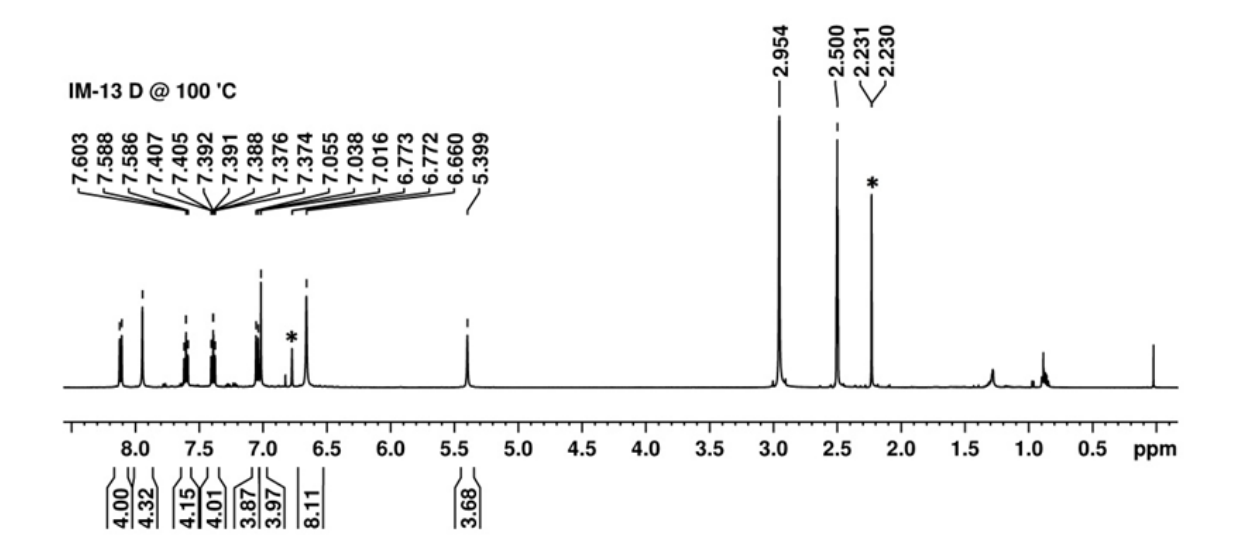


**Figure 5.**  ${}^{1}\text{H-NMR}$  spectrum of cage 1 in DMSO- $d_{6}$  at 298 K.



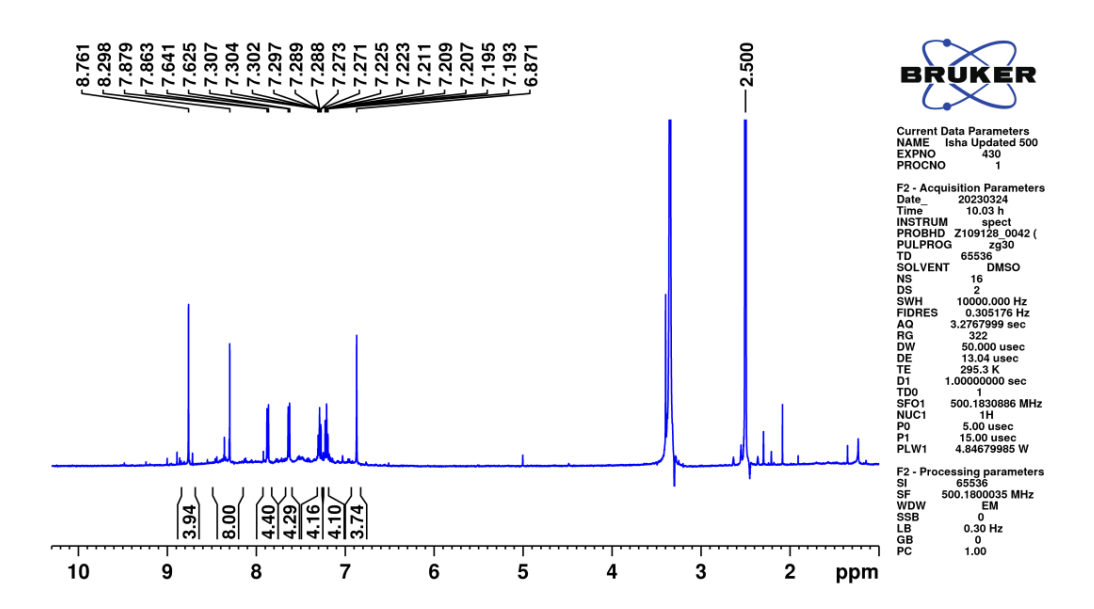
**Figure 6.** Partial  ${}^{1}\text{H-NMR}$  of free ligands and **1** (at 295 K, 333 K and 373 K) in DMSO- $d_6$  (\*mesitylene solvent peak).

In order to understand the behavior of **1**, variable high temperature <sup>1</sup>H NMR spectra were recorded. The spectrum obtained at 373 K showed properly resolved chemical resonances for all the protons (Figure 6-7). More importantly, the H<sup>a</sup> proton of L in **1** was upfield shifted significantly. The above data indicates that the cage remains intact in the solution at both room temperature and high temperature. The cage is flexible at room temperature i.e., possibly two or three conformers are present and are interconverting slowly due to orientation of benzimidazolyl/imidazolate motifs.



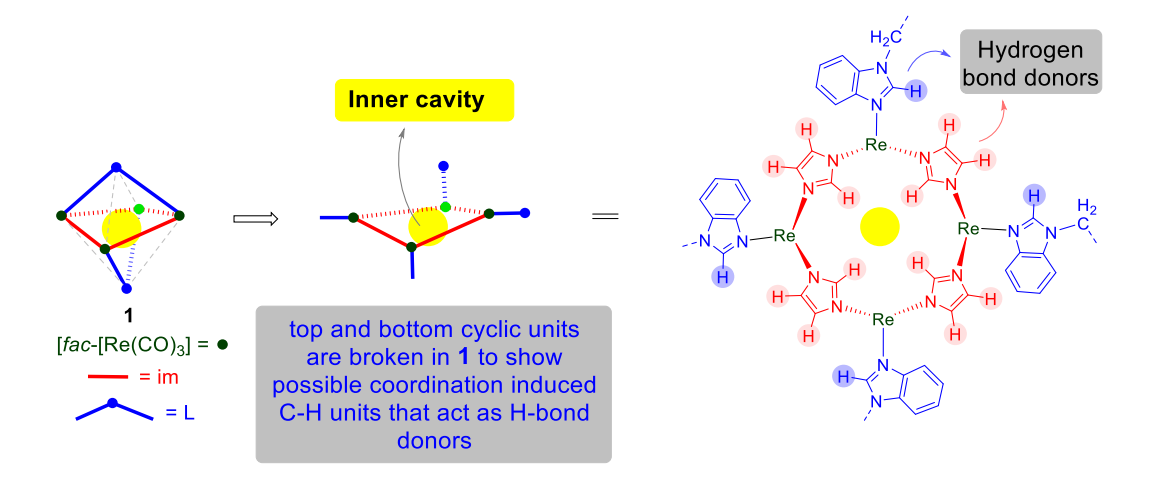
**Figure 7.**  ${}^{1}\text{H-NMR}$  spectrum of cage **1** in DMSO- $d_6$  at 373 K (\* mesitylene peak).

The  ${}^{1}\text{H-NMR}$  spectrum of **2** displayed well-resolved pattern in DMSO- $d_{6}$  at room temperature (Figure 8). The pattern is different from that of **1**, no broad peaks were observed at room temperature. The protons in the complex undergo slight upfield/downfield shift as compared to the free ligand.



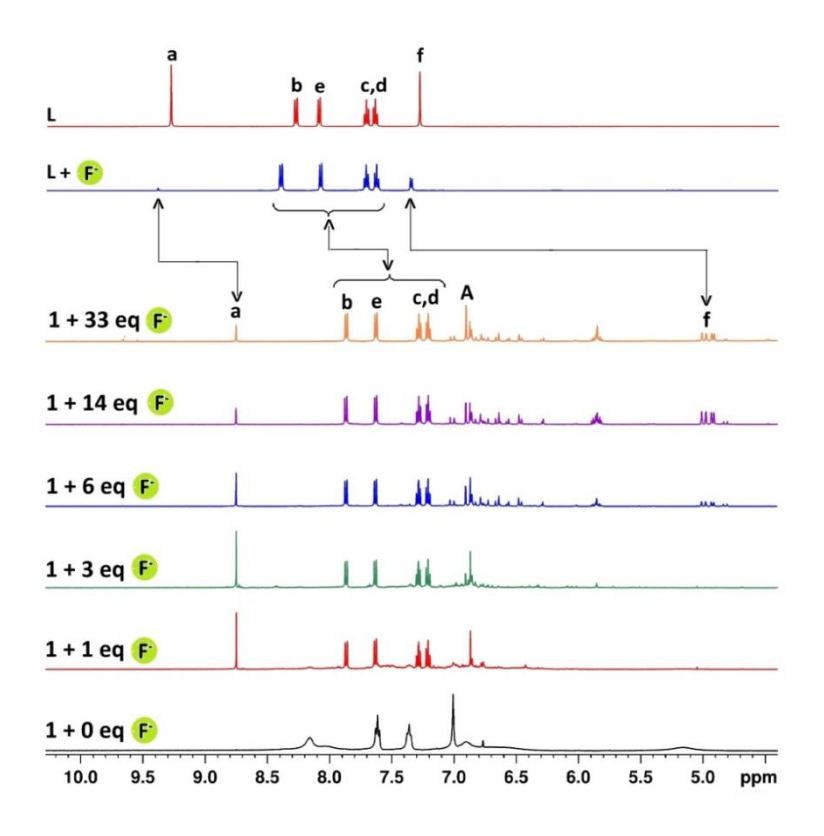
**Figure 8.**  ${}^{1}\text{H-NMR}$  spectrum of cage **2** in DMSO- $d_6$  at 298 K.

Anion recognition studies using <sup>1</sup>H–NMR spectroscopy. Flexible cage 1 possesses small cavity which is surrounded by multiple coordination induced electron deficient C–H groups from four imidazolate (im) and four benzimidazolyl motifs (Figure 9).



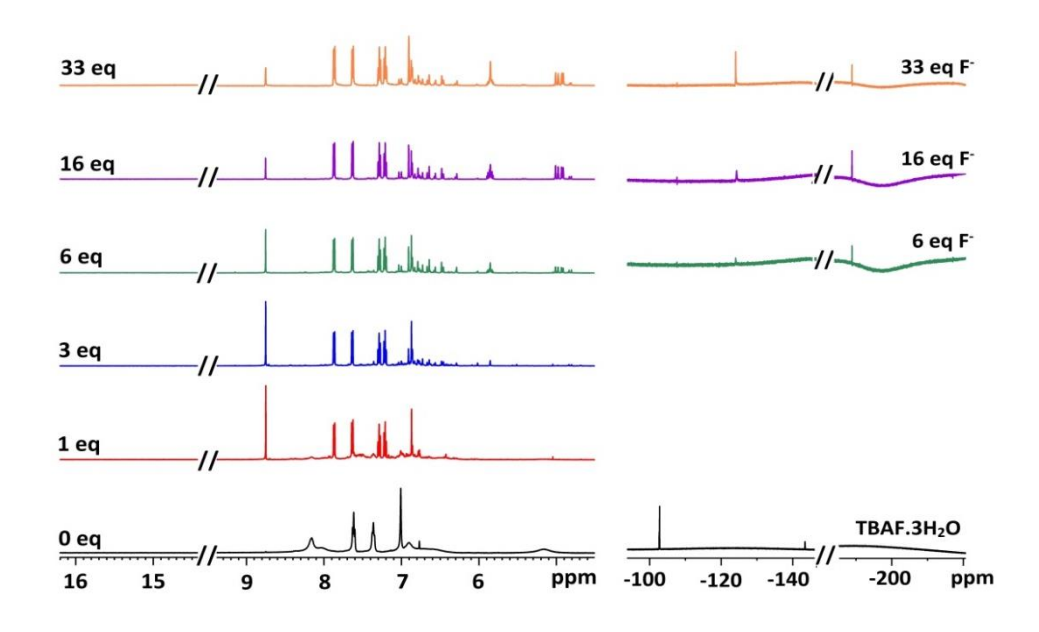
**Figure 9.** Cartoon representation of cage **1** with and without broken L motifs to show possible coordination induced C–H units that act as H–bond donors.

The steric and electronic environment of the flexible frameworks of **1** may make it a suitable host for anions of specific shapes and sizes. To find the ability of **1** as a host for spherical halides, linear, trigonal planar- and tetrahedral anions, the  ${}^{1}H$ -NMR studies of **1** with their respective tetrabutylammonium salts (TBAX) in  $d_6$ -DMSO were carried out. The addition of  $F^-$ ,  $CI^-$ ,  $Br^-$ ,  $\Gamma$ ,  $N_3^-$  and  $SCN^-$  to **1** resulted in significant change in the  ${}^{1}H$ -NMR pattern whereas minor changes were observed for  $CIO_4^-$  anion. No significant change was observed for  $NO_3^-$  and  $HSO_4^-$ . The  ${}^{1}H$  NMR spectrum of **1** +  $F^-$  ( $\sim 0.8$  eq) shows well-resolved sharp peaks for aromatic protons ( $H^{b\text{-e}(L)}\& H^{A(im)}$ ). No peaks for methylene ( $-CH_2$ -) and  $H^{B,C(im)}$  were observed. Further addition of  $F^-$  ( $\sim 3$  eq) did not alter the signals of  $H^{b\text{-e}}$  but a small singlet emerged near to  $H^A$  (Figure 10).



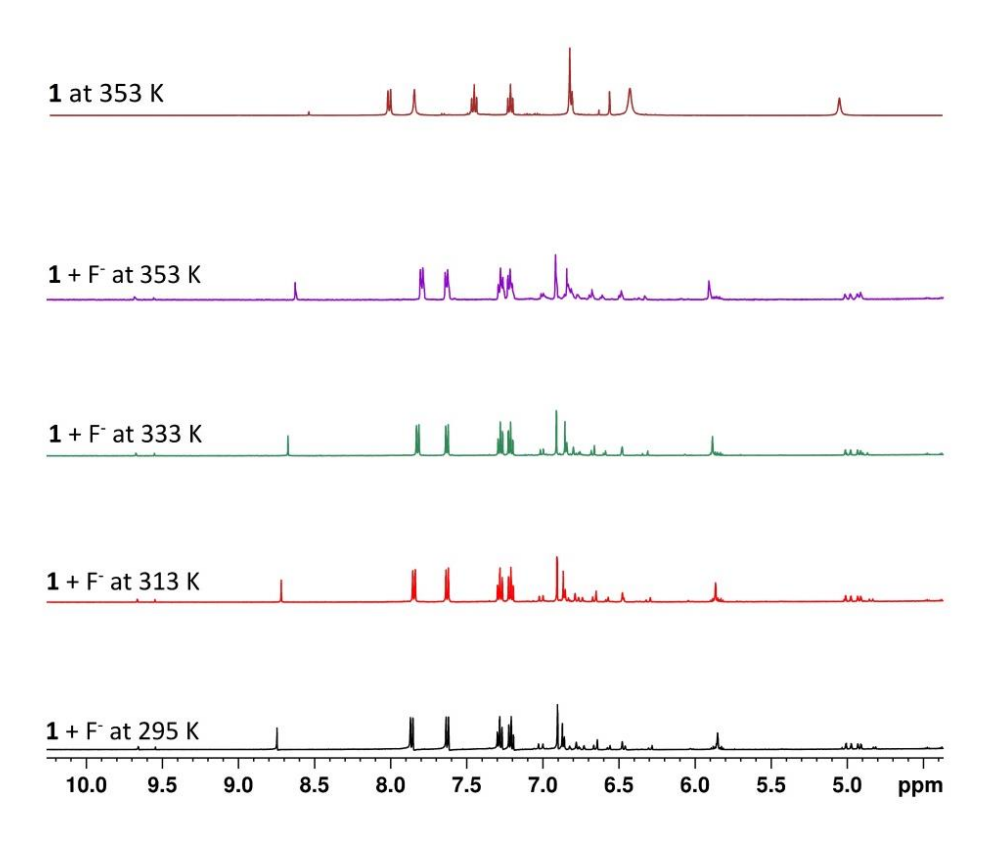
**Figure 10.** Partial  ${}^{1}\text{H}$ –NMR spectra of **1**, **1** (5.2 x  $10^{-3}$  M) with various equivalents of TBAF.3H<sub>2</sub>O in comparison with L and L + TBAF in DMSO- $d_6$  at 298 K.

Upon increasing equivalents of fluoride, the intensity of  $H^a$  (N– $CH_2$ –N of bim) decreases and several tiny peaks in the region of 5.5–7.2 ppm appears. A doublet of doublet with a coupling constant of ~18 Hz corresponding to methylene protons also appears. In the presence of excess  $F^-$  (~ 33.4 eq), the intensity of the singlet around 6.9 ppm increased (Figure 10). The data indicates that the C–H groups of im in 1 interact with  $F^-$  initially. Multiple C–H groups (N– $C^a$ H–N of bim and N– $C^B$ H– $C^C$ H–N/ $C^A$ –H of im) of 1 may interact with  $F^-$  at higher concentration. Further, the encapsulation of fluoride in the cavity of 1 is supported by the coupled  $^{19}$ F-NMR studies. Free TBAF.3H<sub>2</sub>O in DMSO- $d_6$  displayed a singlet at –103 ppm and a triplet at –143 ppm, whereas 1 +  $F^-$  shows upfield shifted singlet at –124 ppm and a pentet at –189 ppm, suggesting  $F^-$  interactions with the cage (Figure 11).  $^{9,10}$ 



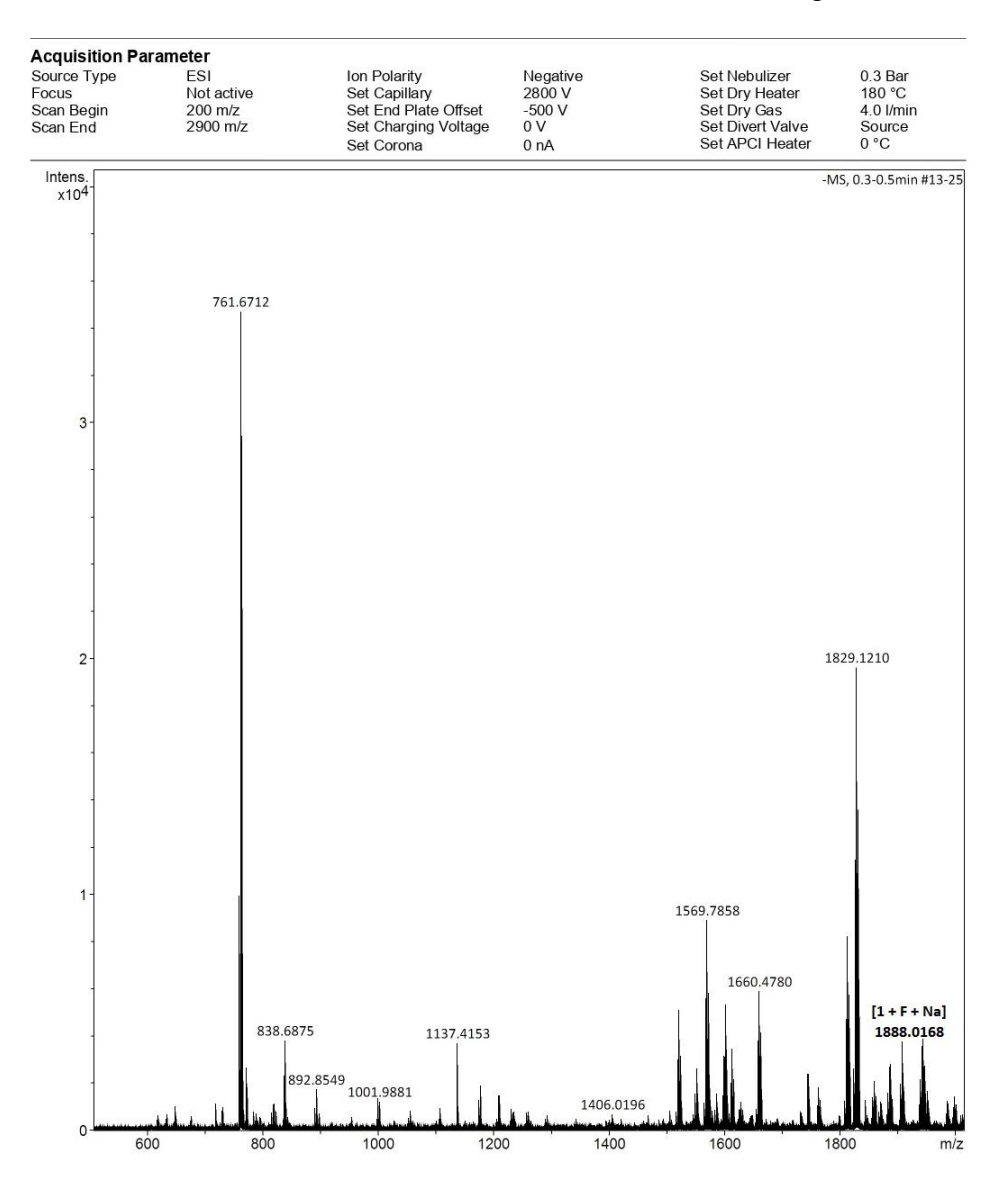
**Figure 11.** a) Partial <sup>1</sup>H–NMR spectra of cage **1** (4.2 x  $10^{-3}$  M) with various equivalents of fluoride in DMSO- $d_6$  at 298 K. b) <sup>19</sup>F–NMR spectra of cage **1** (4.2 x  $10^{-3}$  M) with various equivalents of fluoride in DMSO- $d_6$  at 298 K.

In order to check if any decomposition of the cage occurs in presence of  $F^-$ , the  $^1H$ -NMR spectrum of  $L + F^-$  was recorded and compared with  $1 + F^-$ . The singlet of  $H^a$  disappears, whereas the singlet of methylene becomes doublet (J = 6.5 Hz) without any significant upfield/downfield shift for  $L + F^-$ , in particular, no doublet of doublet was observed at 5 ppm. The  $^1H$ -NMR patterns of  $\mathbf{1} + F^-$  and  $L + F^-$  are different (Figure 10). The data clearly indicates that the cage becomes rigid after accommodating fluoride in its cavity without any decomposition. Further, no significant changes in the chemical resonances of  $\mathbf{1} + F^-$  (excess) were observed even at 353 K (80 °C) (Figure 12). The high temperature NMR spectra of  $\mathbf{1}$  and  $\mathbf{1} + F^-$  are different from each other, suggesting the conformation of the cage changes after interacting with fluoride ion, which is different from the conformation of free  $\mathbf{1}$  at high temperature.



**Figure 12.** Partial  ${}^{1}H$ -NMR spectra of  $1 + F^{-}$  at variable temperature (bottom) and **1** at 353 K (top) in DMSO- $d_6$ .

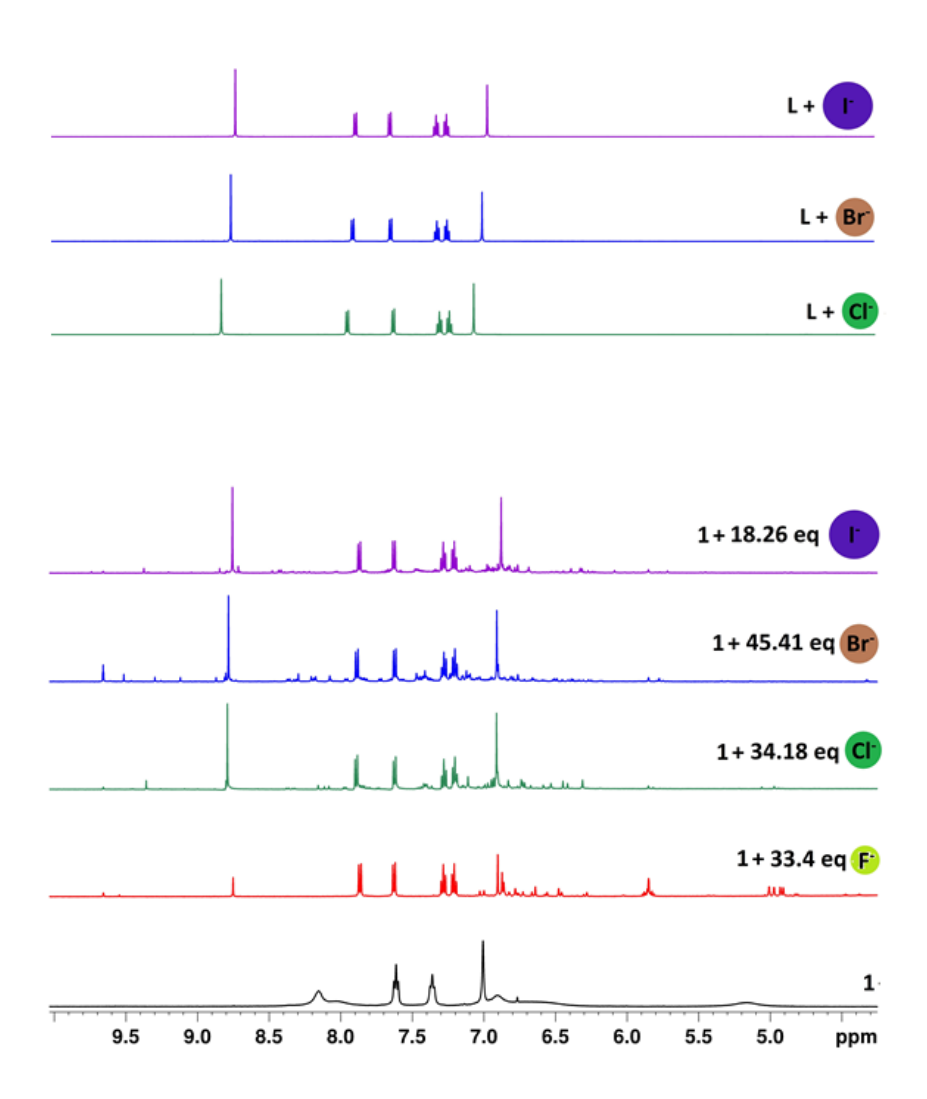
The encapsulation of fluoride to  $\mathbf{1}$  is supported by ESI–MS spectrum, which displays peak for  $[\mathbf{1} + F + Na]$  at m/z 1888.0168 that matches well with the theoretical values (Figure 13).



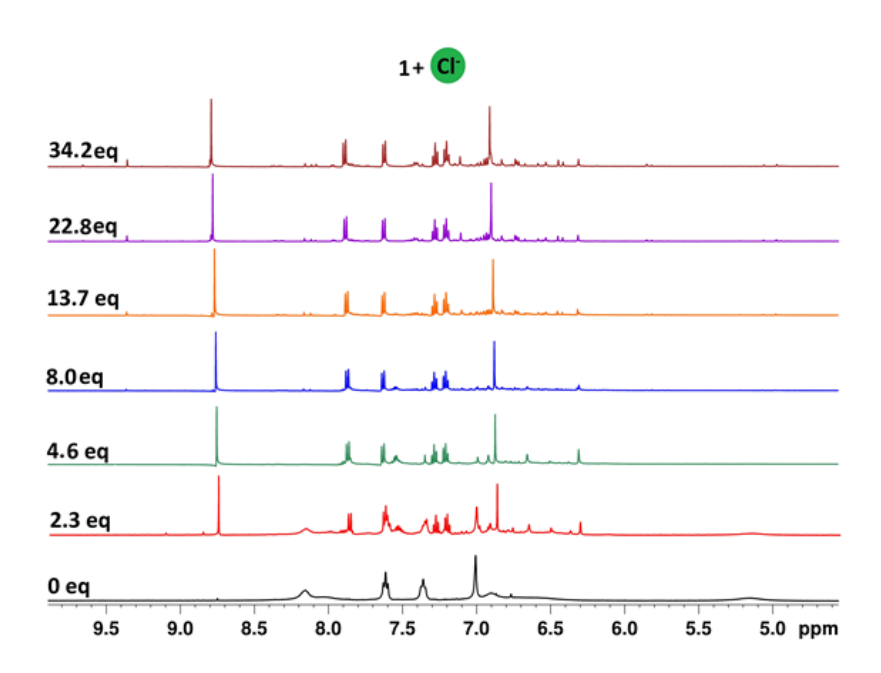
**Figure 13.** Experimental ESI mass spectrum of [1 + F + Na] in negative ion mode.

The detailed recognition ability of  $\mathbf{1}$  with other halides was also studied. The <sup>1</sup>H-NMR spectrum of 1 + X ( $X = Cl^{-}/Br^{-}/\Gamma$ ) displayed well-separated peaks for the aromatic protons with pattern different from that of  $\mathbf{1} + F^{-}$  (Figure 13). The spectrum of  $\mathbf{1} + Cl^{-}$  displayed many small peaks in

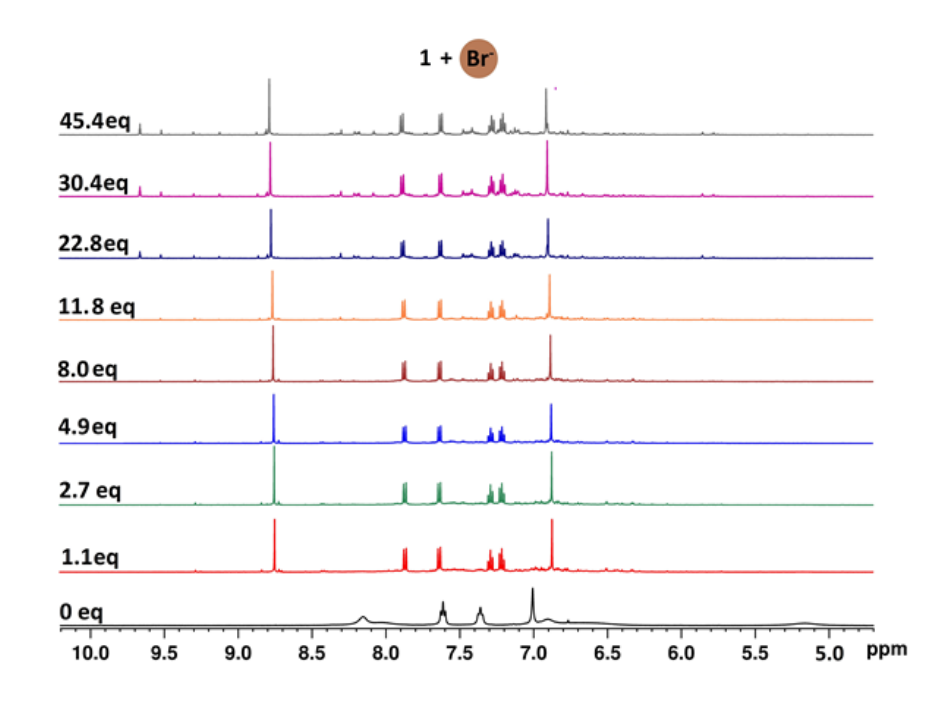
the region 5.5 - 7.2 ppm similar to that of  $1 + F^-$  whereas  $1 + Br^-/1 + \Gamma^-$  also show several small peaks between 8 - 10 ppm (Figure 2.16–2.18). However, the  $^1H$ -NMR spectra of L + X ( $X = C\Gamma^-/Br^-/\Gamma^-$ ) is different from 1 + X (Figure 14–16). The data suggests that the cage interacts with halides and accommodates it either in its inner cavity or exocavity.



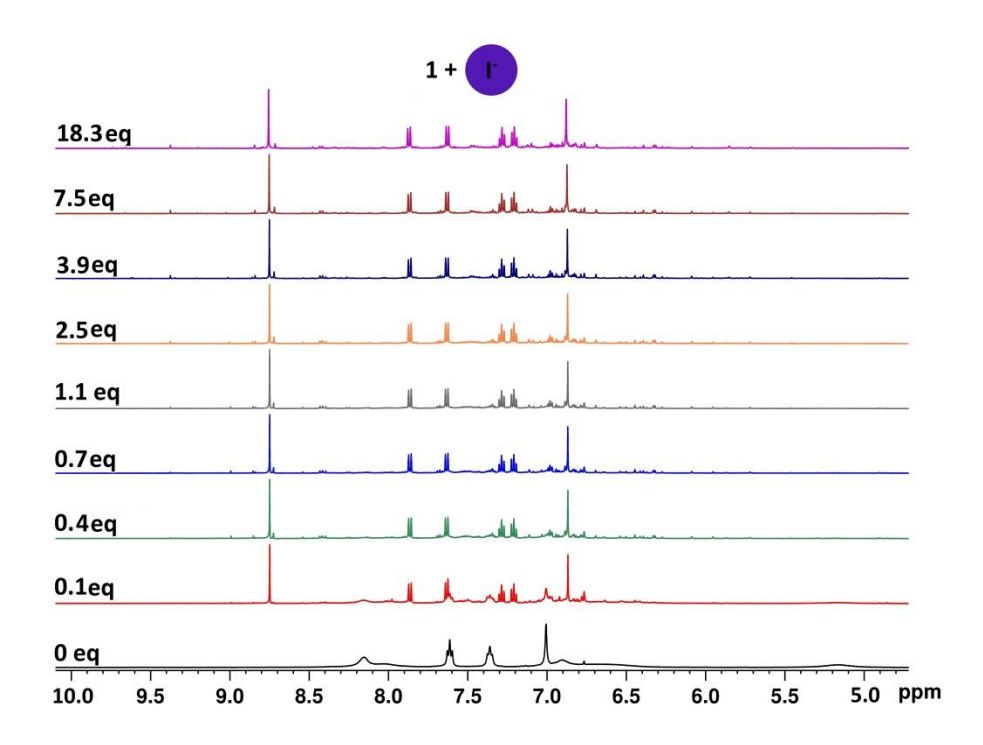
**Figure 14.** Partial <sup>1</sup>H–NMR spectra of **1** and **1** with various tetrabutylammonium salts, TBAX (X = F, Cl, Br, I) (bottom) in comparison with L + Cl<sup>-</sup>/Br<sup>-</sup>/ $\Gamma$  (top) in DMSO– $d_6$  at 298 K.



**Figure 15.** Partial  ${}^{1}\text{H}$ –NMR spectra of **1** and **1** (4.4 x  $10^{-3}$  M) with various equivalents of TBACl in DMSO– $d_6$  at 298 K.

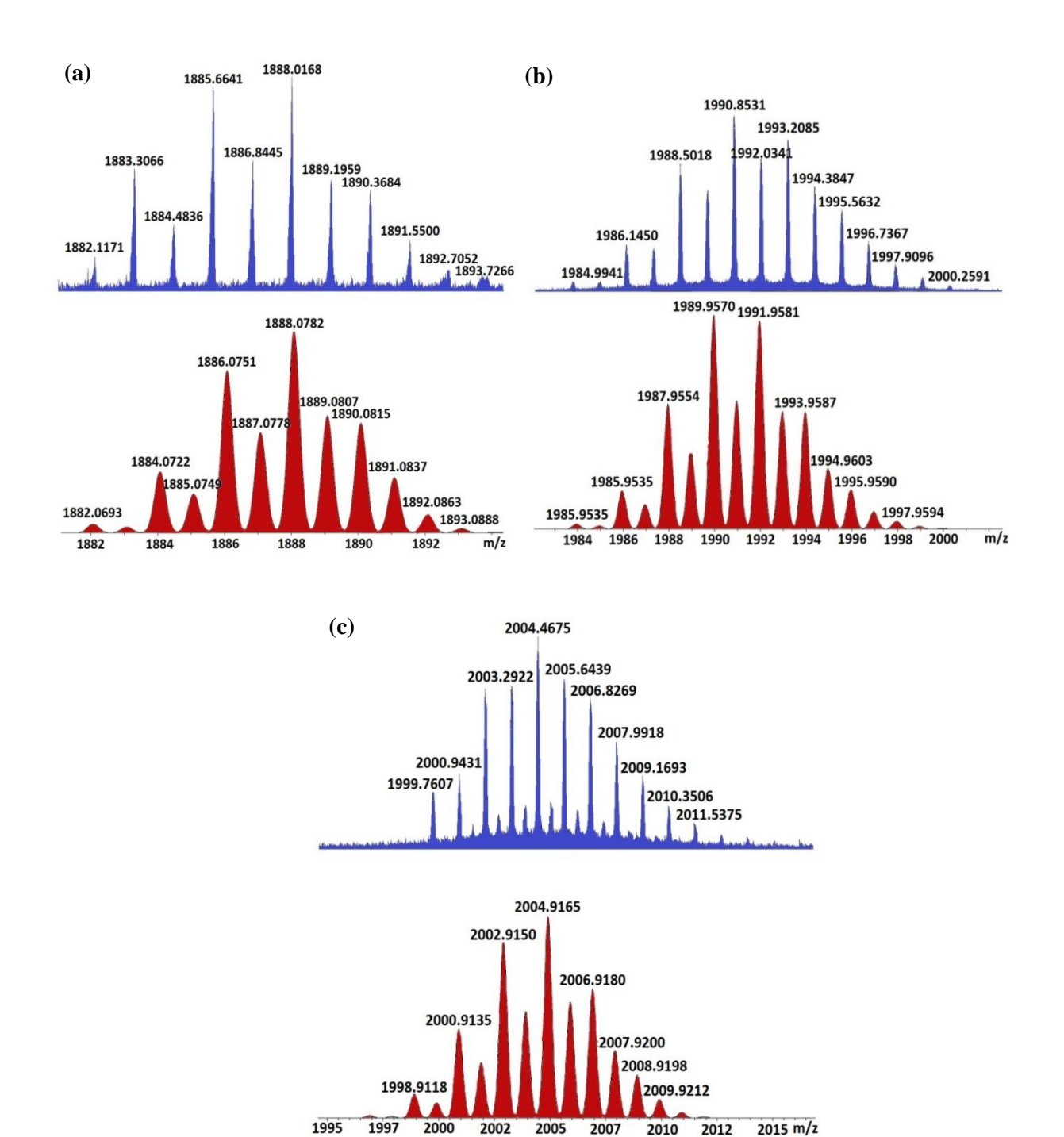


**Figure 16.** Partial <sup>1</sup>H–NMR spectra of **1** and **1** (5.74 x  $10^{-3}$  M) with various equivalents of TBABr in DMSO– $d_6$  at 298 K.



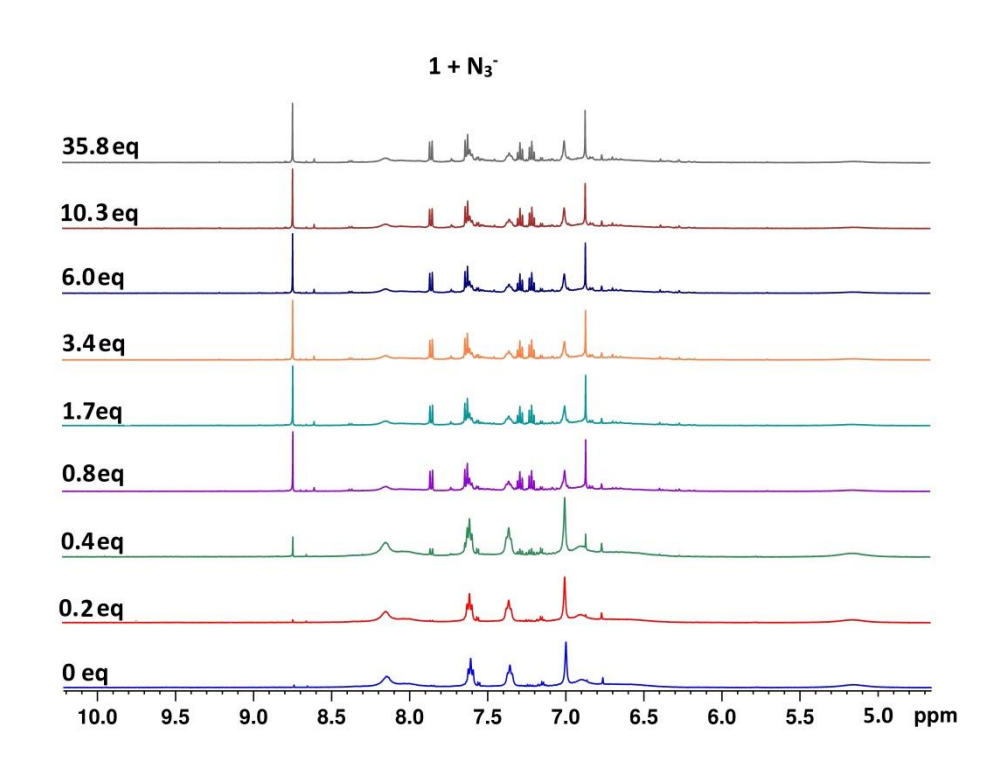
**Figure 17.** Partial <sup>1</sup>H–NMR spectra of **1** and **1** (4.8 x  $10^{-3}$  M) with various equivalents of TBAI in DMSO– $d_6$  at 298 K.

The recognition of **1** for halides is supported by ESI–MS spectra, m/z = 1990.8531 for [**1** + 3Cl + K] and m/z = 2004.4675 for [**1** + 2Br – H] which matches well with the theoretical values (Figure 18).



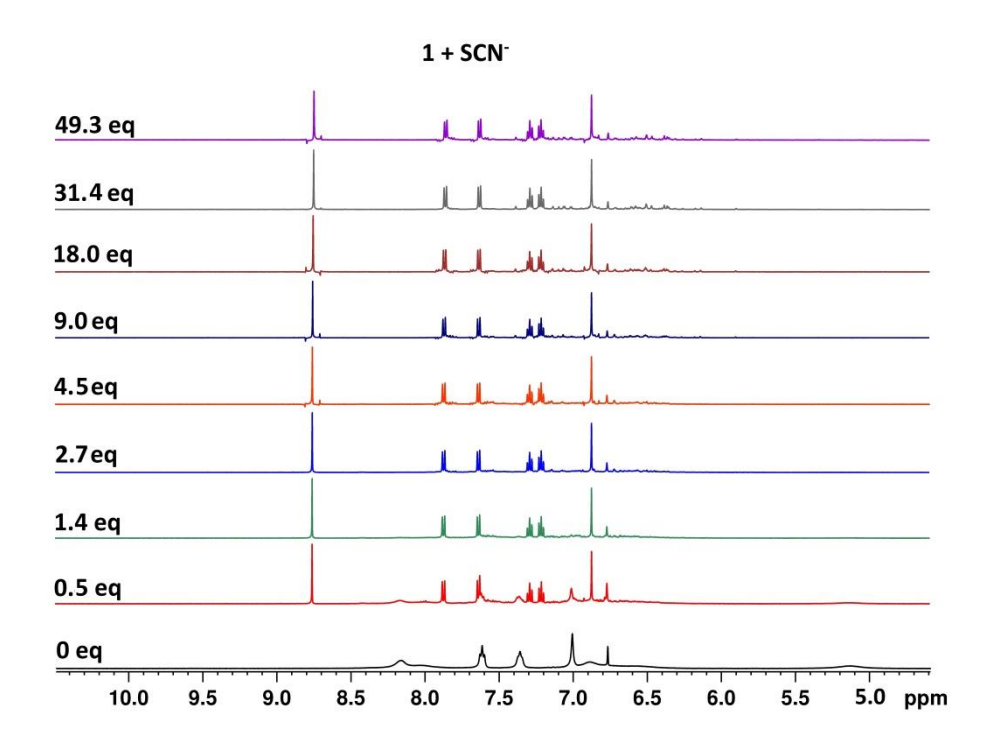
**Figure 18.** Experimental (Top) and calculated (Bottom) ESI mass spectra of (a) [1 + F + Na]; (b) [1 + 3Cl + K]; (c) [1 + 2Br - H] in negative ion mode.

The ability of 1 to interact with anions of other shapes and sizes was also investigated. Upon addition of aliquots of azide ( $\sim 0.85$  eq), the  $^{1}$ H-NMR spectrum of  $1 + N_{3}^{-}$  displayed two set of chemical resonances, the major one closely similar to  $1 + \text{Cl}^{-}$  and the minor set may correspond to free 1 (Figure 19). The above pattern did not alter much in the presence of excess of azide ( $\sim 36$  eq).



**Figure 19.** Partial  ${}^{1}\text{H}-\text{NMR}$  spectra of **1** and **1** (4.8 x  $10^{-3}$  M) with various equivalents of TBAN<sub>3</sub> in DMSO- $d_6$  at 298 K.

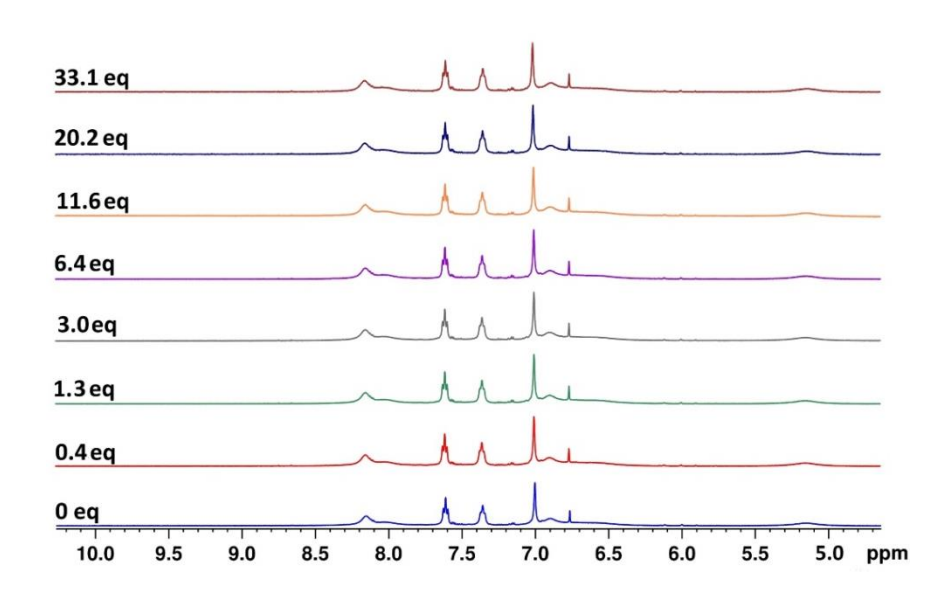
The pattern for  $L + N_3^-$  is different from  $\mathbf{1} + N_3^-$ . The study indicates that the solution contains rigid  $\mathbf{1} + N_3^-$  and flexible  $\mathbf{1}$ . However, addition of SCN $^-$  ( $\sim 0.45$  eq) to  $\mathbf{1}$  displayed the pattern similar to that of  $\mathbf{1} + N_3^-$  but upon increasing the equivalents of SCN $^-$ , well-resolved chemical resonances were observed (Figure 20).



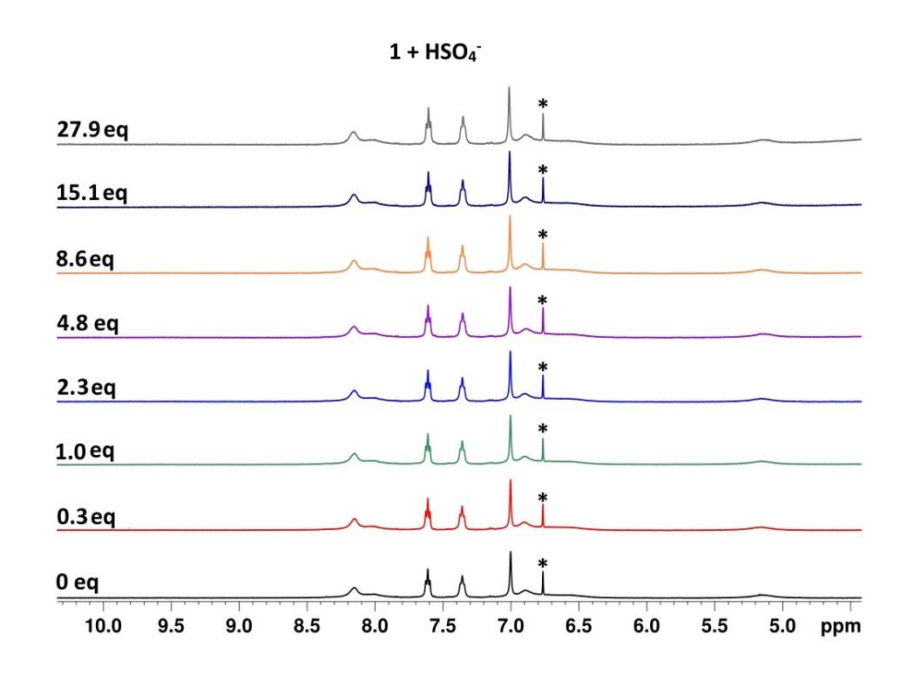
**Figure 20.** Partial  ${}^{1}\text{H}-\text{NMR}$  spectra of **1** and **1** (4.76 x  $10^{-3}$  M) with various equivalents of TBASCN in DMSO- $d_6$  at 298 K.

No significant changes were observed in the <sup>1</sup>H–NMR pattern of **1** for NO<sub>3</sub><sup>-</sup> and HSO<sub>4</sub><sup>-</sup> anions (Figure 21–22). The addition of ClO<sub>4</sub><sup>-</sup> does induce some changes in the conformation of **1** leading to the appearance of two sets of protons, major one corresponding to free **1** (Figure 23). This suggests that the cage does not interact with NO<sub>3</sub><sup>-</sup> and HSO<sub>4</sub><sup>-</sup> but interacts very weakly with ClO<sub>4</sub><sup>-</sup> anions. From the above experiments it can be inferred that the cage favors interaction with spherical and linear anions over other shapes.

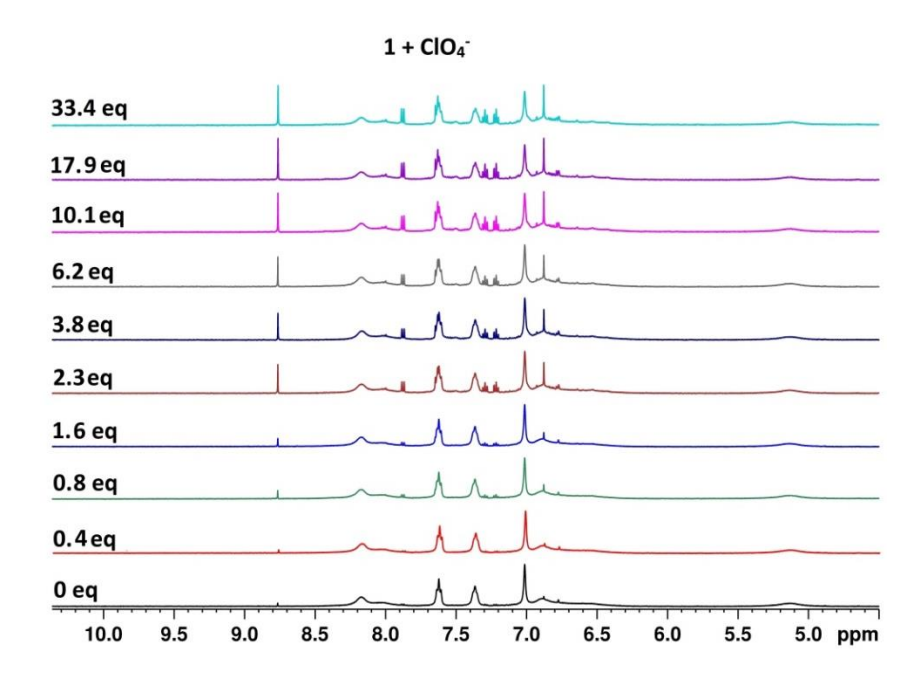




**Figure 21.** Partial <sup>1</sup>H–NMR spectra of **1** and **1** (4.88 x  $10^{-3}$  M) with various equivalents of TBANO<sub>3</sub> in DMSO– $d_6$  at 298 K.



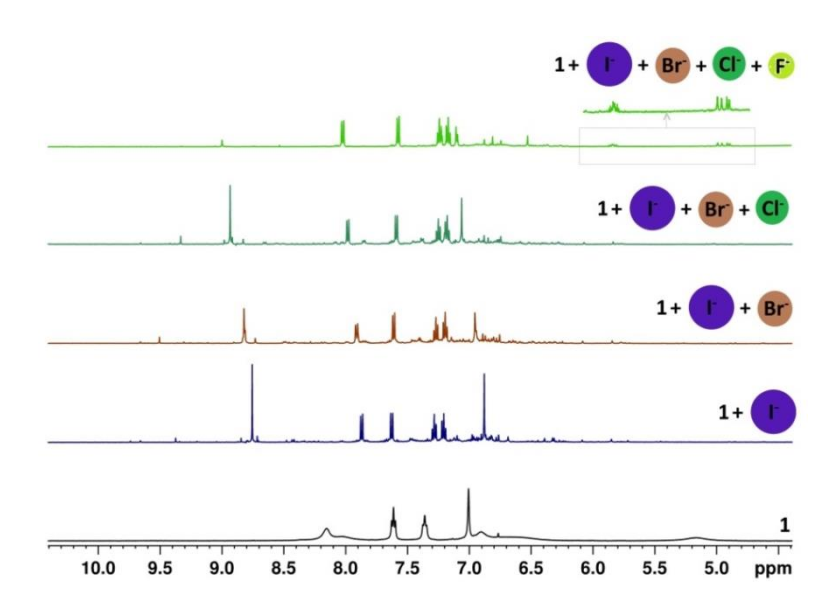
**Figure 22.** Partial  ${}^{1}\text{H-NMR}$  spectra of **1** and **1** (5.3 x  $10^{-3}$  M) with various equivalents of TBAHSO<sub>4</sub> in DMSO- $d_6$  at 298 K (\* mesitylene solvent peak).



**Figure 23.** Partial  ${}^{1}\text{H}-\text{NMR}$  spectra of **1** and **1** (4.56 x  $10^{-3}$  M) with various equivalents of TBAClO<sub>4</sub> in DMSO- $d_6$  at 298 K.

Anion competing studies. The anion competing behavior was investigated by sequential addition of various TBAX ( $X = CI^-$ ,  $Br^-$ ,  $F^-$ ) salts to the solution of  $\mathbf{1} + \Gamma$ . The  $^1H$ -NMR for  $\mathbf{1} + \Gamma + Br^-$  and  $\mathbf{1} + \Gamma + Br^- + CI^-$  shows slight changes in the chemical resonances whereas the addition of  $F^-$  to  $\mathbf{1} + \Gamma + Br^- + CI^-$  results in the disappearance of  $H^{a(L)}$ ; appearance of a new doublet at 7.01 ppm (J = 6.35 Hz), a doublet of doublet at 4.90 ppm for methylene protons and a multiplet at 5.8 ppm (Figure 24). Similarly, the addition of  $CI^-$  to  $\mathbf{1} + Br^-$  results in decreased intensity and splitting for  $H^{a(L)}$  and  $H^{A(im)}$ . Both the protons are downfield shifted as compared to  $\mathbf{1} + Br^-$ . The intensity of triplet at 9.65 ppm is increased w.r.t other aromatic protons. Addition of  $F^-$  to the same solution resulted in the appearance of a very prominent doublet of doublet at 4.90 ppm along with a multiplet at 5.8 ppm as observed for  $1 + F^-$ . The peak intensity of  $H^b$  is enhanced whereas for  $H^a$  is decreased. The

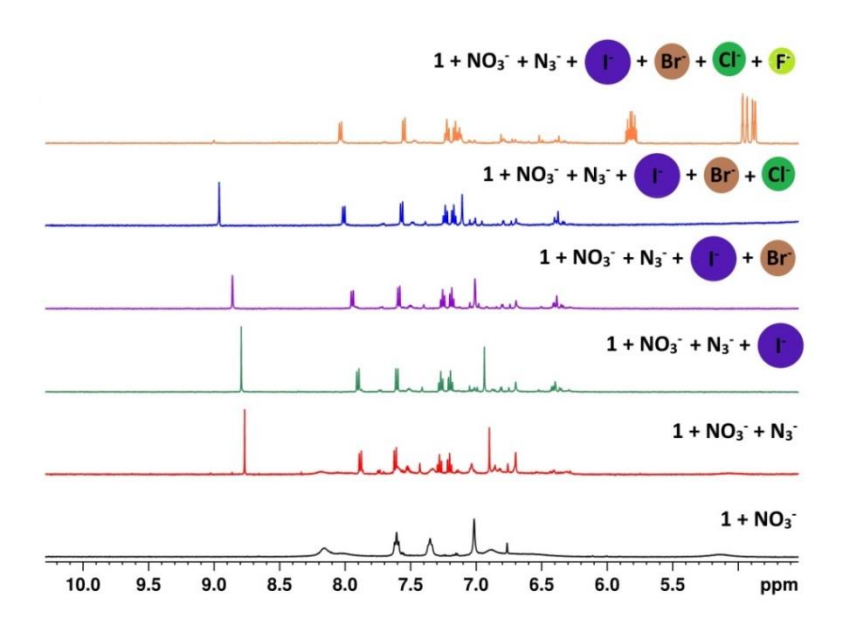
small peaks in the region 8–10 ppm completely disappeared. Both the studies suggest that  $F^-$  interacts more strongly with **1** as compared to  $\Gamma/Br^-/Cl^-$ .



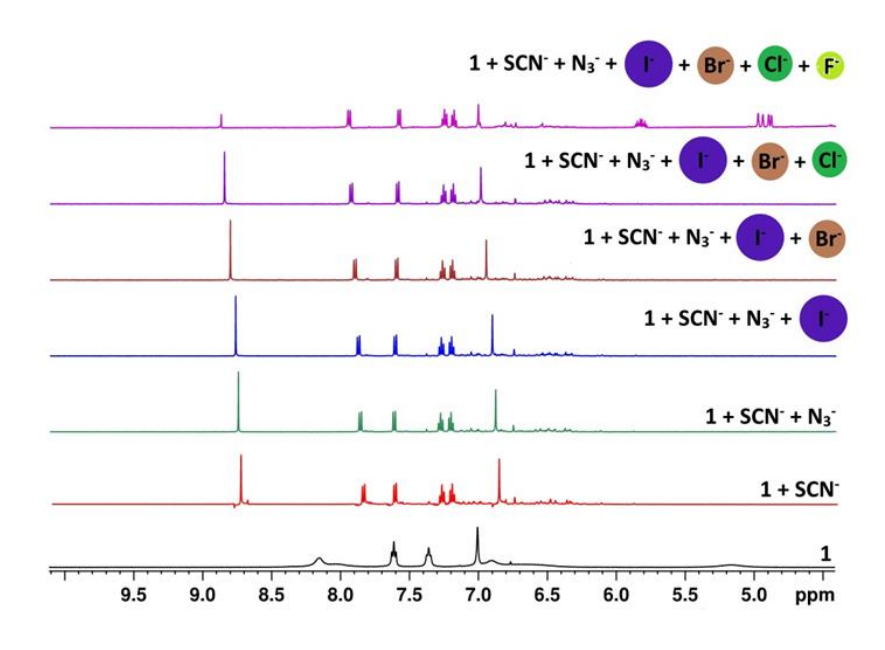
**Figure 24.** Partial <sup>1</sup>H–NMR of **1** +  $\Gamma$  and 1 +  $\Gamma$  with various tetrabutylammonium salts, TBAX (X = Br<sup>-</sup>, Cl<sup>-</sup>, F<sup>-</sup>) sequentially added in DMSO– $d_6$  at 298 K.

To further check the selectivity of the system, the competing experiments were carried out by adding TBAX salts ( $X = N_3^-$ ,  $\Gamma$ ,  $Br^-$ ,  $Cl^-$ ,  $F^-$ ) to the solution of  $\mathbf{1} + NO_3^-$  and  $\mathbf{1} + SCN^-$ . The changes in the spectrum of  $\mathbf{1} + NO_3^-$  suggests that upon sequential addition of  $N_3^-$ ,  $\Gamma$ ,  $Br^-$  and  $Cl^-$ , slight downfield shifts were observed for all the protons except  $H^{c,d}$ , whereas the addition of  $F^-$ , results in a different pattern with the disappearance of  $H^{a(L)}$  and  $H^{A(im)}$  and appearance of new peaks at 4.9 ppm and 5.8 ppm as observed for  $\mathbf{1} + F^-$  (Figure 25). Similar results were observed for the addition of various TBAX salts ( $X = N_3^-$ ,  $\Gamma$ ,  $Br^-$ ,  $Cl^-$ ,  $F^-$ ) in the solution of  $\mathbf{1} + SCN^-$  with prominent changes on addition of fluoride (Figure 26). The competing studies suggest that as the

size of spherical anion decreases, the anion interacts more favorably with 1.

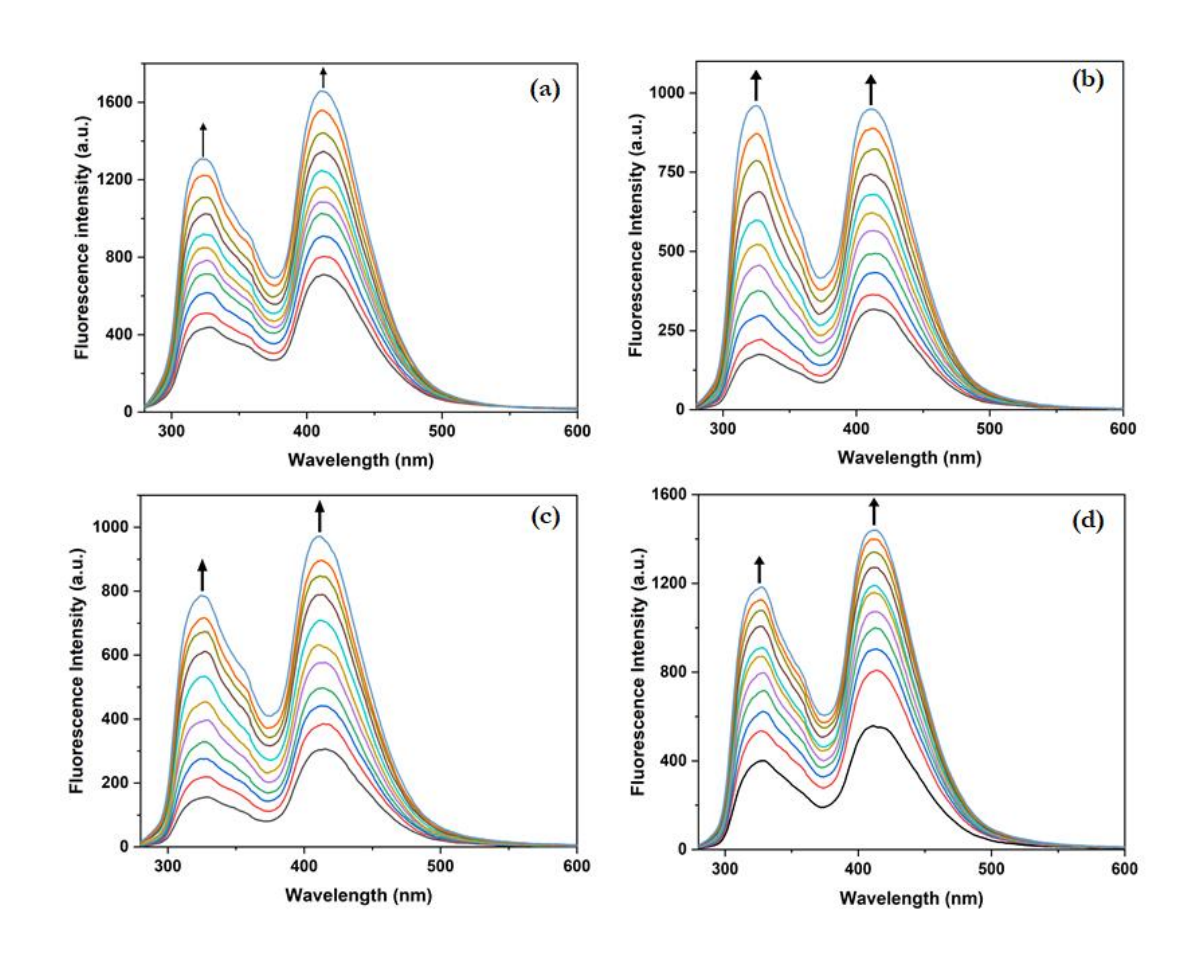


**Figure 25.** Partial  ${}^{1}\text{H-NMR}$  of  $\mathbf{1} + \mathrm{NO_3}^{-}$  and  $\mathbf{1} + \mathrm{NO_3}^{-}$  with various tetrabutylammonium salts, TBAX (X = N<sub>3</sub><sup>-</sup>,  $\Gamma$ , Br<sup>-</sup>, Cl<sup>-</sup>, F<sup>-</sup>) sequentially added in DMSO- $d_6$  at 298 K.



**Figure 26.** Partial  ${}^{1}H$ -NMR of  $\mathbf{1} + SCN^{-}$  and  $\mathbf{1} + SCN^{-}$  with various tetrabutylammonium salts, TBAX (X = N<sub>3</sub> $^{-}$ ,  $\Gamma$ , Br $^{-}$ , Cl $^{-}$ , F $^{-}$ ) sequentially added in DMSO- $d_6$  at 298 K.

Anion binding studies of 1 using fluorescence spectroscopy. To quantify the binding affinity of 1 towards spherical (F<sup>-</sup>, Cl<sup>-</sup>, Br<sup>-</sup> and  $\Gamma$ ), linear (N<sub>3</sub><sup>-</sup> and SCN<sup>-</sup>) and anions of other shapes (NO<sub>3</sub><sup>-</sup>, HSO<sub>4</sub><sup>-</sup>, ClO<sub>4</sub><sup>-</sup>), fluorescence titration studies were performed in acetonitrile solution at room temperature. During the titration host concentration was kept constant and addition of appropriate aliquots of guest (F<sup>-</sup>/Cl<sup>-</sup>/Br<sup>-</sup>/ $\Gamma$ /N<sub>3</sub><sup>-</sup>/SCN<sup>-</sup>) to 1 resulted in enhancement of the emission intensity for both the bands (317 and 411 nm) (Figure 27). A slight red-shift of 2–4 nm was observed for both the bands upon addition of fluoride anion. However, the addition of NO<sub>3</sub><sup>-</sup>, HSO<sub>4</sub><sup>-</sup> and ClO<sub>4</sub><sup>-</sup> to 1 did not show any constant enhancement or quenching instead fluctuating emission intensities were observed for each set. Thus, the value of binding constant cannot be determined for these anions.



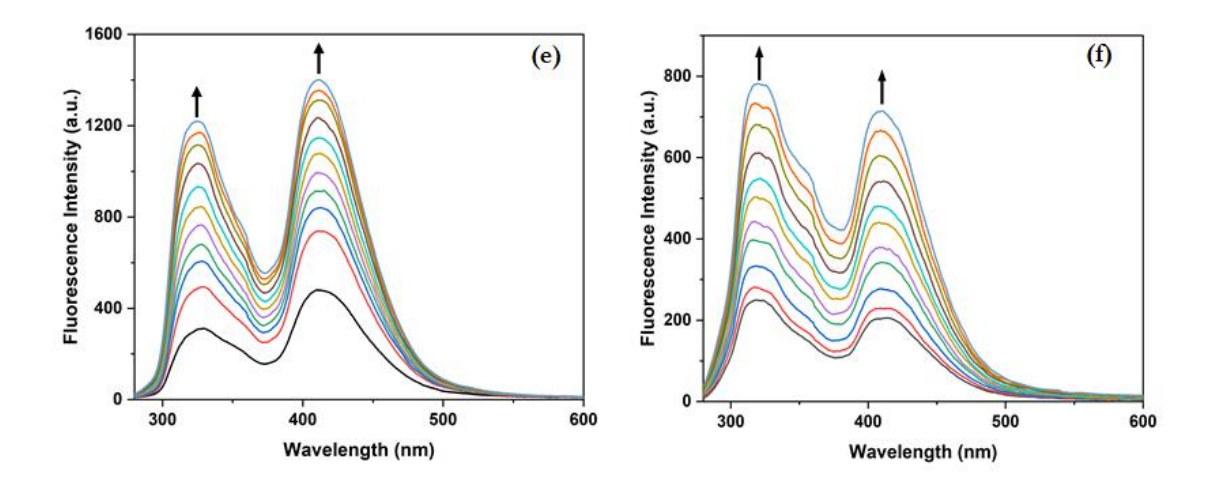


**Figure 27.** Fluorescence spectra of **1** (8.67 × 10<sup>-5</sup> M) upon titration with appropriate aliquots of tetrabutylammonium salts of spherical anions; (a)  $F^-$ ; (b)  $CI^-$ ; (c)  $Br^-$ ; (d)  $\Gamma$  and linear anions; (e)  $N_3^-$ ; (f)  $SCN^-$  in  $CH_3CN$  at room temperature.

The binding constant values for spherical and linear anions were calculated using Benesi-Hildebrand equation.<sup>11</sup> The linear regression analysis carried out at 411 nm suggested 1 : 1 host: guest stoichiometry (Figure 28–33).

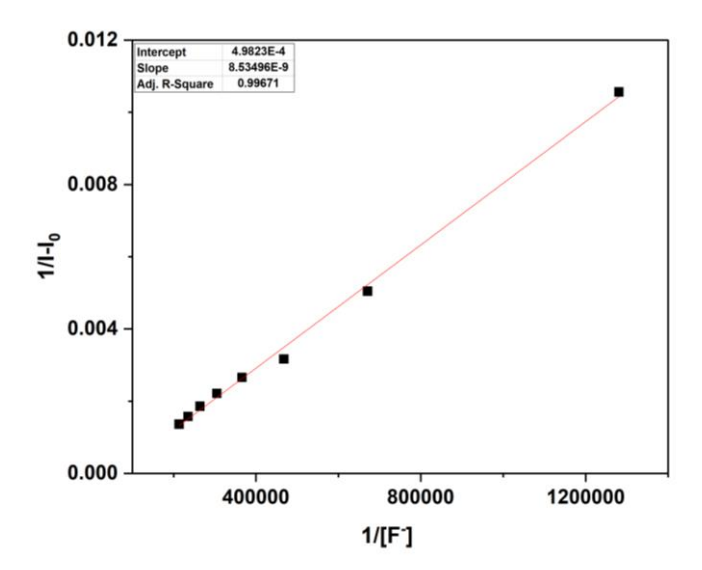


**Figure 28**. Benesi-Hildebrand plot for the emission enhancement of host **1** (at 411 nm) with increasing fluoride (F<sup>-</sup>) concentration in CH<sub>3</sub>CN at room temperature.

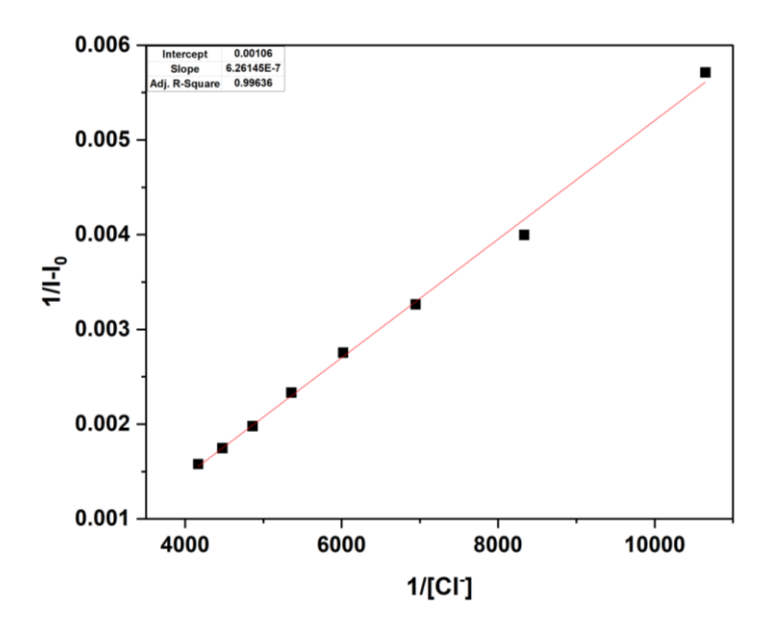


**Figure 29**. Benesi–Hildebrand plot for the emission enhancement of host **1** (at 411 nm) with increasing chloride (Cl<sup>-</sup>) concentration in CH<sub>3</sub>CN at room temperature.

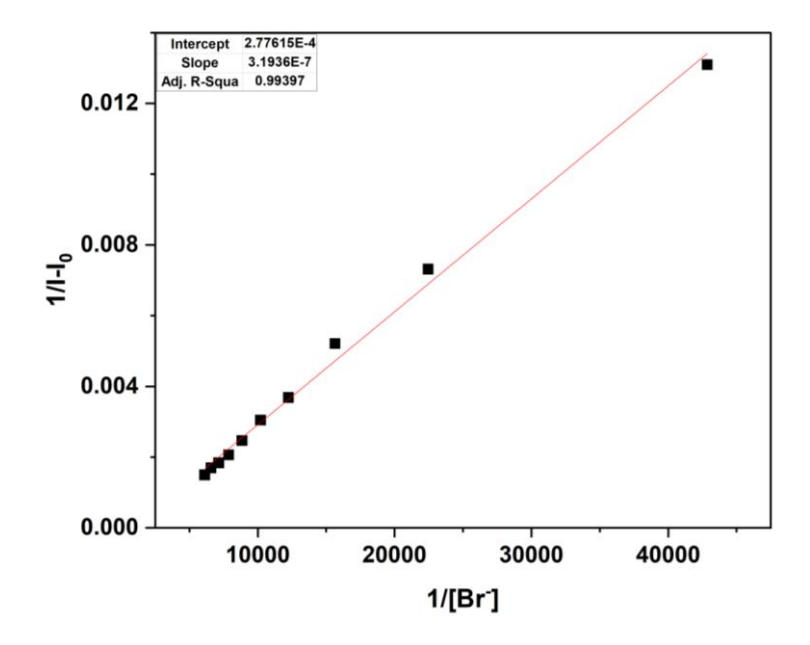


**Figure 30**. Benesi–Hildebrand plot for the emission enhancement of host **1** (at 411 nm) with increasing bromide (Br<sup>-</sup>) concentration in CH<sub>3</sub>CN at room temperature.

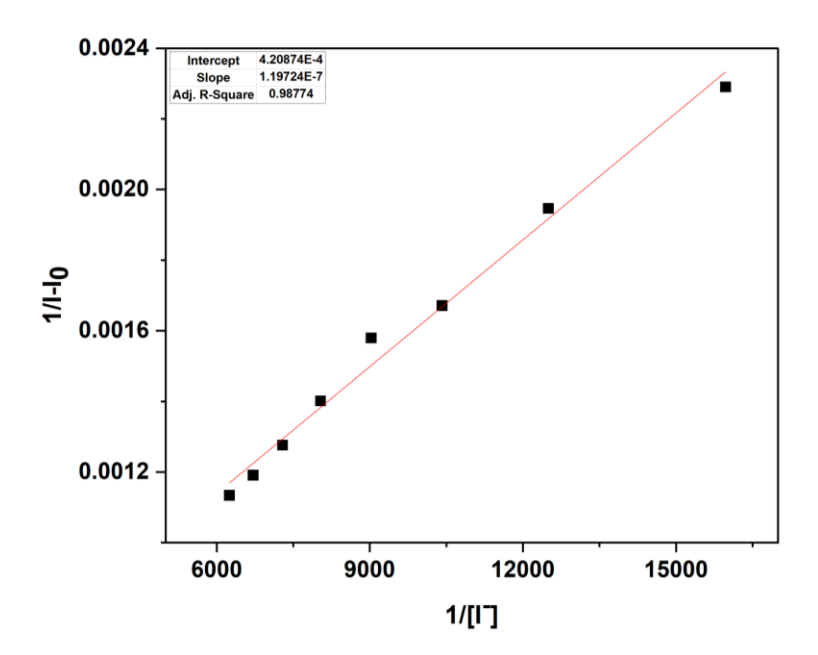


**Figure 31**. Benesi–Hildebrand plot for the emission enhancement of host **1** (at 411 nm) with increasing iodide ( $\Gamma$ ) concentration in CH<sub>3</sub>CN at room temperature.

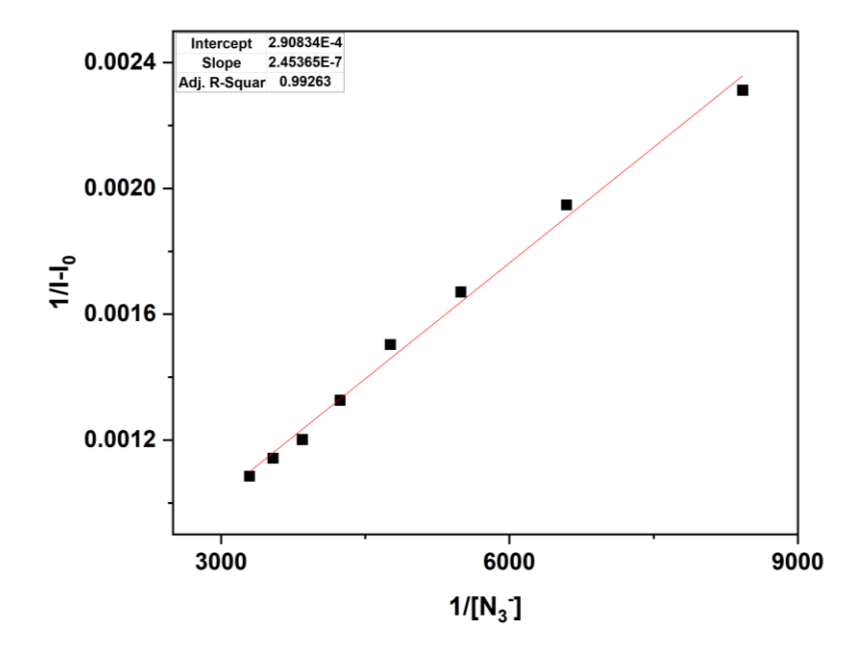


**Figure 32.** Benesi-Hildebrand plot for the emission enhancement of host **1** (at 411 nm) with increasing azide  $(N_3^-)$  concentration in CH<sub>3</sub>CN at room temperature.

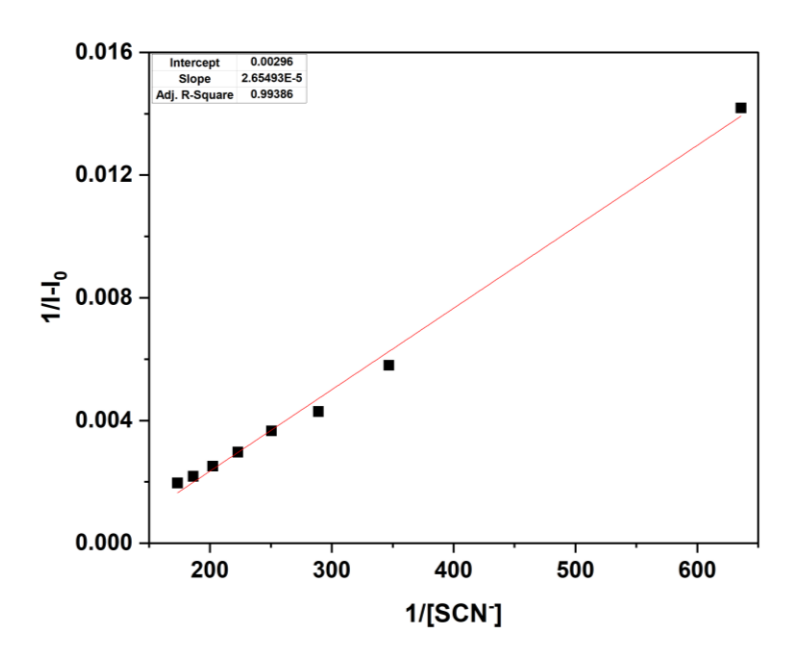


**Figure 33.** Benesi–Hildebrand plot for the emission enhancement of host **1** (at 411 nm) with increasing thiocyanate (SCN<sup>-</sup>) concentration in CH<sub>3</sub>CN at room temperature.

**Table 2.** Binding constant,  $K_b$  ( $M^{-1}$ ) for cage 1 with various spherical and linear anionic guests calculated using fluorescence titration in CH<sub>3</sub>CN at 298 K.

Anions	Binding constant, $K_b$ (M <sup>-1</sup> ) with 1
F	$5.84 \times 10^4$
Cl <sup>-</sup>	$2.65 \times 10^{3}$
$\mathrm{Br}^-$	$8.69 \times 10^2$
Γ	$3.52\times10^3$
$N_3^-$	$1.14 \times 10^{3}$
$SCN^-$	$1.1\times10^2$

The values of binding constant for spherical and linear anions are in the range of  $10^4$ – $10^2$  M<sup>-1</sup> (Table 2). The studies suggest that host **1** interacts strongly with fluoride anion whereas moderate to weak association was observed in case of other anions.

# 2.3. Experimental Section

#### General Data

Re<sub>2</sub>(CO)<sub>10</sub>, carbonyldiimidazole (CO-im<sub>2</sub>), 1,2,4-triazole (tz), NaH (55–60 %) in mineral oil, TBAX·nH<sub>2</sub>O (X = F/Cl/Br/I/N<sub>3</sub>/SCN/NO<sub>3</sub>/HSO<sub>4</sub>/ClO<sub>4</sub>), mesitylene and spectroscopic solvents DMSO and acetonitrile were purchased from commercial sources and used as received. Bis(benzimidazolyl)methane ligand (L) was prepared by modifying the previously reported method. ATR-IR spectrum was recorded on a Nicolet iS5 IR spectrophotometer. NMR spectra were recorded on a Bruker AVANCE III 500 MHz instrument. ESI-MS spectra were recorded on Bruker-maXis mass spectrometer. Fluorescence spectra were recorded on a JASCO FP8500 spectrophotometer.

**Synthesis of** [{fac-Re(CO)<sub>3</sub>(im)}<sub>4</sub>L<sub>2</sub>] (1). A mixture of Re<sub>2</sub>(CO)<sub>10</sub> (100.2 mg, 0.153 mmol), L (28.5 mg, 0.115 mmol), CO-im<sub>2</sub> (24.81 mg, 0.153 mmol), and mesitylene (10 mL) was taken in a teflon vessel. The vessel was placed inside a stainless steel bomb and kept in an oven maintained at 160 °C for 48 h further allowed to cool up to 30 °C. The white crystals were obtained, washed with hexane and air-dried. Yield: 27 % (37.7 mg). AT-IR ( $v_{max}$ , cm<sup>-1</sup>): 2008, 1896 and 1854 (CO). ESI-MS. Calcd. for C<sub>54</sub>H<sub>36</sub>N<sub>16</sub>O<sub>12</sub>Re<sub>4</sub> [1 + H]<sup>+</sup>: m/z 1847.0767, found: m/z 1847.0978. <sup>1</sup>H NMR (500 MHz, DMSO- $d_6$ , at 298 K):  $\delta$  8.16–8.05 (br, 8H), 7.63–7.59 (t, 6H), 7.37–7.34 (t, 5H), 7.01 (s, 5H), 6.9–6.59 (br, 9H), 5.15-5.14 (br, 3H). At 373 K:  $\delta$  8.12 (d, 4H, J = 8.3 Hz, H<sup>e</sup>), 7.94 (s, 4H, H<sup>a</sup>), 7.62–7.59 (t, 4H, H<sup>c</sup>), 7.41–7.37 (t, 4H, H<sup>d</sup>), 7.05 (d, 4H, J = 8.3 Hz, H<sup>b</sup>), 7.02 (s, 4H, H<sup>A</sup>), 6.67 (s, 8H, H<sup>B,C</sup>), 5.39 (s, 4H, H<sup>f</sup>).

**Synthesis of** [ $\{fac\text{-Re}(CO)_3(tz)\}_4L_2$ ] (2). A mixture of Re<sub>2</sub>(CO)<sub>10</sub> (100.1 mg, 0.153 mmol), L (38.05 mg, 0.153 mmol), 1,2,4-tz (21.2 mg, 0.306 mmol), and toluene : acetone (8:1 mL) was

taken in a teflon vessel. The vessel was placed inside a stainless steel bomb and kept in an oven maintained at 180 °C for 48 h further allowed to cool up to 30 °C. White powder was obtained, washed with hexane and air-dried. Yield: 74 % (104 mg). ATR-IR ( $v_{max}$ , cm<sup>-1</sup>): 2020 and 1872 (CO). ESI-MS. Calcd. for  $C_{50}H_{32}N_{20}O_{12}Re_4$  [2 + H]<sup>+</sup>: m/z 1851.0789, found: m/z 1851.0884. <sup>1</sup>H NMR (500 MHz, DMSO-  $d_6$ , at 298 K):  $\delta$  8.76 (s, 4H, H<sup>a</sup>), 8.30 (s, 8H, H<sup>A,B</sup>), 7.88 (d, 4H, J = 8 Hz, H<sup>b</sup>), 7.64 (d, 4H, J = 8 Hz, H<sup>b</sup>), 7.31-7.27 (m, 4H, H<sup>c</sup>), 7.22-7.19 (m, 4H, H<sup>d</sup>), 6.87 (s, 4H, H<sup>f</sup>).

NMR titration procedure for anion recognition. Complex 1 was dissolved in 0.5 mL DMSO- $d_6$  and TBAX.nH<sub>2</sub>O (X = F/Cl/Br/I/N<sub>3</sub>/SCN/NO<sub>3</sub>/HSO<sub>4</sub>/ClO<sub>4</sub>) stock solution was prepared in DMSO- $d_6$  (0.6 mL). Aliquots of the anion solutions were sequentially added to the 0.5 mL host solution. The solution was heated, allowed to cool at room temperature and then NMR spectra were recorded at 298 K.

General procedure for the calculation of binding constants using fluorescence spectroscopy. The anion binding ability of **1** with spherical (F̄, Cl̄, Br̄ and  $\Gamma$ ), linear (N<sub>3</sub>¯ and SCN¯) and anions of other shapes (NO<sub>3</sub>¯, HSO<sub>4</sub>¯, ClO<sub>4</sub>¯) was determined using fluorescence spectroscopy. The stock solution of cage **1** (1.73 × 10<sup>-4</sup> M) was prepared by dissolving 3.2 mg of **1** in a mixture of DMSO: CH<sub>3</sub>CN (0.5/9.5 mL, v/v). The guest stock solutions (10<sup>-5</sup> M) were prepared by dissolving appropriate amount of tetrabutylammonium salts in CH<sub>3</sub>CN (5 mL). During the titration, the concentration of host was kept constant and the appropriate amount of guest was added sequentially. The emission spectra were recorded for each set at an excitation wavelength of 265 nm and slit width of 5 nm. The value of binding constant was calculated using Benesi–Hildebrand equation for a 1:1 host–guest stoichiometry. <sup>11</sup>

 $[1/\Delta I = 1/\Delta I_{\text{max}} + (1/K[G]\Delta I_{\text{max}})]$ 

Here,  $\Delta I_{\text{max}} = I_{\text{max}} - I_0$ ,  $\Delta I = I - I_0$ ,  $I_0$  is the emission intensity of free host 1,

I is the emission intensity after addition of guest to 1

 $I_{max}$  is the emission intensity after adding excess of guest

K is the binding constant, and [G] is the concentration of guest.

**X-ray crystallography.** The single crystal X-ray diffraction data were collected at 296(2) K on Rigaku Oxford XtaLAB synergy and Bruker D8 quest diffractometer equipped with Mo–K $\alpha$  radiation ( $\lambda = 0.71073$ Å) source. Cell refinement and data reduction was performed using CrysAlisPro and Bruker APEX 2 software programs. The structure solutions and refinements were performed with OLEX and SHELX program package. Non–hydrogen atoms were refined anisotropically. Some of the lattice solvent molecules in  $\mathbf{1} \cdot (H_2O) \cdot (DMSO)$  could not be modelled. The detailed crystallographic data of  $\mathbf{1}$  and  $\mathbf{1} \cdot (H_2O) \cdot (DMSO)$  are given in Table 1.

## 2.4. Conclusion

Two flexible neutral heteroleptic tetranuclear coordination cages, [ $\{fac\text{-Re}(CO)_3(L')\}_4L_2$ ] (where L' = carbonyldiimidazole for 1/1,2,4-tetrazole for 2 possessing flexible multiple electron deficient C–H donors were self–assembled via one pot solvothermal approach. The cages are thermally stable and flexible in solution. The anion recognition and anion competing studies using  $^1H$ -NMR spectroscopy suggested that the cage 1 reorganizes itself on addition of spherical and linear anions. However, it selectively recognizes fluoride in the presence of mixture of anions. The fluorescence titration studies further suggested that among all spherical and linear anions showing moderate to weak association, fluoride interacts more strongly with 1. The research provides a new approach towards the synthesis of fac-Re(CO) $_3$  core based flexible cages using semi-rigid linker motifs. The research on cages of different shape, sizes and nuclearity by tuning the ligand motifs and/or by incorporating long aliphatic linkers is under progress in our laboratory.

### 2.5. References

- (a) R. Saha, B. Mondal, P. S. Mukherjee, *Chem. Rev.* 2022, 122, 12244–12307; (b) S. Samantray, S. Krishnaswamy, D. K. Chand, *Nat. Commun.* 2020, 11, 1-8; (c) N. Busschaert, C. Caltagirone, W. V. Rossom, P. A. Gale, *Chem. Rev.* 2015, 115, 8038–8155; (d) C. Liu, Y. Zhang, Q. An, *Chem Asian J.* 2021, 16, 1–19; (e) D. Chakraborty, P. S. Mukherjee, *Chem. Commun.*, 2022, 58, 5558–5573; (f) J. M. Stauber, G. E. Alliger, D. G. Nocera, C. C. Cummins, *Inorg. Chem.* 2017, 56, 7615–7619; (g) H. Xie, T. J. Finnegan, V. W. L. Gunawardana, R. Z. Pavlovic, C. E. Moore, J. D. Badjic, *J. Am. Chem. Soc.* 2021, 143, 3874–3880; (h) J. Esteban, M. Font–Bardia, A. Escuer, *Inorg. Chem.* 2014, 53, 1113-1121.
- (a) E. G. Percastegui, T. K. Ronson, J. R.Nitschke, *Chem. Rev.* 2020, **120**, 13480–13544; (b)
   D. L. Caulder, R. E. Powers, T. N. Parac, K. N. Raymond, *Angew. Chem. Int. Ed.* 1998, **37**, 1840–1843; (c) X. Zhu, D. Luo, X. Zhou, D. Li, *Coord. Chem. Rev.*, 2022, **455**, 214354; (d)
   A. Escuer, J. Esteban, M. Font-Bardia, *Chem. Commun.* 2012, **48**, 9777–9779; (e) G. H. Clever, P. Punt, *Acc. Chem. Res.* 2017, **50**, 2233–2243; (f) R. Li, A. Marcus, F. Fadaei-Tirani, K. Severin, *Chem. Commun.*, 2021, **57**, 10023–10026.
- (a) L. Liang, W. Zhao, X. Yang, B. Wu, Acc. Chem. Res. 2022, 55, 3218–3229; (b) S. Bandi, A. K. Pal, G. S. Hanan, D. K. Chand, Chem. Eur. J. 2014, 20, 13122–13126; (c) C. Klein, C. Gütz, M. Bogner, F. Topic´, K.Rissanen, A. Lützen, Angew. Chem. Int. Ed. 2014, 53, 3739–3742; (d) G. Sarada, A. Kim, D. Kim, O. Jung, Dalton Trans., 2020, 49, 6183–6190. (e) A. Schmidt, A. Casini, F. E. Kühn, Coord. Chem. Rev. 2014, 275, 19–36; (f) I. Mishra, M. Bhol, P. Kalimuthu, M. Sathiyendiran, Chem.Rec. 2021, 21, 594–614. (g) H. Takesawa, M. Fujita, Bull. Chem. Soc. Jpn. 2021, 94, 2351–2369.
- (a) P. D. Beer, P. A. Gale, Angew. Chem. Int. Ed. 2001, 40, 486–516.
   (b) U. Manna, S. Kayal, B. Nayak, G. Das, Dalton Trans., 2017, 46, 11956–11969.
   (c) T. Xie, C. Guo, S. Yu,

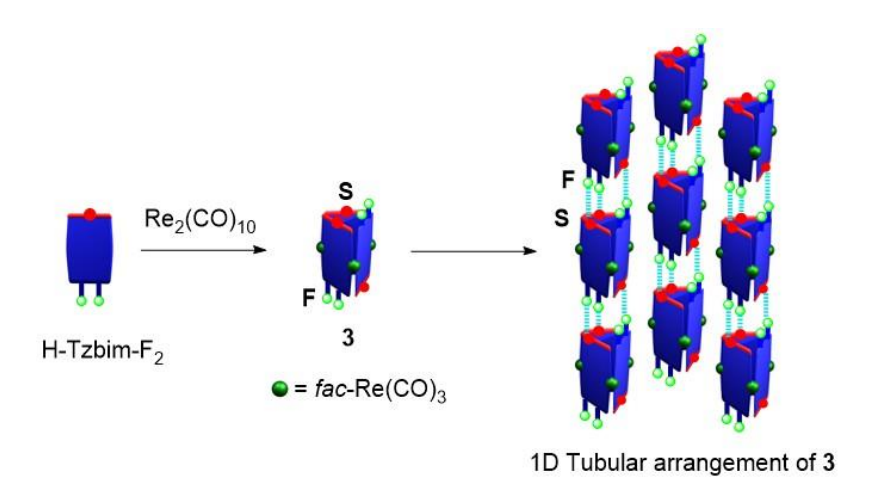
- Y Pan, Angew. Chem. Int. Ed. 2012, **51**, 1177–1181; (d) V. Amendola, L. Fabbrizzi, L. Mosca, Chem. Soc. Rev., 2010, **39**, 3889–3915; (e) J. Esteban, M. Font–Bardia, A. Escuer, Inorg. Chem. 2014, **53**, 1113-1121.
- (a) T. Zhang, L. Zhou, X. Guo, L. Cai, Q. Sun, *Nat. Commun.* 2017, 8, 15898; (b) W. Deng,
   Z. Yu, H. Ma, S. Yu, *Chem. Asian J.* 2018, 13, 2805–2811; (c) H. Lü, Y. Mu, J. Li, D. Wu,
   H. Hou, Y. Fan, *Inorg. Chim. Acta* 2012, 387, 450–454; (d) J. Li, X. Li, H. Lü, Y. Zhu, H.
   Sun, X. Y.Guo, Z. Yue, J. Zhao, M. Tang, H.Hou, Y. Fan, J. Chang, *Inorg. Chim. Acta*,
   2012, 384, 163–169.
- (a) S. Li, T. Zhang, X. Deng, X.Guo, L. Zhou, F.Guo, Q. Sun, *Inorg. Chem. Commun.*, 2018, 92, 69–73;
   (b) W. Du, J. Tong, W. Deng, M. Wang, S. Yu, *Chinese Chemical letters*, 2021, 32, 485-488;
   (c) R. Dutta, P. Ghosh, *Chem. Commun.* 2014, 50, 10538–10554;
   (d) Y. Wu, C. Zhang, S. Fang, D. Zhu, Y. Chen, C. Ge, H. Tang, H. Li, *Angew. Chem. Int. Ed.* 2022, 61, 1–6.
- (a) M. C. Naranthatta, V. Ramkumar, D. K. Chand, *J. Chem. Sci.*, 2015, 127, 273–280; (b)
   R. Saha, A. K. Ghosh, R. N. Samajdar, P. S. Mukherjee, *Inorg. Chem.* 2018, 57, 6540–6548; (c) M. Karthikeyan, R. Govindarajan, C. A. Kumar, U. Kumar, B. Manimaran, *J. Organomet. Chem.* 2018, 866, 27–34; (d) T. Tateishi, M. Yoshimura, S. Tokuda, F. Matsuda, D. Fujita, S. Furukawa, *Coord. Chem. Rev.* 2022, 467, 214612; (e) S. Pal, T. K. Ghosh, R. Ghosh, S. Mondal, P. Ghosh, *Coord. Chem. Rev.* 2020, 405, 213128.
- 8. (a) M. Kedia, B. Shankar, M. Sathiyendiran, *Inorg. Chem.* 2022, **61**, 14506–14510; b) B. Shankar, F. Hussain, M. Sathiyendiran, *J. Organomet. Chem.* 2012, **719**, 26–29; (c) B. Shankar, P. Elumalai, R. Shanmugam, M. Sathiyendiran, *J. Organomet. Chem.* 2014, **749**, 224–232; (c) S. M. Lin, M. Velayudham, C. H. Tsai, C. H. Chang, C. C. Lee, C. C. Luo, P. Thanasekaran, K. L. Lu, *Organometallics* 2014, **33**, 40–44. (d) M. Kedia, M. Priyatharsini,

- S. D. Sathiyashivan, B. Shankar, R. V. Krishnakumar, M. Sathiyendiran, *J. Organomet. Chem.* 2022, **959**, 122123–122129.
- (a) S. Guha, S. Saha, J. Am. Chem. Soc. 2010, 132, 17674–17677. (b) S. K. Dey, G. Das, Chem. Commun. 2011, 47, 4983–4985. (c) Z. Xu, N. J. Singh, S. K. Kim, D. R. Spring, K. S. Kim, J. Yoon, Chem. Eur. J. 2011, 17, 1163–1170.
- (a) V. Amendola, M. Boiocchi, L. Fabbrizzi, N. Fusco, Eur. J. Org. Chem. 2011, 32, 6434–6444.
   (b) H. J. Han, J. Hyun Oh, J. L. Sessler, S. K. Kim, Chem. Commun. 2019, 55, 10876–10879.
- 11. H. A. Benesi, J. H. Hildebrand, J. Am. Chem. Soc. 1949, **71**, 2703–2707.
- 12. N. Ahmed, B. Shirinfar, I. S. Youn, M. Yousuf, K. S. Kim, *Org. Biomol. Chem.*, 2013, **11**, 6407–6413.
- (a) SAINT and XPREP, version 5.1; Siemens Industrial Automation Inc.: Madison, WI, 1995.
   (b) G. M. Sheldrick, A short history of SHELX. *ActaCrystallogr. Sect. A: Found. Crystallogr.* 2008, 64, 112–122.
   (c) G. M. Sheldrick, Crystal structure refinement with SHELXL. *ActaCrystallogr., Sect. C: Struct. Chem.* 2015, 71, 3–8.

# **Chapter-3**

# Fluorine assisted self-assembly approach for tubular architecture of cyclic trinuclear rhenium(I)-fluorothiabendazolate complex

**ABSTRACT.** Three neutral trinuclear rhenium(I)-organic complexes, fac-[{Re(CO)<sub>3</sub>(L)}<sub>3</sub>] (1–3), were self-assembled from Re<sub>2</sub>(CO)<sub>10</sub> and thiabendazole/thiazolylnaphthanoimidazole/difluorothiabendazole (H–L) via one-pot approach. The molecular structures established by X-ray analysis revealed that 1–3 adopt M<sub>3</sub>L<sub>3</sub>-type triangular structure which consists of alternatively arranged three fac-[Re(CO)<sub>3</sub>] cores and three anionic ligand motifs. All three complexes possess uncoordinated sulfur atoms from thiazolyl motif that are directed along the complex axis. Complex 3 additionally possesses six C–F bonds, four at one end and two at rear, lateral to the complex axis which further self-organizes into 1D supramolecular tubular architecture via fluorine assisted noncovalent C–F···S contacts.



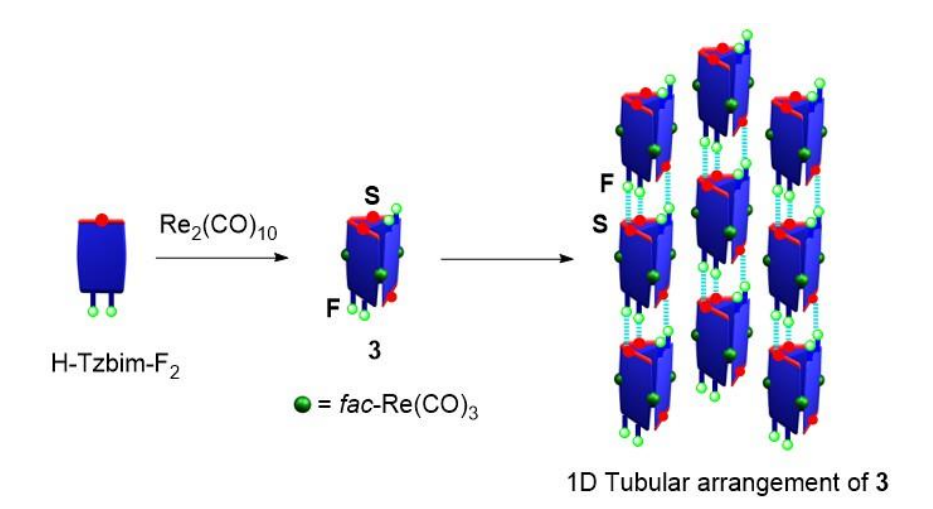
The photophysical properties of 1–3 were studied using UV-visible and fluorescence spectroscopy and further validated using time-dependent density functional theory (TDDFT) calculations. The

electrochemical properties of **1–3** were studied using cyclic voltammetry. The solution state studies for the formation of tubular structure were elucidated using concentration dependent NMR and UV-Visible spectroscopy along with low temperature NMR.

### 3.1. Introduction

The design and synthesis of simple to complex supramolecular coordination complexes (SCCs) are increasing tremendously due to their potential utility in various fields. <sup>1-8</sup> Among various SCCs, fac-[Re(CO)<sub>3</sub>] core-based SCCs are one of the important class of complexes having potential applications in molecular recognition, catalysis, sensors, bio-imaging and as anticancer agents.<sup>4-7</sup> Due to their significance, different shapes and sizes of Re(I) SCCs mono-/di-/trinuclear cycles, helicates, mesocates, squares, tetrahedrons, spheroids, and prisms have been emerging continuously.<sup>4-7</sup> Currently, the efforts are being directed towards incorporating functional groups on the cyclic framework of SCCs to construct higher order superstructures and functional materials. The design of ligand with precisely arranged donors and functional groups plays a vital role in deciding the structure and properties of SCCs. Until now, the use of ligands possessing both coordinating donors and properly embedded chalcogen/halogen donor/acceptor groups that can be utilized to construct higher order superstructures from self-assembled Re(I) SCCs is scarce. The literature reports show the increasing use of fluorine substituted ligands to construct functional metal-organic materials owing to their interesting properties and utility in various fields including catalysis, sensors, gas adsorption and drug delivery. 8 As a part of current study, electron rich heterocycles, thiabendazole and its derivatives, which fulfil both the criterion of possessing coordinating atoms and functional atom/groups (sulfur and fluorine) were utilized to construct Re(I) based SCCs. The studies on supramolecular architectures involving thiabendazole as coordinating ligand are limited.<sup>9</sup> This chapter reports new synthetic combinations for self-assembling discrete neutral homoleptic rhenium(I) core-based metal-organic triangular complexes possessing chalcogen (S)/halogen(F) donors/acceptors, which further self-organize into 1D tubular structure via

# C-F···S contacts (Scheme 1).



**Scheme 1**. Synthetic approach for discrete complex **3** and its self-organisation into 1D-tubular architecture *via* fluorine assisted C–F···S non–covalent contacts.

## 3.2. Results and Discussions

### Synthesis of complexes 1–3.

The discrete triangular complexes (1-3) with functional atoms on their cyclic framework are constructed using  $Re_2(CO)_{10}$  and 2-(4-thiazolyl)benzimidazole (H–Tzbim) for 1/2-(4-thiazolyl)naphthanoimidazole (H–Tznim) for 2/2-(4-thiazolyl)-5,6-difluorobenzimidazole (H–Tzbim–F<sub>2</sub>) for 3 in a one-pot solvothermal approach (Scheme 2). The complexes 1-3 are air, moisture stable and are soluble in DMSO,  $CH_3COCH_3$  and  $CH_3CN$ .

Scheme 2. Synthesis of 1–3.

The ATR-IR spectra of **1–3** displayed two strong bands in the region 1874–2022 cm<sup>-1</sup>, corresponding to the fac-[Re(CO)<sub>3</sub>] motif (Figure **1–3**).<sup>4-9</sup> The ESI-MS spectra of the compounds displayed molecular ion peak (m/z = 1411.9047 for [**1** + H]<sup>+</sup>, 1560.9608 for [**2**+

2H]<sup>+</sup>, and 1518.9047 for [**3**+ 2H]<sup>+</sup>) and their isotopic distribution peaks matches well with the theoretical values (Figure 4–6).

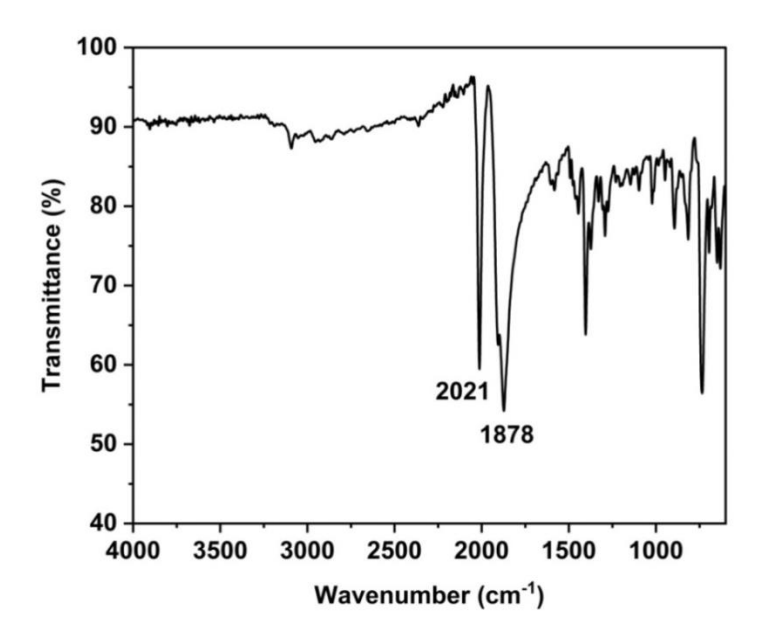


**Figure 1.** ATR–IR spectrum of complex **1**.

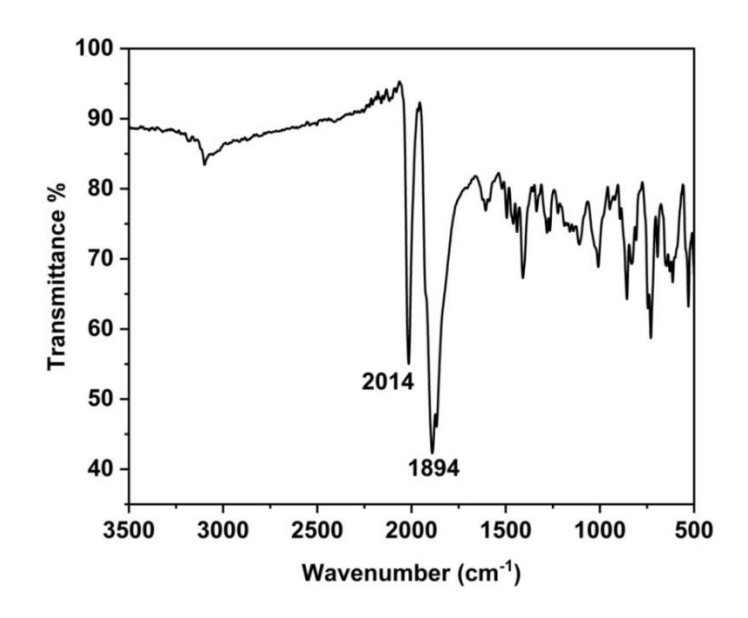
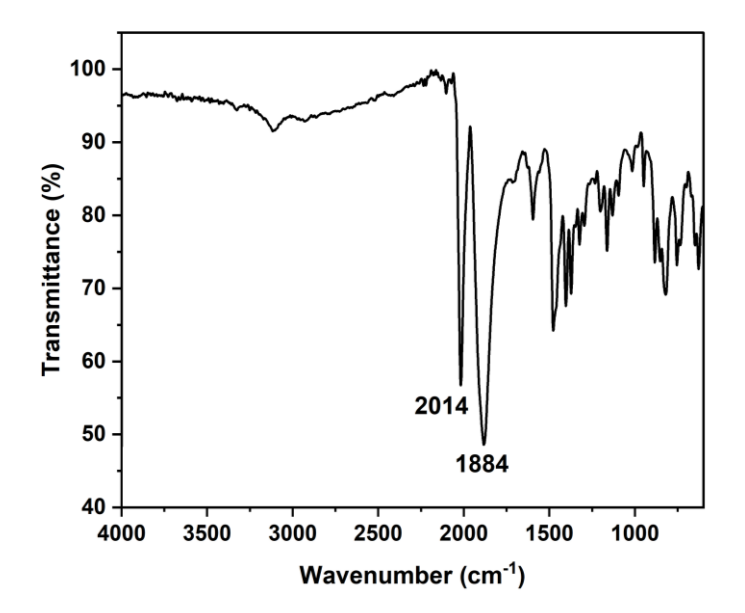
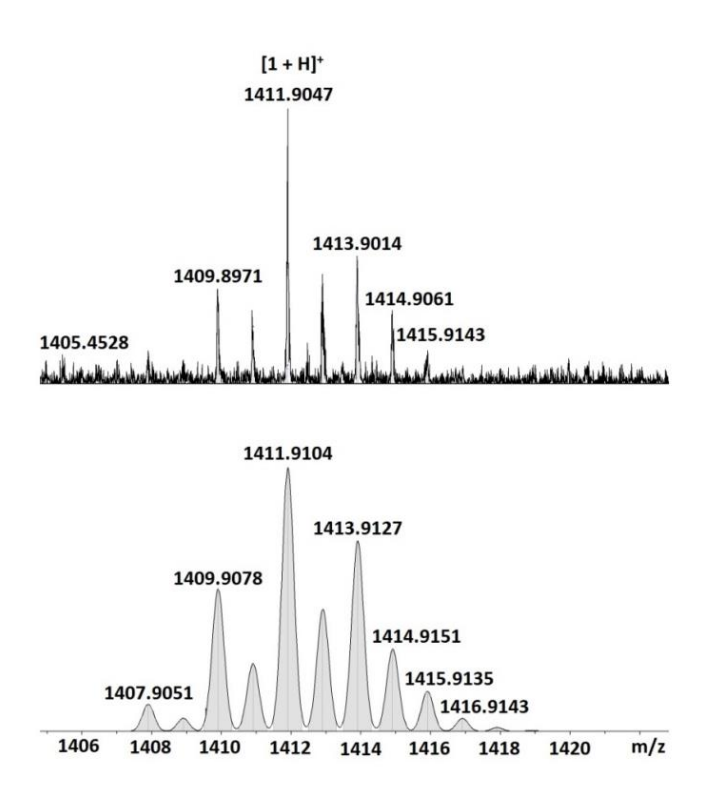


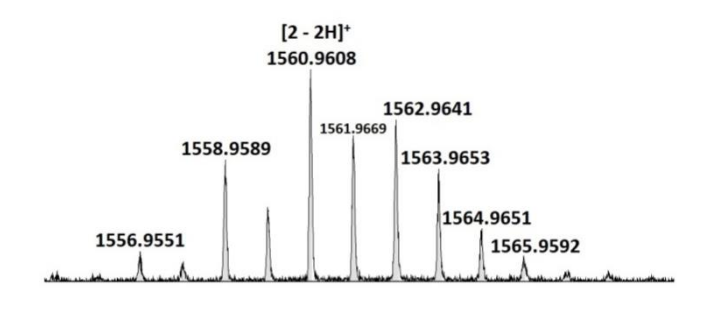
Figure 2. ATR–IR spectrum of complex 2.



**Figure 3.** ATR–IR spectrum of complex **3.** 



**Figure 4.** Experimental (Top) and calculated (Bottom) ESI mass spectra of  $[1 + H]^+$  in positive ion mode.



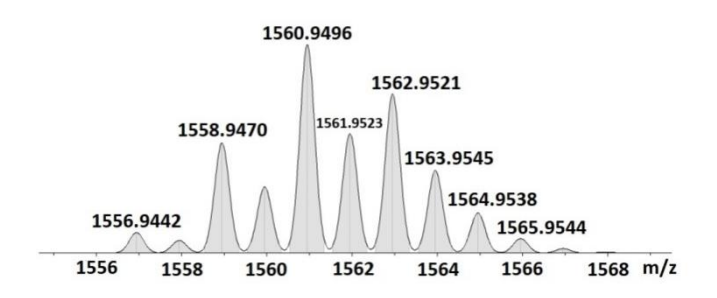


**Figure 5.** Experimental (Top) and calculated (Bottom) ESI mass spectra of  $[2 - 2H]^+$  in positive ion mode.

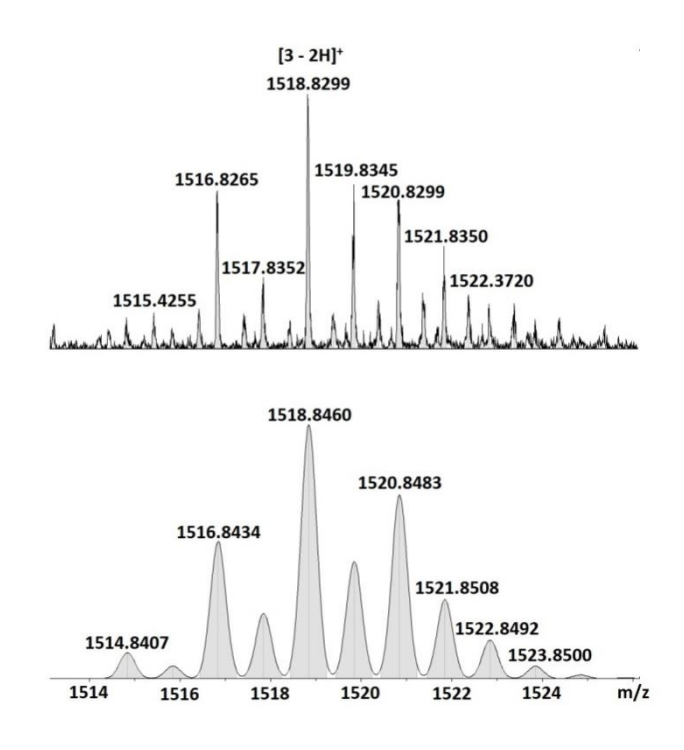


**Figure 6.** Experimental (Top) and calculated (Bottom) ESI mass spectra of  $[3 - 2H]^+$  in positive ion mode.

The  ${}^{1}\text{H-NMR}$  spectrum of 1-3 in  $d_{6}$ -DMSO displayed a set of well-resolved peaks with the absence of NH proton of the anionic Tzbim/Tznim/F<sub>2</sub>-Tzbim (Figure 7-15). All the protons are assigned using <sup>1</sup>H-<sup>1</sup>H COSY spectrum. The Diffused-ordered spectroscopy (DOSY) NMR spectrum of 1 displayed single band, confirming the presence of single product in the solution. Complex 1 displayed eighteen peaks including six singlets, six doublets and six triplets which are different from the free ligand. The protons of Tzbim in 1 were upfield/downfield shifted as compared to free H-Tzbim. The three H<sup>a</sup> protons (N-CH<sup>a</sup>-S) of thiazolyl (Tz) unit were significantly downfield shifted, suggesting the coordination of thiazolyl unit using its nitrogen atom to the rhenium centre. The downfield shift and noticeable upfield shifts for H<sup>e-f</sup> protons suggest that both the nitrogen atoms of the benzimidazolate motif coordinated to the rhenium cores and the adjacent protons experience neighbouring ring current effect. The above data clearly suggests that complex 1 adopts cyclic structure having three Tzbim motifs which are arranged unsymmetrically. Complexes 2 and 3 also displayed similar <sup>1</sup>H-NMR pattern to that of 1 (Figure 11–15). The <sup>19</sup>F-NMR spectrum of 3 displayed five different signals (1:2:1:1:1) suggesting the presence of six fluorine atoms under different chemical environment due to asymmetric arrangement of ligand motifs (Figure 14). The above data suggests that the solid state discrete complex structures retain in the solution state.

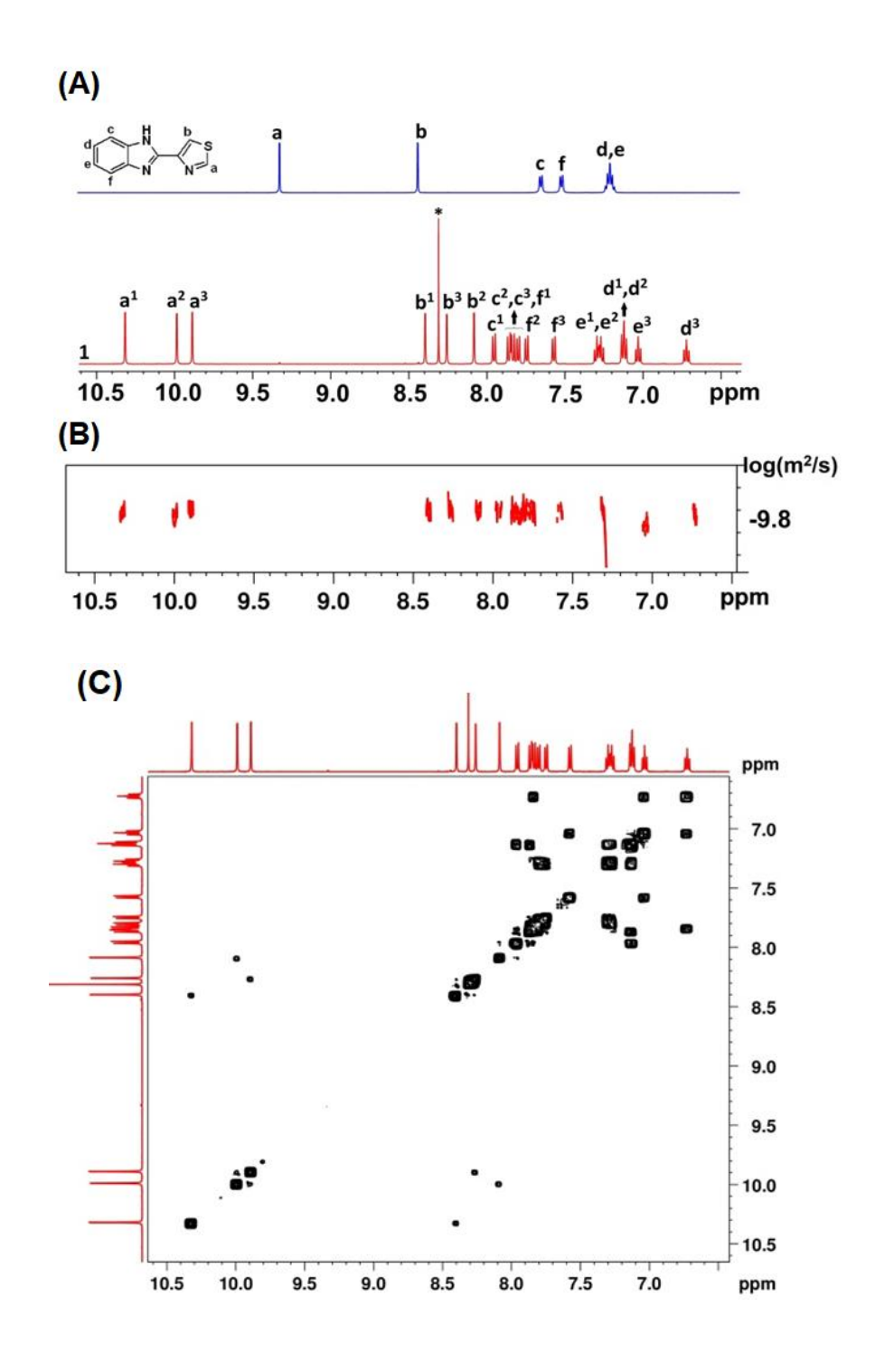


**Figure 7.** (A) Partial  ${}^{1}\text{H}$ –NMR spectra of H–Tzbim and **1**. (B–C) DOSY and  ${}^{1}\text{H}$ – ${}^{1}\text{H}$  COSY spectra of **1** in  $d_{6}$ -DMSO (\*chloroform solvent peak).

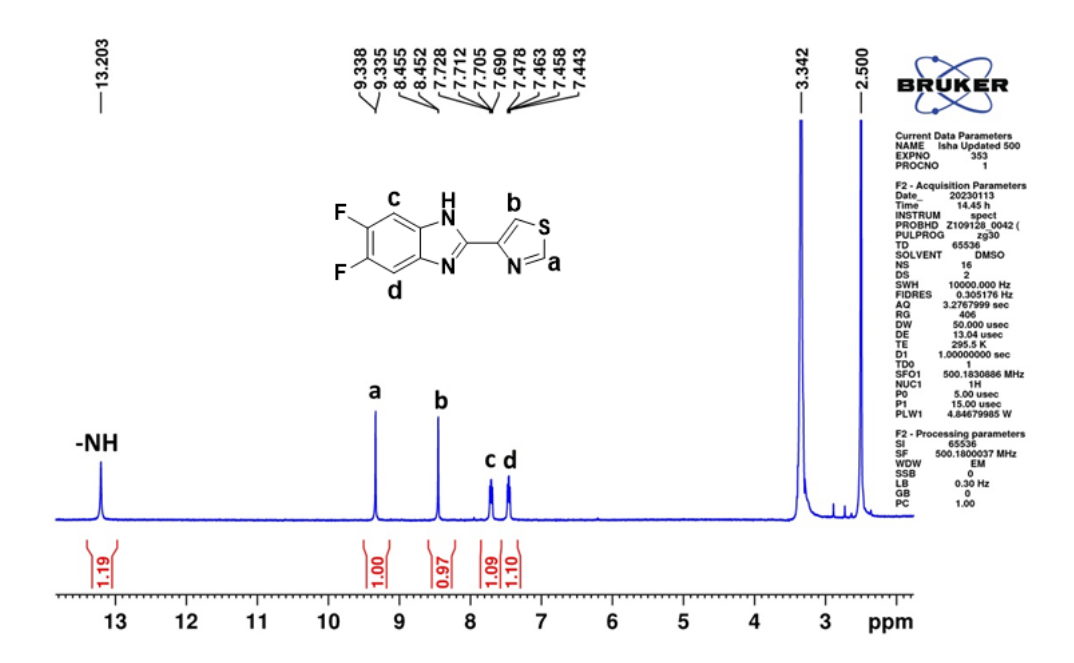


**Figure 8.** Partial  ${}^{1}H$ -NMR spectra of H-Tzbim-F<sub>2</sub> in  $d_6$ -DMSO.

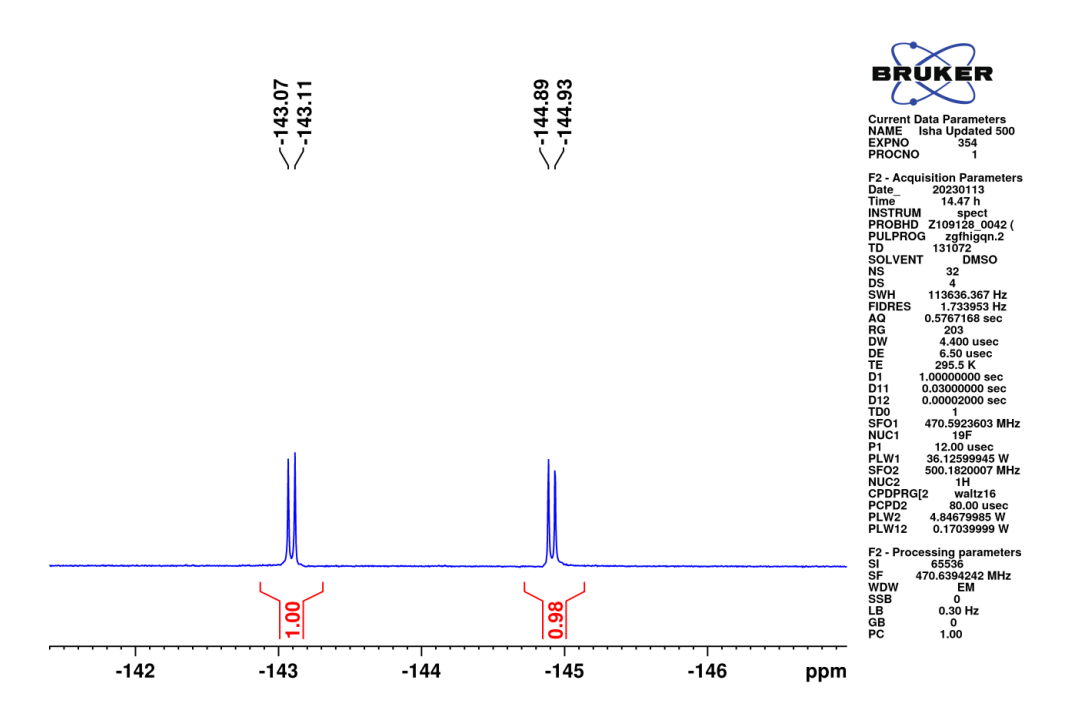


**Figure 9.**  $^{19}$ F-NMR spectrum of H-Tzbim-F<sub>2</sub> in DMSO- $d_6$  at 298 K.

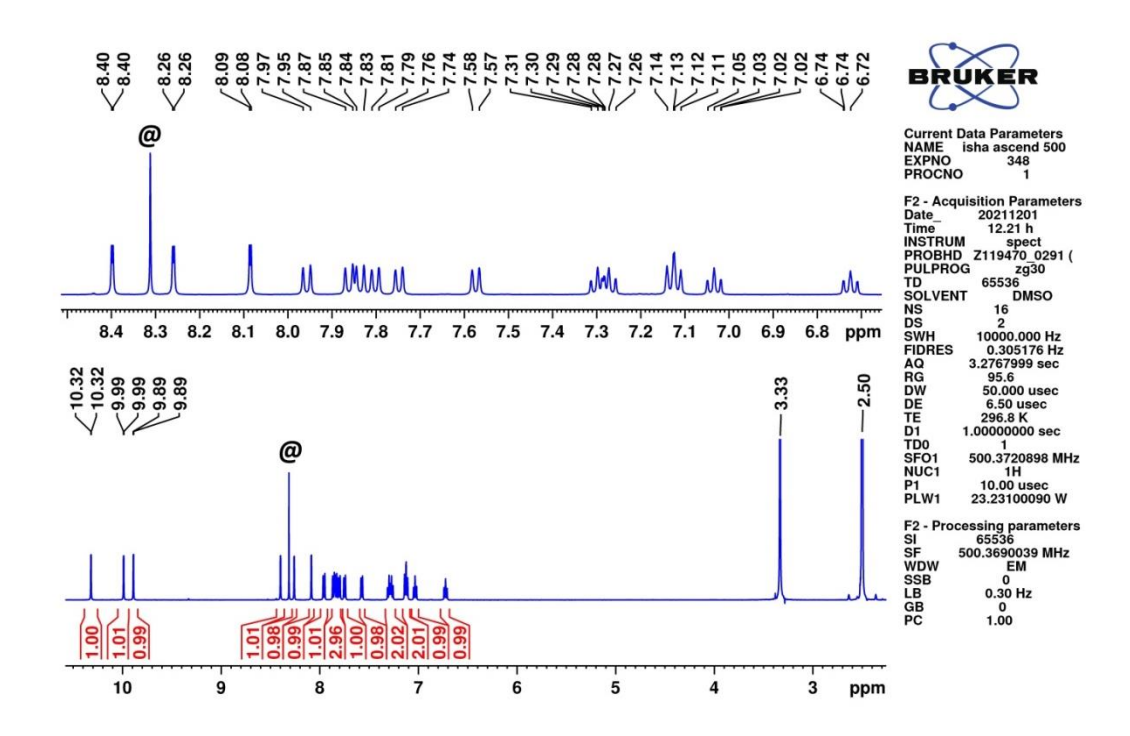


**Figure 10.**  $^{1}$ H-NMR spectrum of molecular complex **1** in DMSO- $d_6$  at 298 K ( $^{@}$ CHCl<sub>3</sub> solvent peak).

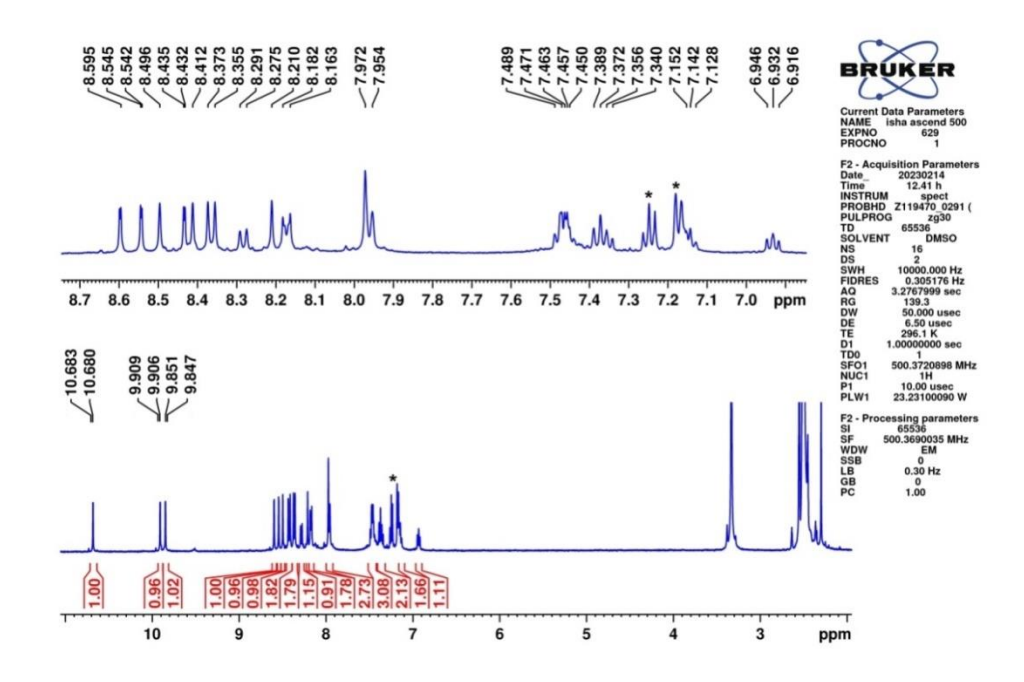


**Figure 11.**  $^{1}$ H-NMR spectrum of molecular complex **2** in DMSO- $d_6$  at 298 K (\*toluene solvent peaks).

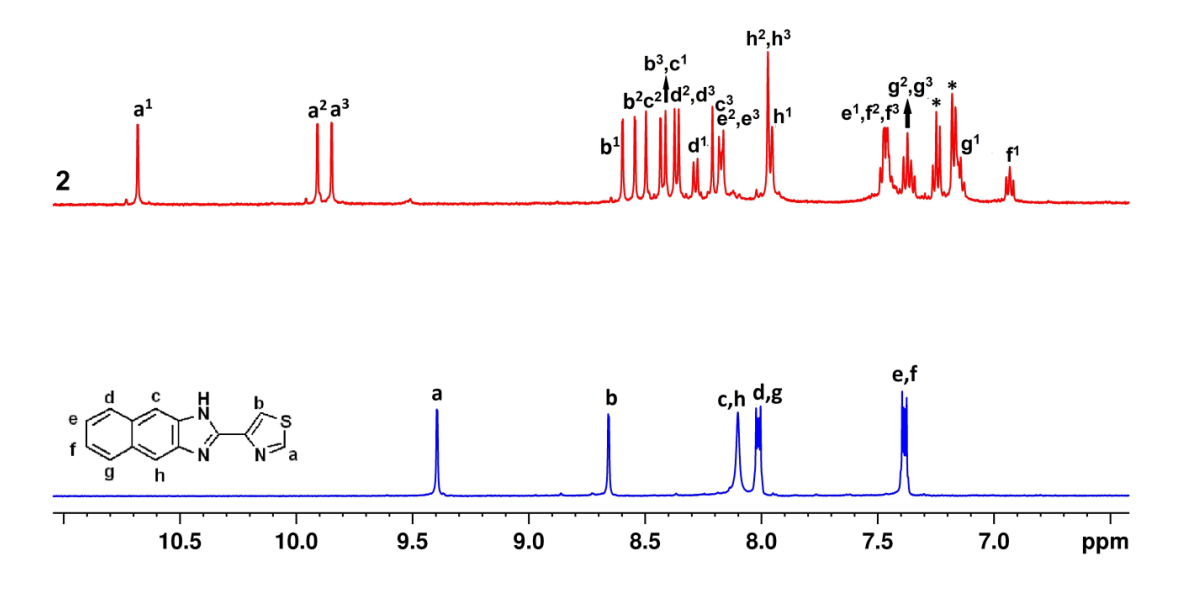


**Figure 12.** Partial H-NMR spectra of H-Tznim (blue) and molecular complex **2** (red) in DMSO- $d_6$  at 298 K (\*toluene solvent peaks).

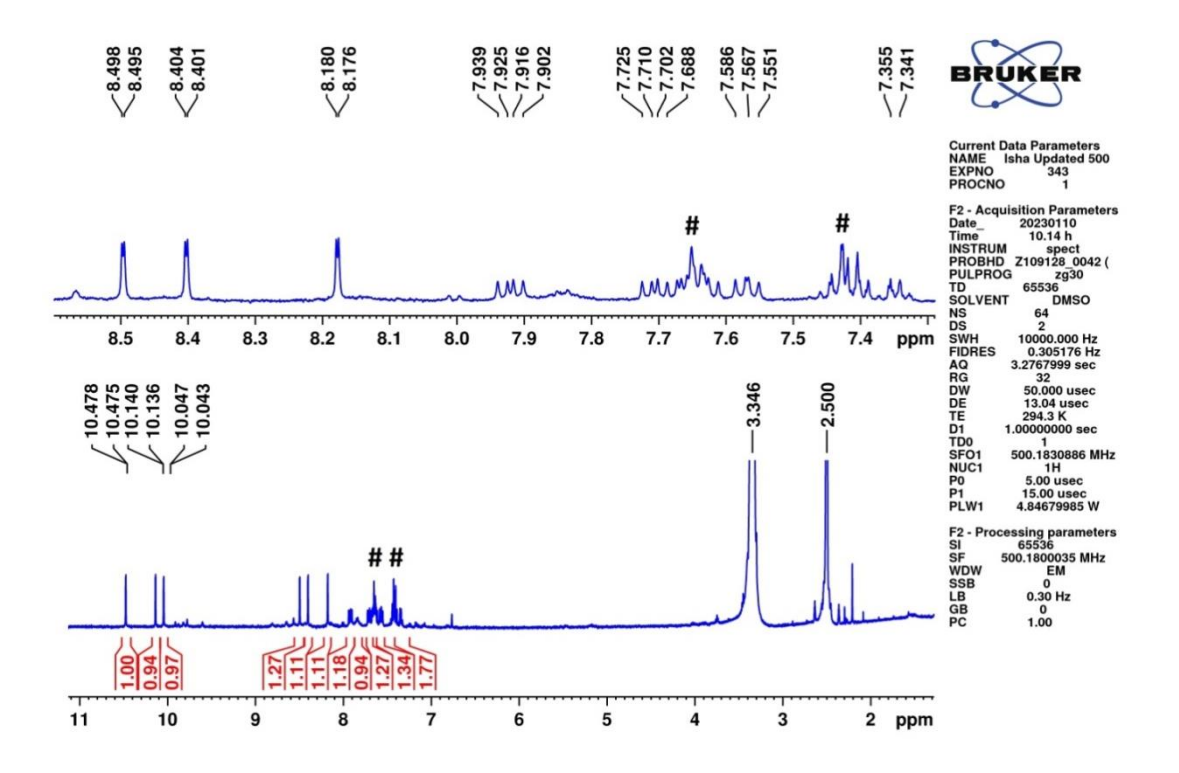


**Figure 13.**  $^{1}$ H-NMR spectrum of molecular tube **3** in DMSO- $d_6$  at 298 K ( $^{\#}$ chlorobenzene solvent peaks).

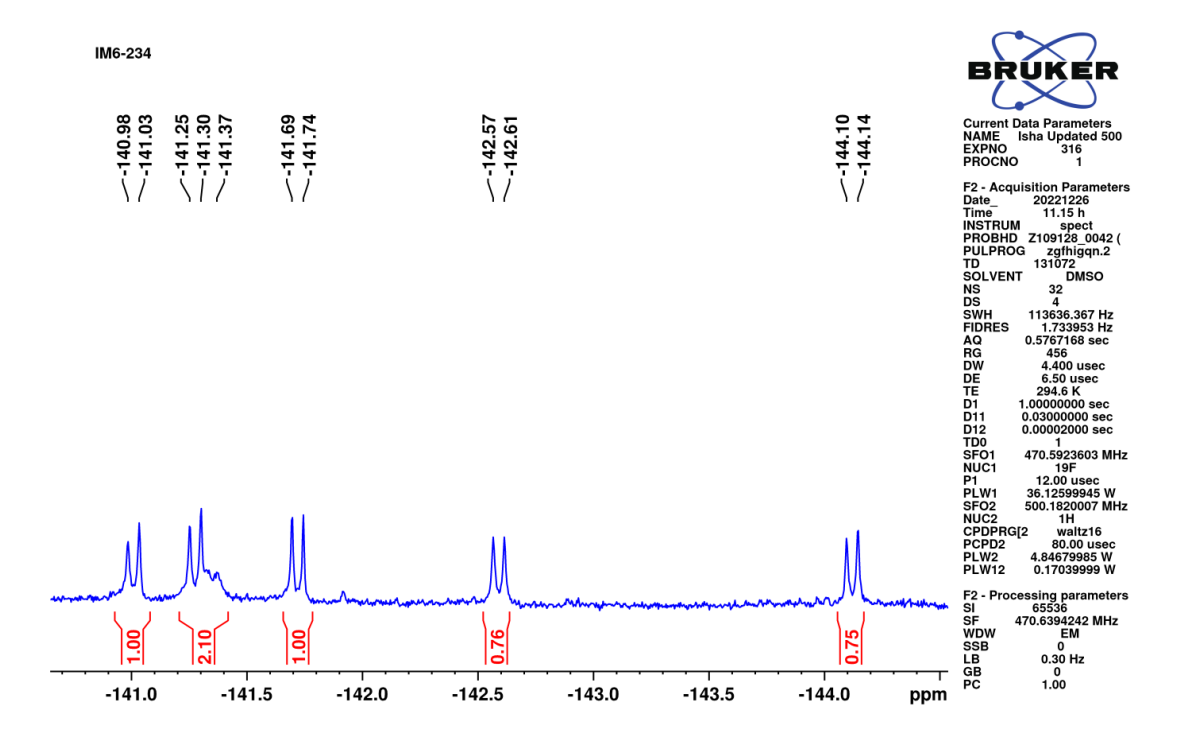


**Figure 14.**  $^{19}$ F-NMR spectrum of molecular tube **3** in DMSO- $d_6$  at 298 K.

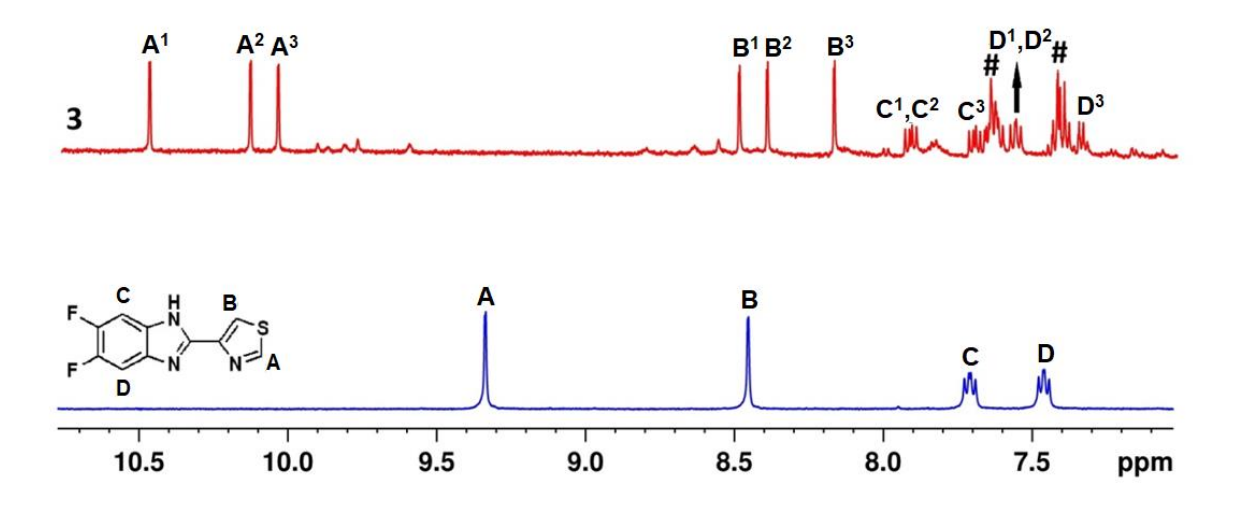


**Figure 15.** Partial  ${}^{1}\text{H-NMR}$  spectra of H-Tzbim-F<sub>2</sub> and molecular tube **3** in DMSO- $d_6$  at 298 K ( ${}^{\#}$ chlorobenzene solvent peaks).

**Molecular structures of 1–3.** The molecular structures were established by X–ray analysis which revealed that **1–3** adopt  $M_3L_3$ -type metal-organic triangular complex structure (Figure 16). The lengths of the molecular complexes are ~9.2 Å for **1**, ~15.8 Å for **2**, and ~9.5 Å for **3**. The complex consists of alternatively arranged three fac-[Re(CO)<sub>3</sub>] cores and three anionic ligand motifs (Tzbim/Tznim/Tzbim-F<sub>2</sub>). The rhenium cores in the complexes possess distorted octahedral geometry. The three rhenium centres are arranged in the equilateral triangle form with Re···Re distances of ~6.28, ~6.30 and ~6.35 Å.

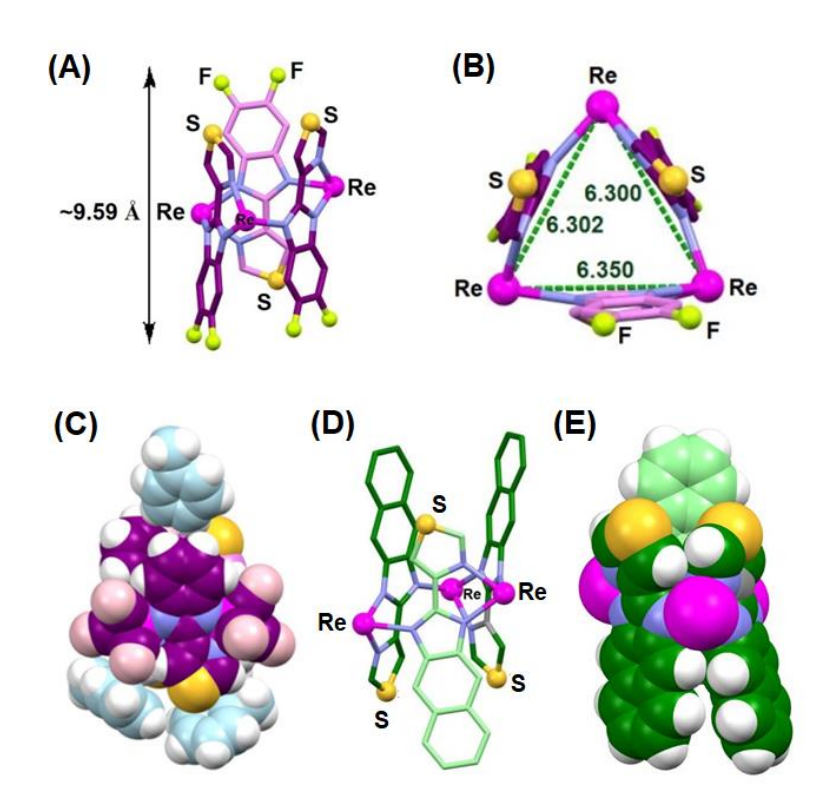


**Figure 16.** (A-B) Side and top views of discrete tube **3**; (C) Molecular structure of **1** showing three toluene molecules shielding both the ends of the complex (space-fill view); (D-E) Side view for **2** (capped stick and space-fill view) (H atoms and CO groups are removed for clarity); (Color code: Re = magenta, C = purple and green, N = light blue, S = yellow, F = light green).

The coordinated carbonyl groups in the complexes are directed outward. Ligand Tzbim/Tznim/Tzbim- $F_2$  in the complexes act as N^N-N donors using three nitrogen atoms with  $\mu_2-\eta^2$ : $\eta^1$  coordination mode to bridge two rhenium centres. Both Tz and bim/nim/bim- $F_2$  are bent with respect to each other's plane. The three anionic ligands are arranged in syn,syn,anti-manner in the cycle to avoid the steric repulsion between the phenyl/thiazolyl units. All three complexes (1–3) contain three sulfur atoms from the three thiazolyl units, which are directed along the complex axis. In addition, complex 3 contains six fluorine atoms on its cyclic framework.

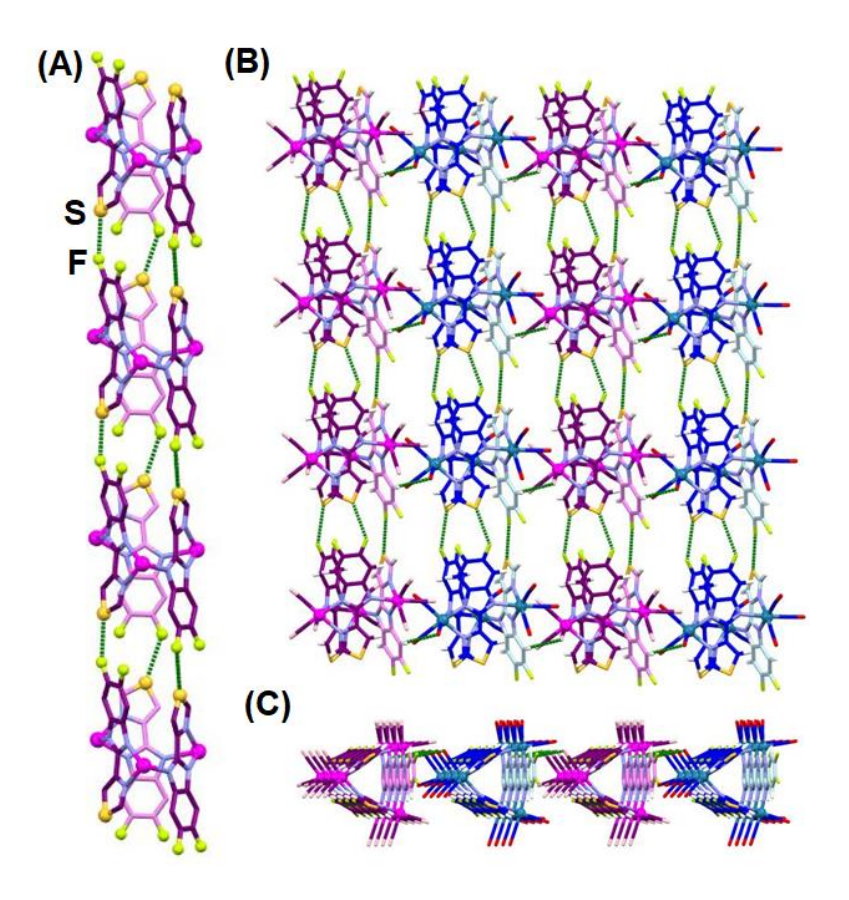


**Figure 17.** (A) 1D-tubular structure of **3** formed *via* intermolecular C–F···S contacts; (B–C) Side and top view of partial packing diagrams of **3** (Color code: Re = magenta, C = purple/blue, N = light blue, F = light green, S = yellow).

The presence of fluorine atoms on the periphery of the cyclic framework and the orientation of ligand motifs influences the packing arrangement of 3. Each discrete molecular complex stacks on top of each other to form a regular 1D-linear arrangement in 3 (Figure 17). Two neighbouring complexes in 3 have three close intermolecular contacts between the sulfur of thiazolyl of one molecule and fluorine atom on the phenyl motif of another molecule. The distance between the fluorine and the sulfur  $(d(F \cdot \cdot \cdot S) = \sim 3.06 \text{ Å}, \sim 3.16 \text{ Å} \text{ and } \sim 3.21 \text{ Å})$  is shorter than the sum of van der Waals radii of fluorine and sulfur (1.47 Å + 1.8 Å = 3.27 Å). As evidenced from the literature, the short contacts C-F...S in solid state can greatly impact the arrangement of the molecules in the crystal lattice. 10 The array of C-F...S contacts in 3 determines the tubular arrangement of the complex in the crystal packing. As per our knowledge, the studies on rhenium(I)-based SCCs possessing intermolecular C-F···S interaction are scarce. 11 Among the few examples of molecules possessing intermolecular C-F...S contacts, pentafluorophenyl-2,2'-bisthiazole (I) is one of the example containing both thiazole motifs and fluorophenyl units. Compound I features an intermolecular interactions C–F···S (d = 3.286 Å,  $\theta = 162^{\circ}$ ) in the crystal packing structure in which fluorine bonded to carbon acts as halogen bond donor and sulfur of thiazole acts as acceptor. Thus, the intermolecular contacts found in 3 are convincingly indicative of C-F...S ( $\theta = 160^{\circ}$ , 134° and 136°) halogen bonding interactions which play prominent role in forming a one dimensional tubular arrangement. Upon extending the 1D-tubular arrangement, it forms an array of tubular structure connected via hydrogen bonding interactions, C-H···O $\equiv$ C-Re (d=2.65 Å). The influence of C-F...S interactions in dictating the tubular arrangement of 3 was indirectly evidenced from the packing arrangement of fluorine unsubstituted complex 1. In the crystal packing of complex 1, discrete molecular complex structure is surrounded by three toluene molecules, stabilized via  $CH \cdot \tau$  interactions, which shield both the ends of the complex (Figure 16). Further, each molecule

of 1 interacts with neighbouring molecules sideways via C-H··· $\pi$ ,  $\pi$ ··· $\pi$ , C-H···O=C-Re and S··· $\pi$  interactions. No intermolecular 1D tubular arrangement was observed for 1. On the other hand, the crystal packing diagram of 2 shows that the two adjacent molecules are arranged in a head-to-head manner forming a dimeric tubular structure with the length of ~26.68 Å. The two complexes are held together by C-H··· $\pi$  interactions between thiazolyl sulfur and naphthanozolyl unit (Figure 18). This arrangement provides a rectangular prism shaped cavity. Further, the two adjacent dimeric complexes interacts with each other via C-H··· $\pi$ , C-H···O, and S··· $\pi$  contacts and forms 1D ladder type arrangement (Figure 18).

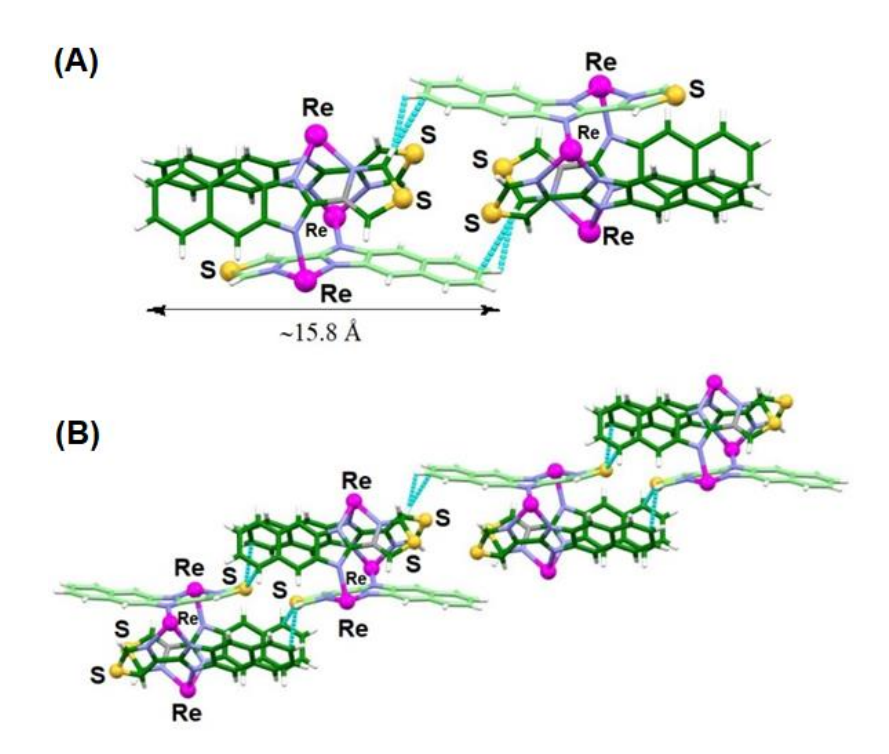


**Figure 18.** (A) Two adjacent molecules of **2** forming dimeric nonlinear tubular structure *via*  $C-H\cdots\pi$  contacts. (B) Two adjacent dimeric complexes forming 1D-ladder type arrangement in the crystal packing (Color code: Re = magenta, C = green, N = light blue). (CO groups are removed for clarity).

**Table 1.** Crystallographic parameters of **1–3**.

	1			2	3	,	
Empirical formula	C <sub>60</sub> H <sub>42</sub> N <sub>9</sub> O <sub>9</sub> Re <sub>3</sub> S <sub>3</sub>		$C_{58}H_{32}N_9O_9Re_3S_3$		$C_{39}H_{12}F_6N_9O_9Re_3S_3$		
Formula weight	1687.8	30	165	53.70	1519	0.36	
Temperature	296(2)	K	296	5(2) K	296(2	2) K	
Wavelength	0.71073	3 Å	0.71	073 Å	0.710	0.71073 Å	
Crystal system	Monocl	inic	Tri	clinic	Tricl	inic	
Space group	P 21/	c	F	P-1	P -	-1	
Unit cell dimensions	a = 13.1805(4) Å	α= 90°	a = 11.9109(2) Å	$\alpha = 73.6540(10)^{\circ}$	a = 11.1802(2) Å	α= 92.8420(10)°	
	b = 24.0955(7) Å	β= 104.90 (3)	b = 11.9143(2) Å	β = 84.0880(10)°	b = 12.56650(10) Å	β= 90.7940(10)°	
	c = 19.5208(6) Å	$\gamma = 90^{\circ}$	c = 21.0550(3) Å	$\gamma = 69.721(2)^{\circ}$	c = 15.3357(2) Å	γ = 99.2100(10)°	
Volume	5991.1(3	) Å <sup>3</sup>	2689.3	38(8) Å <sup>3</sup>	2123.69	$O(5) \text{ Å}^3$	
Z	4			2	2	,	
ρ	1.871 Mg	$g/m^3$	2.042	$Mg/m^3$	2.376 N	$Mg/m^3$	
$\mu$	6.215 m	<sub>m</sub> -1	6.920	) mm <sup>-1</sup>	8.771	mm <sup>-1</sup>	
Crystal size	0.100 x 0.070 mm <sup>3</sup>		0.120 x 0.10	0 x 0.080 mm <sup>3</sup>	0.120 x 0.100	x 0.080 mm <sup>3</sup>	
Independent reflections	10560 [R( 0.0954		9442 [R(ir	nt) = 0.0862	7485 [R(int	) = 0.0454]	
GooF	1.019	)	1.	059	1.0	41	
[I>2sigma(I)]	R1 = 0.0609 0.147		R1 = 0.0551,	wR2 = 0.1551	R1 = 0.0338, v	vR2 = 0.0787	
R indices (all data)	$R1 = 0.1093$ $0.175$ $F \parallel / \sum_{k=1}^{\infty} b_{k}$	, wR2 =		wR2 = 0.1604	R1 = 0.0461, v	wR2 = 0.0838	

 ${}^{a}R_{1} = \sum ||F_{o}| - |F_{c}|| / \sum |F_{o}| \cdot {}^{b}wR_{2} = \{ \sum [w(F_{o}^{2} - F_{c}^{2})^{2}] / \sum [w(F_{o}^{2})^{2}] \}^{1/2}$ 

**Photophysical Studies.** The electronic properties of the ligands and complexes **1–3** were studied using UV–Visible and emission spectroscopy (Figure 19-21, Table 3A-B). The UV–Visible spectra of **1** and **3** in DMSO shows one broad absorption band in the region 250–400 nm with three minor humps ( $\lambda_{max} = 261$ , 300, 340 nm) corresponding to ligand centered transitions in higher energy region as both H–Tzbim and H–Tzbim–F<sub>2</sub> showed structured absorbance with three shoulders in the same region (Figure 20, 21). Complex **2** displayed one strong absorption band ( $\lambda_{max} = 266$  nm) and four weak absorption bands ( $\lambda_{max} = 317$ , 345, 398, 424 nm). The H-Tznim displayed four absorption bands with two weak bands at 267 and 328 nm, two sharp bands at 276 and 341 nm (Figure 21). Based on time-dependent density functional theory calculations, the higher energy absorptions in **1–3** can be attributed to the ligand centered transitions (Figure 19, 22).

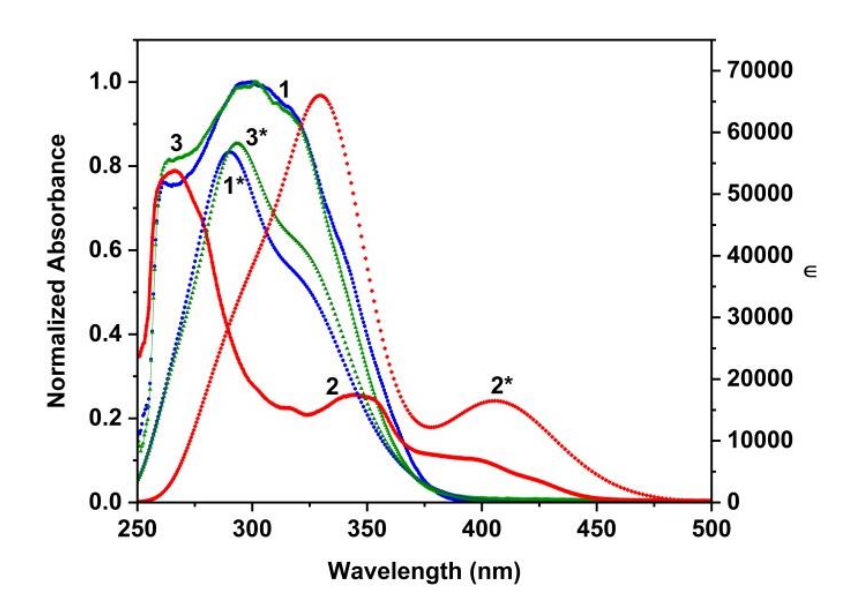


**Figure 19.** Absorption spectra of 1-3 (experimental) and 1\*-3\* (theoretical) in DMSO at room temperature.

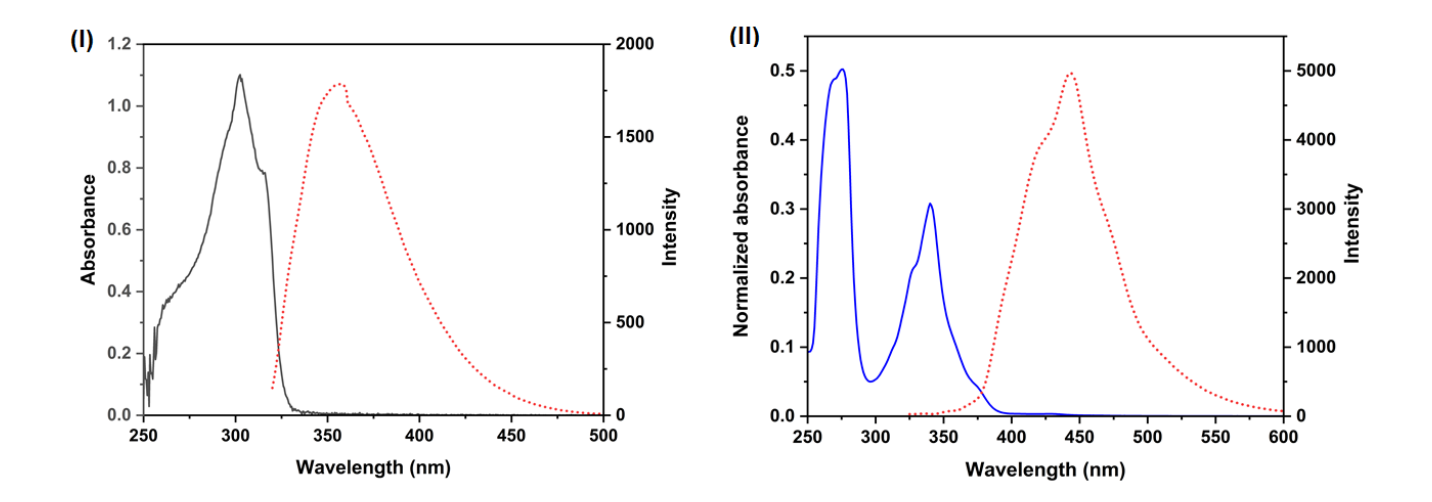


**Figure 20.** Absorption (solid line) and emission (dotted line) spectra of (I) H–Tzbim and (II) H–Tznim in DMSO at room temperature.

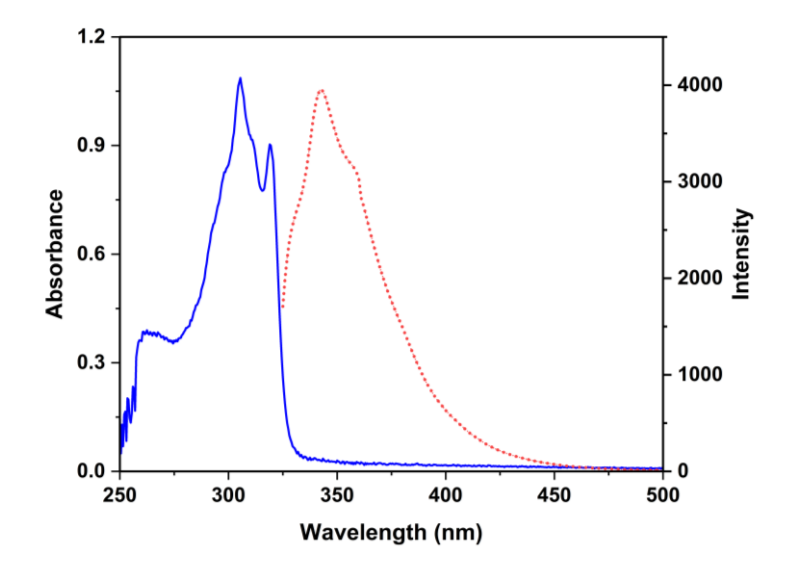


**Figure 21.** Absorption (solid line) and emission (dotted line) spectra of H–Tzbim–F<sub>2</sub> in DMSO at room temperature.

The lower energy absorption bands of 1 and 3 can be attributed to admixture of metal-to-ligand charge transfer (MLCT,  $d\pi$  (Re)  $\rightarrow \pi^*$ ) and ligand centered electronic transitions ( $\pi \rightarrow \pi^*$ ; Tzbim  $\rightarrow$  Tzbim/F<sub>2</sub>-Tzbim  $\rightarrow$  F<sub>2</sub>-Tzbim). However, the lower energy visible absorptions of 2 mainly correspond to Tznim  $\rightarrow$  Tznim transitions. The composition and energy levels of frontier molecular orbitals are presented in Table 2 and Figure 22. The highest occupied molecular orbitals of 1 (HOMO, HOMO-1) is concentrated on Re-center, bim unit of Tzbim and CO ligands. The HOMO-3 is particularly centered on Tzbim with less contribution from Re(CO)<sub>3</sub> (15%). The lowest unoccupied orbitals (LUMO, LUMO + 1 and LUMO + 4) are predominantly based on Tzbim with  $\pi^*$  character, mainly accumulated on thiazolyl unit. In complex 2, the lower energy bands majorly correspond to Tznim  $\rightarrow$  Tznim transitions (Table 2).

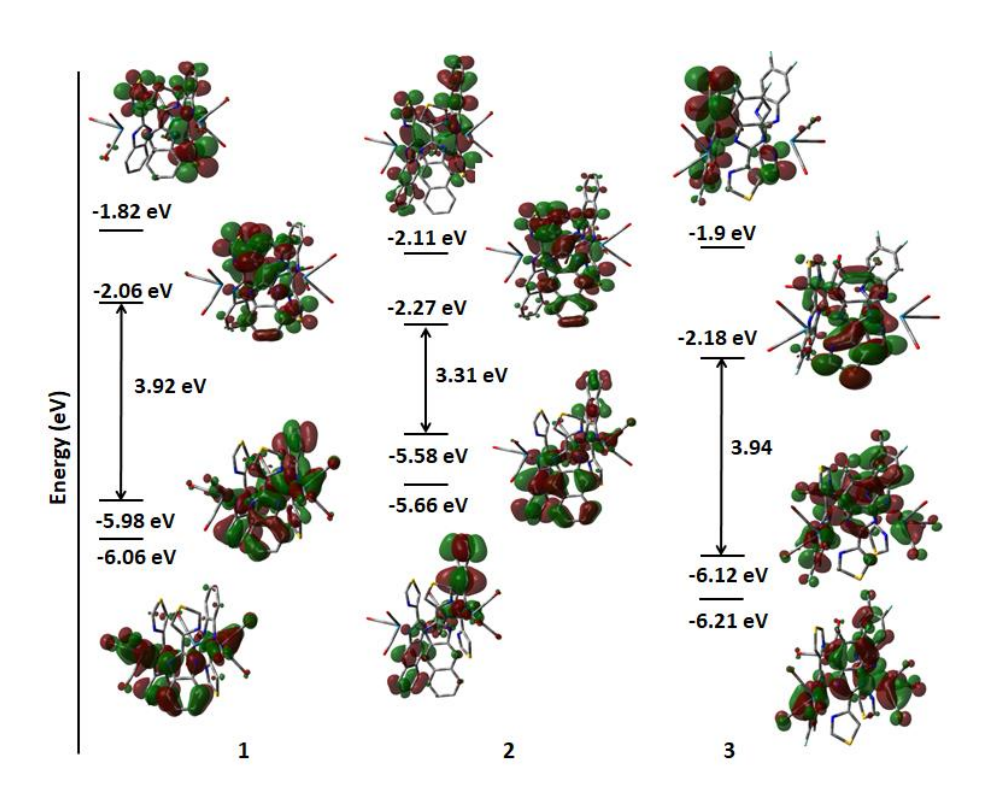


Figure 22. Frontier molecular orbitals involved in TDDFT/IEF–PCM transitions of 1–3.

HOMO of 2 is centered on nim unit of Tznim with minor contribution from Re(CO)<sub>3</sub> core (11%), the HOMO-2 has contribution from two nim units of the Tznim motif. However, HOMO-3 spreads over entire Tznim ligand framework. Similarly, LUMOs are particularly centered on Tznim moieties with  $\pi^*$  character. Complex 3 exhibits similar character to that of 1. Thus, transitions in the lower energy region correspond to admixture of MLCT and ligand centered transitions. The LUMOs are centered on one of the F2-Tzbim units and thiazolyl unit, completely having ligand  $\pi^*$  character. Complex 1 and 3 showed structured emission with two bands between 350-600 nm. The higher energy bands correspond to ligand centered emission as both H-Tzbim and H-Tzbim-F<sub>2</sub> are emissive at 343 and 356 nm, respectively. The pattern exhibited by 2 is different from 1 and 3 (Figure 23). The lower energy transitions mainly correspond to LC transitions as H-Tznim also displayed emission bands at 420 and 443 nm (Figure 20(II)). The increase in the  $\pi$ -conjugation resulted in higher HOMO levels and decreased LUMO levels causing the decrease in the band gap which is consistent with the changes in absorption and emission spectra. The solid state absorption spectra of the crystals of 1 and 3 showed structured band with three prominent shoulders in the region, 200-440 nm due to both LC and MLCT transitions. The single crystal of 1 and 3 displayed broad emission spectrum at 624 nm and 628 nm, which is redshifted as compared to that in solution state (Figure 24, Table 3B). Complex 2 exhibited four absorption bands 261, 329, 421 and 600 nm, with a broad and less-defined emission band in the range of 450–750 nm. The lifetime measurements were performed both in the solution and solid state. All the complexes displayed ultrafast decay in solution state due to which lifetime for each component could not be determined precisely. In solid state, complex 1 and **3** displayed tri-exponential decay with an average lifetime of 0.297 ns and 0.254 ns, respectively.

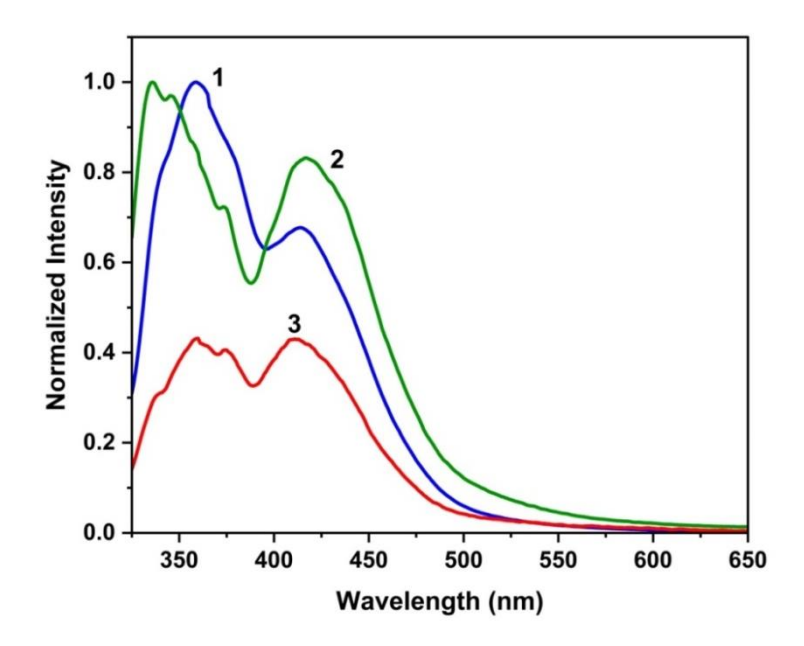
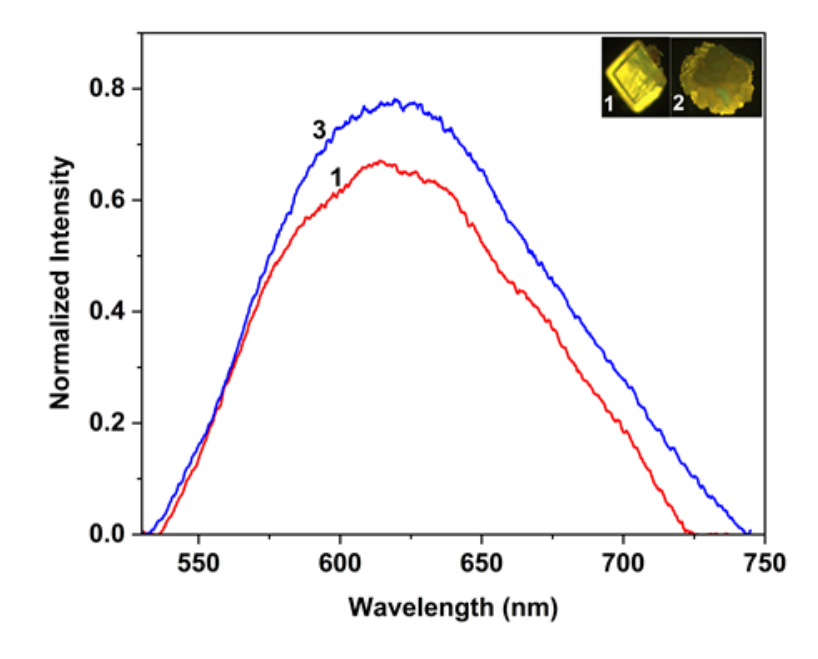


Figure 23. Emission spectra of 1–3 in DMSO at room temperature.



**Figure 24.** Emission spectra of **1** and **3** in solid state (crystal) at room temperature. Inset: Photograph of emission under irradiation from a 405 nm excitation source.

**Table 2.** Major singlet excited state transitions for 1–3 from TDDFT/IEF–PCM calculations with DMSO as the solvent model.

Trans band	λ (nm)	Oscillator strength (f)	Major contribution [%]	Character
Complex 1				
1	367	0.0056	HOMO →LUMO (94%)	Re (23%), CO (13%), Tzbim $^-$ (65%) $\rightarrow$
				Tzbim (98%)
	251	0.0000		(MLCT, IL)
2	361	0.0283	HOMO <b>-</b> 1 →LUMO (93%)	Re (31%), CO (18%), Tzbim $^-$ (51 %) $\rightarrow$
				Tzbim (98%)
6	338	0.0476	HOMO 2 - HIMO (640)	(MLCT, IL)
0	336	0.0470	HOMO−3 →LUMO (64%)	Re (10%), CO (5%), Tzbim <sup>-</sup> (85%) → Tzbim <sup>-</sup> (98%)
			HOMO NUMO (2/199/)	120lm (98%)
			HOMO →LUMO + 2 (18%)	
13	330	0.0992	HOMO →LUMO + 4 (56%)	Re (23%), CO (13%), Tzbim <sup>-</sup> (65%) $\rightarrow$
			HOMO →LUMO + 5 (11%)	Tzbim <sup>-</sup> (80%)
			110.110 / 120.110 / 5 (11/4)	(MLCT, IL)
16	321	0.0699	HOMO – 3 →LUMO + 1 (17%)	
			HOMO – 1 →LUMO + 3 (11%)	Re (10%), CO (5%), Tzbim $^{-}$ (85%) $\rightarrow$
			HOMO – 1 →LUMO + 4 (16%)	Tzbim (96%)
			HOMO →LUMO + 3 (15%)	
Complex 2			, ,	
2	427	0.0227	HOMO – 2 →LUMO (59%)	Re (5%), CO (3%), $Tznim^-$ (92%) $\rightarrow$
			HOMO − 1 →LUMO (34%)	Tznim <sup>-</sup> (98%)
				(IL)
4	412	0.0624	HOMO →LUMO + 1 (89%)	Re (6%), CO (5%), Tznim $^-$ (89 %) $\rightarrow$
				Tznim <sup>-</sup> (97%)
				(IL)
7	401	0.0544	$HOMO -2 \rightarrow LUMO + 1(44\%)$	Re (5%), CO (3%), Tznim $^-$ (92 %) $\rightarrow$
			HOMO-1 → $LUMO + 1$ (11%)	Tznim <sup>-</sup> (97%)
			HOMO →LUMO + 2 (38%)	(IL)
22	338	0.3551	HOMO −5 →LUMO (17%)	Re (7%), CO (4%), Tznim⁻ (90 %) →
			HOMO −3 →LUMO + 1 (63%)	Tznim <sup>-</sup> (97%)
Complex 3				
1	365	0.0078	HOMO →LUMO (94%)	Re (20%), CO (11%), $F_2$ -Tzbim $^-$ (69%) $\rightarrow$
				F <sub>2</sub> -Tzbim <sup>-</sup> (98%)
				(MLCT, IL)
2	358	0.0284	HOMO −1 →LUMO (90%)	Re (32%), CO (18%), $F_2$ -Tzbim <sup>-</sup> (50 %) $\rightarrow$
				F <sub>2</sub> -Tzbim <sup>-</sup> (98%)
				(MLCT, IL)
7	335	0.0575	HOMO −4 →LUMO (39%)	Re (11%), CO (6%), $F_2$ -Tzbim <sup>-</sup> (83%) $\rightarrow$
			HOMO−2 →LUMO + 1 (12%)	$F_2$ -Tzbim $^-$ (98%)
			HOMO →LUMO + 2 (28%)	
13	324	0.0709	HOMO−2 →LUMO + 2 (74%)	Re (19%), CO (10%), $F_2$ -Tzbim <sup>-</sup> (72 %) $\Rightarrow$
13	327	0.0707	1101VIO-2 ->LUIVIO + 2 (14%)	Re (19%), CO (10%), $F_2$ -12bim (72%) $\Rightarrow$ $F_2$ -Tzbim (93%)
17	318	0.0858	HOMO-3 →LUMO + 2 (60%)	Re (7%), CO (4%), $F_2$ -Tzbim (93 %) $\rightarrow$
			2 2 (00,0)	F <sub>2</sub> -Tzbim <sup>-</sup> (89%)

**Table 3A.** Absorption and emission spectral data for the ligands and complexes 1−3 in solution.

Compound	$\lambda_{abs}$ , nm (DMSO)	$\lambda_{em}$ , nm (DMSO)	фет (DMSO)
H–Tzbim	302, 316	356	
1	300, 345	354, 410	0.74 %
H–Tznim	267, 276, 328, 341	420, 443	
2	347, 400	332, 348, 374, 418	1.34 %
H-Tzbim-F <sub>2</sub>	264, 304, 321	343, 359	
3	263, 305	359, 373, 410	0.82 %

**Table 3B.** Absorption and emission spectral data of 1–3 in solid state.

Compound	$\lambda_{abs}$ , nm (solid)	$\lambda_{em}$ , nm (crystal)	τ <sub>av</sub> (ns) (FLIM)	ф (solid)
1	203, 302, 380	624	0.297	1.48 %
2	261, 329, 421, 600	-	-	2.13 %
3	263, 305	628	0.254	1.56 %

Electrochemical Studies. The electrochemical properties of ligands H-Tzbim, H-Tznim, H-Tzbim-F<sub>2</sub> and complexes 1-3 were investigated using cyclic voltammetry in DMSO with 0.1 M Bu<sub>4</sub>NPF<sub>6</sub> as the supporting electrolyte under nitrogen atmosphere (Table 4, Figure 25). Ligands H-Tzbim and H-Tzbim-F<sub>2</sub> displayed irreversible reductions at -2.75 and -2.61, -3.23 V respectively whereas H-Tznim showed a quasi-reversible process (E<sub>1/2</sub> = -2.05 V). The cyclic voltammogram of 1 showed two distinct irreversible reductions at -2.07 V and -2.73 V (vs Fc<sup>+</sup>/Fc). The correlation of voltammetric measurements with computational analysis shows that LUMOs are mainly located on the ligand cores and are electronically independent of Re(I) center. Thus, the reductions occurring in 1 can be attributed to reduction of Tzbim ligands, mainly thiazolyl cores. Complex 2 also displayed two irreversible reductions (-2.37, -2.58 V) and one quasi reversible redox process ( $E_{1/2}$  = -1.93 V). The increase in  $\pi$ -conjugated cores in complex 2, lowers the LUMO levels and increases the HOMO energy levels as evident from TD-DFT. The stabilization of LUMO energy levels resulted in lower reduction potentials of 2 compared to 1 and 3. The cyclic voltammogram of 3 exhibited three irreversible reductions at -2.31 V, -2.65 V and -2.78 V and one poorly resolved irreversible oxidation at -2.6 V. The anodic region for 3 displayed an irreversible oxidation at +1.34~V (vs  $Fc^+/Fc$ ), ascribed to metal-centered  $Re^{I/II}$  oxidation process.<sup>12</sup> However, similar oxidation process was not observed in the anodic region of 1 and 2. The incorporation of electron withdrawing fluorine group leads to systematic stabilization of HOMO and LUMO orbitals resulting in increased band gap. 13 Thus, complex 3 have more positive reduction potentials than 1 and 2.

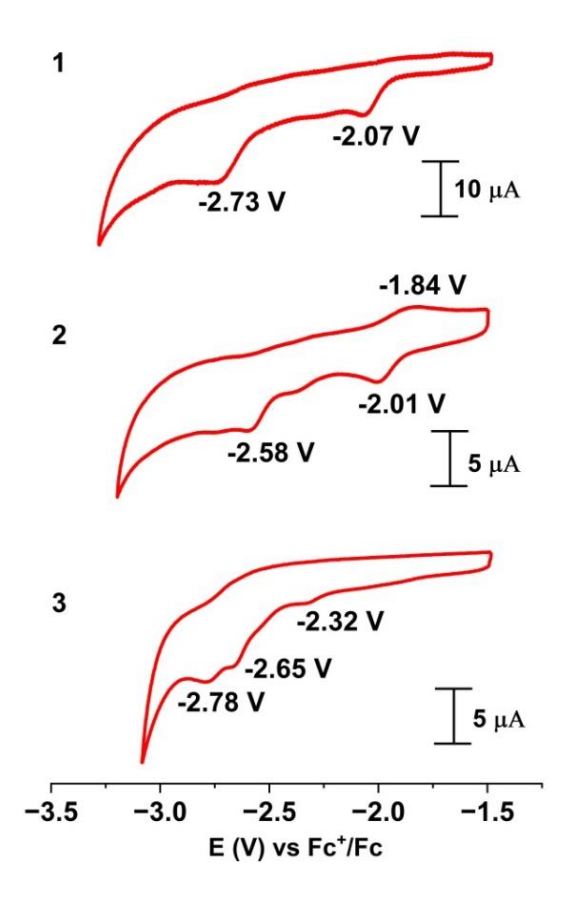
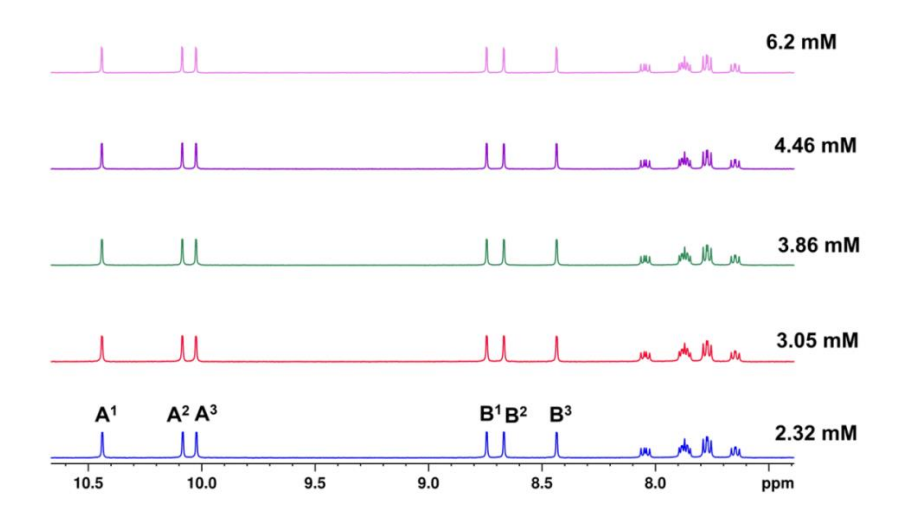


Figure 25. Cyclic voltammograms for 1–3 in DMSO (NBu<sub>4</sub>PF<sub>6</sub>, 0.1 M), scan rate 300 mVs<sup>-1</sup>.

**Table 4.** Electrochemical data of ligands and complexes **1–3**.

compounds	cathodic peak curre	ent (V vs Fc <sup>+</sup> /Fc)	LUMO	
			(eV	)
	1 <sup>st</sup> Reduction	2 <sup>nd</sup> Reduction	CV	DFT
H-Tzbim	-2.75	-	-	-
1	-2.07	-2.73	-2.07	-2.06
H-Tznim	-1.98	-2.11	-	-
2	-2.01	-2.58	-2.22	-2.27
H-Tzbim- F <sub>2</sub>	-2.61	-3.23	-	-
3	-2.65	-2.78	-2.15	-2.18

**Solution State Studies.** The ability of **3** to form tubular architecture in the solution state was studied using concentration dependent and variable low temperature NMR analysis in acetone- $d_6$ . Upon increasing the concentration of **3**, minor shifts were observed for protons of H<sup>A1-A3</sup> (N-CH-S) and H<sup>B1-B3</sup>, whereas no shifts were observed for the other protons (Figure 26-27).



**Figure 26.** Partial  ${}^{1}\text{H-NMR}$  spectra of **3** in acetone- $d_{6}$  at variable concentration at 300 K.

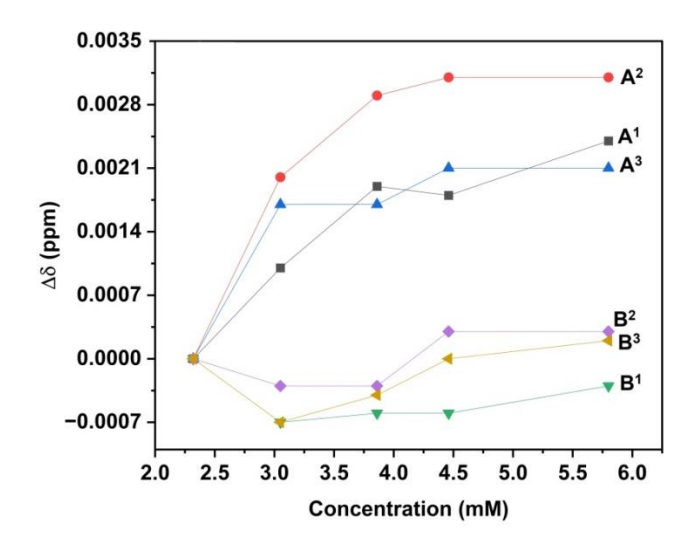


**Figure 27.** Changes in the chemical shift for protons of  $H^{A1-A3}$  and  $H^{B1-B3}$  with varying concentration in acetone- $d_6$  at room temperature.

The <sup>19</sup>F-NMR spectra also displayed minor downfield shifts upon increasing the concentration (Figure 28).

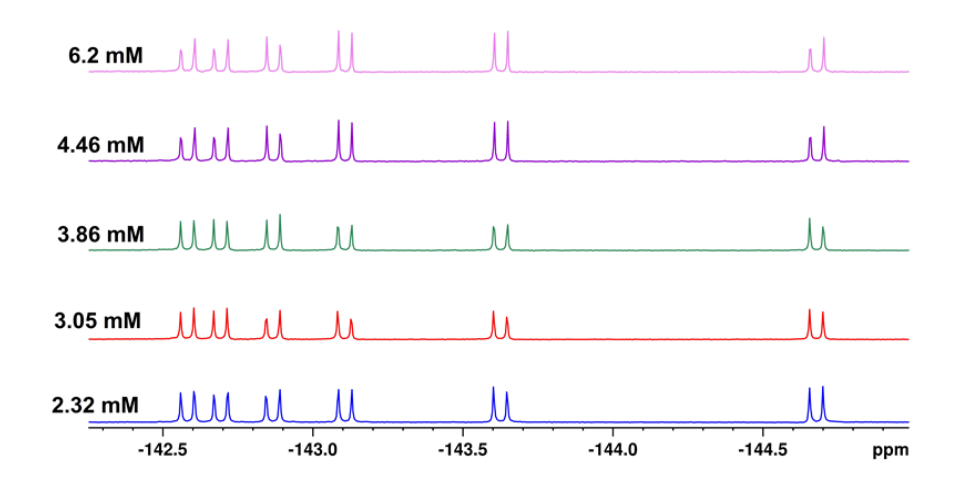


**Figure 28.** <sup>19</sup>F–NMR spectra of **3** in acetone- $d_6$  at variable concentration at 300 K.

Further, the low temperature experiments showed significant downfield shifts for H<sup>A1-A3</sup> (N-CH-S) and H<sup>B1-B3</sup> protons of **3**. The <sup>19</sup>F-NMR spectra also displayed downfield shifts for all six fluorine atoms with three fluorine signals getting merged and appear as a multiplet at 193 K (Figure 29–30). The results of <sup>19</sup>F-NMR spectra are indicative of interaction of fluorine atoms in the concentrated solution as well as at low temperature, which could be cumulative C-F···S contacts as evidenced from the crystal packing diagram. The spatial proximity of molecules upon lowering the temperature can result in C-F···S contacts along with other non-covalent interactions causing the deshielding of protons (H<sup>A1-A3</sup> and H<sup>B1-B3</sup>) adjacent to sulfur atom. At 193 K, H<sup>D3</sup> protons are also shifted downfield and merged with H<sup>D1,D2</sup> possibly due to non-traditional intermolecular hydrogen bonding interactions with O-atom of the neighboring carbonyl group (C-H<sup>D3</sup>···O=C-Re). To

establish the role of fluorine atoms in the formation of tubular architecture in solution state, the low temperature <sup>1</sup>H-NMR studies of **3** were compared with its non-fluorinated analogue, complex **1** (Figure 31–33). The low temperature <sup>1</sup>H-NMR spectra of **1** was different from that of **3**. The H<sup>a1</sup> (N-CH<sup>a1</sup>-S) protons of **1** displayed almost similar trend like H<sup>A1</sup> of **3** whereas H<sup>a2, a3</sup> protons shifted downfield and appeared as a singlet at 213 K (Figure 32). The H<sup>b2,b3</sup> protons of **1** showed upfield shifts unlike that of H<sup>B1-B3</sup> of **3** which appeared downfield (Figure 33). The intermolecular noncovalent interactions of fluorine with sulfur (C–F···S) in complex **3** can result in deshielding of adjacent protons (H<sup>B1-B3</sup>), thereby resulting in significant downfield shift. The results are indicative of the involvement of fluorine atoms in forming non-covalent interactions presumably forming tubular architecture via C–F···S contacts in solution.

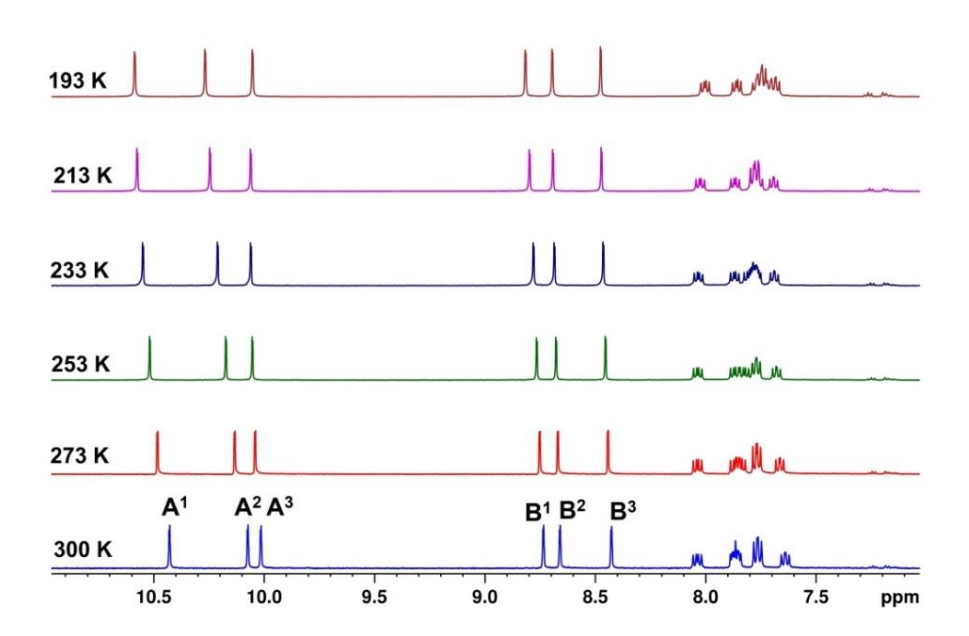


**Figure 29.** Variable low temperature  ${}^{1}H$ -NMR spectra of **3** in acetone- $d_6$ .

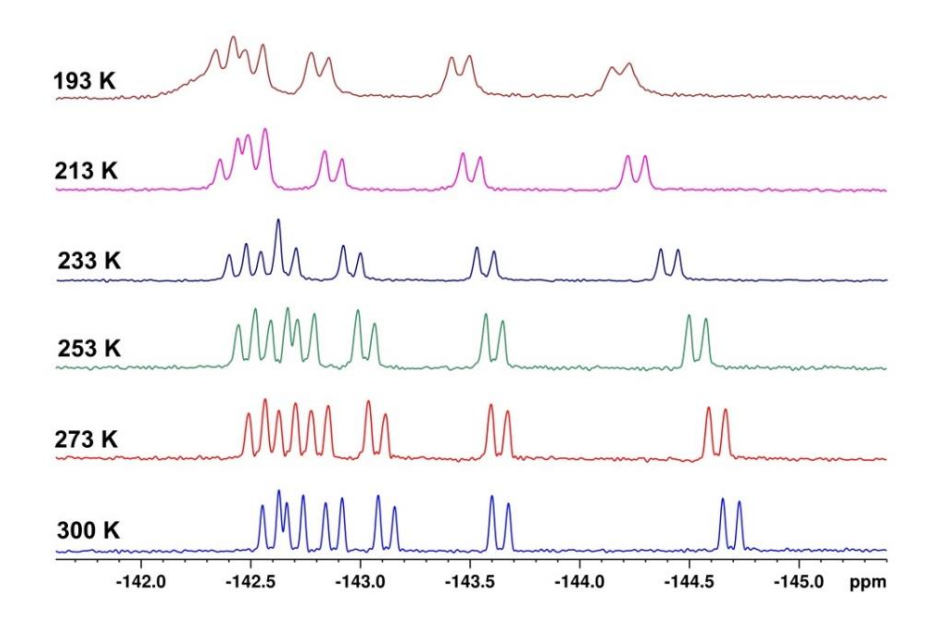


**Figure 30.** Variable low temperature  $^{19}$ F-NMR spectra of **3** in acetone- $d_6$ .

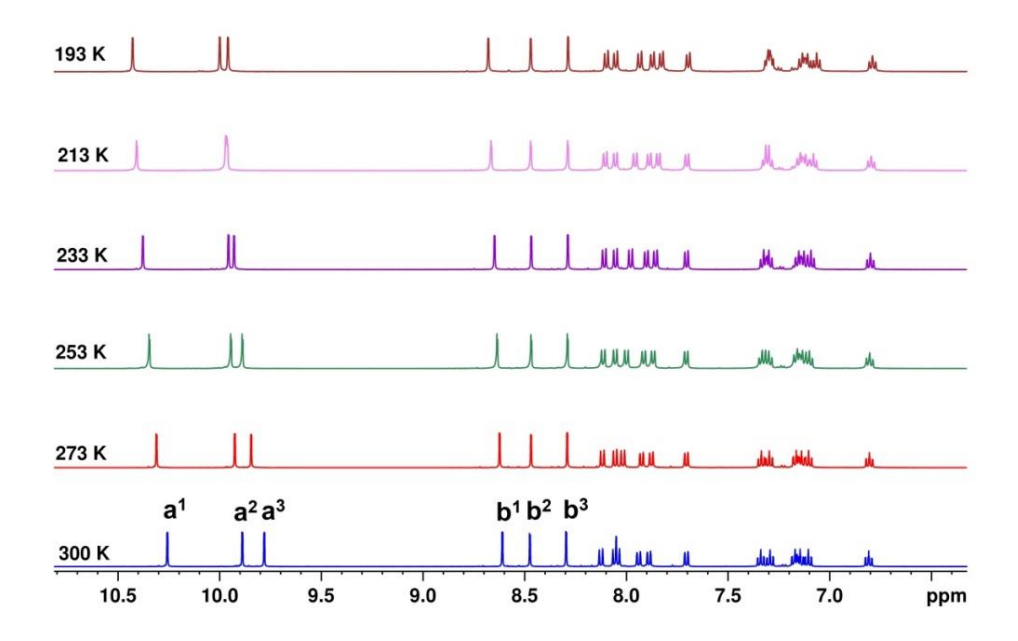


**Figure 31.** Variable low temperature  ${}^{1}H$ -NMR spectra of **1** in acetone- $d_6$ .

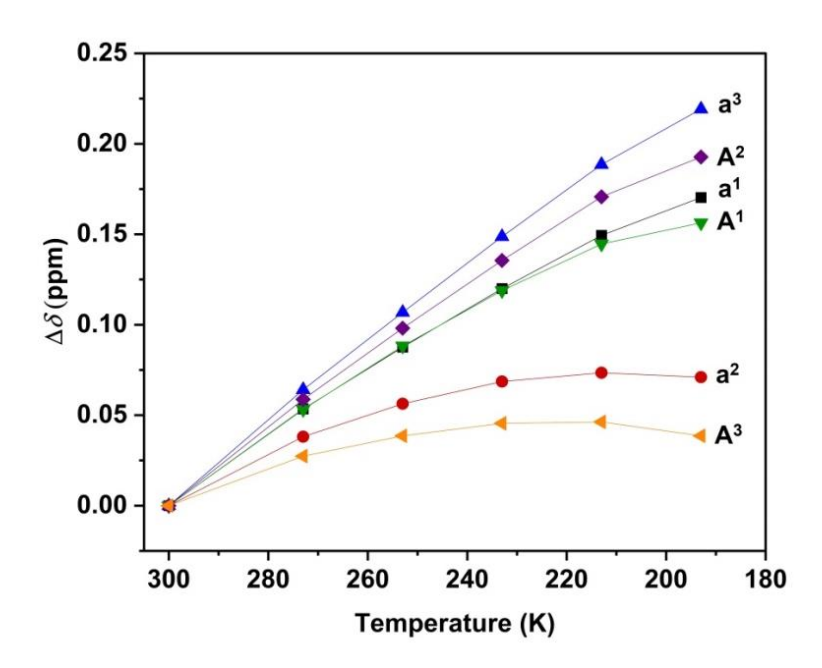


**Figure 32.** Changes in the chemical shift for  $H^{a1-a3}$  and  $H^{A1-A3}$  of **1** and **3** protons upon varying temperature in acetone- $d_6$ .

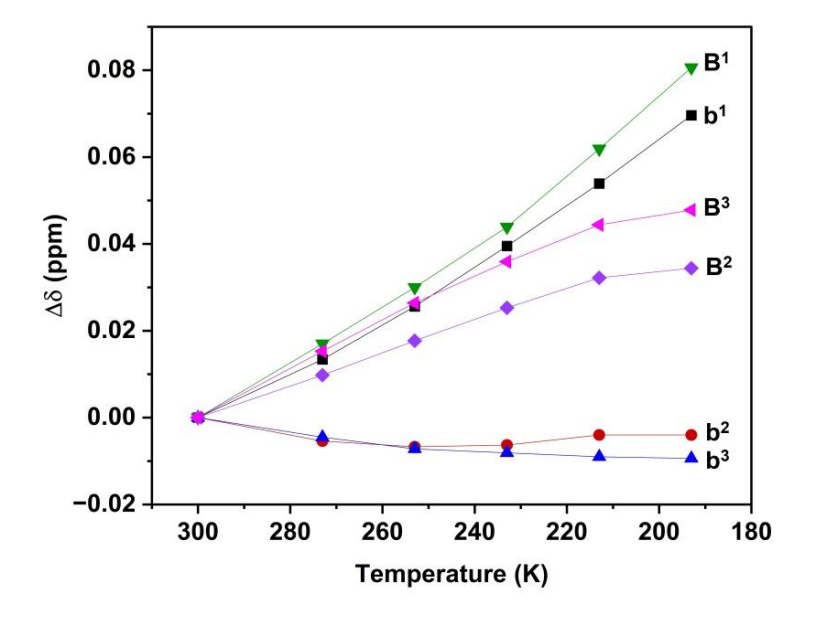


**Figure 33.** Changes in the chemical shift for  $H^{b1-b3}$  and  $H^{B1-B3}$  of **1** and **3** protons upon varying temperature in acetone- $d_6$ .

The UV-Visible and fluorescence spectroscopic methods were further used to corroborate the formation of tubular structure of 3 in solution state by varying the concentration in acetonitrile. The increase in the concentration of 3 resulted in a less defined, broadened absorption band with a significant red shift of ~34 nm. The broadening of absorption band at higher concentration can be attributed to the collisional broadening taking place due to increased molecular collisions and interactions between the molecules. 14a The emission spectra of 3 also exhibited remarkable red shifted emission at 640 nm (Figure 34). The redshift in the absorption and emission bands can be attributed to J-type aggregation which occurs when the molecules are arranged in a head to tail manner due to increase in intermolecular interactions. 14b,c Similarly, complex 1 also displayed a red shift (~ 23 nm) in the absorption band at 234 nm which is comparatively lesser than that of 3 (Figure 35). The emission spectra of 1 unlike that of 3 showed quenching for the band at 286 nm with an emergence of new band at 376 nm upon increasing the concentration, indicating the aggregation of molecules at higher concentration (Figure 36). Complex 2 exhibited very less red-shift (~ 4 nm) in absorption band as compared to 1 and 3, the emission profile of 2 also displayed an emergence of new band between 434-444 nm with a quenching of band at 286 nm (Figure 37-38). The comparison of the above data clearly suggests that the presence of additional fluorine atoms on 3 influence intermolecular interactions which may be cumulative C-F...S interactions responsible for significant changes in absorption and emission properties of 3 as compared to its non-fluorinated analogues 1 and 2.

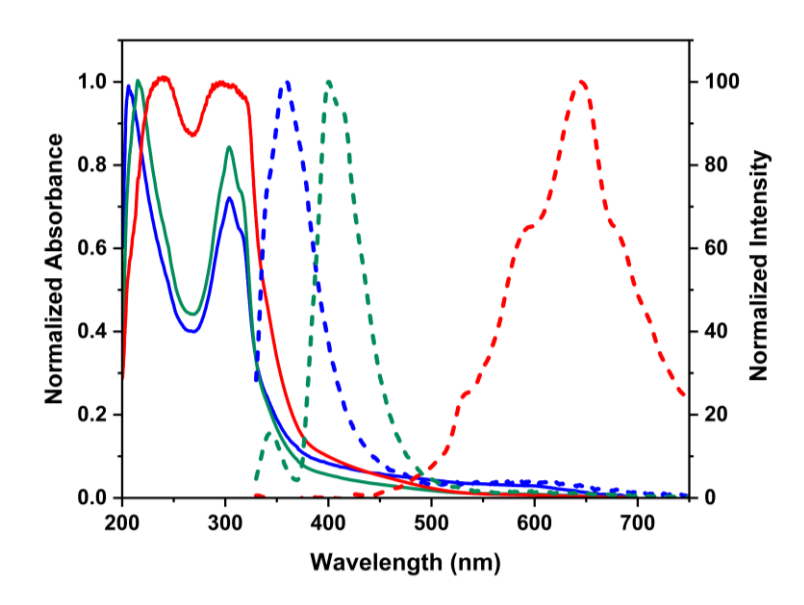


**Figure 34.** Absorption (solid line) and emission (dash line) spectra of **3** at  $1.42 \times 10^{-4}$  M (red),  $1.45 \times 10^{-5}$  M (green) and  $1.42 \times 10^{-6}$  M (blue) in CH<sub>3</sub>CN at room temperature.

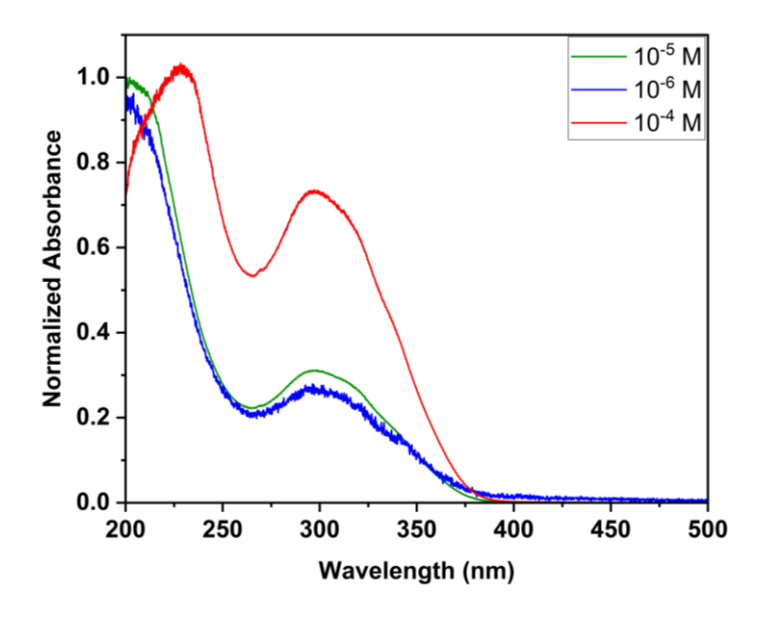


Figure 35. Absorption spectra of 1 at various concentrations in CH<sub>3</sub>CN.

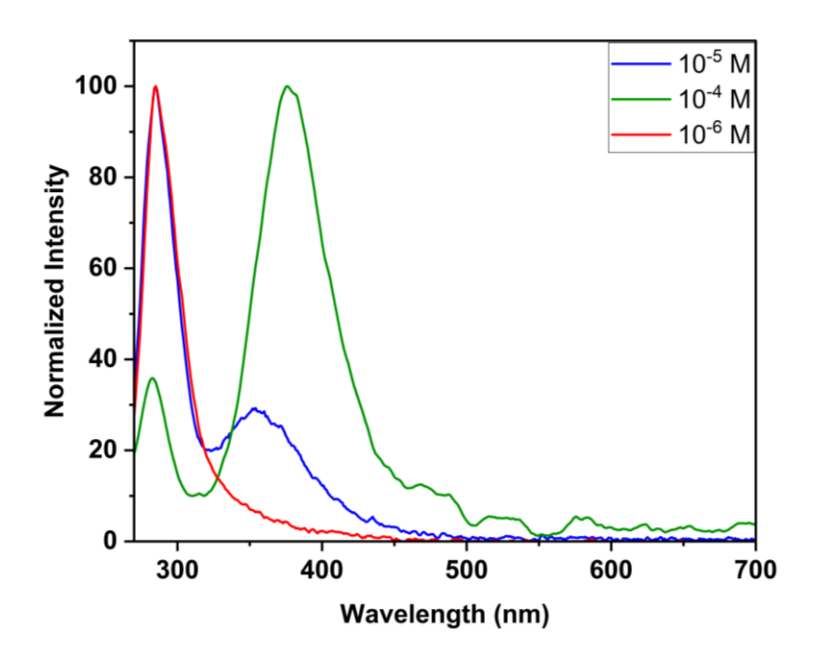


Figure 36. Emission spectra of 1 at various concentrations in CH<sub>3</sub>CN.

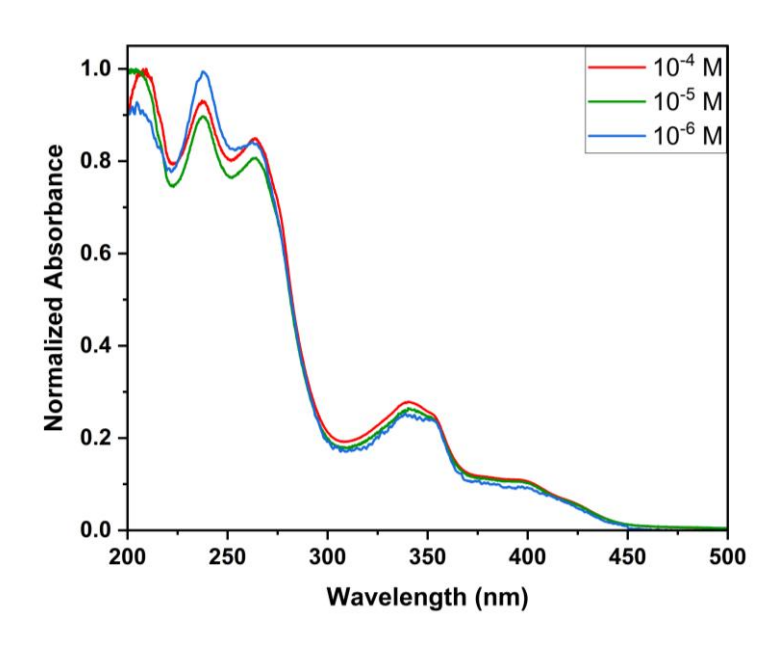


Figure 37. Absorption spectra of 2 at various concentrations in CH<sub>3</sub>CN.

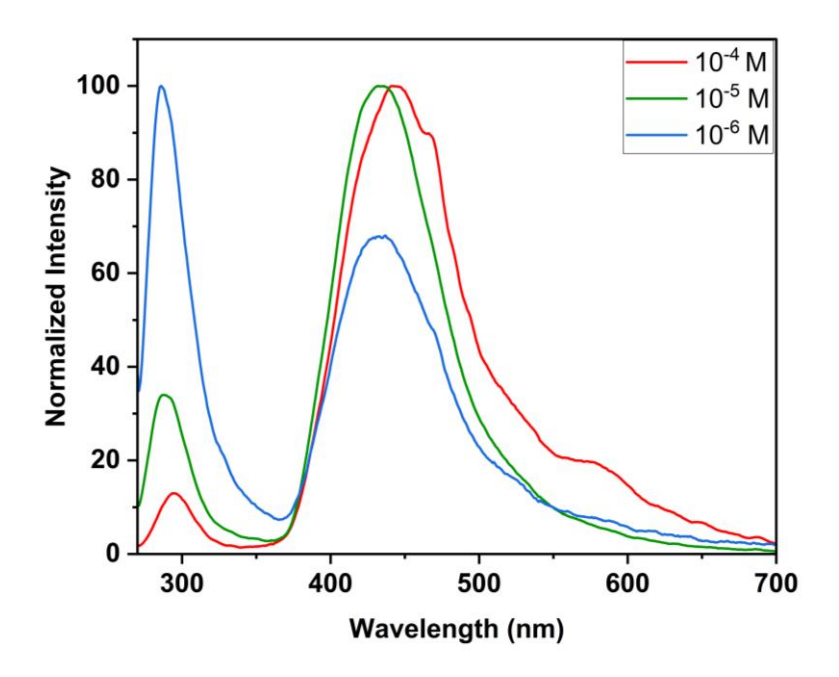
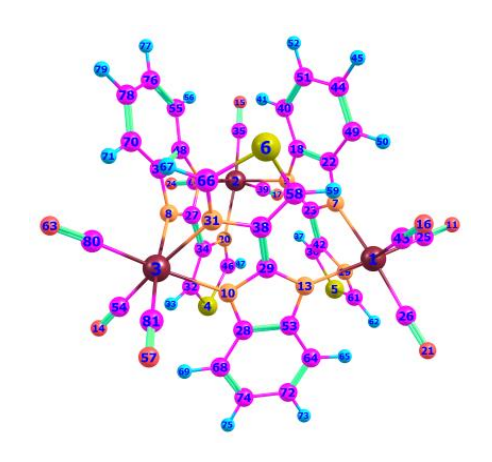


Figure 38. Emission spectra of 2 at various concentrations in CH<sub>3</sub>CN.

## **Optimized Coordinates of 1**

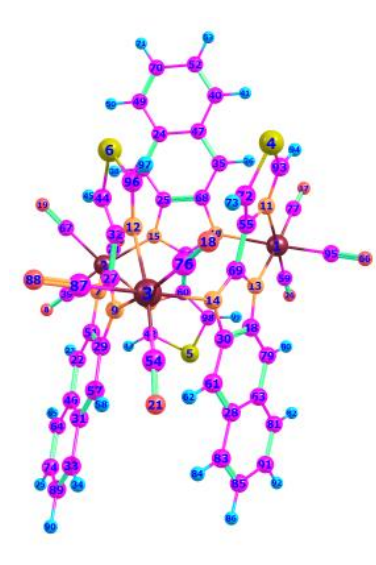


75	3.300930000	-1.611327000	0.695495000
75	-0.193266000	3.635712000	-0.399944000
75	-3.093369000	-2.106101000	-0.403598000
16	-0.508064000	0.884274000	-4.258087000
16	4.162826000	1.275874000	-2.989158000

16	-1.212474000	-2.203953000	3.957058000
7	2.304499000	0.273199000	1.312690000
7	-2.799455000	0.161713000	-0.012791000
7	1.177960000	2.183118000	0.778000000
7	-0.927978000	-2.231749000	-0.857761000
8	6.004471000	-0.555626000	1.756542000
7	-1.764556000	2.183585000	0.201247000
7	1.271704000	-2.175836000	-0.265209000
8	-4.305384000	-1.826187000	-3.232000000
8	-0.376398000	5.796289000	1.804296000
8	3.098297000	-3.356812000	3.234363000
8	2.103124000	5.299940000	-1.629183000
6	1.051525000	1.949899000	2.148304000
7	3.420945000	-0.168709000	-1.023474000
7	-0.346342000	2.094857000	-2.018832000
8	4.804739000	-4.004538000	-0.572885000
6	1.777147000	0.777933000	2.475835000
6	1.981515000	1.179495000	0.359057000
8	-2.242437000	5.321030000	-1.984928000
6	4.997224000	-0.957410000	1.369081000
6	4.214021000	-3.129856000	-0.105602000
6	-1.922526000	1.053749000	-0.526963000
6	-0.194715000	-2.534622000	-1.978896000
6	-0.021316000	-2.086636000	0.136266000
6	-3.304553000	0.812514000	1.114498000
7	-1.988183000	-2.172640000	1.530173000
6	-1.454368000	0.299245000	-2.940629000
1	-2.120800000	-0.527787000	-3.085676000
6	-1.249350000	1.047929000	-1.820093000
6	-0.289277000	4.958648000	1.015637000
6	3.025380000	1.937039000	-1.868459000
1	2.717957000	2.962411000	-1.955543000
6	-0.593190000	-2.057702000	1.481974000
6	1.250301000	4.685785000	-1.140988000
6	0.406986000	2.665596000	3.167417000
1	-0.165193000	3.556020000	2.964907000
6	2.725414000	1.035797000	-0.888792000
6	3.145966000	-2.705129000	2.280637000
6	1.301759000	1.082644000	4.792938000
1	1.412000000	0.787735000	5.831246000
6	0.108288000	2.123753000	-3.244660000
1	0.794043000	2.872735000	-3.608828000
6	-2.657399000	2.066921000	1.240102000
6	1.926310000	0.347667000	3.800989000
1	2.542956000	-0.510864000	4.043108000
6	0.539866000	2.222896000	4.473215000
1	0.058346000	2.780635000	5.269267000
6	1.173859000	-2.490339000	-1.620954000
6	-3.854182000	-1.928372000	-2.171884000
	-2.993778000	2.970624000	2.255445000
6 1	-2.516467000 -2.516467000	3.940401000	2.320273000
8	-3.215746000	-5.184871000	-0.646341000
0	-3.213/40000	-3.1040/1000	-0.040341000

-0.021919000	-2.062919000	2.718032000
1.013027000	-1.998584000	2.981443000
-1.477355000	4.701159000	-1.388572000
4.191678000	-0.179240000	-2.077028000
4.816049000	-1.015458000	-2.352607000
-6.005161000	-2.253707000	0.636115000
2.145733000	-2.800620000	-2.584181000
3.197347000	-2.818757000	-2.342653000
-2.435186000	-2.258883000	2.753707000
-3.481169000	-2.352702000	3.000395000
-0.610087000	-2.900661000	-3.265463000
-1.662810000	-2.978528000	-3.510712000
-4.301009000	0.456896000	2.036515000
-4.851661000	-0.467447000	1.954759000
1.729688000	-3.151009000	-3.859515000
2.473336000	-3.416671000	-4.603743000
0.365143000	-3.203512000	-4.200415000
0.075156000	-3.508829000	-5.200214000
-3.978493000	2.600221000	3.153744000
-4.269064000	3.284132000	3.944112000
-4.623737000	1.354486000	3.042442000
-5.408037000	1.097511000	3.746974000
-4.921698000	-2.142337000	0.250605000
-3.176659000	-4.037205000	-0.564370000
	1.013027000 -1.477355000 4.191678000 4.816049000 -6.005161000 2.145733000 3.197347000 -2.435186000 -3.481169000 -0.610087000 -1.662810000 -4.301009000 -4.851661000 1.729688000 2.473336000 0.365143000 0.365143000 0.375156000 -3.978493000 -4.623737000 -5.408037000 -4.921698000	1.013027000       -1.998584000         -1.477355000       4.701159000         4.191678000       -0.179240000         4.816049000       -1.015458000         -6.005161000       -2.253707000         2.145733000       -2.800620000         3.197347000       -2.818757000         -2.435186000       -2.258883000         -3.481169000       -2.352702000         -0.610087000       -2.978528000         -4.301009000       0.456896000         -4.851661000       -0.467447000         1.729688000       -3.151009000         2.473336000       -3.416671000         0.365143000       -3.508829000         -3.978493000       2.600221000         -4.623737000       1.354486000         -5.408037000       1.097511000         -4.921698000       -2.142337000

# **Optimized Coordinates of 2**

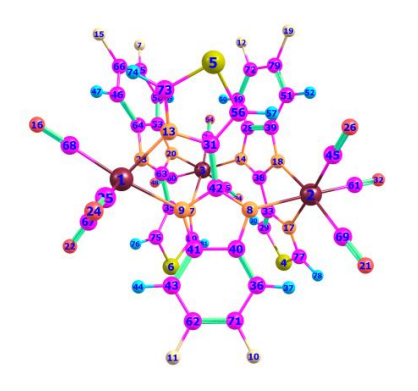


75	2.582580000	-2.104708000	-1.898444000
75	-0.230871000	3.635570000	-0.650621000
75	-1.638452000	-1.546302000	2.880971000
16	3.737812000	-3.004524000	2.630169000
16	-1.750785000	0.688060000	-4.055069000
16	1.999509000	1.349962000	3.856447000

7	-1.520849000	2.162454000	0.589218000
8	-2.465086000	5.715673000	-1.163960000
7	-2.135774000	0.245967000	1.671569000
7	2.279700000	0.123027000	-1.339647000
7	2.905204000	-2.343726000	0.312069000
7	0.086818000	-0.123685000	3.031577000
7	0.607223000	-2.450904000	-0.949910000
7	-0.766467000	-2.301458000	0.870384000
7	1.373572000	2.108267000	-0.665727000
7	-0.731841000	2.124395000	-2.211980000
8	5.524957000	-1.718001000	-2.785574000
8	-0.466039000	-3.830441000	4.603446000
8	0.635645000	5.415087000	1.721752000
8	1.506769000	5.324196000	-2.569981000
8	-4.255481000	-3.186716000	2.756367000
6	-3.798021000	2.561533000	-0.474767000
1	-3.569811000	3.492160000	-0.971491000
6	4.699179000	2.693867000	0.930094000
6	2.652572000	2.054605000	-0.155924000
8	1.880461000	-1.908632000	-4.899177000
6	-1.181615000	1.176813000	1.448868000
6	-3.417411000	-3.035832000	-1.714904000
6	-3.237740000	0.684476000	0.967927000
6	-1.549893000	-2.541605000	-0.268444000
6	-5.485377000	0.859473000	0.140433000
6	0.004390000	1.057583000	2.290865000
6	-6.831083000	0.399184000	0.043143000
1	-7.109654000	-0.505632000	0.575678000
6	4.528097000	0.509221000	-0.217035000
1	5.010187000	-0.399800000	-0.543689000
6	3.370269000	2.987932000	0.567504000
1	2.941218000	3.949201000	0.826027000
6	-1.667173000	4.912163000	-0.934171000
6	6.638275000	1.176625000	0.887467000
1	7.087452000	0.239013000	0.571753000
6	-1.703433000	2.103344000	-3.083586000
1	-2.422922000	2.899531000	-3.193601000
6	0.966277000	1.965197000	2.621111000
1	1.109950000	2.959855000	2.247470000
6	-5.116052000	2.064318000	-0.559175000
6	5.283304000	1.438224000	0.530051000
6	-0.677810000	-2.670305000	-1.394448000
6	5.499086000	3.614196000	1.668606000
1	5.060963000	4.563905000	1.961891000
6	-2.860962000	1.884132000	0.285490000
6	7.373367000	2.085861000	1.600706000
1	8.404845000	1.869308000	1.859219000
6	-3.270346000	-2.585978000	2.755350000
6	1.763613000	-2.430104000	1.112707000
6	1.232896000	0.981854000	-1.400882000
6	-4.522165000	0.179884000	0.909450000
1	-4.802709000	-0.707315000	1.464781000

```
6
     2.129919000
                    -1.959437000
                                   -3.771734000
6
     0.058621000
                    0.970582000
                                   -2.273389000
6
     -2.912433000
                    -2.703007000
                                   -0.440235000
1
     -3.609304000
                    -2.605911000
                                    0.376693000
6
     -2.522612000
                                   -2.831681000
                    -3.214376000
6
     -6.116080000
                    2.743290000
                                   -1.315322000
1
     -5.843679000
                    3.658973000
                                   -1.832685000
8
     2.956461000
                                   -2.278441000
                    -5.148414000
6
     0.307775000
                    4.750996000
                                   0.833119000
6
     3.222905000
                    0.809471000
                                   -0.564433000
6
     0.495885000
                    -2.322489000
                                    0.392960000
6
     6.795523000
                    3.320239000
                                    1.997993000
1
     7.389994000
                    4.034459000
                                    2.558403000
6
     2.039018000
                    -2.795325000
                                    2.397897000
1
     1.353973000
                    -3.031467000
                                    3.190621000
6
     -7.397831000
                    2.266442000
                                   -1.386724000
1
     -8.145020000
                    2.798889000
                                   -1.966352000
6
     -0.921796000
                    -2.994604000
                                    3.942886000
6
     4.422990000
                    -1.823945000
                                   -2.458337000
6
     0.861069000
                    4.702048000
                                   -1.848137000
6
     -1.140202000
                    -3.024223000
                                   -2.648020000
1
    -0.454118000
                    -3.187303000
                                   -3.472634000
6
     -3.071484000
                    -3.584534000
                                   -4.094556000
1
     -2.395636000
                    -3.730821000
                                   -4.932409000
6
     -4.814145000
                    -3.226879000
                                   -1.928039000
1
    -5.489895000
                    -3.090637000
                                   -1.089295000
6
    -5.303203000
                    -3.574755000
                                   -3.158593000
1
     -6.369941000
                    -3.713834000
                                   -3.300609000
6
     -2.363419000
                    -0.732270000
                                    4.485491000
8
     -2.781961000
                    -0.238182000
                                    5.437189000
6
    -7.759970000
                    1.078225000
                                   -0.698899000
     -8.779949000
1
                    0.712841000
                                   -0.761159000
6
     -4.420212000
                    -3.757934000
                                   -4.255525000
1
     -4.820669000
                    -4.038906000
                                   -5.224310000
6
     3.996272000
                    -2.605187000
                                    0.979100000
1
     4.982613000
                    -2.596248000
                                    0.540837000
6
     2.816166000
                    -4.012908000
                                   -2.148220000
6
     1.077501000
                    -0.097662000
                                    3.884328000
1
     1.292692000
                    -0.900645000
                                    4.572005000
6
     -0.359551000
                    0.094934000
                                   -3.228843000
1
     0.053961000
                    -0.854664000
                                   -3.497890000
```

# **Optimized Coordinates of 3**



75	1.274255000	3.493563000	-0.135649000
75	-3.335939000	-0.745979000	1.643083000
75	1.686864000	-2.701536000	-1.827547000
16	-3.839796000	-2.684144000	-2.674664000
16	1.056516000	1.641523000	4.239389000
16	-0.597488000	0.540637000	-4.435907000
9	6.393721000	-1.241211000	1.851101000
7	-2.280397000	1.091588000	0.695811000
7	-0.700815000	2.487475000	-0.173401000
9	-5.443794000	2.284800000	-2.840938000
9	-3.572083000	3.941580000	-3.820686000
9	3.160215000	-3.418292000	3.840404000
7	0.966829000	2.508307000	1.843337000
7	0.253772000	-2.574183000	-0.004838000
9	6.153961000	1.376496000	2.381643000
8	3.939007000	4.974619000	0.404755000
7	-3.291833000	-1.558910000	-0.452468000
7	-1.398136000	-1.786419000	1.357582000
9	1.159218000	-2.574462000	5.412985000
7	2.466104000	-0.800207000	-0.980588000
8	-6.141407000	0.566053000	1.573016000
8	1.447673000	4.591586000	-3.017255000
7	2.249787000	1.433721000	-0.569865000
8	-0.161883000	6.079323000	0.761717000
6	0.376035000	5.121967000	0.418623000
8	-3.218342000	0.130251000	4.600551000
7	0.545998000	-1.020960000	-2.773583000
6	0.700154000	-2.603600000	1.314150000
6	-2.230834000	-2.821821000	-2.060742000
1	-1.514239000	-3.443968000	-2.563908000
6	-0.149938000	1.675387000	1.985311000
8	-4.645171000	-3.379617000	2.590670000
6	-2.102084000	-2.157032000	-0.875748000
8	0.219636000	-5.043198000	-3.213495000
6	0.850460000	0.274775000	-2.348936000
6	-4.030963000	1.583200000	-1.090324000
1	-4.842435000	0.981111000	-0.714347000
6	-1.019711000	-2.130102000	0.102304000

```
6
     -0.336998000
                    -2.130530000
                                    2.154167000
6
    -2.781656000
                    1.682347000
                                   -0.460397000
6
    -1.800145000
                     2.552589000
                                   -0.990868000
6
    -1.055070000
                     1.658653000
                                    0.837241000
6
     -2.043156000
                     3.338973000
                                   -2.125123000
1
     -1.323624000
                    4.046586000
                                   -2.516395000
6
     -3.243041000
                    -0.176943000
                                    3.486386000
     4.246132000
                                    1.014390000
6
                    1.571063000
1
     4.241157000
                    2.628373000
                                    1.225424000
8
                    -2.537801000
     3.651892000
                                   -4.206961000
6
     1.906749000
                    -3.036656000
                                    1.883054000
1
     2.735686000
                    -3.421045000
                                    1.312717000
6
     -0.215808000
                    -2.123418000
                                    3.550149000
1
     -1.023740000
                    -1.830705000
                                    4.208529000
6
     3.459160000
                    -0.445598000
                                   -0.102192000
8
     3.592029000
                    -4.803139000
                                   -0.599657000
6
     0.776381000
                    -4.184274000
                                   -2.672368000
     -0.247262000
                     1.133762000
                                    3.231619000
6
1
     -1.005910000
                    0.491873000
                                    3.628651000
6
     4.492275000
                    -1.211193000
                                    0.454039000
1
     4.630733000
                    -2.261652000
                                    0.235747000
6
     2.924393000
                    -2.608986000
                                   -3.318641000
6
     -4.161021000
                    -2.393583000
                                    2.248184000
6
     -3.274658000
                    3.216356000
                                   -2.727261000
6
     1.811527000
                    0.352732000
                                   -1.255668000
6
     3.330018000
                    0.940465000
                                   0.158585000
6
     5.375486000
                    -0.568259000
                                    1.289598000
6
     5.249373000
                    0.804358000
                                    1.564501000
6
     1.389599000
                    4.179634000
                                   -1.938271000
6
     2.971648000
                    4.384258000
                                   0.185669000
                                   1.601271000
6
     -5.083993000
                    0.105918000
6
     2.861884000
                    -4.015079000
                                   -1.019130000
6
     -4.252927000
                    2.348626000
                                   -2.213824000
6
     2.023430000
                    -3.003131000
                                    3.254329000
6
     1.674860000
                    2.575397000
                                    2.938830000
1
     2.571410000
                    3.168185000
                                   3.034836000
6
     0.314127000
                    1.239523000
                                   -3.149152000
1
     0.434122000
                    2.303627000
                                   -3.094296000
6
                                   -1.299468000
     -4.268097000
                    -1.749745000
1
     -5.270458000
                    -1.376561000
                                   -1.152850000
6
     0.976137000
                    -2.557883000
                                    4.080189000
6
     -0.198615000
                    -1.021307000
                                   -3.848878000
     -0.519795000
                    -1.920386000
                                   -4.351532000
```

## 3.3. Experimental Section

#### General Data

Re<sub>2</sub>(CO)<sub>10</sub>, 2-(4-thiazolyl)benzimidazole (H–Tzbim), 1,2-diamino-4,5-difluorobenzene, thiazole-4-carboxaldehyde, DMF, DMSO, toluene and chlorobenzene were purchased from commercial sources and used as received. The ligand 2-(4-thiazolyl)naphthanoimidazole (H–Tznim) and 2-(4-thiazolyl)-5,6-difluorobenzimidazole (H-Tzbim-F<sub>2</sub>) were prepared by following the modified procedure. The ATR–IR spectra were recorded on a Nicolet iS5 IR spectrophotometer. NMR spectra were recorded on a Bruker AVANCE III 500 MHz instrument. ESI-MS spectra were recorded on Bruker maXis mass spectrometer. UV–Visible spectra were recorded on JASCO V–750 spectrophotometer and fluorescence spectra were recorded on WI-Tec confocal Raman spectrometer. Solid state emission spectra were recorded on WI-Tec confocal Raman spectrometer with 405 nm as the excitation source. The lifetime of the complexes was measured using a time-correlated single-photon counting (TCSPC) fluorescence spectrometer (Horiba JobinYvon, IBH). The relative quantum yield for the complexes was calculated using [Ru(bpy)<sub>3</sub>](PF<sub>6</sub>)<sub>2</sub> as standard in acetonitrile solution.

#### Synthesis of 4-(5,6-difluoro-1*H*-benzimidazol-2-yl)thiazole (H–Tzbim–F<sub>2</sub>)

1,2-Diamino-4,5-difluorobenzene (1.00 g, 6.94 mmol), thiazole-4-carboxaldehyde (784.97 mg, 6.94 mmol) and NaHSO<sub>3</sub> (2.17 g, 20.82 mmol) were dissolved in DMF (15 mL) and allowed to stir at 80  $^{\circ}$ C for 6 h. The progress of the reaction was monitored using thin layer chromatography and  $^{19}$ F-NMR spectroscopy. After completion, the reaction mixture was poured into ice-water and stirred thoroughly. The brown precipitate obtained was collected, washed with water, diethyl ether and air-dried. Yield: 52 % (858.7 mg).  $^{1}$ H-NMR (500 MHz, DMSO- $d_6$  at 298 K):  $\delta$  13.20 (s, 1H, -

NH), 9.33 (d, 1H, J = 1.85 Hz, H<sup>a</sup>), 8.45 (d, 1H, J = 1.9 Hz, H<sup>b</sup>), 7.72–7.68 (m, 1H, H<sup>c</sup>) and 7.47–7.44 (m, 1H, H<sup>d</sup>). <sup>19</sup>F-NMR (500 MHz, DMSO- $d_6$  at 298 K): –143.05 (d, J = 20 Hz) and –144.87 (d, J = 20 Hz).

## Synthesis of fac-[{Re(CO)<sub>3</sub>(Tzbim)}<sub>3</sub>] (1)

Re<sub>2</sub>(CO)<sub>10</sub> (100.1 mg, 0.153 mmol), H–Tzbim (138.8 mg, 0.689 mmol), toluene (10 mL) were taken in a teflon vessel which was then placed in a stainless steel bomb. The bomb was placed in an oven maintained at 180 °C for 48 h and allowed to cool up to 30 °C. The filtered mother liquor was kept undisturbed for 2–3 days to yield pale yellow crystals. The crystals were washed with hexane and air-dried. Yield: 52% (73.3 mg). ATR-IR ( $v_{max}$ , cm<sup>-1</sup>): 2021 and 1878 (CO). ESI–MS Calcd. for C<sub>39</sub>H<sub>18</sub>N<sub>9</sub>O<sub>9</sub>Re<sub>3</sub>S<sub>3</sub> [**1** + H]<sup>+</sup>: m/z 1411.9104, found: m/z 1411.9047. <sup>1</sup>H NMR (500 MHz, DMSO- $d_6$ , at 298 K):  $\delta$  10.32 (d, 1H, J = 1.75 Hz, H<sup>a1</sup>), 9.99 (d, 1H, J = 1.75 Hz, H<sup>a2</sup>), 9.89 (d, 1H, J = 1.75 Hz, H<sup>b1</sup>), 8.26 (d, 1H, J = 1.75 Hz, H<sup>b3</sup>), 8.08 (d, 1H, J = 1.75 Hz, H<sup>b2</sup>), 7.96 (d, 1H, J = 8.4 Hz, H<sup>c1</sup>), 7.86 (d, 1H, J = 8.4 Hz, H<sup>c2</sup>), 7.84 (d, 1H, J = 8.4 Hz, H<sup>c3</sup>), 7.31–7.25 (m, 2H, H<sup>c1</sup>, 2), 7.14–7.10 (m, 2H, H<sup>d1,d2</sup>), 7.05–7.01 (t, 1H, J = 7.4 Hz, H<sup>c3</sup>) and 6.74–6.70 (t, 1H, J = 8 Hz, H<sup>d3</sup>).

### Synthesis of fac-[{Re(CO)<sub>3</sub>(Tznim)}<sub>3</sub>] (2)

Reddish-brown crystals of **2** were obtained by following the procedure similar to that of **1**, using Re<sub>2</sub>(CO)<sub>10</sub> (100.3 mg, 0.153 mmol), H–Tznim (70.3 mg, 0.276 mmol) and toluene (7 mL). Crystals were washed with pentane and air-dried. Yield: 42 % (43.7 mg). ATR–IR ( $\nu_{max}$ , cm<sup>-1</sup>): 2014, 1894 (CO). ESI–MS Calcd. for C<sub>51</sub>H<sub>24</sub>N<sub>9</sub>O<sub>9</sub>Re<sub>3</sub>S<sub>3</sub> [**2**– 2H]<sup>+</sup>: m/z 1560.9504, found: m/z 1560.9608. <sup>1</sup>H NMR (500 MHz, DMSO- $d_6$ , at 298 K):  $\delta$  10.68 (d, 1H, J = 1.75 Hz, H<sup>a1</sup>), 9.91 (d, 1H, J = 1.75 Hz,

 $H^{a2}$ ), 9.85 (d, 1H, J = 1.75 Hz,  $H^{a3}$ ), 8.59 (d, 1H, J = 1.75 Hz,  $H^{b1}$ ), 8.55 (d, 1H, J = 1.75 Hz,  $H^{b2}$ ), 8.49 (s, 1H,  $H^{c2}$ ), 8.43 (d, 1H, J = 1.75 Hz,  $H^{b3}$ ), 8.41 (s, 1H,  $H^{c1}$ ), 8.37 (d, 2H, J = 9 Hz,  $H^{d2,d3}$ ), 8.29 (d,1H, J = 8.24 Hz,  $H^{d1}$ ), 8.21 (s,1H,  $H^{c3}$ ), 8.18 (dd, 2H, J = 9.5 Hz,  $H^{e2,e3}$ ), 7.97 (d, 3H,  $H^{b1,b2,b3}$ ), 7.48–7.45 (m, 3H,  $H^{e1,f2,f3}$ ) 7.38–7.34 (m, 2H,  $H^{g2,g3}$ ), 7.14 (t, 1H,  $H^{g1}$ ) and 6.95 (t, 2H, J = 7.75 Hz,  $H^{f1}$ ).

## Synthesis of fac-[{Re(CO)<sub>3</sub>(Tzbim-F<sub>2</sub>)}<sub>3</sub>] (3)

Yellow crystals of **3** were obtained by following the procedure similar to that of **1**, Re<sub>2</sub>(CO)<sub>10</sub> (100.1 mg, 0.153 mmol), H–Tzbim–F<sub>2</sub> (60.6 mg, 0.255 mmol) and chlorobenzene (6 mL). Crystals were washed with hexane and air-dried. Yield: 72 % (84.9 mg). ATR-IR ( $v_{max}$ , cm<sup>-1</sup>): 2014, 1884 (CO). ESI–MS. Calcd. for C<sub>39</sub>H<sub>12</sub>F<sub>6</sub>N<sub>9</sub>O<sub>9</sub>Re<sub>3</sub>S<sub>3</sub> [3 – 2H]<sup>+</sup>: m/z 1518.8469, found: m/z 1518.8299. <sup>1</sup>H NMR (500 MHz, DMSO- $d_6$ , at 298 K):  $\delta$  10.48 (d, 1H, J = 1.7 Hz, H<sup>a1</sup>), 10.14 (d, 1H, J = 1.75 Hz, H<sup>a2</sup>), 10.05 (d, 1H, J = 1.7 Hz, H<sup>a3</sup>), 8.49 (d, 1H, J = 1.75 Hz, H<sup>b1</sup>), 8.40 (d, 1H, J = 1.75 Hz, H<sup>b2</sup>), 8.18 (d, 1H, J = 1.75 Hz, H<sup>b3</sup>), 7.94–7.90 (m, 2H, J = 8.4 Hz, H<sup>c1</sup>), 7.73–7.69 (m, 1H, H<sup>c2</sup>) 7.59–7.57 (m, 1H, H<sup>c3</sup>) and 7.36–7.34 (m, 1H, H<sup>c4</sup>).

Electrochemical studies. The cyclic voltammetry measurements of 1–3 (1 mM), H–Tzbim, H–Tznim and H–Tzbim– $F_2$  were studied using an AMETEK Princeton Applied Research VersaSTAT 3 potentiostat. Tetrabutylammoniumhexafluorophosphate (0.1 M) was used as supporting electrolyte. Glassy carbon was used as the working electrode, Pt wire as counter electrode, Ag/AgCl as reference electrode and ferrocene as an internal standard. All the measurements were performed under nitrogen atmosphere at room temperature. The LUMO energy levels were calculated from the reduction potential using the equation; LUMO = - ( $E_{red}$  + 4.8) eV.  $^{13b}$ 

Computational studies. The structure optimizations of 1–3 were performed in the gas phase using B3LYP function in the Gaussian 09 program package. The coordinates for optimizations were taken from X-ray crystal structure of 1–3. The Stuttgart-Dresden-Effective Core Potential (SDD-ECP) basis set was used for Re-centers and 6-311G\* was used for C, H, N and O atoms. The absorption studies were validated by time-dependent density functional theory (TD-DFT) calculations using integral equation formalism for the polarizable continuum model (IEF-PCM) with DMSO as solvent model. The TDDFT calculations were performed using B3LYP function and SDD/6-311G\* basis set for 1–3. The stimulated absorption spectra and corresponding molecular orbitals were obtained from the GaussSum program and GaussView program package, respectively.

**X-ray crystallography.** The single crystal X-ray diffraction data were collected at 296(2) K on Rigaku Oxford XtaLAB synergy and Bruker D8 quest diffractometer equipped with Mo-K $\alpha$  radiation ( $\lambda = 0.71073$  Å) source. Cell refinement and data reduction was performed using CrysAlisPro and Bruker APEX 3 software programs. The structure solutions and refinements were performed with OLEX and SHELX program package. Non-hydrogen atoms were refined anisotropically. Due to high disorder the solvent lattice molecules for **1** have been fixed isotropically.

#### 3.4. Conclusion

Three new fac-[Re(CO)<sub>3</sub>] core-based neutral homoleptic discrete triangular complexes were selfassembled using Re<sub>2</sub>(CO)<sub>10</sub> and thiabendazole motif via one-pot solvothermal approach. All three triangular complexes possess uncoordinated sulfur atoms from thiazolyl motif that are directed along the complex axis. The complex possessing fluorine substituents on the periphery of benzimidazolate (3) undergo self-organization into 1D tubular architecture via complementary intermolecular unusual non-covalent C-F...S contacts. To the best of our knowledge, the current result is the first report on fac-[Re(CO)<sub>3</sub>] core-based discrete complexes functionalized with fluorine atoms which self-organizes into 1D tubular architecture. The photophysical properties of 1-3 were studied using UV-Visible and emission spectroscopy and validated using TD-DFT calculations. The electrochemical properties were studied using cyclic voltammetry. The solution state studies using concentration dependent and low temperature NMR, UV-Visible and fluorescence spectroscopic methods are suggestive of the prominent role of fluorine atoms in forming intermolecular interactions presumably C-F...S contacts in the solution. The study provides the insight for the design of neutral metal-organic complexes and metallacycles with fluorine and heteroatom functional groups that can be utilized to build tubular and hierarchical supramolecular architectures from discrete SCCs.

#### 3.5. References

- a) G. Moreno-Alcantarand, A. Casini, FEBS Letters 2023, 597, 191–202; b) D. Chakraborty, R. Saha, J. K. Clegg, P. S. Mukherjee, Chem. Sci., 2022, 13, 11764–11771; c) Z. Cui, G. Jin, Nat. Synth., 2022, 1, 635–640; c) D. Zhang, T. K. Ronson, Y. Zou, J. R. Nitschke, Nat Rev Chem., 2021, 5, 168–182.; d) N. Dey, C. J. Haynes, ChemPlusChem 2021, 86, 418–433; e) I. Mishra, M. Bhol, P. Kalimuthu, M. Sathiyendiran, Chem. Rec. 2021, 21, 1–22; f) A. Kumar, P. S. Mukherjee, Chem. Eur. J. 2020, 26, 4842–4849.
- a) Y. Sun, C. Chen, J. Liu, P. J. Stang, *Chem. Soc. Rev.* 2020, 49, 3889–3919; b) S. Samantray,
   S. Krishnaswamy, D. K. Chand, *Nat Commun.* 2020, 11, 880; c) J. E. M. Lewis, J. D. Crowley,
   *ChemPlusChem* 2020, 85, 815–827.
- a) H. Sepehrpour, W. Fu, Y. Sun, P. J. Stang, J. Am. Chem. Soc. 2019, 141, 14005–14020; b) M. PanKai, W. Zhang, C. Su, Coord. Chem. Rev. 2019, 378, 333–349; c) T. Tateishi, Y. Yasutake, T. Kojima, S. Takahashi, S. Hiraoka, Chem Commun, 2019, 2, 25.
- a) K. R. Soumya, I. Mishra, M. Kedia, U. Phukon, R. Borkar, M. Sathiyendiran, Rhenium (I)-based supramolecular coordination complexes: Synthesis and functional properties. In Supramolecular Coordination Complexes: Design, Synthesis and Applications, 1st Ed.; Elseiver, 2022, pp 133-153. b) A. A. Haase, E. B. Bauer, F. E. Kühn, D. C. Crans, *Coord. Chem. Rev.* 2019, 394, 135–161. c) W. Gao, H. Zhang, G. Jin, *Coord. Chem. Rev.*, 2019, 386, 69–84. d) D. Gupta, M. Sathiyendiran, *ChemistrySelect* 2018, 3, 7439 7458. e) R. Govindarajan, R. Nagarajaprakash, V. Veena, N. Sakthivel, B. Manimaran, *Polyhedron* 2018, 139, 229 236. f) J. Rohacova, O. Ishitani, *Dalton Trans.*, 2017, 46, 8899–8919. g) V. Sathish, A. Ramdass, M. Velayudham, K. L. Lu, P. Thanasekaran, S. Rajagopal, *Dalton Trans.*, 2017, 46, 16738–16769.

- a) J. Varghese, U. Kumar, S. Jose, A. A. Magray, S. Y. Kumar, R. Padmanaban, B. Manimaran, New J. Chem., 2023, 47, 3582–3590. b) M. Bhol, B. Shankar, M. Sathiyendiran, Inorg. Chem. 2022, 61, 11497-11508. c) M. Kedia, B. Shankar, M. Sathiyendiran, Inorg. Chem. 2022, 61, 14506-14510. d) U. Phukon, B. Shankar, M. Sathiyendiran, Dalton Trans., 2022, 51, 16307; e) B. Tzeng, A. Chao, M. Lin, G. Lee, T. Kuo, Chem. Eur. J. 2017, 23, 18033-18040.
- a) P. Rajakannu, P. Elumalai, B. Shankar, F. Hussain, M. Sathiyendiran, *Dalton Trans.*, 2013,
   42, 11359–11362; b) D. Gupta, P. Rajakannu, B. Shankar, R. Shanmugam, F. Hussain, B. Sarkar, M. Sathiyendiran, *Dalton Trans.*, 2011, 40, 5433–5435; c) D. Bhattacharya, C. Chang, Y. Cheng, L. Lai, H. Lu, C. Lin, K. Lu, *Chem. Eur. J.* 2012, 18, 5275 5283.
- a) B. Laramée-Milette, N. Zaccheroni, F. Palomba, G. S. Hanan, *Chem. Eur. J.* 2017, 23, 6370 6379; b) P. J. Wright, S. Muzzioli, B. W. Skelton, P. Raiteri, J. Lee, G. Koutsantonis, D. S. Silvester, S. Stagni, M. Massi, *Dalton Trans.*, 2013, 42, 8188–8191; c) F. L. Thorp-Greenwood, V. Fernández-Moreira, C. O. Millet, C. F. Williams, J. Cable, J. B. Court, A. J. Hayes, D. Lloyd, M. P. A. Coogan, *Chem. Commun.* 2011, 47, 3096–3098. d) P. Barbazán, R. Carballo, J. S. Casas, E. García-Martínez, G. Pereiras-Gabián, A. Sánchez, E. M. Vázquez-López, *Inorg. Chem.* 2006, 45, 7323-7330; c) T. Brasey, A. Buryak, R. Scopelliti, K. Severin, *Eur. J. Inorg. Chem.* 2004, 964–967.
- a) S. Kumar, B. Mohan, C. Fu, V. Gupta, P. Ren, *Coord. Chem. Rev.* 2023, 475, 214876. b) H.
   R. Khavasi, N. Rahimi, *ChemistrySelect* 2017, 2, 11314–11321. c) J. Vincent, *Chem. Commun.* 2012, 48, 11382–11391. d) M. Kleinwächter, L. Vendier, C. Dinoi, M. Etienne, *Dalton Trans.* 2013, 42, 10102–10105.
- a) J. Santolaya, N. Busto, M. Martínez-Alonso, G. Espino, J. Grunenberg, G. Barone, B. García,
   J. Bio. Inorg. Chem., 2020, 25, 1067–1083. b) A. Tian, X. Ji, N. Sun, R. Xiao, Y. Zhao, H. Ni,
   Y. Tian, J. Ying, J Chem Crystallogr, 2017, 47, 1–9. c) A. Tian, Y. Yang, N. Sun, J. Li, J. Ying,

- J. Zhang, X. Wang, J. Coord. Chem. 2014, 67, 1550-1561. d) M. Devereux, M. McCann, D. Shea, R. Kelly, D. Egan, C. Deegan, K. Kavanagh, V. McKee, G. Finn, J. Inorg. Biochem. 2004, 98, 1023–1031.
- a) K. J. Thorley, I. McCulloch, *J. Mater. Chem. C*, 2018, 6, 12413–12421. b) M. S. Pavan, K. D. Prasad, T. N. G. Row, *Chem. Commun.* 2013, 49, 7558–7560. c) S. K. Nayak, V. Kumar, J. S. Murray, P. Politzer, G. Terraneo, T. Pilati, P. Metrangolo, G. Resnati, *CrystEngComm* 2017, 19, 4955.
- 11. K. E. Splan, C. L. Stern, J. T. Hupp, *Inorg. Chim. Acta* 2004, **357**, 4005–4014.
- a) S. Sinha, E. K. Berdichevsky, J. J. Warren, *Inorg. Chim. Acta* 2017, 460, 63–68. b) A. Comia, L. Charalambou, S. A. E. Omar, P. A. Scattergood, P. I. P. Elliott, A. Sinopoli, *Inorganics* 2020, 8, 1–13. e) P. H. Dinolfo, K. D. Benkstein, C. L. Stern, J. T. Hupp, *Inorg. Chem.* 2005, 44, 8707-8714. c) M. M. Lee, J. Lin, C. Chang, C. Hung, C. Chen, C. Hsu, S. Sun, *Eur. J. Inorg. Chem.* 2017, 5224–5237.
- a) A. K. Narsaria, J. Poater, C. F. Guerra, A. W. Ehlers, K. Lammertsma, F. M. Bickelhaupt, J. Comp. Chem. 2018, 39, 2690-2696. b) Y. Cho, S. Kim, M. Cho, W. Han, H. Son, D. W. Cho, S. O. Kang, Phys. Chem. Chem. Phys. 2016, 18, 9702–9708.
- 14. a) V. Karunakaran, D. D. Prabhu, S. Das, *J. Phys. Chem. C* 2013, **117**, 9404–9415. (b) P. Pang,
  X. Miao, L. Ying, G. Kong, C. Che, W. Deng, *J. Phys. Chem. C* 2020, **124**, 5665–5671. (c) M.
  Zhang, S. Yin, J. Zhang, Z. Zhou, M. L. Saha, C. Lu, P. J. Stang, *PNAS* 2017, **114**, 3044–3049.
- 15. X. Han, H. Ma, Y. Wang, Russ. J. Org. Chem. 2008, 44, 863.
- 16. a) Gaussian 09, Revision C.01, M. J. Frisch, G. W. Trucks, H. B. Schlegel, G. E. Scuseria, M. A. Robb, J. R. heeseman, G. Scalmani, V. Barone, B. Mennucci, G. A. Petersson, H. Nakatsuji, M. Caricato, X. Li, H. P. Hratchian, A. F. Izmaylov, J. Bloino, G. Zheng, J. L. Sonnenberg, M.

Hada, M. Ehara, K. Toyota, R. Fukuda, J. Hasegawa, M. Ishida, T. Nakajima, Y. Honda, O. Kitao, H. Nakai, T. Vreven, J. A. Montgomery, Jr., J. E. Peralta, F. Ogliaro, M. Bearpark, J. J. Heyd, E. Brothers, K. N. Kudin, V. N. Staroverov, T. Keith, R. Kobayashi, J. Normand, K. Raghavachari, A. Rendell, J. C. Burant, S. S. Iyengar, J. Tomasi, M. Cossi, N. Rega, J. M. Millam, M. Klene, J. E. Knox, J. B. Cross, V. Bakken, C. Adamo, J. Jaramillo, R. Gomperts, R. E. Stratmann, O. Yazyev, A. J. Austin, R. Cammi, C. Pomelli, J. W. Ochterski, R. L. Martin, K. Morokuma, V. G. Zakrzewski, G. A. Voth, P. Salvador, J. J. Dannenberg, S. Dapprich, A. D. Daniels, O. Farkas, J. B. Foresman, J. V. Ortiz, J. Cioslowski, and D. J. Fox, Gaussian, Inc., Wallingford CT, 2010.

17. a) G. M. Sheldrick, SHELXS-97: Program for Crystal Structure Solution, University of Göttingen, Göttingen, Germany, 1997; (b) G. M. Sheldrick, *Acta Crystallogr. Sect. A: Found Crystallogr.* 2008, **64**, 112–122; (c) G. M. Sheldrick, *Acta Crystallogr. Sect. C: Struct. Chem.* 2015, **71**, 3–8; (d) A. L. Spek, *J. Appl. Crystallogr.* 2003, **36**, 7–13.

# Chapter – 4

# Luminescent [fac-Re(CO)<sub>3</sub>-N $\cap$ O-phenylimidazole] complexes with parallel arrangement of twisted ligand motifs

**ABSTRACT.** Luminescent complexes [fac-Re(CO)<sub>3</sub>(Y $\cap$ X)(ph-imz)] where (Y $\cap$ XH) = H<sub>2</sub>-PBI= 2-(2'-hydroxyphenylbenzimidazole) for **1**, H-PBO= 2-(2'-hydroxyphenylbenzoxazole) for **2**, and H-PBT = 2-(2'-hydroxyphenylbenzothiazole) for **3** and ph-imz = 2-phenylimidazole) were synthesized using Re<sub>2</sub>(CO)<sub>10</sub>, H<sub>2</sub>-PBI/H-PBO/H-PBT and ph-imz via one pot approach. All three complexes were characterized using FT-IR, <sup>1</sup>H-NMR spectroscopy and X-ray diffraction analysis. The two coordinated and twisted ligand motifs arrange closely parallel to each other and interact through  $\pi$ ··· $\pi$  stacking interactions in solid state. All the complexes displayed moderate to strong emission both in solution and solid state at room temperature.

Re<sub>2</sub>(CO)<sub>10</sub>

$$Re_{2}(CO)_{10}$$

$$Re_{2}(CO)_{10}$$

$$Re_{2}(CO)_{10}$$

$$Re_{2}(CO)_{10}$$

$$Re_{2}(CO)_{10}$$

$$Re_{3}(CO)_{10}$$

$$Re_{4}(CO)_{10}$$

$$Re_{2}(CO)_{10}$$

$$Re_{3}(CO)_{10}$$

$$Re_{4}(CO)_{10}$$

$$Re_{5}(CO)_{10}$$

$$Re_{5}(CO)_{10$$

## 4.1. Introduction

Tricarbonyl rhenium(I)-based complexes possessing chelating N∩N units (2,2'-bipyridine (bpy), 1,10-phenanthroline and their derivatives) and monodentate neutral donors (pyridine, phosphine and their derivatives) have been gaining much interest in materials and biology. <sup>1-3</sup> The key properties associated with these complexes are kinetic inertness, photo-stability,<sup>4</sup> and metal-to-ligand charge-transfer absorptions and emissions. <sup>5</sup> Research has been intensely focusing on the area to increase absorption and emission towards the red region. To achieve these properties, both chelating ligands and monodentate ligands are tuned by either introducing the substituted groups on the ligands or using structurally similar ligands like those of bpy but possessing different electronic properties.<sup>6</sup> In this category, 2-(2'hydroxyphenylbenzimidazole) (H<sub>2</sub>-PBI)/ 2-(2'-hydroxyphenylbenzoxazole) (H-PBO)/ 2-(2'hydroxyphenylbenzothiazole) (H-PBT) are used to enhance the absorption in the visible region (350-450 nm). The complexes display emission at room temperature, both in solid and solution state. Recently, attempts have been made by incorporating nitrogen atom(s) in the anionic chelating ring and substituting various alkyl groups on the neutral monotopic nitrogen donor to enhance the photophysical properties.<sup>7</sup> The arrangement of these two ligand cores in the complexes is crucial for the solid state photophysical properties. The intra and inter molecular  $\pi \cdots \pi$  stacking interactions between these two organic units in the complexes in the solid state play a significant role in photophysical properties. Up to now, tricarbonyl rhenium(I) complexes with H<sub>2</sub>-PBI/H-PBO/H-PBT motifs were centered on pyridine/pyridine derivatives. These complexes were synthesized using two steps synthetic approach. 8a Attempt to use other monodentate heterocyclic donors like imidazole in place of pyridine motif in the complexes is also scarce. Similarly, one-step synthetic approach for the complexes, surprisingly, scarce.<sup>8</sup> Herein, we report three fac-Re(CO)<sub>3</sub>-core based complexes

[Re(CO)<sub>3</sub>(Y $\cap$ X)L] ((Y $\cap$ XH) = HN-N $\cap$ O for **1**, O-N $\cap$ O for **2**, and S-N $\cap$ O for **3**) and L = 2-phenylimidazole) which were synthesized using Re<sub>2</sub>(CO)<sub>10</sub>, H<sub>2</sub>-PBI/H-PBO/H-PBT and 2-phenylimidazole (ph-imz) *via* one-pot approach. Complexes **1—3** were characterized using various analytical and spectroscopic methods. The molecular structures of the complexes were determined using single crystal X-ray diffraction methods. The photophysical properties of the complexes were studied both in the solution and solid state.

## 4.2. Results and Discussions

# Synthesis of complexes 1–3

The treatment of  $Re_2(CO)_{10}$  with  $H_2$ -PBI/H-PBO/H-PBT and ph-imz in toluene resulted crystalline products **1–3** (Scheme 1). The complexes are air and moisture stable and soluble in polar organic solvents. The FT–IR spectra of the complexes display three carbonyl stretching bands in the range 2014–1856 cm<sup>-1</sup>, corresponding to the *fac*-tricarbonyl rhenium (I) motif. <sup>9a</sup>

$$Re_{2}(CO)_{10}$$

$$Re_{2}(CO)_{10}$$

$$Re_{2}(CO)_{10}$$

$$Re_{2}(CO)_{10}$$

$$Re_{2}(CO)_{10}$$

$$Re_{2}(CO)_{10}$$

$$Re_{3}(CO)_{10}$$

$$Re_{4}(CO)_{10}$$

$$Re_{5}(CO)_{10}$$

**Scheme 1.** Synthetic approach for complexes **1–3**.

The  ${}^{1}\text{H-NMR}$  spectrum of complex **3** in DMSO- $d_{6}$  shows two types of pattern which are assigned using  ${}^{1}\text{H-}{}^{1}\text{H}$  COSY spectroscopic methods. The presence of two sets of peaks may be considered to correspond for major and minor isomers due to the rotation of the phenyl ring in ph-imz motif in solution. In particular, triplet and doublet were observed for the protons ( $\text{H}^{3'-6'}$  and  $\text{H}^{4,7}$ ) in the high-field region (Figure 1–3). The data clearly indicates that moderate to strong intramolecular interactions exist between the two aromatic ligand motifs. A similar kind of pattern was observed for complexes **1** and **2**.

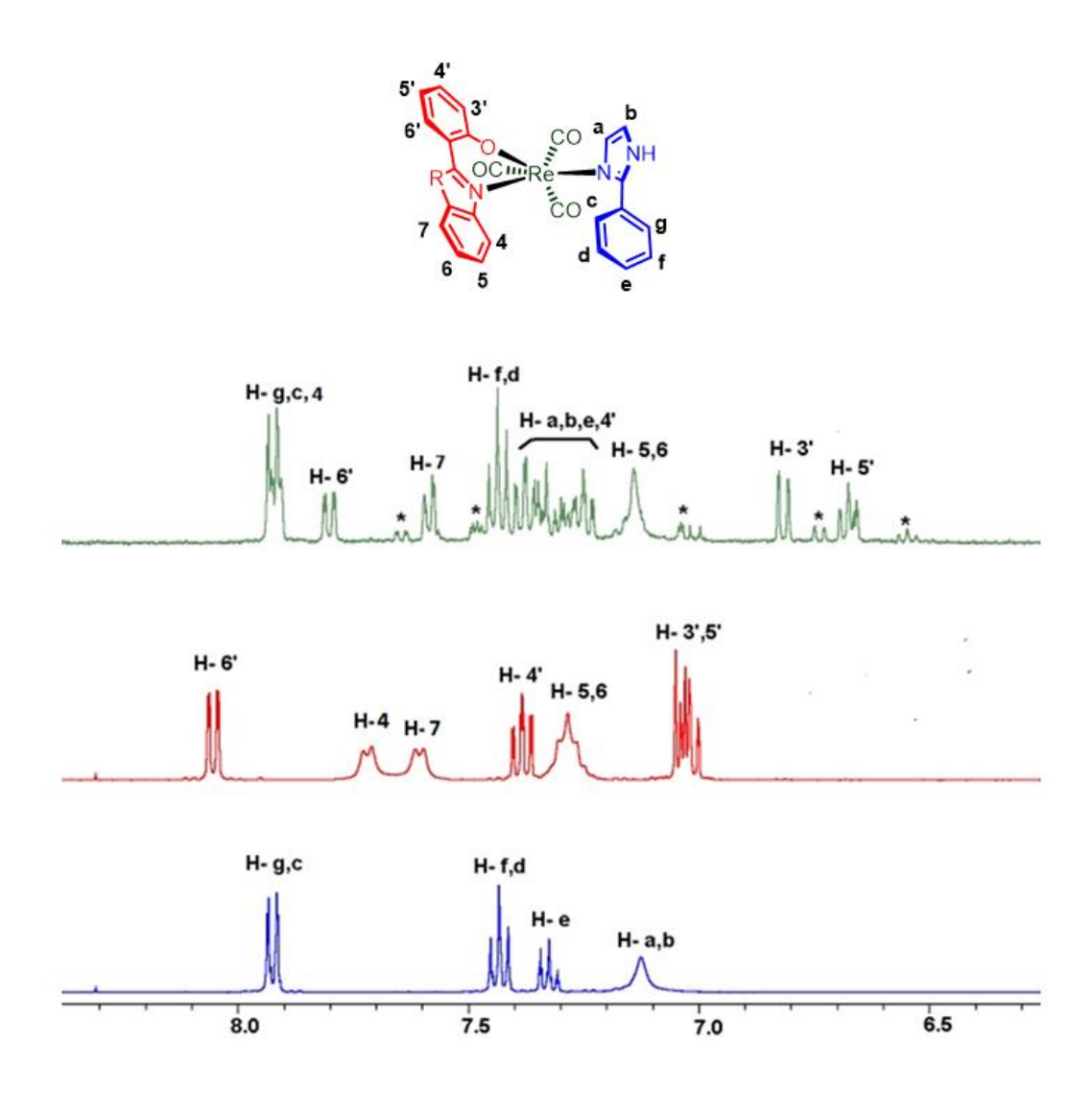


**Figure 1.**  $^{1}$ H-NMR spectra of ph-imz (blue), H<sub>2</sub>-PBI (red) and **1** (green) in DMSO- $d_6$  (\*indicates minor isomer peaks).

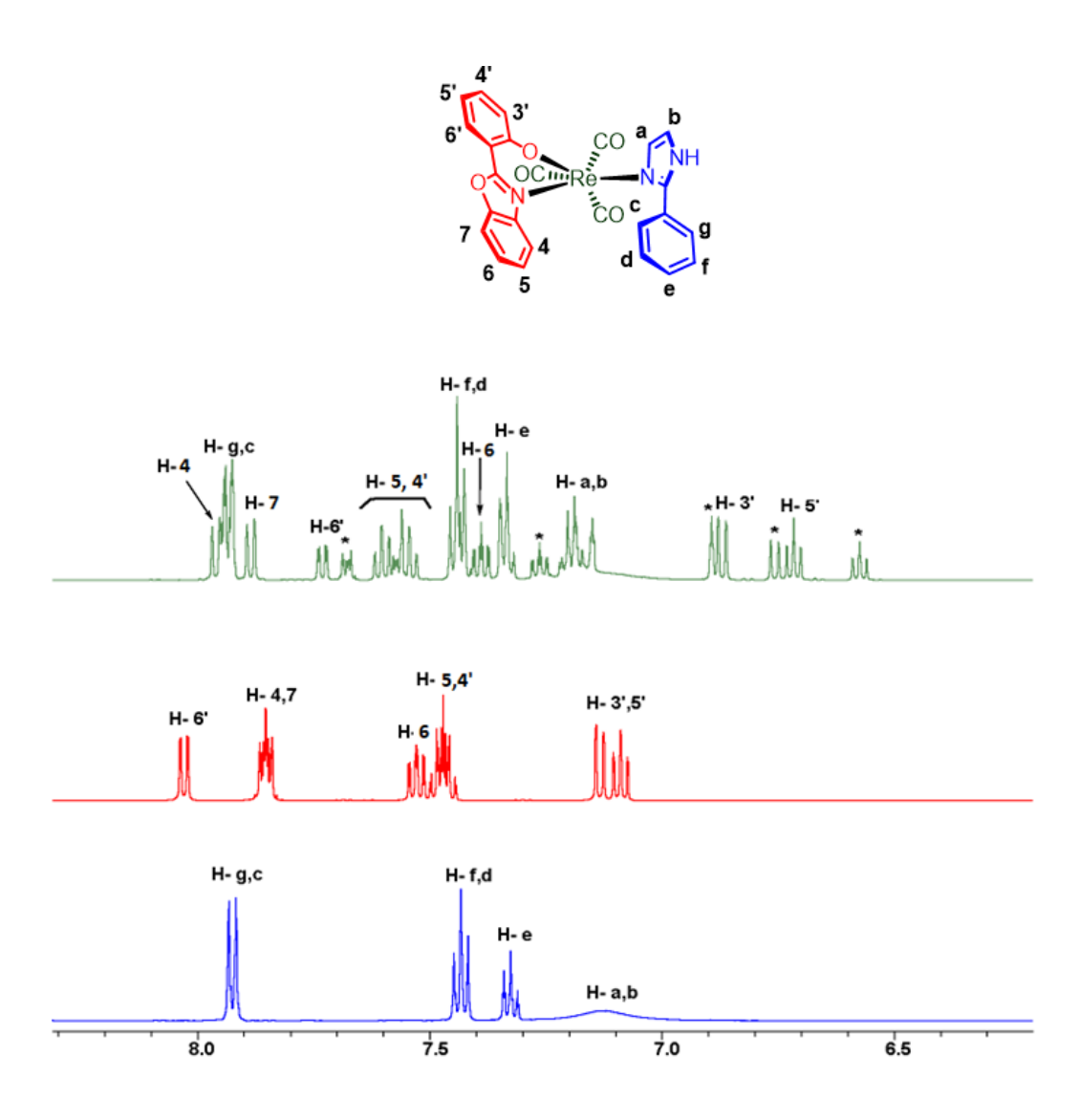


**Figure 2.**  $^{1}$ H-NMR spectra of ph-imz (blue), H-PBO (red) and **2** (green) in DMSO- $d_6$  (\*indicates minor isomer peaks).

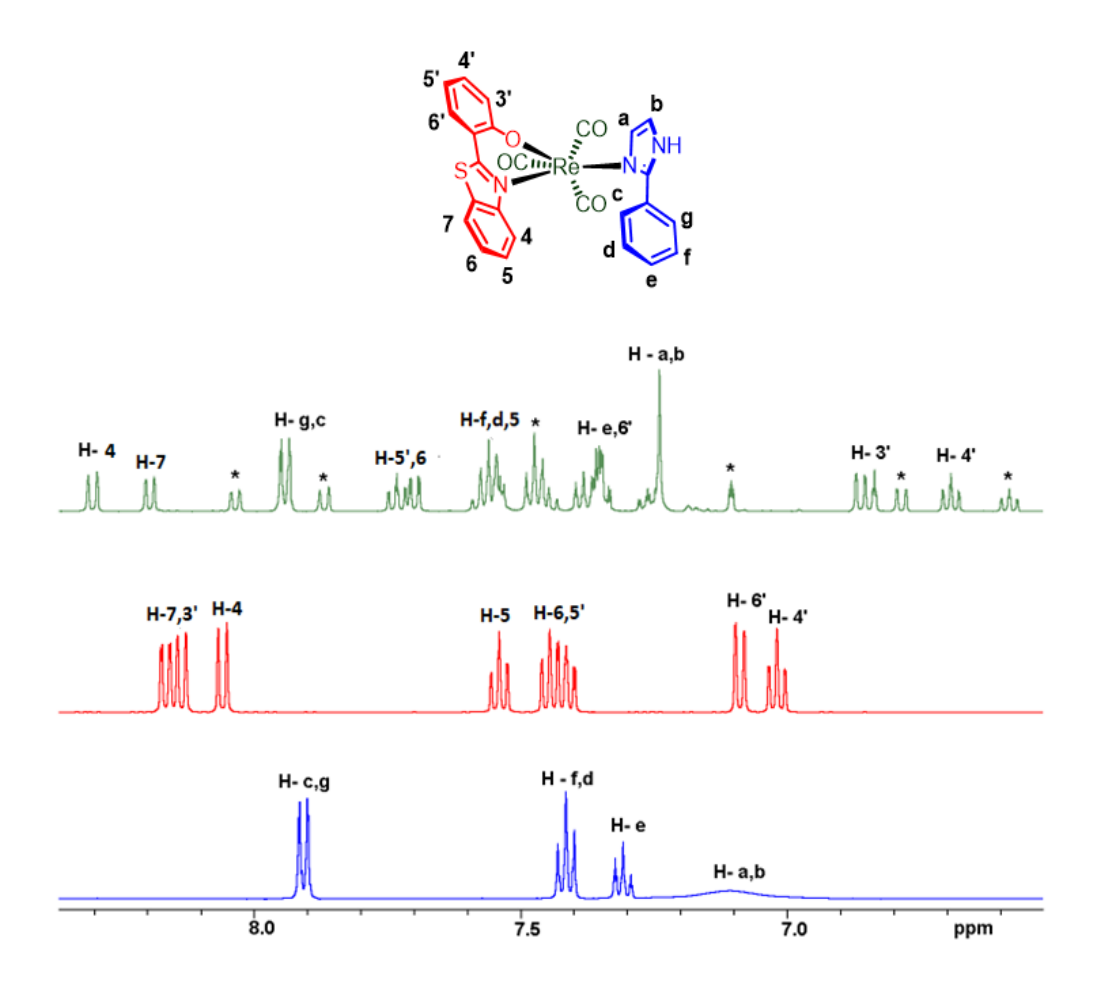


**Figure 3.**  $^{1}$ H-NMR spectra of ph-imz (blue), H-PBT (red) and **3** (green) in DMSO- $d_6$  (\*indicates minor isomer peaks).

The molecular structures of 1-3 were determined using single crystal X-ray diffraction analysis. The geometry around the rhenium core and the arrangement of two organic ligands in the complexes are similar to each other. The rhenium is in distorted octahedral geometry in the complexes. Two chelating atoms (NOO atoms) and two carbonyl carbon atoms are in the square planar geometry. The axial position of octahedral geometry is occupied by N from imidazole and one carbonyl carbon. The Re-O(PBI)/Re-N(ph-imz) distance is 2.137(5)/2.203(6) Å for 1, 2.167(3)/2.214(3) Å for 2, 2.209(4)/2.202(4) Å for 3, which indicate the ionic/coordination interactions between these two atoms. The Re-N(ph-imz) distance is 2.202-2.214 Å, which is in the expected range for Re-N(neutral heterocyclic donor).8-11 It is noteworthy to discuss the arrangement of the two organic donors in the complexes. Though the stoichiometry and bonding parameters of 1-3 are very similar to the complexes reported previously, 8a the two organic units are twisted significantly in 1-3 due to the intramolecular  $\pi \cdots \pi$  stacking interactions (Figure 4). Though N $\cap$ O atoms are in the square plane, the benzimidazole as well as phenolate motifs are not in the square plane. The phenolate is above the square plane whereas benzimidazole is below to it. The Re-N(imidazolyl) bond is bent towards chelating unit. In particular, the imidazolyl unit is bent with respect to Re-N plane. The dihedral angle between the phenolate and the imidazole is (10.14° in 1, 5.06° in 2 and 6.81° in 3). A similar kind of arrangement is found in those complexes possessing imidazole and phenanthroline units. 11 In general, the phenyl unit and imidazole unit in 2-phenyl imidazole are orthogonal to each other to avoid steric repulsion (H···H). 12 The phenyl unit of ph-imz is positioned over the chelating unit in 1-3 with the distance of 3.6 Å (centre of mass,  $COM_{ph} \cdots COM_{NS/NO}$ ), which indicates the strong  $\pi \cdots \pi$ stacking interactions between these units. The intramolecular interactions found between these units are slipped co-facial  $\pi\cdots\pi$  stacking interactions (Figure 4, Table 2). The *fac*-Re(CO)<sub>3</sub> core based complexes containing 8-hydroxyquinolate and 2-phenylimidazole motifs have phenyl unit of ph-imz positioned at a distance of 3.8 Å (COM<sub>ph</sub>····COM<sub>quinolate</sub>) with dihedral angle of 29.08°, indicating comparatively weaker intramolecular  $\pi\cdots\pi$  stacking interactions than complexes 1-3. <sup>8d</sup>

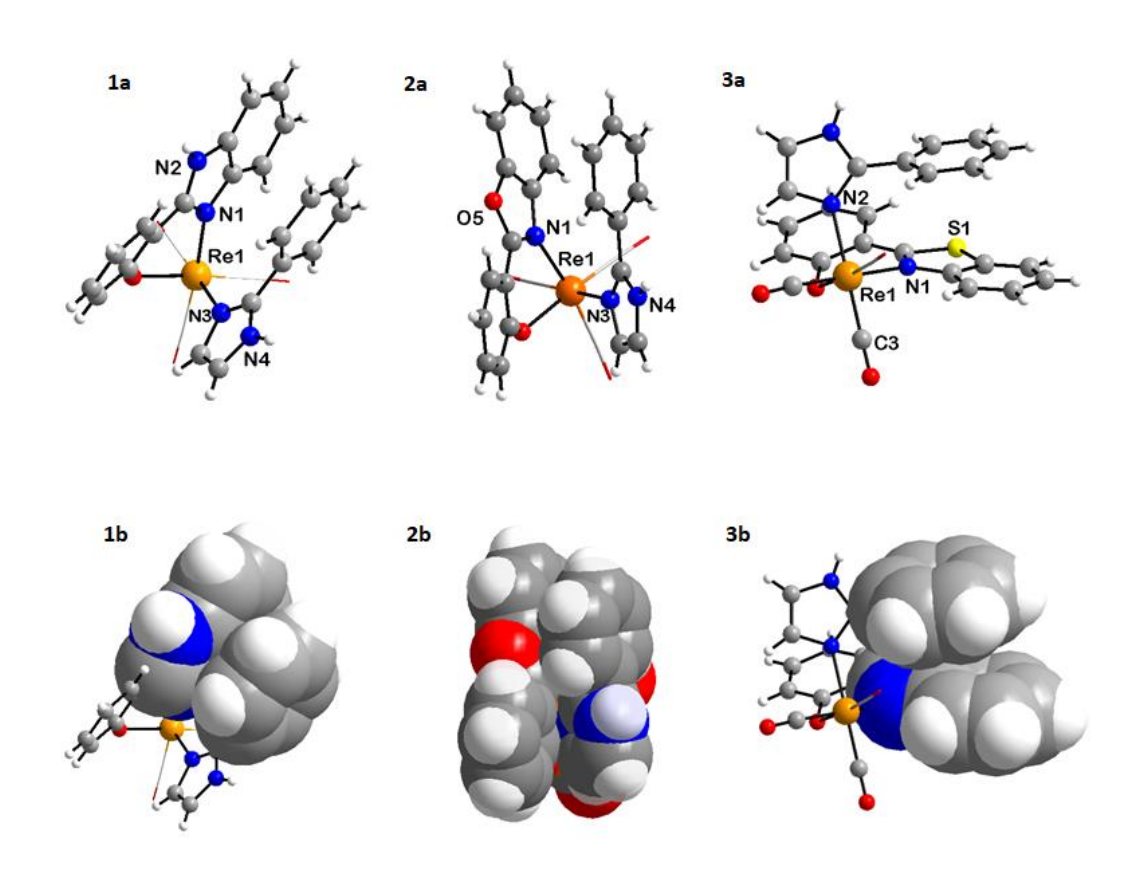


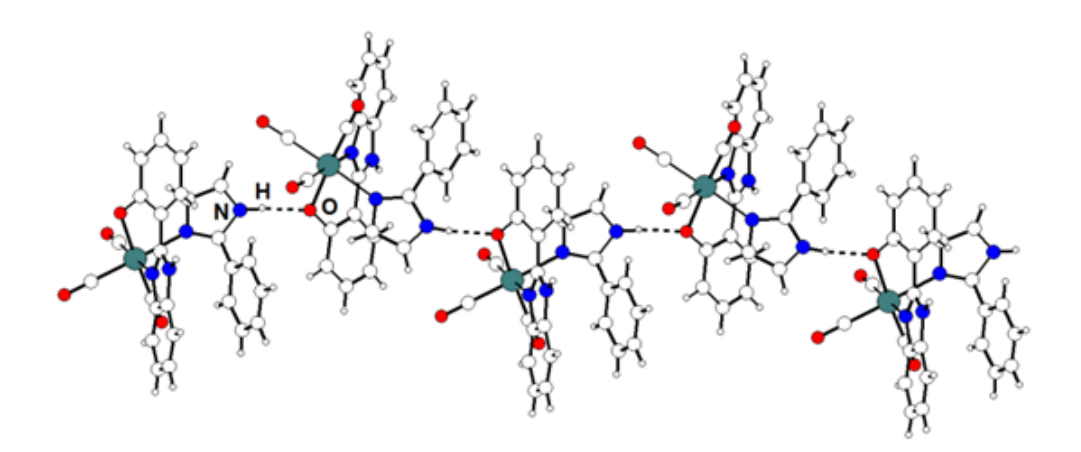
Figure 4. Molecular structures of 1–3, ball and stick model and space–fill model showing  $\pi \cdots \pi$  stacking interactions. (C = gray, H = white, N = blue, O = red, S = yellow, Re = orange).

Table 1. Crystallographic data for the structure determination of 1–3.

	1	2	3
Empirical Formula	$C_{25}H_{17}N_4O_4Re$	$C_{25}H_{16}N_3O_5Re$	$C_{25}H_{16}N_3O_4ReS$
Formula Weight	623.62	624.61	640.67
Crystal System	Monoclinic	Orthorhombic	Monoclinic
Space group	P 21/n	P 21 21 21	P 21/n
a (Å)	11.6361(9)	11.2382(12)	11.681(3)
b (Å)	14.3182(10)	13.9677(13)	14.324(3)
c (Å)	14.8078(10)	14.2375(15)	14.835(3)
α (°)	90	90	90
β (°)	110.556(2)	90	111.161(7)
γ (°)	90	90	90
$V(\mathring{A}^3)$	2310.0(3)	2234.9(4)	2314.8(9)
Z	4	4	4
T (K)	300(2)	298(2)	298(2)
λ (Å)	0.71073	0.71073	0.71073
$\rho_{calcd} (mg m^{-3})$	1.793	1.856	1.838
$\mu \ (mm^{-1})$	5.300	5.480	5.377
R1 $[I>2\sigma(I)]^a$	0.0610	0.0133	0.0558
wR2 (all data) <sup>b</sup>	0.1719	0.0409	0.1432
GOF	1.107	1.332	1.076

 $= \sum ||F_o| - |F_c|| / \sum |F_o| \cdot |wR_2| = \{ \sum [w(F_o^2 - F_c^2)^2] / \sum [w(F_o^2)^2] \}^{1/2}$ 

Intermolecular interactions. In the crystal lattice of complex 1–3, each molecule is involved in intermolecular N–H···O hydrogen bonding interactions between the imidazole N–H groups and the metal coordinated O atoms of the phenolate motif in the chelating unit. The N···O distances are in the range 2.697–2.742 Å and the N–H···O angles are within range  $170^{\circ}$ – $176^{\circ}$ . In each case, self-assembly of the complexes through intermolecular N–H···O hydrogen bonds result in the formation of a one dimensional chain (Figure 5). Complex 2 and 3 are further stabilized by intermolecular C—H··· $\pi$  interactions between the two adjacent molecules (imidazole unit to benzoxazole/benzothiazole unit, dihedral angle =  $54^{\circ}$ /64°, distance = 5.049/5.296Å). However, these kinds of interactions are not observed for 1. H<sub>2</sub>-PBI/H-PBO/H-PBT based Re(CO)<sub>3</sub> complexes with pyridine/pyridine derivatives adapt the structure in which the N∩O chelating ligand and pyridyl unit are arranged orthogonally.<sup>8</sup>



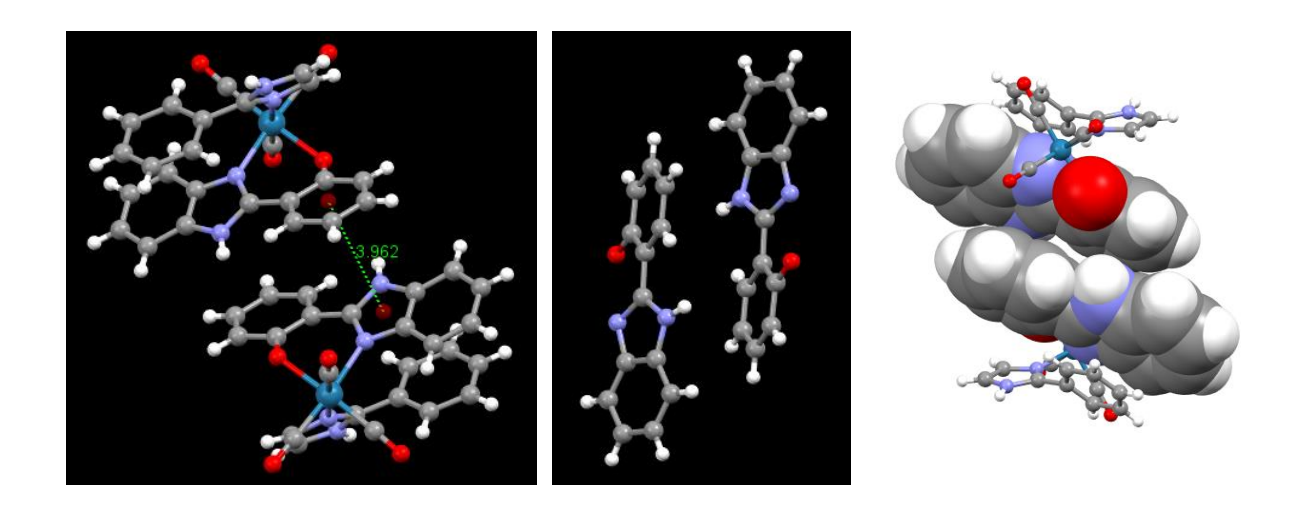
**Figure 5.** Partial packing diagram for complex **1** showing a one-dimensional chain formed by hydrogen bonding interactions between the two discrete molecules.

In the complexes 1–3, though the imidazole unit is similar to pyridyl unit, based on the structure and coordinating ability, presence of phenyl in ph-imz motif alter the arrangement

of these two units. In the complexes, the H<sub>2</sub>-PBI/H-PBO/H-PBT and ph-imz ligand motifs are twisted significantly, thereby, lying closely parallel to each other.

**Table 2.** Intermolecular slipped  $\pi \cdots \pi$  stacking interactions for 1 [Å and °].

$d\left(C_{g}\cdots C_{g}\right)$	$\tau$ (arenearene)
3.962	0



#### **Photophysical Studies of complexes 1-3**

The absorption properties of complexes 1–3 were studied both in dichloromethane (DCM) and dimethylsulfoxide (DMSO) at room temperature (Figure 6-7). The UV-Vis spectra of 1–3 in DCM closely match with those of 1–3 in DMSO. The intense absorptions in the range of 200–350 nm can be assigned to predominantly ligand-based electronic transitions ( $\pi$ ··· $\pi$ \* including N $\cap$ X  $\rightarrow$  N $\cap$ X and N $\cap$ X  $\rightarrow$  ph-imz). The higher energy absorption ( $\sim$ 300–350 nm) may also contains significant amount of MLCT electronic transitions (Re  $\rightarrow$  N $\cap$ X). The moderate absorptions in the visible region of 350–500 nm can be attributed to the metal to ligand charge transfer (MLCT) electronic transitions with small contribution of intraligand charge transfer (ILCT) electronic transitions.

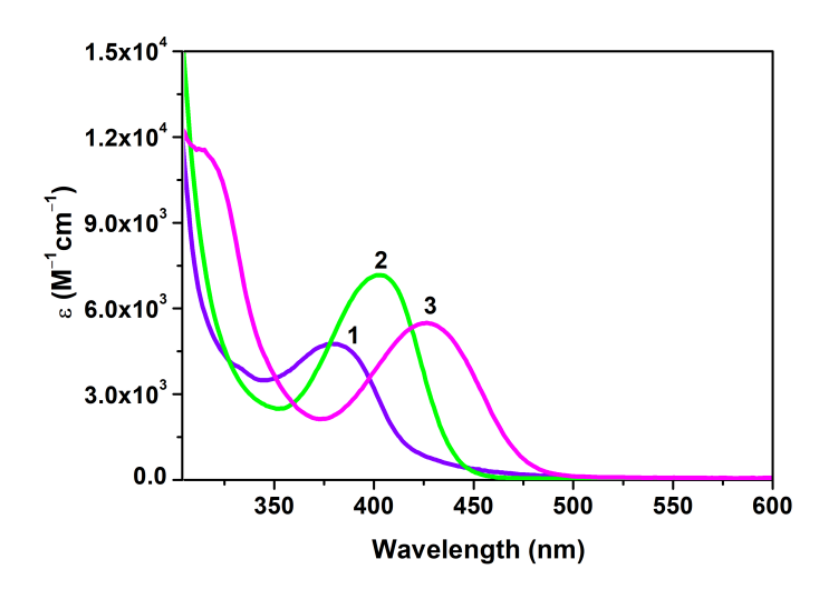


Figure 6. Absorption spectra of 1–3 in DMSO.

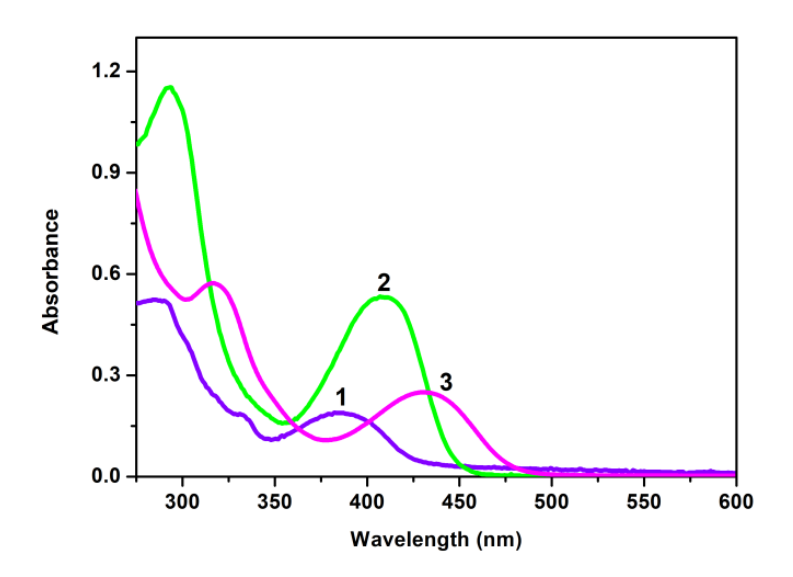


Figure 7. Absorption spectra of 1–3 in DCM.

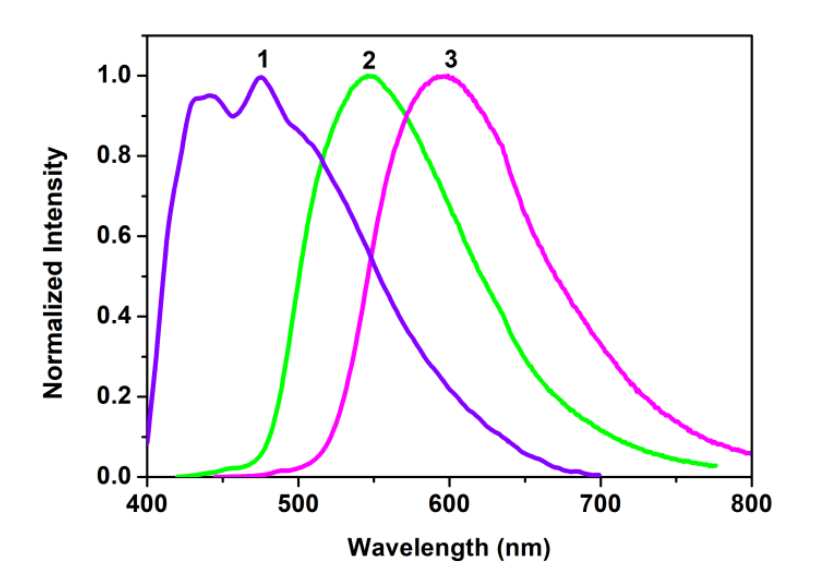


Figure 8. Emission spectra of 1–3 in DMSO.

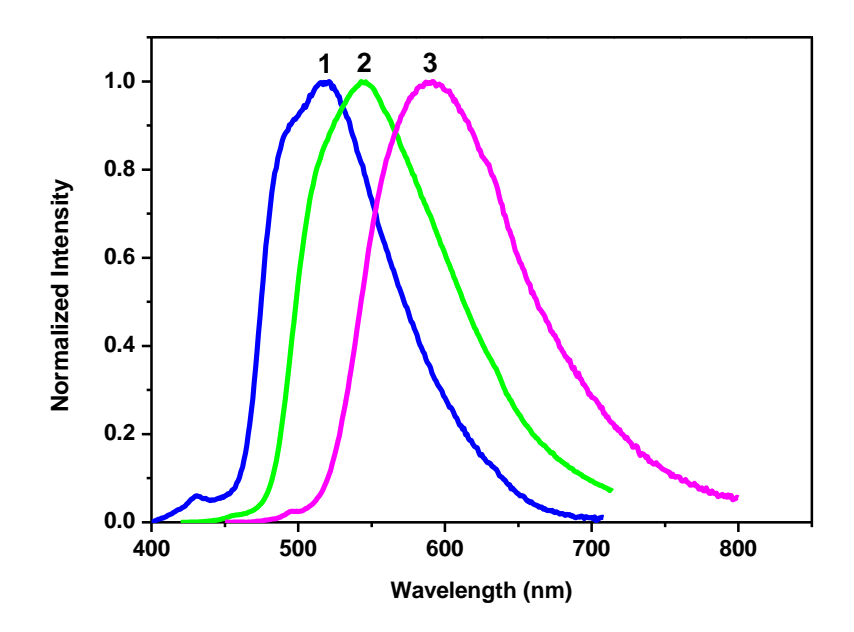


Figure 9. Emission spectra of 1–3 in DCM.

All the complexes display emission both in solution and solid state. The emission properties of the complexes in DCM/DMSO were studied with and without nitrogen purged solution (Figure 8–21). Complex 1 displayed poorly structured emission band in DCM. The emission intensity of 1 is slightly enhanced in nitrogen purged solution with red shift by 4 nm (Figure 10). Excitation spectrum of 1 at 516 nm displayed three structured bands below 350 nm (Figure 11). The broad band with maximum at 388 nm for 1 in the UV-Vis absorption spectrum is absent in the excitation spectrum of 1. The emission of 1 from the <sup>1</sup>MLCT/<sup>3</sup>MLCT excited state is omitted/less because the main absorption maxima for MLCT electronic transition is absent in the excited state spectrum. The results indicate that the emission of 1 in DCM is mainly originated from the ligand centered (LC) excited state or intra ligand centered (IL) excited state. The emission spectrum of 1 in DMSO showed structured emissions which are blue shifted by 40 nm compared to those emission in DCM. The excitation spectrum of 1 in DMSO at 476 nm displayed bands similar to those of 1 in DCM except intensities. This can be explained that the emission of 1 in DMSO is also originated from the LC or IL excited states. However, the population of these two excited states is reversed in DMSO as compared to those in DCM. The blue shifted emission of 1 in DMSO by 40 nm may be due to rigidochromic effect.<sup>13</sup> The solvent DMSO molecules may interact with ligand motifs of 1 through hydrogen bonding interactions [N-H···O=S(CH<sub>3</sub>)<sub>2</sub>] which provides rigidity to the ligand centered excited state.<sup>14</sup>

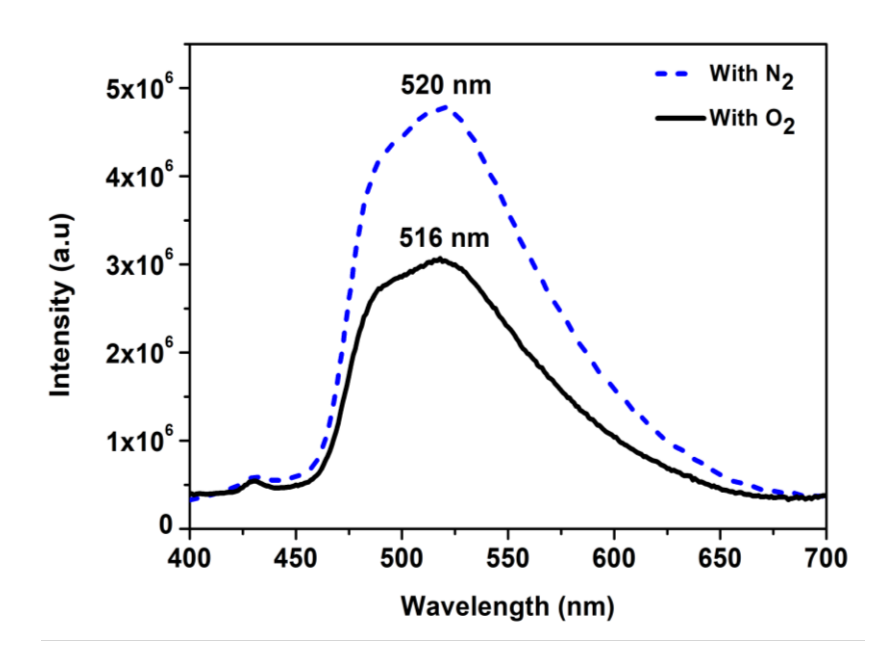
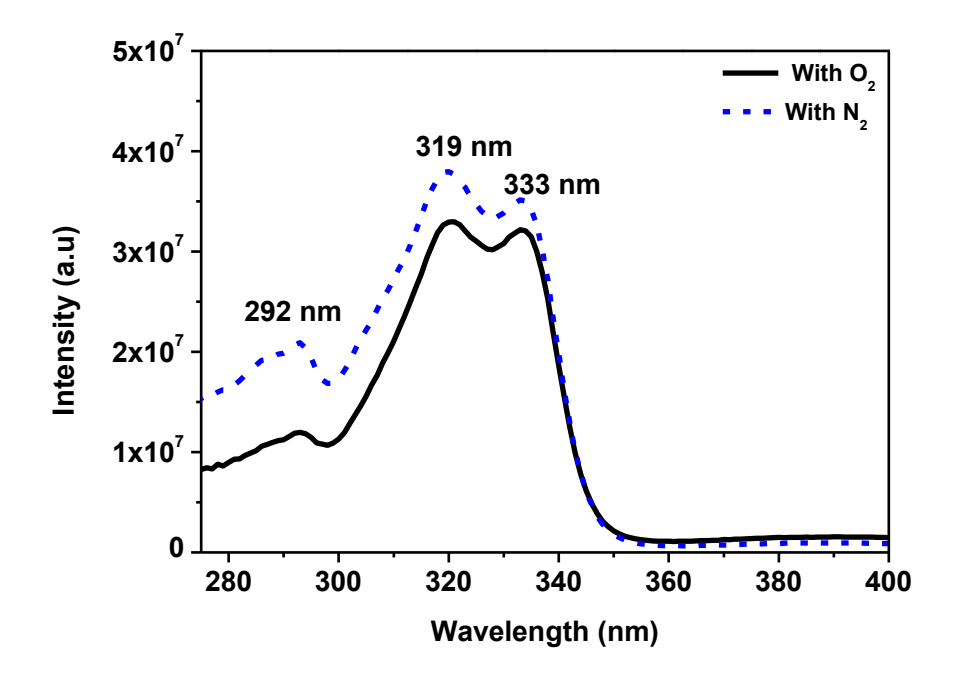
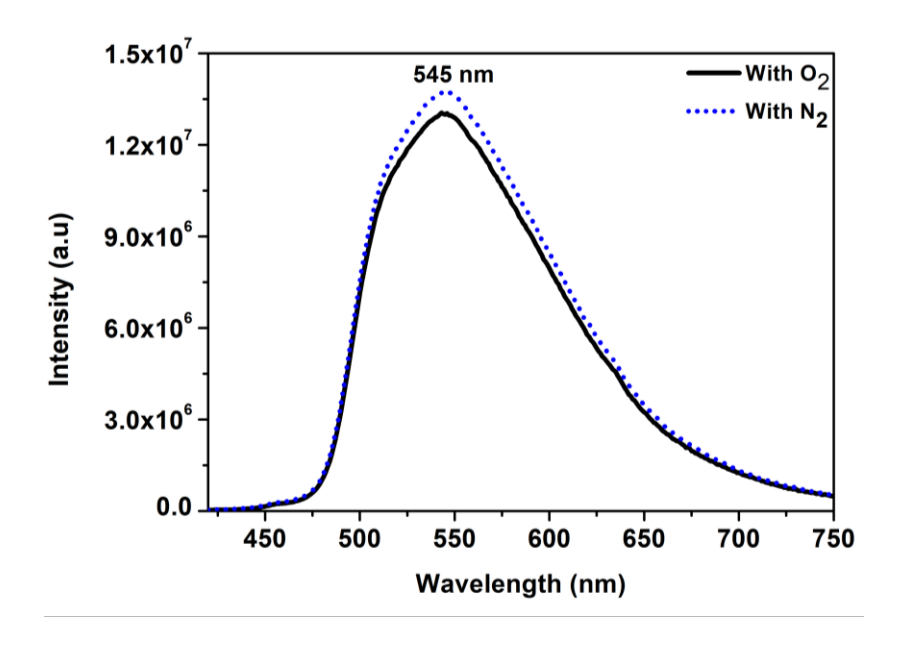


Figure 10. Emission Spectra of 1 in DCM (in presence and absence of air),  $\lambda_{ex}$ = 380 nm.



**Figure 11.** Excitation Spectra of **1** in DCM (in presence and absence of air),  $\lambda_{em}$ = 516 nm.



**Figure 12.** Emission spectra of **2** in DCM (in presence and absence of air),  $\lambda_{ex}$ = 410 nm.

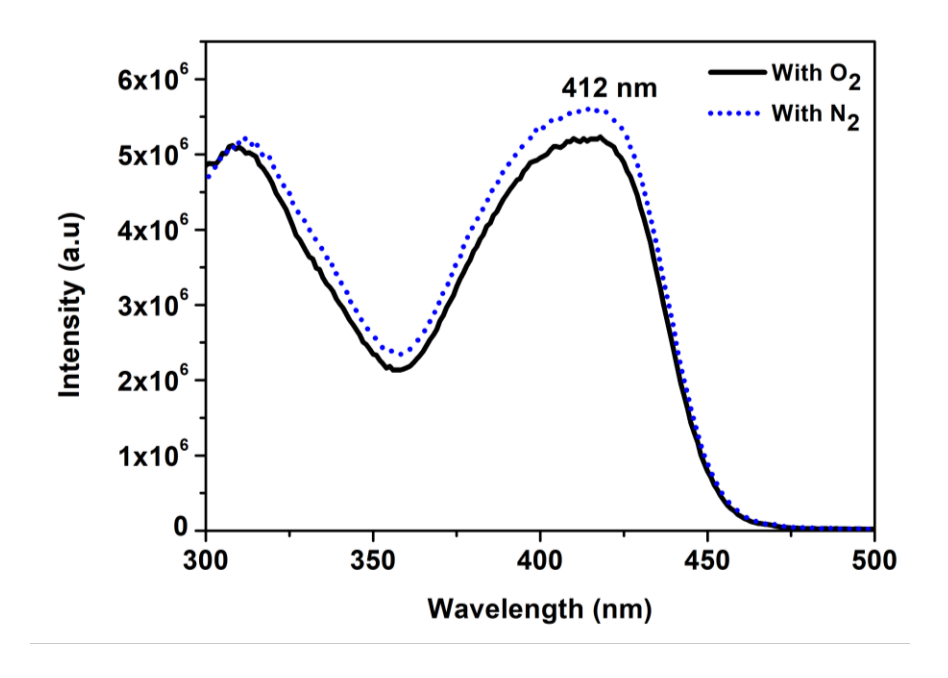


**Figure 13.** Excitation spectra of **2** in DCM (in presence and absence of air),  $\lambda_{em}$ = 545 nm.

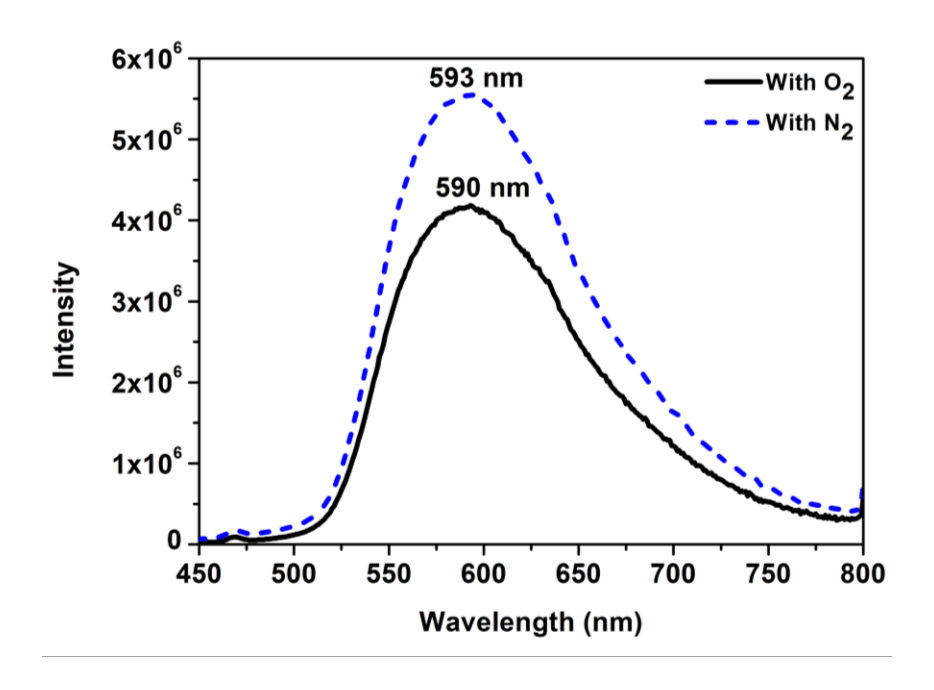


**Figure 14.** Emission spectra of **3** in DCM (in presence and absence of air),  $\lambda_{ex}$ = 410 nm.

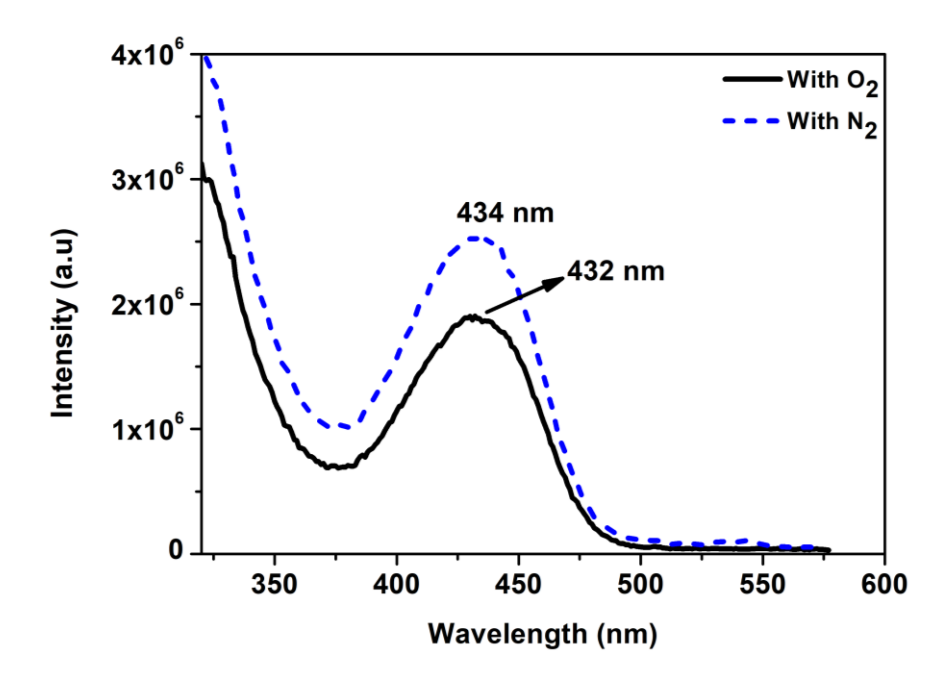


**Figure 15.** Excitation spectra of **3** in DCM (in presence and absence of air),  $\lambda_{em}$ = 592nm.

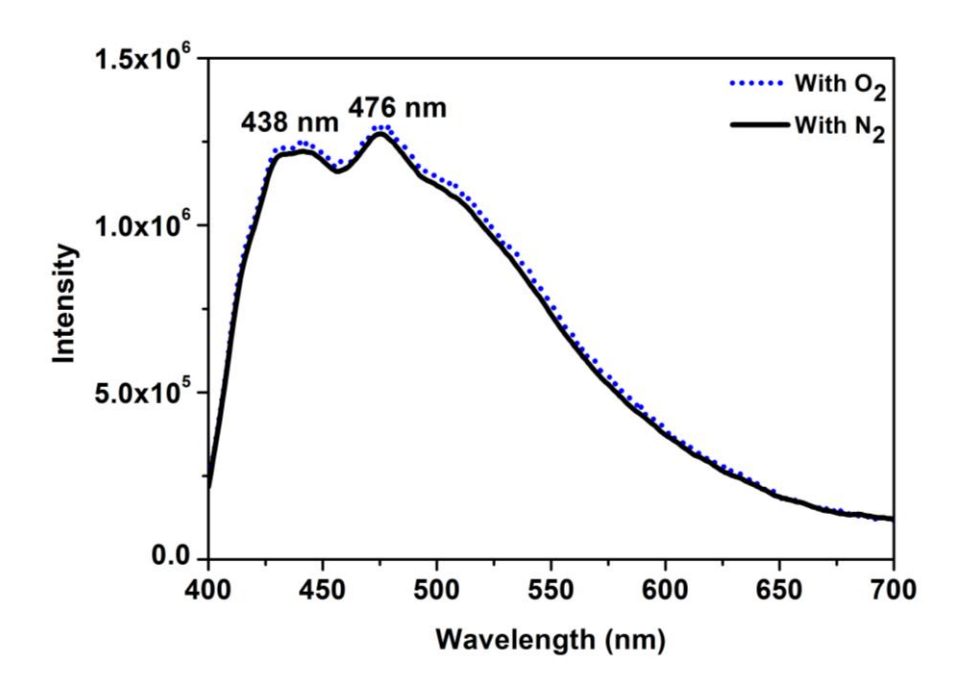


**Figure 16.** Emission Spectra of **1** in DMSO (in presence and absence of air),  $\lambda_{ex}$ = 380 nm.

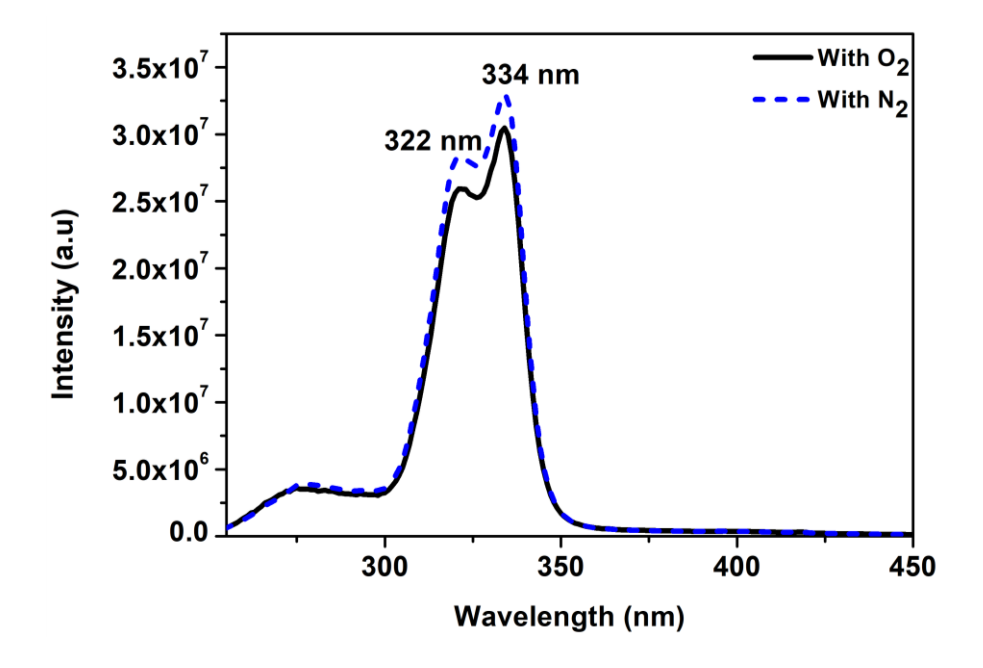


**Figure 17.** Excitation Spectra of 1 in DMSO (in presence and absence of air),  $\lambda_{em}$ = 476 nm.

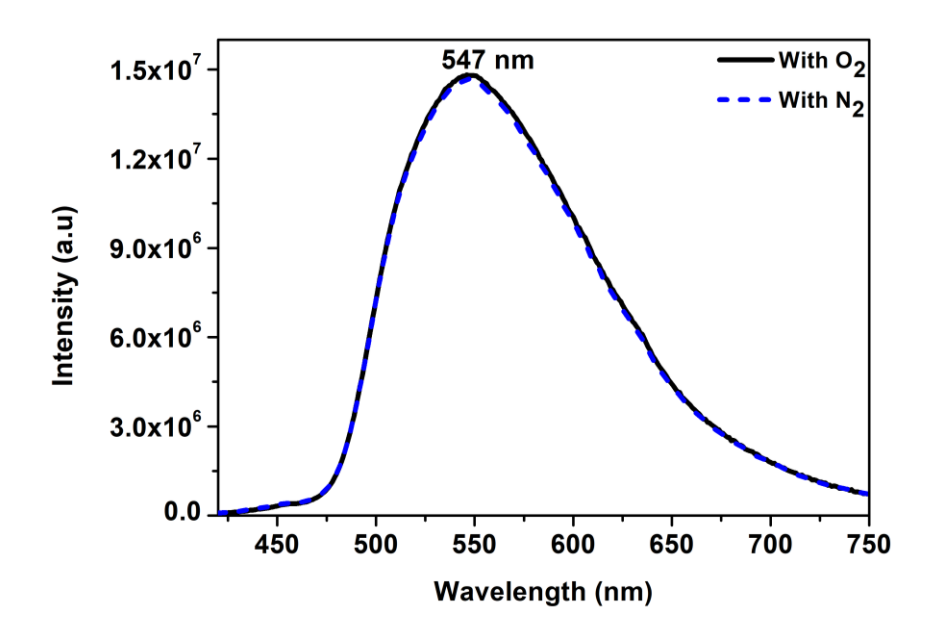


**Figure 18.** Emission spectra of **2** in DMSO (in presence and absence of air),  $\lambda_{ex}$ = 400 nm.

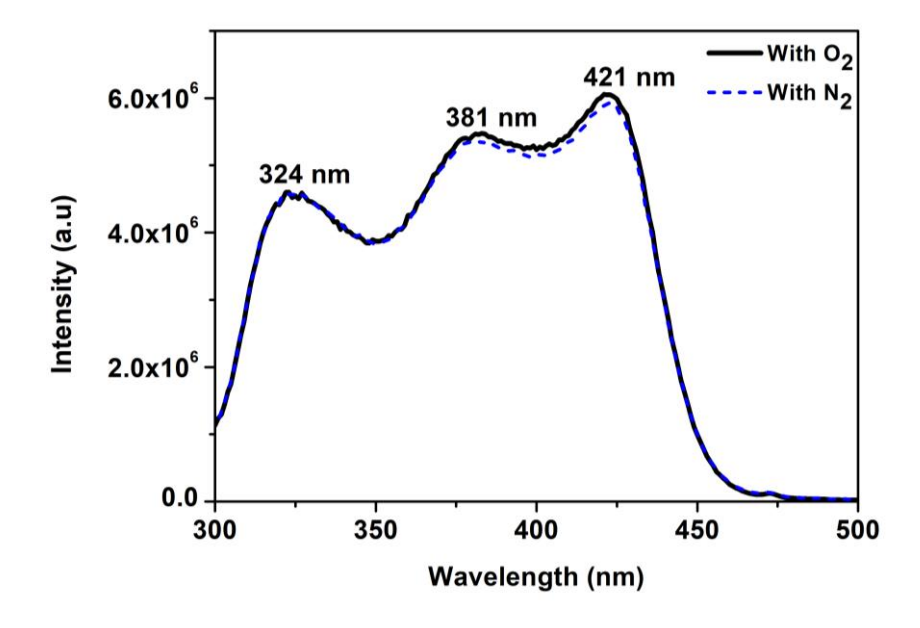


**Figure 19.** Excitation spectra of **2** in DMSO (in presence and absence of air),  $\lambda_{em}$ = 548 nm.

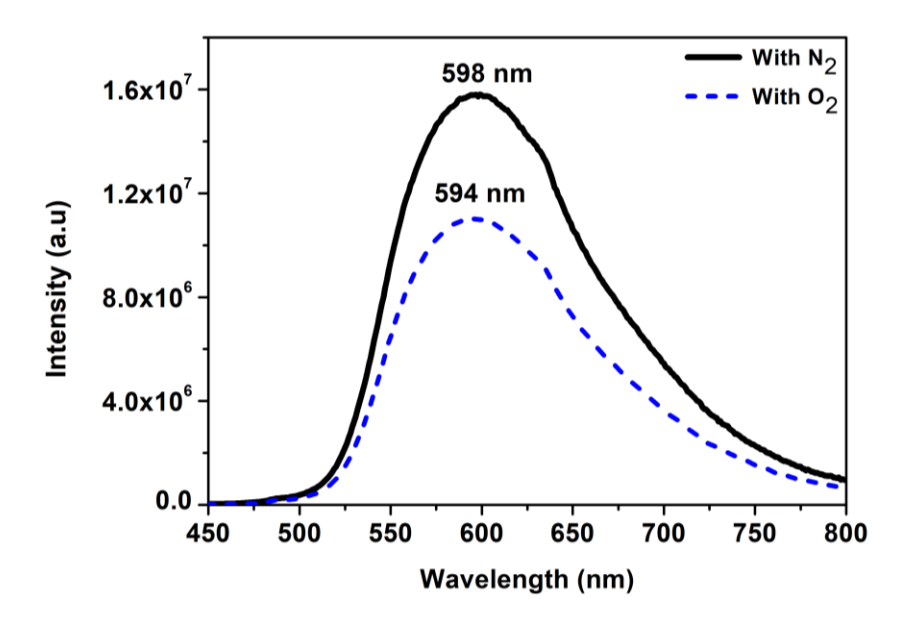


**Figure 20.** Emission spectra of **3** in DMSO (in presence and absence of air),  $\lambda_{ex}$ = 425 nm.

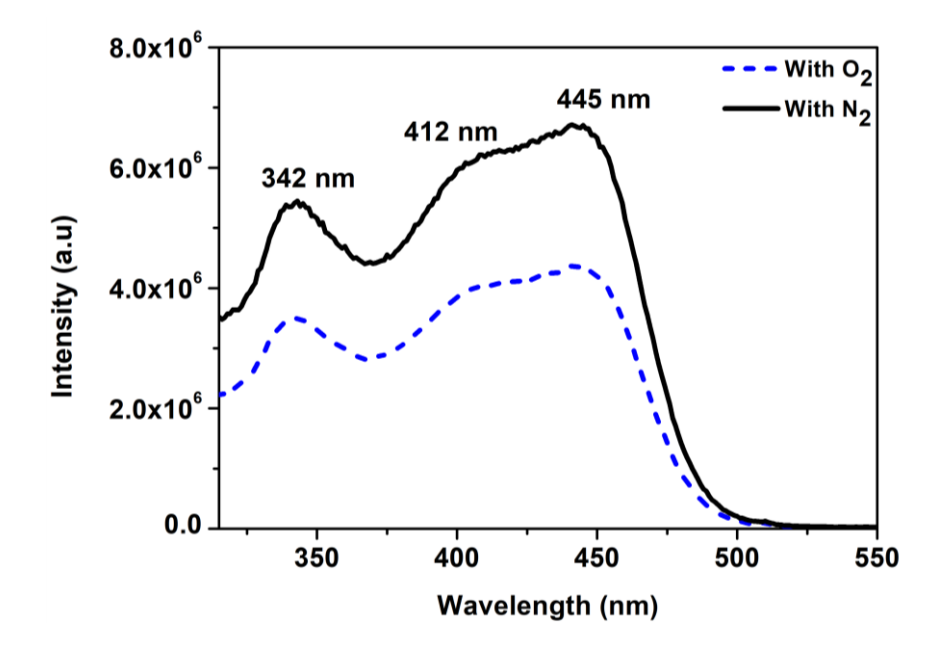


Figure 21. Excitation spectra of 3 in DMSO (in presence and absence of air),  $\lambda_{em} = 595$  nm.

**Table 3.** Absorption and Emission data for 1–3 in solution and solid state (Crystal).

	$\lambda^{abs}_{max}$ , nm $(\varepsilon, \mathbf{M}^{-1} \mathbf{cm}^{-1})$	λ <sup>em</sup> max (λ <sup>e</sup>	ф <sub>ет</sub> <sup>19</sup>	
	DMSO	DMSO	crystal	
$H_2$ -PBI <sup>15</sup>		464 (320, 334)	443 (350)	-
1	290 (19641) 382 (4831)	440, 474 (380)	535 (405)	-
H-PBO <sup>17</sup>		370	481(320)	-
2	292 (28607) 403 (7240)	547 (400)	556 (405)	$0.0212 \pm 0.0007$
H-PBT <sup>18</sup>			525(345)	-
3	315 (11598) 426 (5576)	594 (425)	556 (405)	$0.019 \pm 0.003$

Single crystal/powder 1 displays well–structured emission spectrum, which is red-shifted as compared to that in DCM/DMSO (Figure 22). It is noteworthy to mention that the free  $H_2$ –PBI in solid state displays poorly structured emission with emission maximum of 443/470 nm. <sup>15</sup> The results clearly indicates that crystal 1 emits from three different excited states which may be assigned as LC,  ${}^3$ MLCT, and metal-to-ligand-ligand charge transfer ( ${}^3$ MLLCT) excited states. <sup>16</sup> The slipped co-facial  $\pi$ --- $\pi$  stacking interactions caused due to conformational rotation of phenyl motif in phenylimidazolyl ligand in the complexes plays a major role for the red-shifted emission in the solid state. A similar kind of red-shifted emission was observed in helicate containing  $Re(CO)_3$  core, anionic PBI motif, and benzimidazolyl core. <sup>9a</sup> Closely looking the crystal structure of 1 indicates that two neighbouring PBI motifs interact each other through weak  $\pi$ --- $\pi$  stacking interactions.

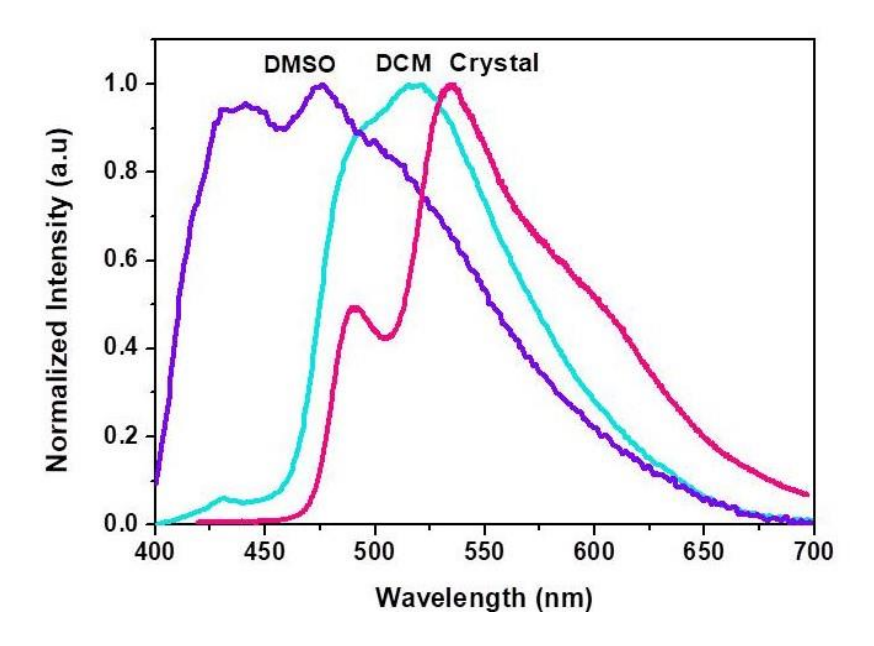


Figure 22. Emission spectra of 1 in DMSO, DCM, and crystal (solid state).

Compound **2** in DCM/DMSO is emissive (Figure 12,18). Similar to the absorption spectrum, the emission maximum of **2** in solution is red shifted as compared to complex **1**. No significant shift in the emission pattern as well as life-time data of **2** was observed while changing solvent from DCM to DMSO. Crystal **2** displays poorly resolved emission pattern (Figure 23). The emission pattern is different from that of crystal **1**. The emission of **2** is redshifted in compared to crystal of H-PBO (free ligand). <sup>17</sup>

The emission pattern of **3** in DCM is almost similar to that in DMSO. Complex **3** displays broad emission, the emission maximum is red-shifted as compared to **1** and **2** in DMSO and DCM. The life-time data of complex **2** and **3** were studied both in DCM and DMSO and were found to be similar (Table 4). The emission decays of both complexes are biexponential. From the data, it can be inferred that the complexes emit from two different

excited states denoted by  $\tau_1$  and  $\tau_2$  (Table 4). Similar emission decays with shorter lifetime were observed for other rhenium complexes.<sup>9</sup>

In addition, the crystal emission of **3** is identical to that of crystal **2** (Figure 23). The results reveals that complexes **2** and **3** display emission which may be originated from the <sup>3</sup>MLCT and <sup>3</sup>MLLCT excited states because changing the anionic unit in the complexes from H-PBO to H-PBT did not alter the emission pattern in the solid-state. It is noteworthy to mention that the photophysical properties of complexes with similar anionic ligands (HPBI/PBO/PBT) but different neutral donor (pyridine) at low temperature (77 K) are blue shifted. <sup>8a</sup> However, the complexes **1–3** shows red shifted emission in the solid state. The results clearly indicate that tuning of the coordinating donor motif can shift the emission properties towards the red region.

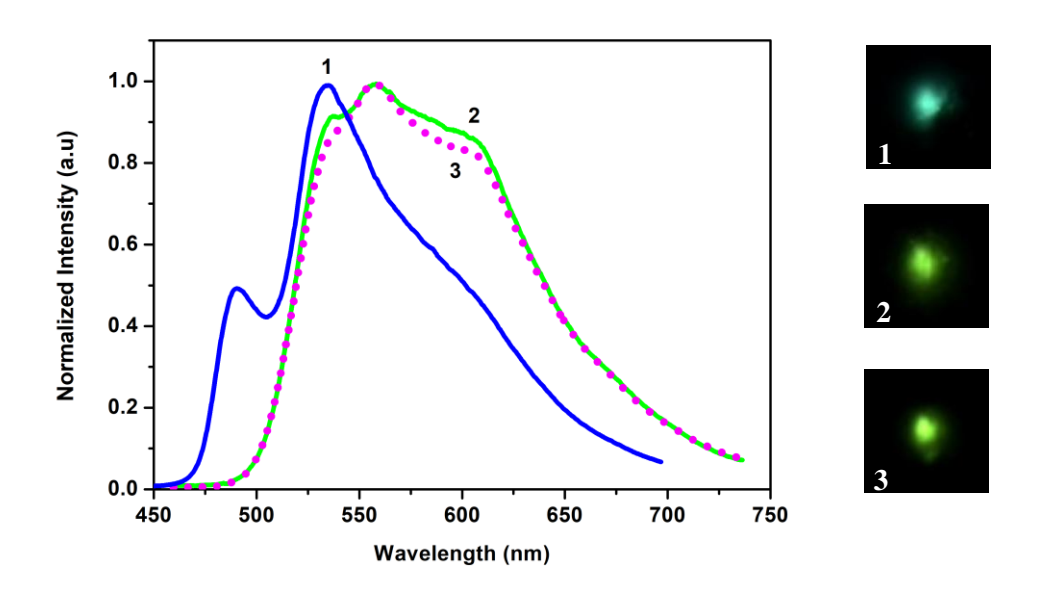


**Figure 23.** Normalized emission spectra of **1–3** in solid state at room temperature ( $\lambda_{ex} = 405$  nm). Right: Photograph of the emission under irradiation from a 405 nm excitation source.

**Table 4.** Fluorescence lifetime  $(\tau, ns)$  of 2 and 3 in solution.

Complex	Medium	$\lambda_{ ext{mon}}$	$ au_1$	$ au_2$	$\chi^2$
2	DCM	526	10670	1160	0.99
	DMSO	526	1730	11890	0.99
3	DCM	572	1730	11890	0.99
	DMSO	576	1730	11890	0.99

 $\lambda_{mon} =$  monitoring wavelength,  $\tau =$  lifetime for each component,  $\chi^2 =$  indicating the goodness of the fit to the data.

# 4.3. Experimental Section

#### **General Data**

Starting materials such  $Re_2(CO)_{10}$ , 2-(2'-hydroxyphenyl)benzoxazoleas (H-PBO),2-(2'-hydroxyphenyl)benzothiazole (H-PBT), 2-phenylimidazole (ph-imz), toluene spectroscopic grade solvents such as dimethylsulfoxide (DMSO, Finar), dichloromethane (DCM, Finar) were obtained from commercial sources and used as received. 2-(2'-hydroxyphenyl)-1Hbenzimidazole (H<sub>2</sub>-PBI) was synthesized by previously reported method. <sup>7a</sup> Elemental analyses were performed on Flash EA 1112 series CHNS analyzer. FT-IR spectra were recorded on a Nicolet iS5 FT-IR spectrometer. NMR spectra were recorded on Bruker Avance III 400 and 500 MHz instruments. Absorption spectra were recorded on UV-3600 Shimadzu UV-Vis-NIR spectrophotometer. Fluorescence spectra were measured on Horiba FluoroMax 4 fluorimeter. Solid State emission spectra were recorded on WI-Tec confocal Raman spectrometer with 405 nm as the excitation source. The lifetime of the complexes was measured using a time-correlated singlephoton counting (TCSPC) fluorescence spectrometer (Horiba Jobin Yvon IBH).

#### General Synthetic Approach for 1–3.

 $Re_2(CO)_{10}$ , 2–(2'–hydroxyphenyl)-1*H*-benzimidazole (H<sub>2</sub>–PBI)/ 2-(2'-hydroxyphenyl)benzoxazole (H–PBO)/ 2–(2'–hydroxyphenyl)benzothiazole (H–PBT) and 2-phenylimidazole (ph–imz) in toluene (~10 mL) were kept in a teflor vessel. The vessel was kept in the stainless steel solvothermal bomb and placed in an oven programmed at 160 °C for 48 h and cooled to room temperature. Crystals or powder obtained in the bomb were filtered, washed with hexane, and air dried.

#### Synthesis of [Re(CO)<sub>3</sub>(PBI)(ph-imz)] (1)

Yellow colored needle shaped crystals were obtained using Re<sub>2</sub>(CO)<sub>10</sub> (100.5 mg, 0.154 mmol), H<sub>2</sub>-PBI (64.4 mg, 0.306 mmol) and ph-imz (44.1 mg, 0.306 mmol) in toluene (~10 mL). Yield: 51% (48.5 mg). Anal. calcd. for C<sub>25</sub>H<sub>17</sub>N<sub>4</sub>O<sub>4</sub>Re: C, 48.15; H, 2.75; N, 8.98. Found: C, 48.23; H, 2.72; N, 8.91. FT–IR ( $\nu_{\text{max}}$  (KBr)/cm<sup>-1</sup>): 2009, 1864 (CO). <sup>1</sup>H–NMR (400 MHz, DMSO- $d_6$ ):  $\delta$  7.94–7.91 (m, 3H, H<sup>g,c,7</sup>), 7.80 (dd, 1H, J = 8 Hz, H<sup>6</sup>), 7.60–7.58 (m, 1H, H<sup>4</sup>), 7.44 (t, 3H, J = 7 Hz, H<sup>f,d</sup>), 7.39–7.23 (m, 6H, H<sup>a,b,e,4</sup>), 7.14 (s, 2H, H<sup>5,6</sup>), 6.82 (dd, 1H, J = 8.4 Hz, H<sup>3</sup>), 6.70–6.66 (m, 1H, H<sup>5</sup>)).

## Synthesis of [Re(CO)<sub>3</sub>(PBO)(ph-imz)] (2)

Brown colored needle shaped crystals were obtained using Re<sub>2</sub>(CO)<sub>10</sub> (100.4 mg, 0.1539 mmol), H-PBO (65.1 mg, 0.307 mmol) and ph-imz (44.1 mg, 0.306 mmol) in toluene (~10 mL). Yield: 32% (30.4 mg). Anal. Calcd. for C<sub>25</sub>H<sub>16</sub>N<sub>3</sub>O<sub>5</sub>Re: C, 48.07; H, 2.58; N, 6.73. Found: C, 48.15; H, 2.52; N, 6.68. FT-IR ( $\nu_{\text{max}}$  (KBr)/cm<sup>-1</sup>): 2012, 1902 and 1866 (CO). <sup>1</sup>H-NMR (500 MHz, DMSO- $d_6$ ):  $\delta$  7.95-7.92 (m, 3H, H<sup>g,c,7</sup>), 7.89 (d, J = 8 Hz, 1H, H<sup>4</sup>), 7.74 (dd, J = 8 Hz, 1H, H<sup>6</sup>), 7.62-7.53 (m, 2H, H<sup>6,4</sup>), 7.46-7.43 (m, 3H, H<sup>f,d</sup>), 7.41-7.37 (m, 1H, H<sup>5</sup>), 7.35-7.32 (m, 2H, H<sup>e</sup>), 7.22-7.15 (m, 3H, H<sup>a,b</sup>), 6.90-6.86 (m, 2H, H<sup>3</sup>), 6.77-6.70 (m, 2H, H<sup>5</sup>).

#### Synthesis of $[Re(CO)_3(PBT)(ph-imz)]$ (3)

Yellow colored crystals were obtained using  $Re_2(CO)_{10}$  (100.6 mg, 0.154 mmol), H-PBT (70.1 mg, 0.307 mmol) and ph-imz (44.2 mg, 0.307 mmol) in toluene (~10 mL). Yield: 31% (30.2 mg). Anal. Calcd. for  $C_{25}H_{16}N_3O_4ReS$ : C, 46.87; H, 2.52; N, 6.56, S, 5.00. Found: C, 46.79; H, 2.56; N, 6.51,

S, 4.92. FT–IR ( $v_{\text{max}}$  (KBr)/cm<sup>-1</sup>): 2013, 1904 and 1864 (CO). <sup>1</sup>H–NMR (500 MHz, DMSO– $d_6$ ):  $\delta$  8.30 (d, 1H, J = 8.5 Hz, H<sup>7</sup>), 8.19 (dd, 1H, J = 8 Hz, H<sup>4</sup>), 7.94 (dd, 2H, J = 8.5 Hz, H<sup>g,c</sup>), 7.73–7.68 (m, 2H, H<sup>5', 5</sup>), 7.54–7.53 (m, 3H, H<sup>f, d, 6</sup>), 7.39–7.33 (m, 4H, H<sup>e, 6'</sup>), 7.23 (s, 2H, H<sup>a, b</sup>), 6.86–6.83 (m, 1H, H<sup>3'</sup>), 6.70–6.67 (m, 1H, H<sup>4'</sup>).

X-ray crystal data for complexes 1–3. Crystallography intensity data of crystals of 1–3 were collected on a Bruker D8 QUEST diffractometer [ $\lambda$ (Mo-K $\alpha$ ) = 0.71073 Å]. The structures were solved by direct methods using SHELXS-97<sup>20a</sup> and refined using the SHELXL-2018/3 program (within the WinGX program package). Non-H atoms were refined anisotropically. The crystallographic data for 1 shows higher value of R<sup>int</sup> due to poor crystal quality.

## 4.4. Conclusion

The three luminescent heteroleptic mononuclear fac-Re(CO)<sub>3</sub> core containing complexes were synthesized using H<sub>2</sub>-PBI/H-PBO/H-PBT, 2-phenylimidazole and Re<sub>2</sub>(CO)<sub>10</sub> via one- pot synthetic approach. The molecular structures of the complexes indicated the parallel arrangement of the two organic motifs which are coordinated to metal core and twisted significantly, resulting in slipped co-facial  $\pi \cdots \pi$  interactions between the phenyl unit of ph-imz and benzimidazolyl of chelating motif in solid state. The photo physical properties of the complexes display strong emission both in the solution and solid state at room temperature. The synthesis of various acyclic and cyclic Re(I) based complexes using different nitrogen donors (phenyl benzimidazole/phenylnaphthyl benzimidazole) is under progress.

## 4.5. References

- (a) X. Gong, P. K. Ng, W. K. Chan, *Adv. Mater.* 1998, 10, 1337–1340; (b) X. Liu, H. Xia, W. Gao,
   Q. Wu, X. Fan, Y. Mu, C. Ma, *J. Mater. Chem.* 2012, 22, 3485–3492; (c) A. Kastl, S. Dieckmann,
   K. Wahler, T. Volker, L. Kastl, A. L. Merkel, A. Vultur, B. Shannan, K. Harms, M. Ocker, W. J.
   Parak, M. Herlyn, E. Meggers, *ChemMedChem.* 2013, 8, 924–927; (d) T. M. McLean, J. L. Moody,
   M. R. Waterland, S. G. Telfer. *Inorg. Chem.* 2012, 51, 446–455.
- 2. (a) S. Ranjan, S. Y. Lin, K. C. Hwang, Y. Chi, W. L. Ching, C. S. Liu, Y. T. Tao, C. H. Chien, S. M. Peng, G. H. Lee, *Inorg. Chem.* 2003, **42**, 1248–1255; (b) T. Klemens, A. Świtlicka-Olszewska, B. Machura, M. Grucela, E. Schab-Balcerzak, K. Smolarek, S. Mackowski, A. Szlapa, S. Kula, S. Krompiec, P. Lodowskie, A. Chrobok, *Dalton Trans.* 2016, **45**, 1746–1762.
- 3. (a) H. Tsubaki, A. Sekine, Y. Ohashi, K. Koike, H. Takeda, O. Ishitani, *J. Am. Chem. Soc.* 2005, **127**, 15544–15555; (b) T. Morimoto, C. Nishiura, M. Tanaka, J. Rohacova, Y. Nakagawa, Y. Funada, K. Koike, Y. Yamamoto, S. Shishido, T. Kojima, T. Saeki, T. Ozeki, O. Ishitani, *J. Am. Chem. Soc.* 2013, **135**, 13266–13269; (c) W. K. Chu, C. C. Ko, K. C. Chan, S. M. Yiu, F. L. Wong, C. S. Lee, V. A. L. Roy, *Chem. Mater.* 2014, **26**, 2544–2550.
- 4. (a) A. J. Amoroso, M. P. Coogan, J. E. Dunne, V. Fernandez-Moreira, J. B. Hess, A. J. Hayes, D. Lloyd, C. Millet, S. J. A. Pope, C. Williams, *Chem. Commun.* 2007, 3066–3068; (b) V. Fernandez-Moreira, F. L. Thorp-Greenwood, M. P. Coogan, *Chem. Commun.* 2010, 46, 186–202; (c) S. Clede, F. Lambert, C. Sandt, Z. Gueroui, M. Refregiers, M. Plamont, P. Dumas, A. Vessieres, C. Policar, *Chem. Commun.* 2012, 48, 7729–7731.
- (a) M. Wrighton, D. L. Morse, J. Am. Chem. Soc. 1974, 96, 998–1003; (b) L. Sacksteder, A. P. Zipp, E. A. Brown, J. Streich, J. N. Demás, B. A. DeGraff, Inorg. Chem. 1990, 29, 4335–4340; (c)
   A. J. Lees, Chem. Rev. 1987, 87, 711–743; (d) D. J. Stufkens, A. Vlcek Jr., Coord. Chem. Rev. 1998, 177, 127–179; (e) A. Gabrielsson, M. Busby, P. Matousek, M. Towrie, E. Hevia, L. Cuesta, J.

- Perez, S. Zalis, A. VlcekJr, *Inorg. Chem.* 2006, **45**, 9789–9797.
- (a) S. L. Huang, T. S. A. Hor, G. X. Jin, Coord. Chem. Rev. 2017, 333, 1–26; (b) H. N. Zhang, W. X. Gao, Y. X. Deng, Y. J. Lin and G. X. Jin, Chem. Commun. 2018, 54, 1559–1562.
- 7. (a) X. Han, H. Ma, Y. Wang, *Russian J. Org. Chem.* 2008, 44, 863–865; (b) C. Wu, S. Tao, M. Chen, F. L. Wong, Y. Yuan, H. W. Mo, W. Zhao, C. S. Lee, *Chem. Asian J*, 2013, 8, 2575–2578;
  (c) Z. Zhang, H. Zhang, C. Jiao, K. Ye, H. Zhang, J. Zhang, Y. Wang, *Inorg. Chem.* 2015, 54, 2652–2659.
- 8. (a) R. Czerwieniec, A. Kapturkiewicz, R. A. Ostrowskab, J. Nowacki, *J. Chem. Soc., Dalton Trans.* 2002, 3434–3441; (b) C. C. Ju, A. G. Zhang, H. L. Sun, K. Z. Wang, W. L. Jiang, Z. Q. Bian, C. H. Huang, *Organometallics* 2011, **30**, 712–716; (c) Y. Y. Lu, C. C. Ju, D. Guo, Z. B. Deng, and K. Z. Wang, *J. Phys. Chem. C.* 2007, 111, 5211–5217; (d) T. W. Tseng, S. Mendiratta, T. T. Luo, T. W. Chen, Y. P. Lee, *Inorg. Chim. Acta* 2018, 477, 312–317.
- 9. (a) B. Shankar, S. Sahu, N. Deibel, D. Schweinfurth, B. Sarkar, P. Elumalai, D. Gupta, F. Hussain, G. Krishnamoorthy, M. Sathiyendiran, *Inorg. Chem.* 2014, **53**, 922–930; (b) A. E. Nahhas, C. Consani, A. M. Blanco-Rodríguez, K. M. Lancaster, O. Braem, A. Cannizzo, M. Towrie, I. P. Clark, S. Zalis, M. Chergui, A. Vlcek Jr, *Inorg. Chem.* 2011, **50**, 2932–2943; (c) J. Skiba, A. Kowalczyk, P. Staczek, T. Bernas, D. Trzybinski, K. Wozniak, U. Schatzschneider, R. Czerwieniec, K. Kowalski, *New J. Chem.* 2019, **43**, 573–583.
- 10. (a) B. Shankar, P. Elumalai, M. Sathiyendiran, *Inorg. Chem. Commun.* 2013, **36**, 109–112; (b) S. K. Behera, G. Sadhuragiri, P. Elumalai, M. Sathiyendiran, G. Krishnamoorthy, *RSC Adv.* 2016, **6**, 59708–59717; (c) P. Saxena, B. Shankar, M. Sathiyendiran, *J. Organomet Chem.* 2015, **799-800**, 82-89.

- 11. (a) M. Fumanal, E. Gindensperger, and C. Daniel, *Phys. Chem. Chem. Phys.* 2018, **20**, 1134–1141; (b) M. Fumanal, C. Daniel, *J. Computat. Chem.* 2016, **37**, 2454–2466.
- 12. (a) A. Mukhopadhyay, S. Pal, *Eur. J. Inorg. Chem.* 2006, 4879–4887; (b) M. Lousame, A. Fernandez, M. Lopez-Torres, D. Vazquez-Garcia, J. M. Vila, A. Suarez, J. M. Ortigueira, J. J. Fernandez, *Eur. J. Inorg. Chem.* 2000, 2055-2062.
- 13. (a) M. K. Itokazu, A. S. Polo, N. Y. M. Iha, *J. Photochem. Photobiol. A: Chem.* 2003, **160**, 27–32; (b) T. G. Kotch, A. J. Lees, S. J. Fuerniss, K. I. Papathomas, R. W. Snyder, *Inorg. Chem.* 1993, **32**, 2570-2575.
- (a) J. Zukerman-Schpector, E. R. T. Tiekink, *Cryst.Eng.Comm.* 2014, 16, 6398–6407; (b) O. K. Abou-Zied, R. Jimenez, E. H. Z. Thompson, D. P. Millar, F. E. Romesberg, *J. Phys. Chem. A* 2002, 106, 3665–3672.
- 15. (a) T. Shida, T. Mutai, K. Araki, *CrystEngComm*. 2013, **15**, 10179–10182; (b) H. Konoshima, S. Nagao, I. Kiyota, K. Amimoto, N. Yamamoto, M. Sekine, M. Nakata, K. Furukawa, H. Sekiya, *Phys. Chem. Chem. Phys.* 2012, **14**, 16448–16457.
- 16. (a) Y. J. Cho, S. Y. Kim, M. Cho, K. R. Wee, H. J. Son, W. S. Han, D. W. Cho, S. O. Kan,
  Phys. Chem. Chem. Phys. 2016, 18, 15162–15169; (b) K. K. W. Lo, K. Y. Zhang, S. K. Leung,
  M. C. Tang, Angew. Chem. Int. Ed. 2008, 47, 2213–2216.
- (a) F. S. Rodembusch, F. R. Brand, D. S. Correa, J. C. Pocos, M. Martinelli, V. Stefani, *Mat. Chem. and Phy.* 2005, 92, 389–393; (b) J. E. Kwon, S. Y. Park, *Adv. Mater.* 2011, 23, 3615–3642.
   P. Majumdar, J. Zhao, *J. Phys. Chem. B*, 2015, 119, 2384–2394.
- 19. The relative quantum yield for the complexes was calculated using  $[Ru(bpy)_3](PF_6)_2$  as standard in acetonitrile solution. The formula used for the calculation is as follows:
- $\phi_S/\varphi_R = \left(n_S/n_R\right)^2 \left(m_S/m_R\right),\, \phi_S :$  quantum yield efficiency of the sample.
- $\phi_{R:}$  quantum yield efficiency of the reference.

m<sub>s</sub>: Slope of the integrated fluorescence intensity vs absorbance curve for the sample.

m<sub>R</sub>: Slope of the integrated fluorescence intensity vs absorbance curve for the reference.

 $n_s = n_r$ : Refractive index of the respective solvents.

20. (a) G. M. Sheldrick, Program for Crystal Structure Solution. SHELXS-97, University of Göttingen, Göttingen, Germany, 1997; (b) G. M. Sheldrick, *ActaCrystallogr., Sect. A: Found. Crystallogr.* 2008, **64**, 112–122; (c) G. M. Sheldrick, *ActaCrystallogr., Sect. C: Struct. Chem.* 2015, **71**, 3–8.

# **Chapter-5a**

#### **ABSTRACT**

Two fac-Re(CO)<sub>3</sub> core based dinuclear complexes were obtained from Re<sub>2</sub>(CO)<sub>10</sub>, 1,4-phenylene-bis(2-(2'-hydroxyphenyl)benzimidazolyl) (H<sub>2</sub>-L) and neutral N-donors (4-aminopyridine for 1/4-dimethylaminopyridine for 2). Both the complexes are characterized using various analytical and spectroscopic techniques. The molecular structure of 2 obtained from a single crystal X-ray diffraction analysis shows that two anionic phenoxybenzimidazolyl motifs of L<sup>2-</sup> are twisted, resulting in an acyclic dinuclear helical structure. Both the complexes display strong emission in the solution state at room temperature.

#### **5a.1. Introduction**

The rhenium-carbonyl based complexes have been gaining intense research interest in the fields of bio-imaging, anticancer agents, photosensitizer as well as photocatalyst for carbon dioxide reduction to useful chemicals, and molecular sensors due to their intrinsic properties such as kinetic inertness, photo-stability, photo-physical and electrochemical properties. <sup>1-9</sup> The ligand design plays a crucial role in tuning the excited state properties of these complexes. Few organic heteroaromatic motifs including chelating ligands, 2,2'-bipyridine, 1,10-phenanthroline and their structural analogous, and monodentate donors, pyridine, phosphine, and their derivatives, have been widely employed for making the complexes.<sup>1-9</sup> Due to their importance in various fields, designing new complexes have been increasing steadily in order to tune the photophysical properties, in particular, shifting the absorption and emission towards the red region. We have been using commercially known chelating ligands, 2-hydroxyphenylbenzimidazolyl, 2-hydroxyphenylbenzothiazole, 2-hydroxyphenylbenzoxazole, 2-(imidazo[1,2-a]pyridin-2-yl)phenol, and designing new 2hydroxyphenylbenzimidazolyl core based-bis-chelating ligands for making luminescent acyclic mononuclear to polynuclear complexes, and supramolecular coordination complexes including helicates, mesocates and tetrahedrons in the presence of pyridine/benzimidazolyl- based neutral nitrogen donor. 10 The complexes comprising of fac-Re(CO)3, phenoxybenzimidazolyl and pyridine/benzimidazolyl donor are stable and display phosphorescent emission. In continuation of the research in the field, 4-aminopyridine derivatives, rigid bis-chelating ligand containing two 2hydroxyphenylbenzimidazolyl cores and phenyl spacer are chosen instead of benzimidazolyl motif, and flexible bis-chelating ligand with phenylene spacer are used in place of benzimidazole units and bis-chelating flexible ligand to make binuclear fac-[Re(CO)<sub>3</sub>]<sup>+</sup> core containing complexes with improved physico-chemical properties.

This chapter reports dinuclear fac-[Re(CO)<sub>3</sub>]<sup>+</sup> core based complexes, [(Re(CO)<sub>3</sub>(L'))<sub>2</sub>(L)] (L' = 4-aminopyridine = 4-AP for 1/4-dimethylaminopyridine = 4-DMAP for 2, and L = 1,4-phenylene-bis(2-(2'-hydroxyphenyl)benzimidazole) = H<sub>2</sub>-L) were assembled in a solvothermal approach. The molecular structure of 2 was established using single crystal X-ray diffraction analysis. The UV-Visible and emission studies of complexes (1-2) were performed in solution.

#### **5a.2. Results and Discussions**

The complexes were synthesized using  $Re_2(CO)_{10}$ ,  $H_2$ –L, 4-aminopyridine (4-AP) for 1/4-dimethylaminopyridine (4-DMAP) for 2 and mesitylene: hexane/mesitylene in a one-pot approach. (Scheme 1).

HO H<sub>2</sub>-L 
$$\xrightarrow{R}$$
  $\xrightarrow{R}$   $\xrightarrow{R}$ 

#### Scheme 1. Synthesis of 1 and 2.

The complexes are moisture, air stable and sparingly soluble in DMSO. The ATR-IR spectra of 1-2 showed three carbonyl bands between 2008–1864 cm<sup>-1</sup>, corresponding to the fac-[Re(CO)<sub>3</sub>]<sup>+</sup> core.<sup>10</sup> The <sup>1</sup>H-NMR spectrum of **1** was recorded in a mixture of solvent, CDCl<sub>3</sub>:DMSO- $d_6$  (5:1, v/v). (Figure 1). The peak assignment for each related proton was difficult due to the appearance of broad chemical resonances. The <sup>1</sup>H-NMR spectrum showed a broad singlet at 5.87 ppm corresponding to -NH<sub>2</sub> protons of aminopyridine motif whereas complex 2 displayed a set of well-resolved peaks in  $H^{b}$ CDCl<sub>3</sub>. The <sup>1</sup>H–NMR complexes showed spectra of both the protons 4-aminopyridine/dimethyl aminopyridine appearing as a doublet and shifted upfield significantly. The H<sup>a</sup> protons also appeared downfield and as a doublet with respect to uncoordinated ligand, which is because of the coordination of adjacent nitrogen atom to the rhenium metal core.

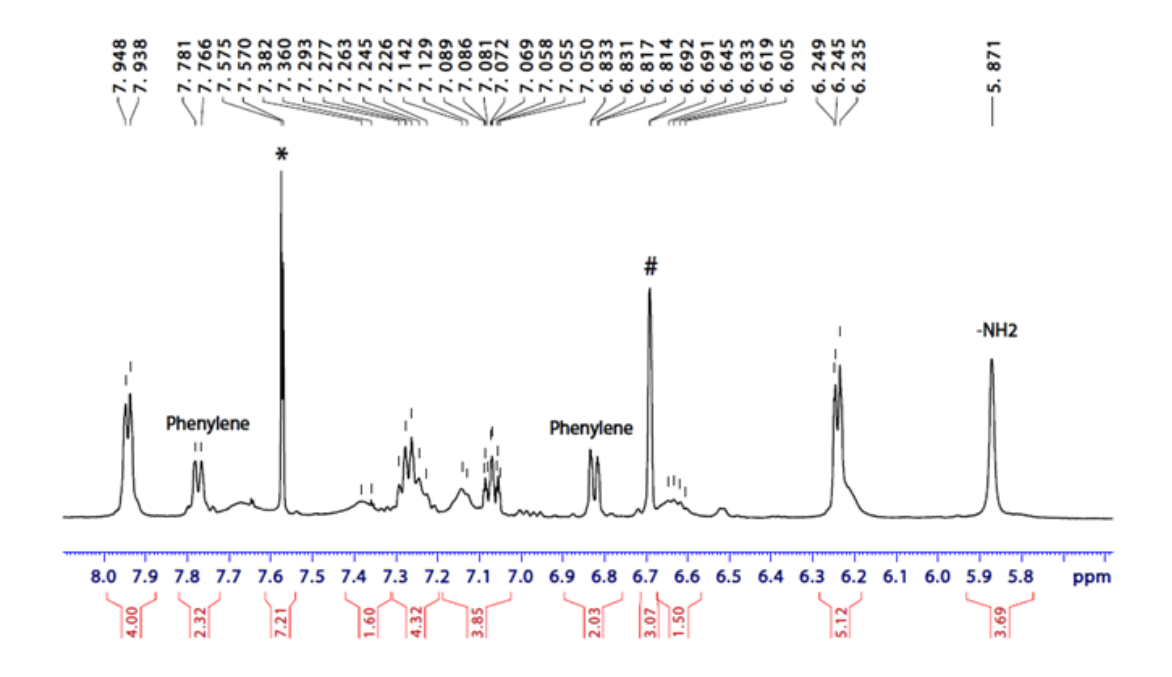


**Figure 1.**  $^{1}$ H-NMR spectrum of **1** in CDCl<sub>3</sub>:DMSO- $d_6$  (5:1, v/v) (\*indicates the solvent peak + compound, # indicates mesitylene peak).

The protons of central phenylene spacer in a rigid bis-chelating ligand split into two doublets for two protons each, indicating the rigidity in arene core in **2** after complexation. The above data suggests that the complex retains structure in solution state. The additional minor peaks ( $\sim$  <1%) present in the  $^{1}$ H–NMR spectra of the complexes can be because of structural isomers present in the solution. (Figure 1–2). Further, the mass spectrometry displayed molecular ion peak at m/z 1222.1466 for [**1**]<sup>+</sup> and 1278.2077 for [**2**]<sup>+</sup> with experimental isotopic distribution pattern matching with the calculated values. (Figure 3–4).

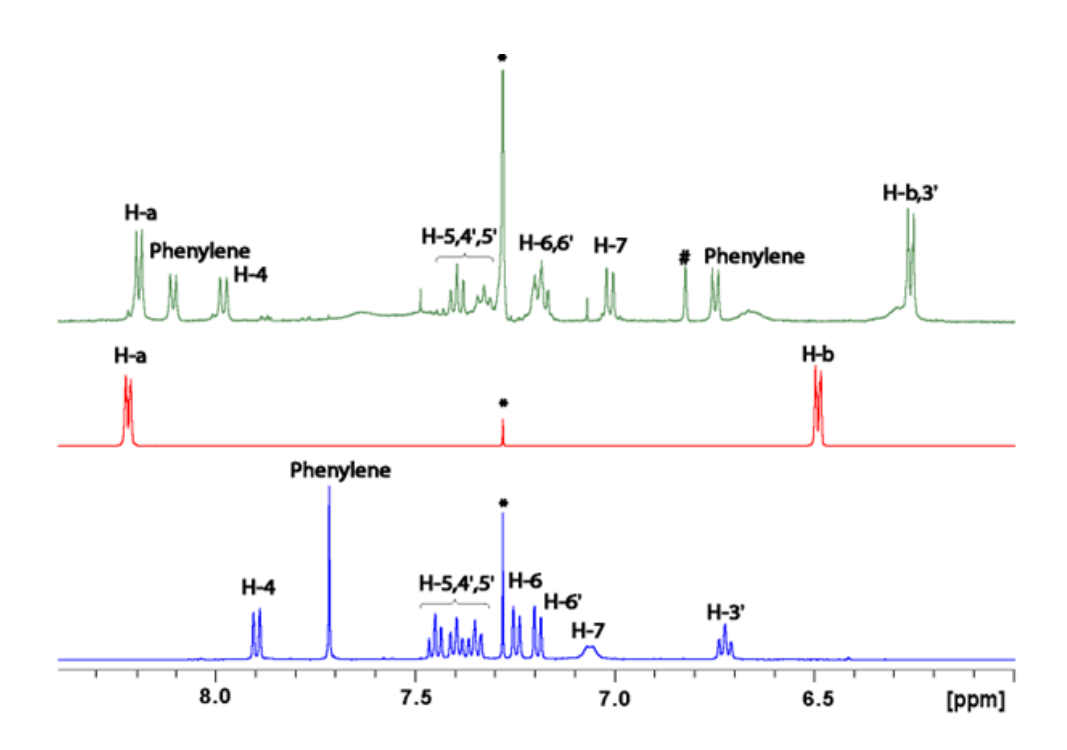


**Figure 2.** <sup>1</sup>H–NMR spectra of H<sub>2</sub>–RBC (blue), 4-DMAP (red) and **2** (green) in CDCl<sub>3</sub> (\*indicates the solvent peak, # indicates the mesitylene peak).

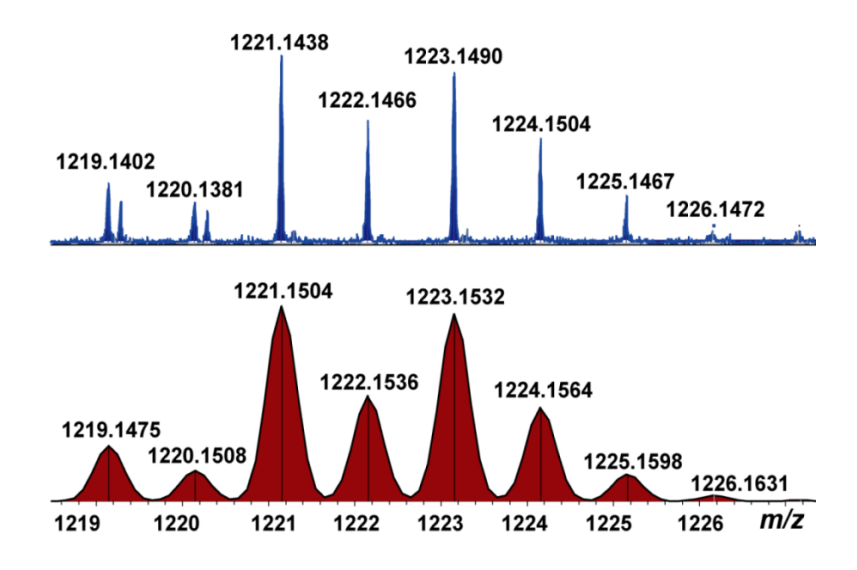


**Figure 3.** Experimental (blue) and calculated (red) ESI-TOF mass spectra of  $[1 + H]^+$ .

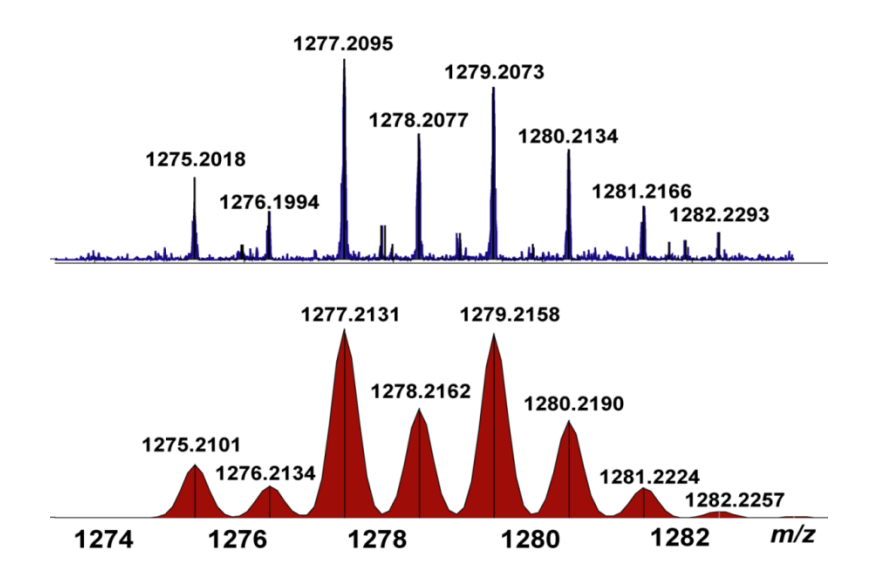


**Figure 4.** Experimental (blue) and calculated (red) ESI-TOF mass spectra of [2+ H]<sup>+</sup>.

The molecular structure of complex 2 was determined using X-ray diffraction analysis. The complex consists of two fac-[Re(CO)<sub>3</sub>]<sup>+</sup> cores, a rigid bis-chelating ligand (L<sup>2-</sup>) and two 4-dimethylaminopyridine. (Figure 5).

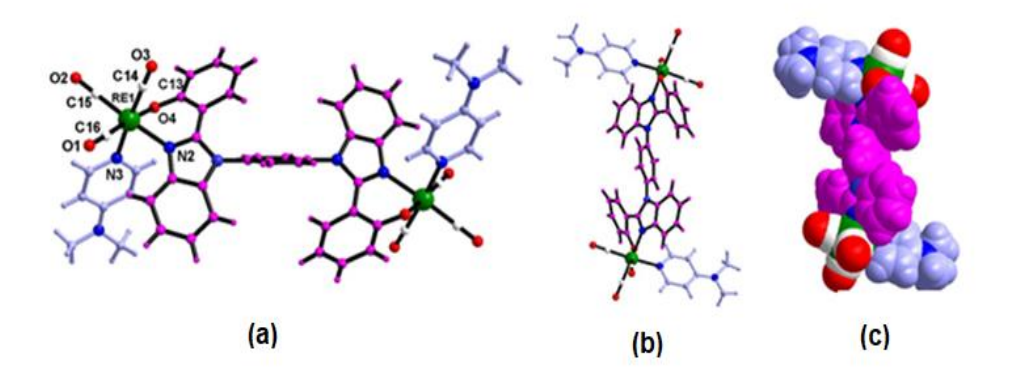


**Figure 5**. (a) Molecular structure of **2**. Side view of **2** showing helical nature of bis-chelating ligand (b-c). C and H atoms of L and 4–DMAP are shown in pink and pale blue color. Six CO units are shown in white and red color. O atoms and N atoms are shown in red and blue color.

Each rhenium centre adopts distorted octahedral geometry and is surrounded by three carbonyl groups, two chelating atoms (N $\cap$ O) from phenoxybenzimidazolyl, and N-atom from 4–DMAP. The L<sup>2-</sup> motif bis-chelates two *fac*-Re(CO)<sub>3</sub> cores using its four donors (O $\cap$ N-O $\cap$ N = bis-chelating donors) symmetrically with Re···Re distance of 13.85 Å. Two anionic benzimidazolylphenolate units of L<sup>2-</sup> are twisted resulting in dinuclear helical architecture of the complex. The Re–N(chel) and Re–O(chel) distances are within the expected range observed for complexes containing fac-[Re(CO)<sub>3</sub>]<sup>+</sup> and phenoxybenzimidazole motifs. The C13–O4 distance (1.321 Å) in 2 indicates the phenolate character of O4–atom, which further supported an ionic interaction between Re1 and O4 atom. The central arene unit of L<sup>2-</sup> is nearly orthogonal to two chelating motifs with a dihedral angle of 66°. The two 4-dimethylaminopyridine motifs are oriented in a 'Z'-type *trans* arrangement. The Re1–N3 (2.173 Å) distance is similar to Re1–N2(chel) (2.171 Å). The axially arranged 4–DMAP in 2 is slightly tilted towards benzimidazolyl core of L, resulting in a V-shaped structure at both ends of the complex.

In the crystal structure of **2**, each molecule interacts with neighbouring molecules via three kinds of non-covalent interactions. The methyl group of 4–DMAP of one molecule interacts with neighbouring molecules via two types of C–H··· $\pi$  contacts, d(C26(H)···C5(arene) = 3.474 Å, d(C26(H)···C16 $\equiv$ O = 3.582 Å. The second pyridine unit interacts with the adjacent phenolate unit through aromatic edge–to–face contacts, d(C21(H)··· $\pi(C12)$  = 3.648 Å. Further, the central arene unit of bis-chelating ligand interacts with neighbouring molecules via H–bonding interactions. This hydrogen bonding interactions is observed between the hydrogen of arene unit to the O–atom of the chelating motif, d(C22(H)···O4 = 3.298 Å and  $\angle C22$ –H···O4 = 140°.

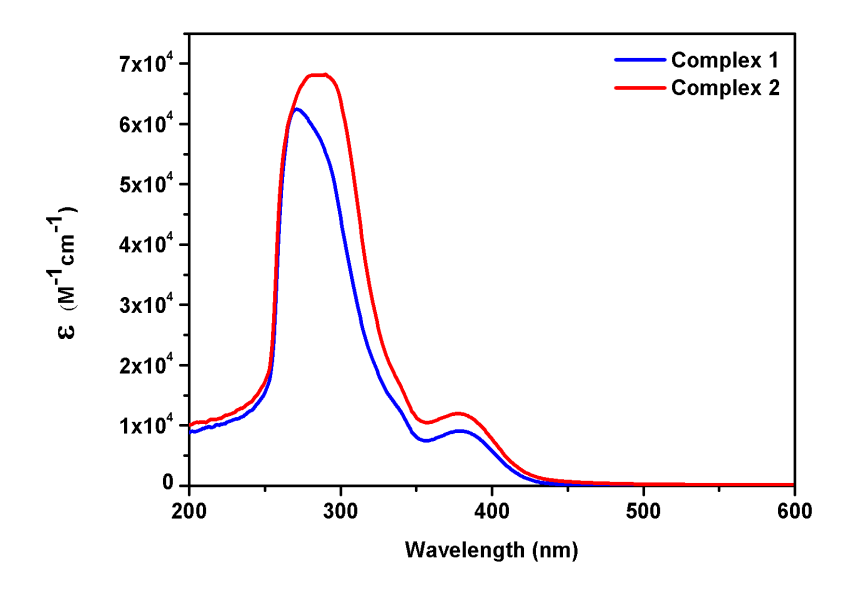


**Figure 6.** UV–Vis spectra of **1** and **2** in DMSO at room temperature.

The photophysical properties of  $\bf 1$  and  $\bf 2$  were studied in DMSO at room temperature (Figure 6–7). Both the complexes displayed a well–resolved band in the high energy UV region ( $\lambda$  < 300 nm), attributed to ligand centered ( $\pi \to \pi^*$ ) transitions. The lower energy band at ~ 380 nm is ascribed to MLCT and ILCT transitions. Complex  $\bf 1$  displayed two emission bands, weak emission band in higher energy region (429 nm), and a strong broad emission centered at 540 nm. Similarly, complex  $\bf 2$  displayed weak emission bands in the higher energy region (418 and 439 nm) and intense broad emission centered at 550 nm. The higher energy emission of both the complexes can be due to ligand centered transitions originating from hydroxyphenylbenzimidazolyl core based bis–chelating ligand as  $\bf H_2$ -L also displayed structured emission band at 370 and 505 nm in DMSO. (Figure 8). The lower energy broad emission is an admixture of  $^3$ MLCT and metal to ligand ligand charge transfer ( $^3$ MLLCT) transitions.

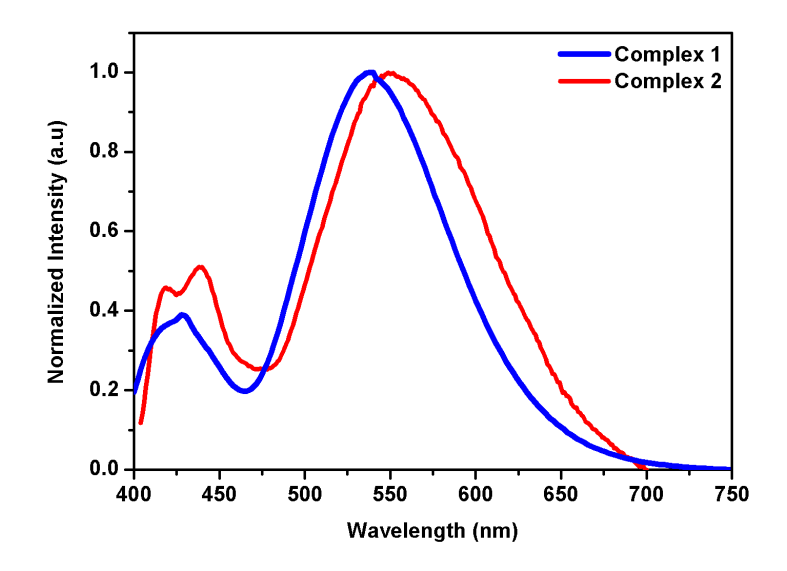
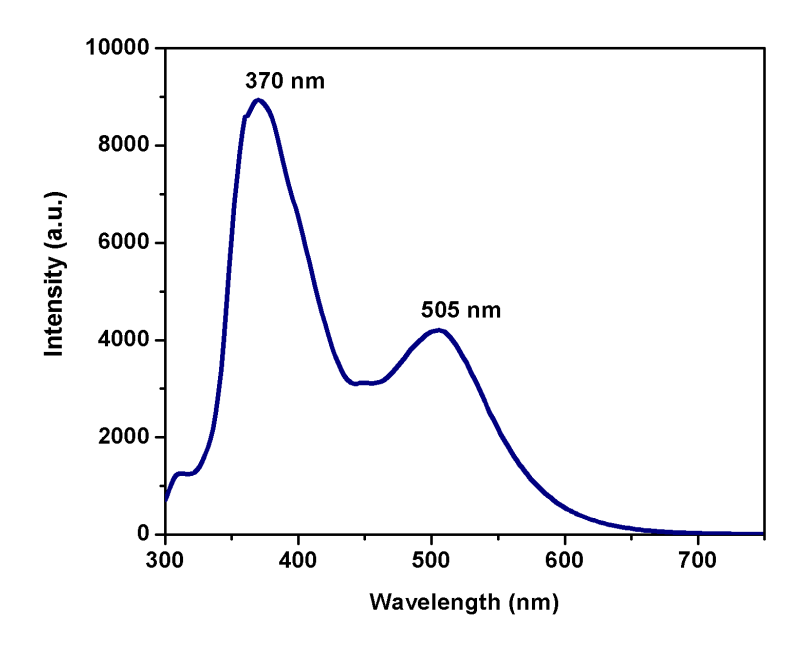


Figure 7. Emission spectra of 1 and 2 in DMSO at room temperature.



**Figure 8.** Emission spectra of H<sub>2</sub>-RBC in DMSO at room temperature,  $\lambda_{ex}$ = 310 nm.

A similar kind of emission was observed for helicate containing fac-[Re(CO)<sub>3</sub>]<sup>+</sup>, hydroxyphenylbenzimidazolyl ligand, and benzimidazolyl containing flexbile motif. Further,

acyclic mononuclear complex containing the structurally similar cores i.e., fac–[Re(CO)<sub>3</sub>]<sup>+</sup>, pyridine, and 2-(1-methyl-1H-benzimidazol-2-yl)phenolate also displayed emission maxima at 515 nm. <sup>11</sup> The results revealed that 4-dimethylaminopyridine is a better choice of ligand for shifting the emission band towards red region as compared to 4-aminopyridine/pyridine/benzimidazolyl motif containing complexes.

# 5a.3. Experimental Section

#### **General Data**

Re<sub>2</sub>(CO)<sub>10</sub>, 4-aminopyridine (4–AP), 4-dimethylaminopyridine (DMAP), *o*-phenylenediamine, 2-hydroxybenzaldehyde, cesium carbonate, copper iodide, 1,10–phenanthroline, mesitylene, hexane and spectroscopic grade solvents, DMSO and DMF, were obtained from commercial sources and used as received. The ligand H<sub>2</sub>–L was synthesized by the previously reported method. <sup>10h</sup>Elemental analyses was performed on the Flash EA 1112 series CHNS analyser. ATR–IR spectra were recorded on a Nicolet iS5 FT–IR spectrometer. High-resolution mass spectra (HR–MS) were measured on a Bruker maXis mass spectrophotometer. NMR spectra were recorded on Bruker Avance III 500 MHz instruments. The electronic absorption spectra were recorded on Jasco V750 UV–Visible spectrophotometer. The emission spectra were recorded on Jasco FP8500 spectrofluorimeter.

## Synthesis of fac-[(Re(CO)<sub>3</sub>(4-AP))<sub>2</sub>(L)] (1).

A mixture of Re<sub>2</sub>(CO)<sub>10</sub> (100.4 mg, 0.153 mmol), H<sub>2</sub>–L (76.2 mg, 0.154 mmol), 4–AP (37.7 mg, 0.400 mmol), and mesitylene:hexane (10:1) was taken in a teflon vessel. The vessel was placed inside a stainless steel bomb. The completely sealed bomb was kept inside an oven maintained at 160 °C for 48 h and then allowed to cool up to 30 °C. The mixture of powder and crystals was obtained were filtered, washed with hexane and air-dried. Yield: 64 % (120.6 mg). Anal. Calcd. for  $C_{48}H_{32}N_8O_8Re_2$ : C, 47.21; H, 2.64; N, 9.18. Found: C, 47.18; H, 2.60; N, 9.20. ATR-IR ( $v_{max}$ , cm<sup>-1</sup>): 2010, 1895 (CO). ESI-TOF-MS. Calcd for  $C_{48}H_{32}N_8O_8Re_2$  [M + H]<sup>+</sup>: m/z 1223.1614, found: m/z 1223.1490. <sup>1</sup>H NMR (500 MHz, CDCl<sub>3</sub>: DMSO- $d_6$  (5:1)):  $\delta$  7.79 (d, 4H, H<sup>a</sup>), 7.78 (d, 2H, J = 7 Hz, phenylene), 7.58 (d, 7H, CDCl<sub>3</sub> + compound), 7.38 (s, br, 2H), 7.29–7.23 (m, 4H), 7.14-7.05 (m,

4H), 6.83 (dd, 2H, phenylene), 6.69 (d, 3H, mesitylene), 6.64–6.60 (m, 2H), 6.25 (d, 5H, H<sup>b</sup> + compound), 5.87 (s, 4H, -NH<sub>2</sub>).

#### Synthesis of fac-[(Re(CO)<sub>3</sub>(4-DMAP))<sub>2</sub>(L)] (2)

A mixture of Re<sub>2</sub>(CO)<sub>10</sub> (100.2 mg, 0.153 mmol), H<sub>2</sub>-L (75.7 mg, 0.153 mmol), DMAP (37.4 mg, 0.306 mmol), and mesitylene (10 mL) was taken in a teflon vessel. The vessel was placed inside a stainless steel bomb. The completely sealed bomb was kept inside an oven maintained at 160 °C for 48 h and then allowed to cool up to 30 °C. The yellow crystals of **2** obtained in the bomb were washed with hexane and air-dried. The yellow solution was decanted and evaporated to half of its volume using a rotary evaporator. The yellow powder **2** was obtained by adding distilled hexane to the solution. The powder was filtered, washed with hexane and air-dried. Yield: Powder, 55 % (107.5 mg). Anal. Calcd. for  $C_{52}H_{40}N_8O_8Re_2$ : C, 48.90; H, 3.26; N, 8.77. Found: C, 48.72; H, 3.21; N, 8.75. ATR–IR ( $v_{max}/cm^{-1}$ ): 2008, 1891, 1864 (CO). ESI–TOF–MS. Calcd for  $C_{52}H_{40}N_8O_8Re_2$  [M + H]\*: m/z 1279.2162, found: m/z 1279.1966. <sup>1</sup>H NMR (500 MHz, CDCl<sub>3</sub>):  $\delta$  8.19 (d, J = 7.25 Hz, 4H, H<sup>a</sup>), 8.10 (d, J = 7.45 Hz, 2H, phenylene), 7.98 (d, J = 8.4 Hz, 2H, H<sup>4</sup>), 7.40-7.36 (m, 3H, H<sup>5.5′</sup>), 7.33–7.30 (m, 3H, H<sup>5.4′</sup>), 7.19-7.15 (m, 4H, H<sup>6.6′</sup>), 7.01 (d, J = 7.75 Hz, 2H, H<sup>7</sup>), 6.81 (d, mesitylene), 6.74 (d, J = 7.5 Hz, 2H, phenylene), 6.25–6.24 (dd, 6H, H<sup>b.3′</sup>).

**X-ray crystal data for complex 2.** Single crystal X-ray data of crystal of **2** were collected on a Bruker D8 QUEST diffractometer [ $\lambda_{(Mo-K\alpha)} = 0.71073$  Å]. The structure was solved by direct methods using SHELXS-2014/5 (Sheldrick 2014) and refined using the SHELXL-2018/3 (Sheldrick, 2018) program (within the WinGX program package). Non-H atoms were refined anisotropically.  $C_{52}H_{40}N_8O_8Re_2$ , M = 1277.32, Tetragonal, space group I 41/a,T = 296(2) K, unit cell: a = 18.3609(8) Å, b = 18.3609(8) Å, c = 33.8197(14) Å,  $c = 90^\circ$ ,  $c = 90^\circ$ 

11401.4(11) ų, Z = 8,  $\mu = 4.297 \text{ mm}^{-1}$ ,  $D_c = 1.488 \text{ g cm}^{-3}$ , F(000) = 4976,  $\theta$  range for data collection, 2.524 to 25.023°, limiting indices,  $-21 <= \eta <= 12$ , -21 <= k <= 21, -37 <= l <= 40, reflections: 19529 collected, 5005 independent ( $R_{int} = 0.0446$ ), completness to  $\theta_{max}$ , 99.3 %; refinement method, full-matrix least-squares of  $F^2$  (5005 data, 0 restraints, 316 parameters); final indices for I > 2 $\sigma$ (I),  $R_1 = 0.0598$ ,  $wR_2 = 0.1638$ ; final indices for all data,  $R_1 = 0.0861$ ,  $wR_2 = 0.1946$ ; GOF on  $F^2$ , 1.019; largest diff. Peak hole, 3.348 and  $-1.491e\text{Å}^{-3}$ .

# 5a.4. Conclusion

Two dinuclear fac–[Re(CO)<sub>3</sub>]<sup>+</sup>–core based complexes were prepared using rigid bis–chelating ligand with hydroxyphenylbenzimidazolyl core and 4-aminopyridine/dimethyl aminopyridine via one–pot synthetic approach. The complexes displayed strong emission in the solution at room temperature. The results further reveal that the emission properties of the complexes can be modulated by remotely tuning the nitrogen donor.

#### 5a.5. References

- 1. E. B. Bauer, A. A. Haase, R. M. Reich, D. C. Crans, F. E. Kühn, Coord. Chem. Rev. 2019, 393, 79.
- 2. A. A. Haase, E. B. Bauer, F. E. Kühn, D. C. Crans, Coord. Chem. Rev. 2019, 394, 135.
- F. L. Thorp-Greenwood, V. Fernandez-Moreira, C. O. Millet, C. F. Williams, J. Cable, J. B. Court, A. J. Hayes, D. Lloyd, M. P. Coogan, *Chem. Commun.* 2011, 47, 3096.
- 4. M. P. Coogan, V. Fernandez-Moreira, B. M. Kariuki, S. J. A. Pope, F. L. Thorp-Greenwood, Angew. Chem. Int. Ed. 2009, 48, 4965.
- D. Gupta, V. Singh, S. Hohloch, M. Sathiyendiran, K. Tedin, B. Sarkar, *Polyhedron* 2015, 100, 243.
- (a) B. Ramakrishna, R. Nagarajaprakash, V. Veena, N. Sakthivel, B. Manimaran, *Dalton Trans*.
   2015, 44, 17629. (b) M. R. Crawley, K. J. Kadassery, A. N. Oldacre, A. E. Friedman, D. C. Lacy,
   T. R. Cook, *Organometallics*2019, 38, 1664 (c) W. Yang, S. S. Roy, W. C. Pitts, R. L. Nelson, F.
   R. Fronczek, J. W. Jurss, *Inorg. Chem.* 2017, 56, 4176.
- 7. A. Vogler, H. Kunkely, *Coord. Chem. Rev.* 2000, **200-202**, 991.
- 8. M. M. Richter, Chem. Rev. 2004, 104, 3003.
- (a) P. H. Dinolfo, J. T. Hupp, *Chem. Mater.* 2001, 13, 3113; (b) P. Thanasekaran, R. T. Liao, Y. H. Liu, T. Rajendran, S. Rajagopal, K. L. Lu, *Coord. Chem. Rev.* 2005, 249, 1085; (c) P. Thanasekaran, C. C. Lee, K. L. Lu, *Acc. Chem. Res.* 2012, 45, 1403; (d) A. Kumar, S. S. Sun, A. J. Lees, *Coord. Chem. Rev.* 2008, 252, 922; (e) D. Gupta, M. Sathiyendiran, *Chemistry Select*, 2018, 3, 7439; (f) S. Sato, O. Ishitani, *Coord. Chem. Rev.* 2015, 282, 50.
- (a) B. Shankar, S. Sahu, N. Deibel, D. Schweinfurth, B. Sarkar, P. Elumali, D. Gupta, F. Hussain, G. Krishnamoorthy, M. Sathiyendiran, *Inorg. Chem.*2014, 53, 922; (b) S. K. Behara, A. Murkherjee, G. Sadhugiri, P. Elumalai, M. Sathiyendiran, M. Kumar, B. B. Mandal, G. Krishnamoorthy, *Faraday Discuss.* 2017, 196, 71; (c) S. S. Ila, B. Shankar, M. Sathiyendiran, G.

Krishnamoorthy, *J. Photochem. Photobiol. A: Chemistry*, 2018, **353**, 416; (d) M. Bhol, M. Priyatharsini, R. V. Krishnakumar, M. Sathiyendiran, *J. Orgomet. Chem.* 2019, **889**, 27; (e) I. Mishra, M. Sathiyendiran, *J. Orgomet. Chem.* 2019, **895**, 1; (f) P. Saxena, B. Shankar, M. Sathiyendiran *J. Orgomet. Chem.* 2015, **799–800**, 82; (g) M. Priyatharsini, B. Shankar, M. Sathiyendiran, N. Srinivasan, R. V. Krishnakumar, *Acta Cryst. E73*, 2017, **310**; (h) M. Bhol, M. Priyatharsini, R. V. Krishnakumar, M. Sathiyendiran, *J. Orgomet. Chem.* 2019, **889**, 27; (i) R. Arumugam, B. Shankar, K. R. Soumya, M. Sathiyendiran, *Dalton Trans.* 2019, **48**, 7425.

- 11. R. Czerwieniec, A. Kapturkiewicz, R. A. Ostrowska, J. Nowacki, *J. Chem. Soc., Dalton Trans.*, 2002, 3434.
- 12. (a) G. M. Sheldrick, A short history of SHELX, *Acta Crystallogr*. 2008, **A64**, 112; (b) A. J. Spek, single crystal structure validation with the program PLATON, *J. Appl. Cryst*. 2003, **36**, 7.

# **Chapter-5b**

Synthesis and characterization of binuclear manganese carbonyl complex of 1,4-bis(2-(2'-hydroxyphenyl)benzimidazol-1-yl)benzene and dimethylaminopyridine

#### **ABSTRACT**

A neutral heteroleptic binuclear complex fac–[{Mn(CO)<sub>3</sub>(Py')}<sub>2</sub>(L)] with Mn···Mn separation of ~13.5 Å was synthesized using Mn<sub>2</sub>(CO)<sub>10</sub>, 1,4-bis(2-(2'-hydroxyphenyl)benzimidazol-1-yl)benzene (H<sub>2</sub>–L<sup>1</sup>), 4-dimethylaminopyridine (Py'), and trimethylamine-N-oxide via one–pot approach. Complex **1** adopts a helical structure in the solid-state.

#### **5b.1. Introduction**

The design and preparation of fac- $[Mn(CO)_3]^+$  core-based heteroleptic complexes using various types of chelating ligands have attracted considerable attention because of their potential applications as photo- and electro-catalysts for CO<sub>2</sub> reduction, photoactivable CO-releasing molecules, and antimicrobial agents. <sup>1-19</sup> The physiochemical properties of fac-[Mn(CO)<sub>3</sub>]<sup>+</sup> core complexes can be tuned by modulating the chelating ligands either by introducing additional functional units on the chelating framework or by changing the complete donor motif. For example, one of the pyridine units in 2,2'-bipyridine, a well-known chelating ligand, can be replaced by fivemembered heterocycle/another coordinating group. 1-19 Up to now, N^N donor-based chelating units are frequently used for constructing fac-[Mn(CO)<sub>3</sub>]<sup>+</sup> core-based complexes. Due to their importance in medicinal chemistry and catalysis, efforts are being focused on designing new chelating donors for fac-[Mn(CO)<sub>3</sub>]<sup>+</sup> complexes. We have recently designed and synthesized bis-chelating ligands  $H_2-L^n$  ( $H_2-L^I=1,4$ -bis(2-(2'-hydroxyphenyl)benzimidazol-1-ylmethyl)benzene,  $H_2-L^{II}=1,3$ -bis(2-(2'-hydroxyphenyl)benzimidazol-1-ylmethyl)-2,4,6-trimethylbenzene, and  $H_2$ - $L^1 = 1,4$ -bis(2-(2'-hydroxyphenyl))hydroxyphenyl)benzimidazol-1-yl)benzene), which were utilized for fac-[Re(CO)<sub>3</sub>]<sup>+</sup> core- based neutral heteroleptic supramolecular coordination complexes including helicate (I), mesocate (II), molecular tetrahedrons (III), and acyclic binuclear helicates (IV). 20-21 Incorporating 2-(2'hydroxyphenyl)benzimidazole (H<sub>2</sub>-PB) and its structural analogues may provide strong visible light absorptions for fac-[Re(CO)<sub>3</sub>]<sup>+</sup> complexes. These rhenium(I) tricarbonyl complexes (**I**, **II**, and **IV**) display attractive photophysical properties that include dual emissions (fluorescence and phosphorescence) in solid-state and solution. Extending the use of 2-(2'hydroxyphenyl)benzimidazolyl (H–PB)-based bis-chelating ligands to manganese(I)tricarbonyl may result in structurally similar complexes with different physiochemical properties. It is worth mentioning that the use of  $H_2$ –PB, 2-(2'-hydroxyphenyl)benzoxazole, 2-(2'-hydroxyphenyl)benzothiazole and their corresponding bis-chelating ligands with or without spacer is less common in the preparation of fac–[Mn(CO)<sub>3</sub>]<sup>+</sup> complexes.<sup>19</sup> This chapter reports a neutral, heteroleptic acyclic binuclear complex fac–[{Mn(CO)<sub>3</sub>(Py')}<sub>2</sub>(L<sup>1</sup>)] (1) where Py' = 4-dimethylaminopyridine. The complex is synthesized using  $H_2$ –L<sup>1</sup>, Py', and Mn<sub>2</sub>CO<sub>10</sub> via a one-pot approach. The complex was characterized by elemental analysis, Electrospray ionization-mass spectrometry (ESI–MS), and spectroscopic techniques (ATR–IR and NMR). The molecular structure of complex 1 was confirmed by single crystal X–ray diffraction analysis.

#### **5b.2. Results and Discussions**

The treatment of  $Mn_2(CO)_{10}$ ,  $H_2-L^1$ , Py', trimethylamine *N*-oxide in dichloromethane under dark conditions in nitrogen atmosphere resulted in the formation of complex **1** (Scheme 1). The general synthetic conditions used for preparing fac– $[Mn(CO)_3]^+$  core-based complexes from  $Mn_2(CO)_{10}$ , oxamide, and ditopic nitrogen donors were followed for complex **1**. The complex is air-stable, light-sensitive, and soluble in most of the polar organic solvents. The ATR–IR spectrum of the complex displayed three strong bands 2014, 1916, and 1886 cm<sup>-1</sup>, corresponding to the stretching bands of fac- $[Mn(CO)_3]^+$  unit (Figure 1).

HO NO HOLD Hard Photo Property of the condition room temp., 
$$Py'$$
  $Py'$   $Py'$ 

**Scheme 1.** Synthetic approach for complex 1.

The <sup>1</sup>H–NMR spectrum of **1** in CDCl<sub>3</sub> displayed slightly broad chemical resonances for the protons of L<sup>2-</sup> and Py' (Figure 2). The chemical resonances in region 7.5–7.00 ppm were complicated due to the overlapping protons of L<sup>2-</sup> motif. An attempt was made to assign the proton signals using the <sup>1</sup>H–<sup>1</sup>H COSY spectrum of **1**. Though complete assignment of protons of **1** was not successful, the chemical resonances of protons of Py' were noticeably unambiguous. The H<sup>a</sup> and H<sup>b</sup> protons of Py' in **1** are slightly upfield shifted compared to that of uncoordinated Py'.

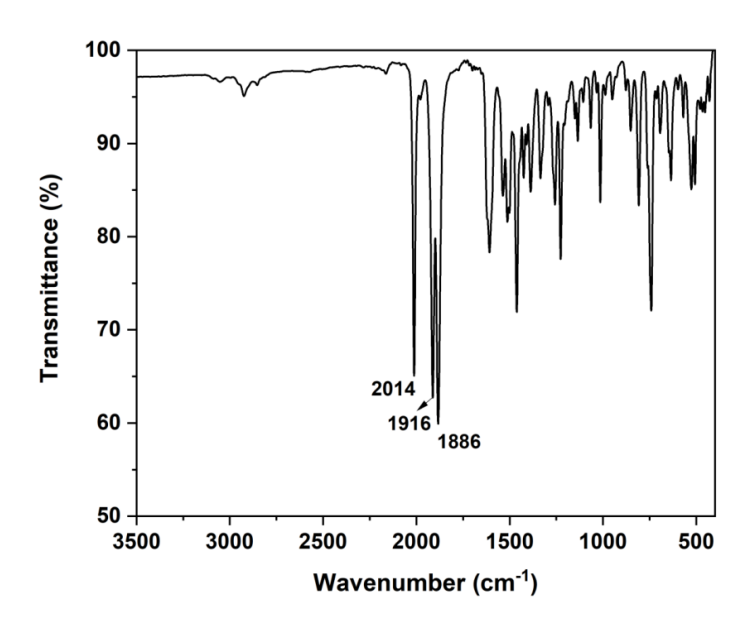
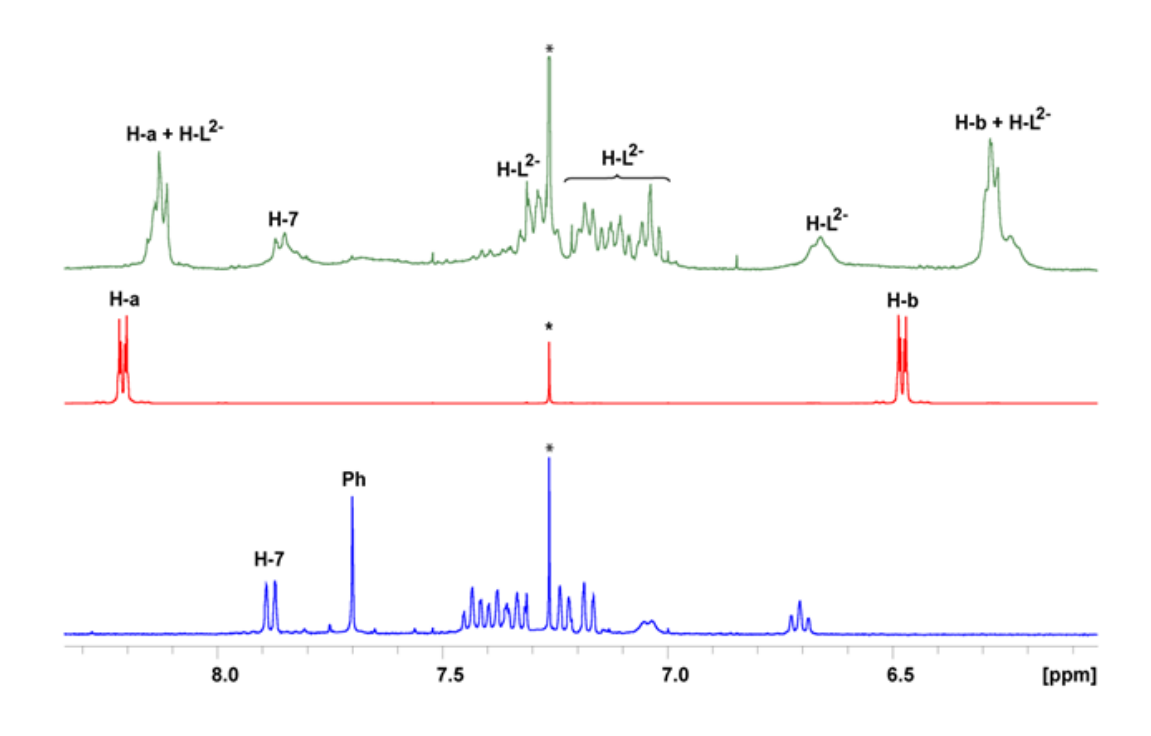


Figure 1. ATR-IR spectrum of complex 1.



**Figure 2.** <sup>1</sup>H NMR spectra of H<sub>2</sub>-L<sup>1</sup> (blue), Py' (red), and **1** (green) in CDCl<sub>3</sub> (\*indicates CDCl<sub>3</sub> peak).

These protons of the complex, in general, are expected to shift downfield because of the close proximity to the coordinated nitrogen atom. The results suggest that these protons lie above or close to the aromatic unit in the complex and experience the ring current effects. Further, an intense single peak ( $\sim$ 7.7 ppm) of protons of the phenylene ring of  $H_2$ –L was not observable in a similar region for the complex. However, peaks of the other protons of  $L^{2-}$  were observed with or without downfield/upfield shifts compared to those of  $H_2$ –L<sup>1</sup>. The results indicate that the phenylene protons split into two chemical resonances and merged with other peaks in 1. The results indirectly suggest that the molecular structure of 1 remains intact in the solution. The  $^{13}$ C–NMR spectrum of 1 displayed two signals around 200 ppm, corresponding to the carbonyl carbon atoms of the complex (Figure 3).

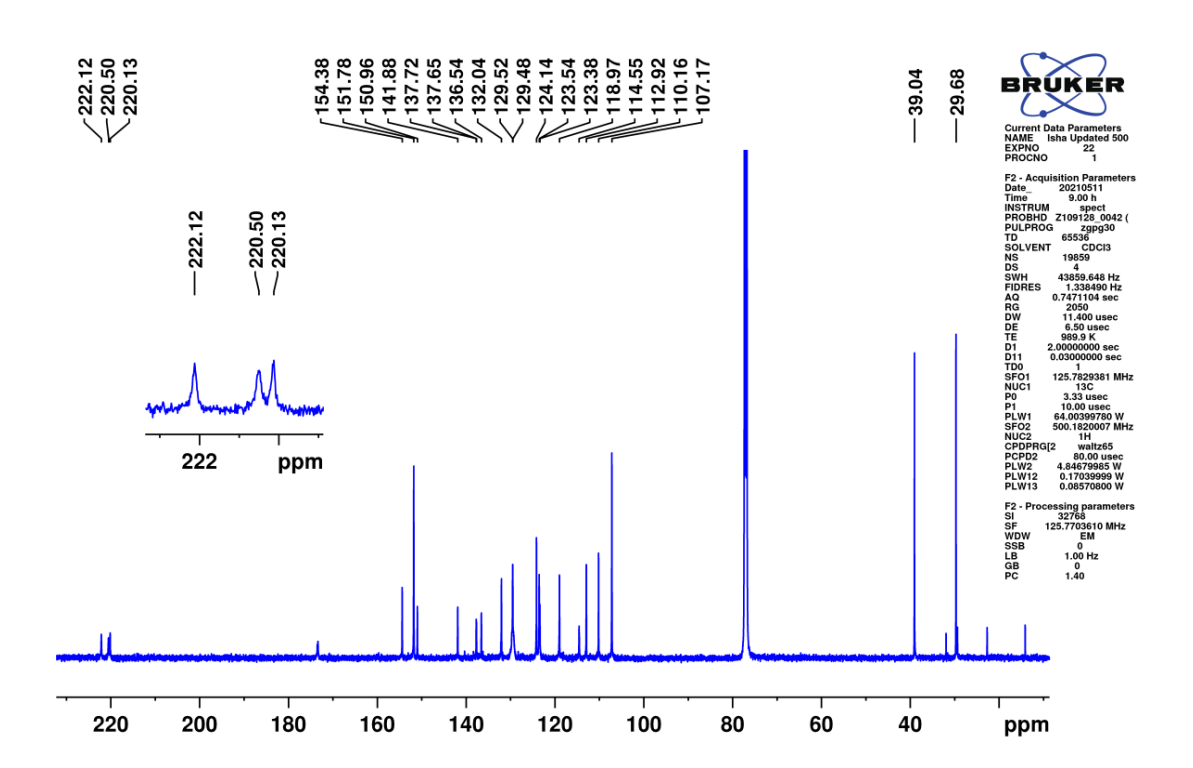
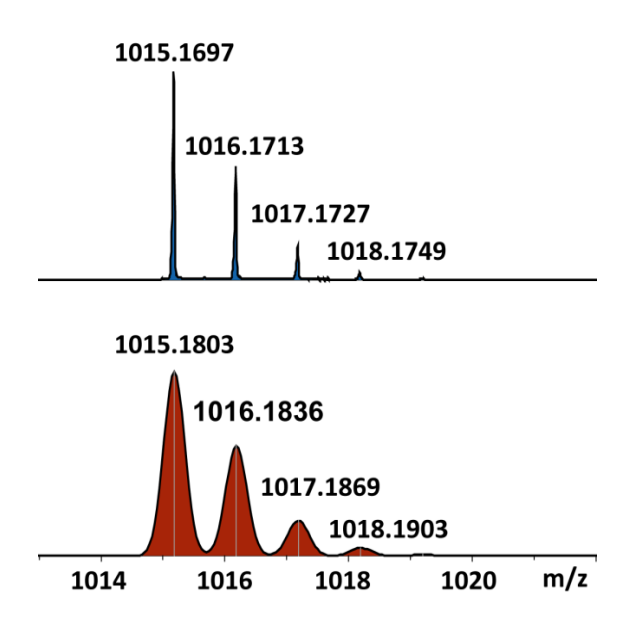


Figure 3. <sup>13</sup>C-NMR spectrum of 1 in CDCl<sub>3</sub>.

The formation of **1** was confirmed by ESI-MS that showed a molecular ion peak at m/z 1015.1697 for  $[\mathbf{1} + \mathbf{H}]^+$ . The experimental isotope pattern of **1** matches the theoretical values (Figure 4).



**Figure 4.** Experimental (blue) and calculated (red) ESI–TOF mass spectra of  $[1 + H]^+$ .

Single crystals of **1** suitable for X-ray diffraction analysis were obtained by slow diffusion of *n*-hexane into its dichloromethane solution. The asymmetric unit of **1** contains half of the complex. The solvent molecules present in the crystal lattice of **1** were squeezed due to the severe disorder of atoms. The molecular structure of **1** contains two fac-[Mn(CO)<sub>3</sub>]<sup>+</sup> cores, one L<sup>2-</sup>, and two Py' motifs (Figure 5). The metal center in the complex adopts distorted octahedral geometry with a C<sub>3</sub>N<sub>2</sub>O environment. The metal core is surrounded by anionic [N^O<sup>-</sup>], one neutral N atom from Py', and three carbonyl carbon atoms. The L<sup>2-</sup> motif acts as bis-chelating donors using its two phenolato-benzimidazolyl (PB<sup>-</sup>) motifs and bis-chelated two Mn(I) cores. Two chelating motifs of L<sup>2-</sup> in the complex adopt a *trans*-conformation mode. The chelating motif (phenolato-benzimidazolyl) deviated from the plane of the central arene core with the dihedral angle of ~66°. The axially coordinated Py' unit bowed towards benzimidazolyl core of L<sup>2-</sup> (dihedral angle = ~64°).

The -NMe<sub>2</sub> motif is coplanar with a pyridine ring in the complex. The two Py' units in **1** acquire *trans*-conformation to each other.

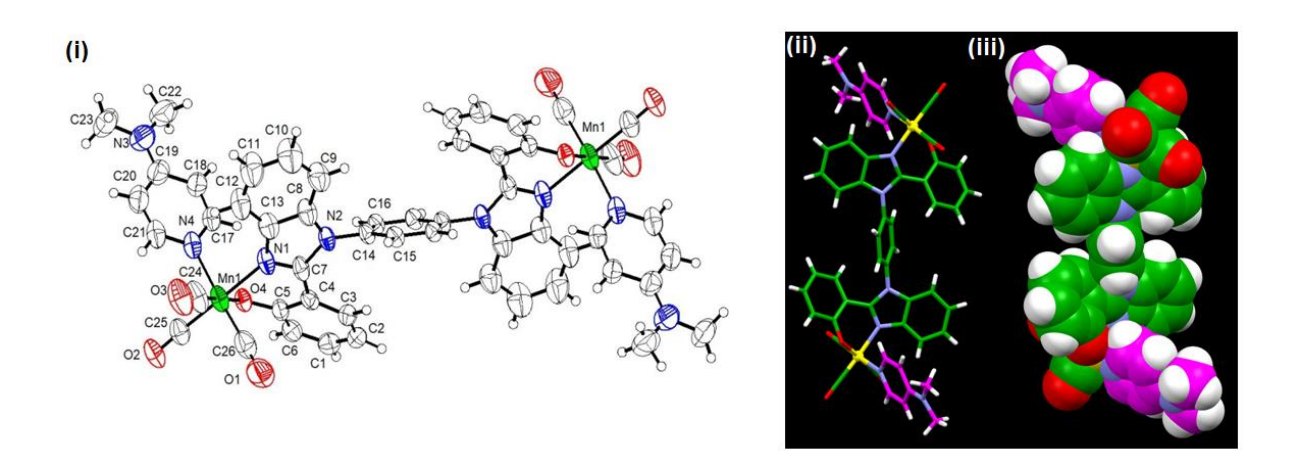


**Figure 5**. Molecular structure of **1** (i) an ORTEP drawing (thermal ellipsoids drawn to 50% probability); Side view of **1**, (ii) capped–stick model, (iii) space–fill view.

The overall arrangement of  $L^{2-}$  and Py' units in the complex results in the helical structure. It is important to mention that a similar helical arrangement of the ligands was also observed in Re(I) analogues (IV).<sup>21</sup> The bonding parameters of 1 are compared with IV. The Mn···Mn distance in 1 is ~13.60 Å that is slightly shorter than that found for complex IV (Re···Re = ~13.85 Å). The bond distances (Mn–N( $L^2$ ), Mn–N(Py'), Mn–O, and Mn–C) are slightly shorter than those found for complex IV (Table 1).<sup>21</sup> A similar observation is found for the several fac–[Mn(CO)<sub>3</sub>]<sup>+</sup> based metallacycles compared to those of complex IV. Further, the C5–O4 distance (~1.325 Å) in 1 is slightly shorter than that found in neutral 2-(2'-hydroxyphenyl) benzimidazole (C–O = ~1.344 Å).<sup>20</sup> The parameter indicates that O4 has a phenolato character in complex 1. Therefore, the interaction

between Mn–O4 may be considered as ionic in nature in the complex.

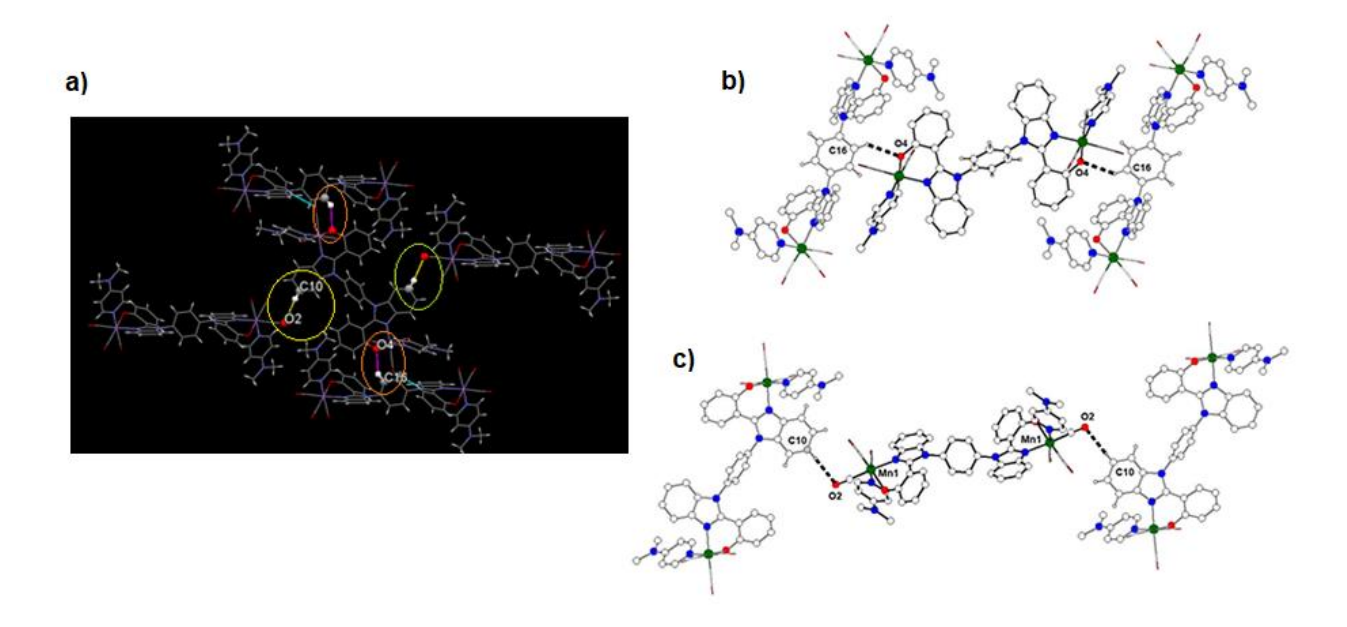


**Figure 6.** Partial packing diagram of **1** showing five molecules. In (a) and (b), the middle molecule is same. (a) Intermolecular H-bonding interactions observed between the phenylene units of  $L^{2-}$  to the oxygen of the phenolate unit of the neighbouring molecule (pink circles). H-atoms except for phenylene units and one CO are removed for clarity. (b) Intermolecular H-bonding contacts between the benzimidazolyl of  $L^{2-}$  to the oxygen atom of the neighboring C $\equiv$ O (yellow circles). All carbonyl units are shown as stick models.

The crystal structure of **1** was stabilized by various types of non-covalent contacts (Figure 6). In particular, the intermolecular hydrogen bonding interactions were observed between the phenylene unit of  $L^{2-}$  to the oxygen of the phenolate unit i.e., coordinated oxygen atom, of the neighbouring molecule ( $d(\mathring{A})$ , C16—H···O4: H···A= ~2.52, D···A = ~3.2915 and  $\angle$ C16—H···O4 = ~140°). This interaction is extended in the crystal structure in both directions. Further, the hydrogen atom of

benzimidazolyl contacts with the oxygen atom of the carbonyl unit of the neighbouring molecule (d (Å), C10—H····O2: H····A= ~2.53, D····A = ~3.448 and  $\angle$ C10—H····O2 = ~167°), resulting in the extended network structure. Dimethylaminopyridine unit of one molecule interacts with the aromatic unit of the adjacent molecule via non-covalent interactions. The methyl group of Py' interacts with the benzimidazolyl core of L<sup>2</sup>-via C-H··· $\pi$  contacts (d (Å): C23(H)···C12/C13 = ~3.419/~3.463 Å). Also, the pyridine unit of Py' interacts with the phenolato unit of L<sup>2</sup>- through C-H··· $\pi$  interactions (d (Å): C17(H)···C6/C1 = 3.347/3.540 Å).

**Table 1.** Selected bond lengths of **1** and **IV**  $(\mathring{A})$ .

	1	IV
$M \cdot \cdot \cdot M$	~13.605	~13.854
M-O	1.991 (3)	2.110(6)
$M-N(L^{2-})$	2.056(3)	2.171(8)
M-N(Py')	2.079 (4)	2.173(11)
$N(L^{2-})-M-C$	1.817 (5)	1.905(11)
N(Py')– $M$ – $C$	1.812 (6)	1.897(17)
$N(L^{2-})-M-C\equiv O$	1.141 (5)	1.160(13)
$N(Py')-M-C\equiv O$	1.136 (6)	1.155(18)
$O(L^{2-})-M-C$	1.780 (5)	1.887(12)
$O(L^{2-})-M-C\equiv O$	1.164 (6)	1.180(16)
O4—C5	1.325 (5)	1.321(11)

# 5b.3. Experimental Section

#### **General Data**

Mn<sub>2</sub>(CO)<sub>10</sub>, 4-dimethylaminopyridine (Py'), trimethylamine *N*-oxide, *o*-phenylenediamine, 2-hydroxybenzaldehyde, cesium carbonate, copper iodide, 1,10-phenanthroline, hexane, and dichloromethane were obtained from commercial sources and used as received. The ligand H<sub>2</sub>-L<sup>1</sup> was synthesized by the previously reported method.<sup>20b</sup> Elemental analysis was performed on Flash EA 1112 series CHNS analyzer. ATR-IR spectrum was recorded on a Nicolet iS5 IR spectrophotometer. A high resolution mass spectrum (HR-MS) was measured on a Bruker maXis mass spectrometer. NMR spectra were recorded on Bruker Avance III 400 MHz instrument.

# Synthesis of fac-[{Mn(CO)<sub>3</sub>(Py')}<sub>2</sub>(L<sup>1</sup>)] (1).

A mixture of  $Mn_2(CO)_{10}$  (100.3 mg, 0.256 mmol),  $H_2$ – $L^1$  (126.6 mg, 0.256 mmol), Py' (62.4 mg, 0.512 mmol), and trimethylamine N-oxide (78.0 mg, 1.024 mmol) was taken in the Schlenk complex equipped with a magnetic bar. The system was purged with nitrogen gas using the Schlenk line. To the mixture, freshly distilled dichloromethane (25 mL) was added. The reaction was performed under dark conditions and allowed to stir at room temperature (~28 °C) for 72 h. The color of the reaction mixture changed from yellow to brown. The brown solution was extracted using water (20 mL × 3) to remove the unreacted trimethylamine N-oxide. The resulting organic solution was concentrated using a rotary evaporator. The mustard yellow powder obtained was washed with hexane several times and air-dried. Yield: 164 mg, 63 % (based on  $Mn_2(CO)_{10}$ ). X-ray quality crystals were obtained by diffusion of hexane to dichloromethane solution of the complex. Anal.Calcd.for  $C_{52}H_{40}N_8O_8Mn_2$ : C, 61.55; H, 3.97; N, 11.04. Found: C, 61.45; H, 3.91; N, 11.09. ATR-IR ( $v_{max}/cm^{-1}$ ): 2014, 1916, 1886 (CO). ESI-MS. Calcd. for  $C_{52}H_{40}N_8O_8Mn_2$  [1 + H]<sup>+</sup>: m/z

1015.1803, found: m/z 1015.1697. <sup>1</sup>H–NMR (400 MHz, CDCl<sub>3</sub>):  $\delta$  8.15–8.11 (m, 5H, H<sup>a</sup>, H(L<sup>2-</sup>), 7.85 (d, J = 8.4 Hz, 2H, H<sup>7</sup>), 7.33–7.00 (m, H(L<sup>2-</sup>), 6.66 (t, 2H, H(L<sup>2-</sup>), 6.28 (m, 6H, H<sup>b</sup>, H(L<sup>2-</sup>), 2.93 (d, J = 2.7 Hz, 12H, -N(CH<sub>3</sub>)<sub>2</sub>).

**X-ray crystal data for 1.** Single crystal X–ray data of crystal of **1** was collected on a Rigaku oxford XtalLAB Synergy [ $\lambda_{(Mo-K\alpha)} = 0.71073$  Å]. The crystal structure of **1** was solved by direct methods using SHELXS-2014/5 (Sheldrick 2014) and refined using the SHELXL-2018/3 (Sheldrick, 2018) program (within the WinGX program package).<sup>22</sup> Non–H atoms were refined anisotropically.  $C_{52}H_{40}N_8O_8Mn_2$ , M = 1014.80, tetragonal, space group I 41/a,T = 293 K, unit cell: a = b = 18.2376(3) Å, c = 33.9154(9) Å,  $\beta = 90^\circ$ , V = 11280.6(5) Å<sup>3</sup>, Z = 8,  $\mu = 0.502$  mm<sup>-1</sup>,  $D_c = 1.195$  g cm<sup>-3</sup>, F(000) = 4176,  $\theta$  range for data collection, 1.984 to 26.235°, limiting indices, -20 <= h <= 22, -22 <= k <= 21, -42 <= l <= 39, reflections: 27067 collected, 5465 independent ( $R_{int} = 0.0523$ ), completness to  $\theta_{max}$ , 1; refinement method, full-matrix least-squares of  $F^2$  (5465 data, 0 restraints, 316 parameters); final indices for  $I > 2\sigma(I)$ ,  $R_1 = 0.0747$ ,  $wR_2 = 0.2471$ ; final indices for all data,  $R_1 = 0.1059$ ,  $wR_2 = 0.2785$ ; GOF on  $F^2$ , 1.017; largest diff. Peak hole, 1.274 and -0.628 e.Å<sup>-3</sup>.

#### **5b.4. Conclusion**

A neutral heteroleptic fac-[Mn(CO)<sub>3</sub>]<sup>+</sup> core-based dinuclear complex 1 was synthesized using the combination of  $Mn_2(CO)_{10}$ , 1,4-bis(2-(2'-hydroxyphenyl)benzimidazol-1yl)benzene and 4-dimethylaminopyridine in a one-pot approach. The complex adopts a helical structure in the solid state. The work facilitates the design of manganese(I) carbonyl-based dinuclear complexes with functional groups such as esters and ethers on the benzimidazolyl or arene spacer motif. The preparation of supramolecular coordination complexes using  $H_2$ -Land neutral ditopic nitrogen donor possessing benzimidazolyl/substituted benzimidazolyl motif is currently progress in our laboratory.

#### **5b.5. References**

- 1. (a) I. Chakraborty, S. J. Carrington, P. K. Mascharak, Acc. Chem. Res. 2014, 47, 2603; (b) I. Chakraborty, S. J. Carrington, P. K. Mascharak, ChemMedChem 2014, 9, 1266; (c) J. Jimenez, I. Chakraborty, A. Dominguez, J. Martinez-Gonzalez, W. M. C. Sameera, and P. K. Mascharak, Inorg. Chem. 2018, 57, 1766; (d) I. Chakraborty, S. J. Carrington, G. Roseman, P. K. Mascharak, Inorg. Chem. 2017, 56, 1534; (e) S. J. Carrington, I. Chakraborty, P. K. Mascharak, Dalton Trans. 2015, 44, 13828; (f) M. A. Gonzalez, M. A. Yim, S. Cheng, A. Moyes, A. J. Hobbs, P. K. Mascharak, Inorg. Chem. 2012, 51, 601; (g) M. N. Pinto, I. Chakraborty, J. Jimenez, K. Murphy, J. Wenger, P. K. Mascharak, Inorg. Chem. 2019, 58, 14522; (h) K. J. Kadassery, S. N. MacMillan, D. C. Lacy, Inorg. Chem. 2019, 58, 10527.
- U. R. Gandra, A. Sinopoli, S. Moncho, M. NandaKumar, D. B. Ninković, S. D. Zarić, M. Sohail,
   S. Al-Meer, E. N. Brothers, N. A. Mazloum, M. Al-Hashimi, H. S. Bazzi, ACS Appl. Mater.
   Interfaces 2019, 11, 34376.
- 3. (a) M. Tinajero-Trejo, N. Rana, C. Nagel, H. E. Jesse, T. W. Smith, L. K. Wareham, M. Hippler, U. Schatzschneider, R. K. Poole, *Antioxidants and Redox signaling* 2016, **24**, 765; (b) W. Huber, R. Linder, J. Niesel, U. Schatzschneider, B. Spingler, P. C. Kunz, *Eur. J. Inorg. Chem.* 2012, 3140; (c) J. Niesel, A. Pinto, H. W. P. N'Dongo, K. Merz, I. Ott, R. Gust, U. Schatzschneider, *Chem. Commun.* 2008, 1798; (d) F. Mohr, J. Niesel, U. Schatzschneider, C. W. Lehmann, *Z. Anorg. Allg. Chem.* 2012, **638**, 543; (e) W. C. Henke, C. J. Otolski, W. N. G. Moore, C. G. Elles, J. D. Blakemore, *Inorg. Chem.* 2020, **59**, 2178.
- 4. S. Pai, M. Hafftlang, G. Atongo, C. Nagel, J. Niesel, S. Botov, H. Schmalz, B. Yard, U. Schatzschneider, *Dalton Trans.* 2014, **43**, 8664.
- 5. (a) S. Karthikeyan, R. Nagarajaprakash, G. Satheesh, C. A. Kumar, B. Manimaran, *Dalton Trans* 2015, **44**, 17389; b) C. A. Kumar, R. Nagarajaprakash, W. Victoria, V. Veena, N. Sakthivel, B.

- Manimaran, Inorg. Chem. Commun. 2016, 64, 39.
- 6. P. P. Mokolokolo, A. Frei, M. S. Tsosane, D. V. Kama, M. Schutte-Smith, A. Brink, H. G. Visser, G. Meola, R. Alberto, A. Roodt, *Inorg. Chim. Acta* 2018, **471**, 249.
- 7. A. M. Mansour, *Appl. Organomet. Chem.* 2017, **31**, 3564.
- 8. U. Sachs, G. Schaper, D. Winkler, D. Kratzert, P. Kurz, Dalton Trans 2016, 45, 17464.
- 9. E. Kottelat, V. Chabert, A. Crochet, K. M. Fromm, F. Zobi, Eur. J. Inorg. Chem. 2015, 5628.
- 10. R. Sakla, A. Singh, R. Kaushik, P. Kumar, D. A. Jose, *Inorg. Chem.* 2019, **58**, 10761.
- 11. E. Üstün, A. Özgür, K. A. Coşkun, S. Demir, İ. Özdemir, Y. Tutar, *J. Coord. Chem.* 2016, **69**, 3384.
- 12. M. Hu, Y. Yan, B. Zhu, F. Chang, S. Yu, G. Alatan, RSC Adv. 2019, 9, 20505.
- 13. H. G. Daniels, O. G. Fast, S. M. Shell, F. A. Beckford, *J. Photochem. Photobio. A Chem.* 2019, 374, 84.
- 14. A. M. Mansour, A. Friedrich, *Polyhedron* 2017, **131**, 13.
- 15. M. McKinnon, K. T. Ngo, S. Sobottka, B. Sarkar, M. Z. Ertem, D. C. Grills, J. Rochford, Organometallics 2019, 38, 1317.
- 16. (a) B. Ramakrishna, D. Divya, P. V. Monisha, B. Manimaran, Eur. J. Inorg. Chem. 2015 5839;
- (b) D. Divya, R. Nagarajaprakash, P. Vidhyapriya, N. Sakthivel, B. Manimaran, ACS Omega 2019,4, 12790.
- 17. J. S. Ward, J. M. Lynam, J. Moir, I. J. S. Fairlamb, *Chem. Eur. J.* 2014, **20**, 15061.
- 18. A. M. Mansour, O. R. Shehab, J. Organomet. Chem. 2016, 822, 91.
- 19. D. Musib, Md K. Raza, Kh. Martina, M. Roy, Polyhedron 2019, 172, 125.
- 20. (a) B. Shankar, S. Sahu, N. Deibel, D. Schweinfurth, B. Sarkar, P. Elumalai, D. Gupta, F.
- Hussain, G. Krishnamoorthy, M. Sathiyendiran, *Inorg. Chem.* 2014, **53**, 922; (b) R. Arumugam, B.
- Shankar, K. R. Soumya, M. Sathiyendian, Dalton Trans. 2019, 48, 7425; (c) M. Bhol, M.

Priyatharsini, R. V. Krishnakumar, M. Sathiyendiran, *J. Organomet. Chem.* 2019, **889**, 27.

21. I. Mishra, M. Priyatharsini, M. Sathiyendiran, *J. Organomet. Chem.* 2020, **927**, 121521.

22. (a) G. M. Sheldrick, A short history of SHELX, *ActaCrystallogr.* 2008, **A64**, 112–122; (b) L. J. Spek, Single-crystal structure validation with the program PLATON, *Appl. Crystallogr.* 2003, **36**,

7–13.

#### **Publications**

- 1. **Mishra, I.**; Sathiyendiran, M. Luminescent [fac-Re(CO)<sub>3</sub>-N∩O-phenylimidazole] complexes with parallel arrangement of twisted ligand motifs, *J. Organomet. Chem.* **2019**, 895, 1-6.
- 2. **Mishra, I.**; Priyatharsini, M.; Sathiyendiran, M. Rhenium(I) complexes from 2-(2'-hydroxyphenyl)benzimidazolyl based bis-chelating ligand and 4-(amino)pyridine/4-(dimethylamino)pyridine, *J. Organomet. Chem.* **2020**, 927, 121521.
- 3. **Mishra, I.**; Priyatharsini, M.; Sathiyendiran, M. Synthesis and characterization of binuclear manganese carbonyl complex of 1,4-bis(2-(2'-hydroxyphenyl)benzimidazol-1-yl)benzene and dimethylaminopyridine, *J. Organomet. Chem.* **2021**, *949*, 121934.
- 4. Priyatharsini, M.<sup>†</sup>; **Mishra, I.**<sup>†</sup>; Shankar, B.; Rajaputi, N. S.; Krishnakumar, V.; Sathiyendiran, M. *fac*-Re(CO)<sub>3</sub> core-based complex featuring benzimidazole as pendant motif from hydroxyquinoline and pyridylbenzimidazole, *J. Organomet. Chem.* **2021**, *953*, 122052. (<sup>†</sup> Equal Contribution)
- 5. **Mishra, I.**<sup>†</sup>; Bhol, M.<sup>†</sup> Palanisamy Kalimuthu, and Malaichamy Sathiyendiran. Emerging Spacers-Based Ligands for Supramolecular Coordination Complexes, *Chem. Rec.* **2021**, *21*, 1–22. (<sup>†</sup> Equal Contribution)
- 6. Soumya, K. R.<sup>†</sup>; **Mishra, I.**<sup>†</sup>; Kedia, M.<sup>†</sup>; Phukon, U.<sup>†</sup>; Borkar, R.<sup>†</sup>; Sathiyendiran, M. Rhenium (I)-based supramolecular coordination complexes: Synthesis and functional properties. In Supramolecular Coordination Complexes Design, Synthesis and Applications; Shanmugaraju. S., Eds., Elsevier, **2022**. (<sup>†</sup> Equal Contribution)
- 7. Kedia, M.; Soumya, K. R.; Phukon, U.; **Mishra, I.**; Borkar, R. L.; Vengadeshwaran, P. Bhol, M.; Sathiyendiran, M. A double ouroboros-shaped noncovalent molecular dimer, *CrystEngComm* **2023**, *25*, 2518 2522.
- 8. **Mishra, I.**; Shankar, B.; Sathiyendiran, M. Fluorine assisted self-assembly approach for tubular architecture of cyclic trinuclear rhenium(I)-fluorothiabendazolate complex, *Dalton Transactions (Under revision)*.
- 9. **Mishra, I.**; Shankar, B.; Sathiyendiran, M. Flexible Coordination Cages with Polarized C–H donors for the Recognition of Spherical and Linear Anions (*To be communicated*).

## **Presentations**

- 1. **Poster:** "Light emitting heteroleptic rhenium complexes" in Chemfest 2018 (In-house symposium) at University of Hyderabad.
- 2. **Poster:** "fac-Mn(CO)<sub>3</sub> core based neutral dinuclear complexes" in Chemfest 2019 at (Inhouse symposium) University of Hyderabad.
- 3. Poster: "Dinuclear Rhenium (I) Acyclic complexes: Photophysical and Electrochemical studies" in Chemfest 2020 (In-house symposium) at University of Hyderabad.
- 4. **Oral and Poster:** "Rhenium(I) based Metallocage and Tubes" in Chemfest 2023 at University of Hyderabad. (Best oral presentation)

# Rhenium(I)/Manganese(I)-based Supramolecular Cages, Tubes and Acyclic Complexes

by Isha Mishra

Submission date: 14-Jun-2023 09:47PM (UTC+0530)

Submission ID: 2116043666

File name: Isha Mishra.pdf (649.25K)

Word count: 15090

Character count: 82733

Libraria

Indira Gandhi Memorial Library

Central University P.O.

# Rhenium(I)/Manganese(I)-based Supramolecular Cages, Tubes and Acyclic Complexes

**ORIGINALITY REPORT** 

SIMILARITY INDEX

INTERNET SOURCES

**PUBLICATIONS** 

STUDENT PAPERS

#### **PRIMARY SOURCES**

Isha Mishra, Malaichamy Sathiyendiran. "Luminescent [fac-Re(CO)3-N∩Ophenylimidazole] complexes with parallel arrangement of twisted ligand motifs", Journal Professor of Organometallic Chemistry, 2019

Publication

Dr. M.Sathiyendiran University of Hyderabad Hyderabad - 500 046, In

Isha Mishra, Maruthupandiyan Priyatharsini, Malaichamy Sathiyendiran. "Synthesis and characterization of binuclear manganese carbonyl complex of 1,4-bis(2-(2'hydroxyphenyl)benzimidazol-1-yl)benzene Dr. M. Sathiyendiran and dimethylaminopyridine", Journal, of Organometallic Chemistry, 2021

M. Satly liva

School of Chemistry University of Hyderabad Hyderabad - 500 046, India.

Publication

Submitted to University of Hyderabad, Hyderabad Student Paper

Isha Mishra, Maruthupandiyan Priyatharsini, Malaichamy Sathiyendiran. "Rhenium(I) complexes from 2-(2-

2%

M. Sattly Dr. M.Sathiyehdiran Professor School of Chemistry University of Hyderabad Hyderabad - 500 046, India. hydroxyphenyl)benzimidazolyl based bischelating ligand and 4-aminopyridine/4dimethylaminopyridine", Journal of Organometallic Chemistry, 2020

Publication

Isha Mishra, Maruthupandiyan Priyatharsini, 5 Malaichamy Sathiyendiran. "Rhenium(I) complexes from 2-(2'hydroxyphenyl)benzimidazolyl based bischelating ligand and 4-(amino)pyridine/4-(dimethylamino)pyridine", Journal of Organometallic Chemistry, 2020 Publication

M. Satly Dr. M.Sathiyendiran Professor School of Chemistry University of Hyderabad Hyderabad - 500 046, India.

medworm.com 6 Internet Source

<1%

www.researchgate.net

Internet Source

Sathiyendiran Malaichamy, Upasana Phukon, Bhaskaran Shankar. "Self-assembly of new class of rhenium(I)-based double stranded dinuclear monohelicates with their photophysical and electrochemical studies", Dalton Transactions, 2022

Publication

Moon Kedia, Bhaskaran Shankar, Malaichamy Sathiyendiran. "Rhenium(I)-Based Neutral Coordination Cages with a Spherical Cavity for Selective Recognition of Fluoride", Inorganic

<1%

K.R. Soumya, Moon Kedia, Malaichamy 10 Sathiyendiran. "Rhenium(I)tricarbonyl M2Cl2Ltype metallocycles from flexible ditopic benzimidazolyl donors", Journal of Organometallic Chemistry, 2023

<1%

Publication

Palanisamy Rajakannu, Bhaskaran Shankar, 11 Anju Yadav, Ramasamy Shanmugam et al. "Adaptation toward Restricted Conformational Dynamics: From the Series of Neutral Molecular Rotors", Organometallics, 2011

<1%

Publication

pubs.acs.org 12

<1%

K. R. Soumya, Ramar Arumugam, Bhaskaran 13 Shankar, Malaichamy Sathiyendiran. "Sulfate Donor Based Dinuclear Heteroleptic Triple-Stranded Helicates from Sulfite and Ditopic Nitrogen Donor Ligands and Their Transformation to Dinuclear Homoleptic Double-Stranded Mesocates", Inorganic Chemistry, 2018 Publication

Mamina Bhol, Bhaskaran Shankar, 14 Malaichamy Sathiyendiran. "Rhenium(I)-Based

<1%

# Heteroleptic Pentagonal Toroid-Shaped Metallocavitands: Self-Assembly and Molecular Recognition Studies", Inorganic Chemistry, 2022

Publication

	1 dolication	
15	Pounraj Thanasekaran, Cheng-Hua Lee, Kuang-Lieh Lu. "Neutral discrete metal- organic cyclic architectures: Opportunities for structural features and properties in confined spaces", Coordination Chemistry Reviews, 2014 Publication	<1%
16	Bhaskaran Shankar, Ramar Arumugam, Palani Elumalai, Malaichamy Sathiyendiran. "Rhenium(I)-Based Monocyclic and Bicyclic Phosphine Oxide-Coordinated Supramolecular Complexes", ACS Omega, 2016 Publication	<1%
17	www.ncbi.nlm.nih.gov Internet Source	<1%
18	worldwidescience.org Internet Source	<1%
19	Isha Mishra, Mamina Bhol, Palanisamy Kalimuthu, Malaichamy Sathiyendiran. "Emerging Spacers - Based Ligands for Supramolecular Coordination Complexes",	<1%

The Chemical Record, 2021

M. Satery Dr. M.Sathiyendiran

School of Chemistry University of Hyderabad Hyderabad - 500 046, India.

Professor

20	Malaichamy Sathiyendiran. "Synthesis of a polynuclear complex possessing four spatially arranged rhenium units", Inorganic Chemistry Communications, 2013 Publication	<1%
21	K.R. Soumya, Isha Mishra, Moon Kedia, Upasana Phukon, Reema Borkar, Malaichamy Sathiyendiran. "Rhenium (I)-based supramolecular coordination complexes: Synthesis and functional properties", Elsevier BV, 2023 Publication	<1%
22	Xian-Lan Hong, Yi-Zhi Li, Jun-Feng Bai. " - Poly[[aquadipyridinezinc(II)]-µ-benzene-1,4- dioxyacetato] ", Acta Crystallographica Section E Structure Reports Online, 2005 Publication	<1%
23	docksci.com Internet Source	<1%
24	WWW.science.gov	<1%

Internet Source